CENTRO INTERNACIONAL DE ESTUDOS
DE DOUTORAMENTO E AVANZADOS
DA USC (CIEDUS)

TESE DE DOUTORAMENTO

IMPROVEMENT OF ANTERIOR AND POSTERIOR SEGMENT OCULAR DRUG DELIVERY: APPLICATION IN OCULAR CYSTINOSIS AND AGE-RELATED MACULAR DEGENERATION

Andrea Luaces Rodríguez

ESCOLA DE DOUTORAMENTO INTERNACIONAL EN CIENCIAS DA SAÚDE

PROGRAMA DE DOUTORAMENTO EN INVESTIGACIÓN E DESENVOLVEMENTO DE MEDICAMENTOS

SANTIAGO DE COMPOSTELA

2020

USC
UNIVERSIDADE
DE SANTIAGO
DE COMPOSTELA

DECLARACIÓN DA AUTORA DA TESE

Improvement of anterior and posterior segment ocular drug delivery: application in ocular cystinosis and age-related macular degeneration

Dna. Andrea Luaces Rodríguez

Presento a miña tese, seguindo o procedemento axeitado ao Regulamento, e declaro que:

1) A tese abarca os resultados da elaboración do meu traballo.
2) De selo caso, na tese faise referencia ás colaboracións que tivo este traballo.
3) A tese é a versión definitiva presentada para a súa defensa e coincide coa versión enviada en formato electrónico.
4) Confirmo que a tese non incorre en ningún tipo de plaxio doutros autores nin de traballos presentados por min para a obtención doutros títulos.

En Santiago de Compostela, 10 de Maio de 2020

Asdo. Andrea Luaces Rodríguez

USC
UNIVERSIDADE
DE SANTIAGO
DE COMPOSTELA

AUTORIZACIÓN DOS DIRECTORES DA TESE

Improvement of anterior and posterior segment ocular drug delivery: application in ocular cystinosis and age-related macular degeneration

D. Francisco J Otero Espinar

D. Anxo Fernández Ferreiro

INFORMAN:

Que a presente tese, correspóndese co traballo realizado por Dna. **Andrea Luaces Rodríguez**, baixo a nosa dirección, e autorizamos a súa presentación, considerando que reúne os requisitos esixidos no Regulamento de Estudos de Doutoramento da USC, e que como directores desta non incorre nas causas de abstención establecidas na Lei 40/2015.

En Santiago de Compostela, 10 de Maio de 2020

Asdo. Francisco J Otero Espinar

Asdo. Anxo Fernández-Ferreiro

USC
UNIVERSIDADE
DE SANTIAGO
DE COMPOSTELA

AGRADECIMIENTOS

Hace cuatro años tomé una decisión muy importante que ha tenido como desenlace la presente tesis. Después de horas y horas realizando experimentos, leyendo artículos, escribiendo y reescribiendo, me encuentro con que la escritura de estos agradecimientos me supone uno de los momentos más complejos de la realización de esta tesis. A pesar de ello, considero que es la parte que nos muestra que esta tesis no es un éxito alcanzado en solitario, ya que sin la ayuda de una forma u otra de todos los que mencionaré a continuación, estoy segura de que no habría llegado a la situación en la que me encuentro ahora.

En primer lugar, me gustaría darles especialmente las gracias a mis dos directores de tesis, a Francisco Otero Espinar y a Anxo Fernández Ferreiro, ya que sin su apuesta en mí esta tesis no habría sido posible.

A **Fran**, por tu dedicación y cariño. Por todos los consejos que me has hecho llegar. Gracias por darme la oportunidad de adentrarme en la investigación y aportarme ese granito de sabiduría y experiencia más que necesario en esta etapa.

A **Anxo**, por creer siempre en mí, valorar mi criterio y apostar por mis ideas. Por tus constantes correcciones a cualquier hora e independientemente de la carga de trabajo que tuvieses. Por tu entusiasmo y trasmitirme que la felicidad en el trabajo es fundamental. Por enseñarme que las ideas más alocadas pueden llegar a ser las mejores ideas del mundo.

Quisiera agradecer también a **Pablo Aguiar**, cuya colaboración me ha permitido llevar a cabo los experimentos de medicina nuclear. A pesar de no estar relacionado directamente con mi tesis, gracias por mostrar una gran predisposición a ayudarme y sacar esta tesis adelante. También a **Miguel Barcia**, por su interés constante y sabios consejos.

A todos los integrantes del Departamento de Tecnología Farmacéutica de la Facultad de Farmacia y de los servicios de Farmacia Hospitalaria y Medicina Nuclear del Hospital Clínico de Santiago de Compostela, por permitirme hacer uso de sus instalaciones y equipamiento y prestarme la ayuda necesaria en cada momento.

Tengo mucho que agradecerles también a mis cómplices investigadores:

A mis compañeros de laboratorio de la facultad de farmacia, **Iria**, **Victoria**, **Rubén**, **Víctor**, **Elena**, **Xurxo**, **Andrea Conde**, **Carlos** y **Guille**. Por todos esos momentos del café, de dejar el trabajo a un lado y reírnos y contar nuestras anécdotas. Por la ayuda prestada por cada uno de ellos en los diversos momentos que la necesité. Por luchar todos por un mismo objetivo.

A mis compañeros de medicina nuclear, **David**, **Manuel**, **Noemí**, **Alexis**, **Jesús** y **Cristina** por aceptarme como una más del grupo y ayudarme en todo lo posible a pesar de dedicarnos a ramas tan dispares de la ciencia. **Cristina**, aunque apareciste a mitad de este largo camino, tu sonrisa constante y palabras de ánimo me han ayudado en la recta final. Gracias por prestarme ayuda en todo momento y ofrecerte a echarme una mano en cualquier cosa que necesitase.

Una de las mejores experiencias que me ha reportado la etapa predoctoral es realizar una estancia en Holanda. Sin duda, **Lara**, tuvo una gran repercusión en esto. Gracias por acogerme y mostrarme tu gran apoyo, allí, y después en la distancia. Gracias por estar ahí para ayudarme en cualquier cosa. También me gustaría agradecer a todos los compañeros de allí que me acogieron desde el primer día y permitieron que llenase esos meses de recuerdos inolvidables.

Asimismo, agradecer una y mil veces más a todas las personas que tengo la suerte de llamar amigos, y particularmente:

A mis farmacéuticas preferidas, **Natalia**, **Bea**, **Clara**, **Carmen** y **Andrea Lafuente**, que aunque nuestros caminos se han separado, siempre me habéis apoyado en el mío, valorando mi esfuerzo y sacrificio. **Natalia**, a pesar de la distancia has sido un apoyo fundamental y una persona con la que siempre podré contar para cualquier cosa. Por tu alegría y por hacerme ver que todo tiene una solución. **Bea**, por tu constante interés en cómo me iba con la tesis y apoyo en los distintos baches que tenía. **Clara**, por ser la mejor vecina de laboratorio que podría tener y aguantar todas mis frustraciones cada vez que un ensayo no salía.

A **Mariña** y a **Uxía**, mis dos grandes pilares en el día a día durante estos años. Gracias por estar ahí todos los días, por escuchar mis quejas y también para vivir conmigo los pequeños logros que iba consiguiendo. Pero, sobre todo, gracias por llenarme esos momentos ajenos a la tesis de alegría y felicidad. Estoy segura de que sin vosotras este camino hubiese sido más difícil.

A **Álvaro**, gracias por todos esos cafés hablando de nuestras vidas y problemas intentando salvar el mundo.

Pero, sobre todo, me gustaría agradecer de forma especial:

A **mi familia**, por creer en mí y darme palabras de apoyo cuando más las necesitaba. Por comprender cuales eran mis inquietudes y deseos y estar pendientes de mis avances en este largo camino.

A **mis padres**, a los que en realidad les debo todo. Gracias una y mil veces más. Por enseñarme a ser perseverante, a que no todo en la vida es fácil y que todo esfuerzo tiene su recompensa. Gracias por vuestro apoyo incondicional, por todas esas palabras alentadoras que tanto necesité en algunos momentos. Gracias por hacerme ser la persona que soy hoy.

A **mi hermana**, por ser esa gran amiga que no tuve que escoger. Gracias por convertirte en un apoyo más que fundamental en mi vida. Gracias por ser un ejemplo a seguir en muchos aspectos, por cuidarme y por tener que hacer de vez en cuando de hermana mayor a pesar de que siempre seguirás siendo mi hermanita pequeña.

A **Dani**, mi compañero en este camino llamado vida. Estas palabras no son representativas de todo lo que te tengo que agradecer, pero creo que se pueden resumir en gracias por estar ahí siempre, en cualquier circunstancia, en cualquier situación. Gracias por escuchar todas las dificultades que me he encontrado durante esta tesis, aun cuando entendías dos palabras de las diez que te estaba contando, y gracias sobre todo por intentar ayudarme a buscar soluciones. Gracias por todas las veces que me acompañaste al laboratorio a horas intempestivas. Gracias por creer en mí aun cuando yo no lo hacía y contagiarme ese positivismo tuyo tan característico. Pero especialmente, gracias por esos abrazos milagrosos acompañados de un “Todo va a salir bien, ya me lo agradecerás cuando termines la tesis”, y efectivamente, tenías razón, ese momento ha llegado.

USC
UNIVERSIDADE
DE SANTIAGO
DE COMPOSTELA

RESUMEN

Las enfermedades oculares afectan a la calidad de vida de millones de personas en todo el mundo. El ojo es un órgano único debido a su compleja anatomía, fisiología y bioquímica, lo que hace que la llegada del medicamento al lugar de acción específico en el ojo sea una de las tareas más difíciles para los farmacéuticos.

El tratamiento de las patologías oculares requiere el uso de vías de administración especializadas debido a la complejidad anatómica del ojo. En consecuencia, los tratamientos oculares presentan grandes desafíos. Por un lado, el tratamiento de las enfermedades de la superficie ocular se realiza mediante la **instilación de soluciones tópicas oftálmicas**, la cual presenta las ventajas de ser una vía de administración fácil y con buen grado de aceptación por parte de los pacientes. Sin embargo, está asociada a un alto grado de aclaramiento ocular y, por tanto, con una baja biodisponibilidad del medicamento, por lo que son necesarias instilaciones frecuentes. Uno de los enfoques para incrementar esta biodisponibilidad es utilizar sistemas de administración de fármacos con permanencia ocular prolongada.

Por otra parte, una de las vías de administración más frecuentes para tratar las enfermedades del segmento posterior del ojo es la **inyección intravítrea de fármacos**. La inyección intravítrea ofrece una liberación local y directa de los fármacos proporcionando una alta biodisponibilidad en el segmento posterior, a la vez que reduce la exposición sistémica. Sin embargo, es una vía muy invasiva que suele requerir inyecciones repetidas. Aunque la incidencia de los efectos adversos debidos a esta invasividad es baja, estas complicaciones pueden ser severas, y además se agravan con el aumento del número de inyecciones intravítreas. Todas estas dificultades hacen que los sistemas de administración de fármacos de liberación sostenida para la inyección intravítrea sean muy deseables, ya que ofrecerían concentraciones terapéuticas en el segmento posterior durante períodos prolongados. Por lo

tanto, evitarían la administración frecuente de fármacos con la asociada disminución del riesgo de efectos secundarios.

Las limitaciones de la instilación tópica de colirios oculares y la inyección intravítrea son un reflejo de los problemas encontrados en el tratamiento de patologías minoritarias como la cistinosis ocular y de enfermedades de alta prevalencia como la degeneración macular asociada a la edad, respectivamente, las dos patologías en las que se centra esta tesis doctoral.

La cistinosis es un desorden metabólico sistémico que también afecta a la córnea. La **cistinosis ocular** se caracteriza por la presencia de cristales de cistina en la córnea, los cuales se tratan mediante la instilación de gotas oculares de cisteamina. La administración tópica de cisteamina durante largos períodos de tratamiento ha demostrado ser eficaz en la disminución de los cristales de cistina. Debido a la baja biodisponibilidad de la formulación actual de cisteamina, las soluciones oculares deben administrarse cada hora que el paciente está despierto para obtener el máximo beneficio. Debido a este uso tan frecuente, el cumplimiento terapéutico de este tratamiento es un problema importante en los pacientes con cistinosis. Teniendo en cuenta estos datos, es necesario reducir la frecuencia de la administración para proporcionar cierto alivio a los pacientes. Para ello, un enfoque consistiría en incluir la cisteamina en sistemas adaptados de liberación de fármacos con un mayor tiempo de permanencia sobre la superficie precorneal, lo que daría lugar a una mejora en la eficacia del tratamiento.

Una enfermedad del segmento posterior que afecta a la retina es la **degeneración macular asociada a la edad** (DMAE), la cual ocupa el tercer lugar entre las causas mundiales de discapacidad visual, aunque es la principal causa de deficiencia visual en los países industrializados. La forma más común de DMAE es la forma neovascular o húmeda. Su tratamiento estándar es la inyección intravítrea periódica de anticuerpos anti-VEGF (entre los que se incluyen bevacizumab, ranibizumab, aflibercept y brolucizumab), los cuales deben ser administrados por un oftalmólogo cada uno o dos meses. Además, son tratamientos costosos que, unido a la alta prevalencia de la DMAE, hace que el impacto económico de esta enfermedad sea elevado. Una posible estrategia para reducir al mínimo el número de inyecciones es el diseño de sistemas de administración prolongada de agentes anti-VEGF. Esto

permitiría aumentar los intervalos entre las inyecciones intravítreas, minimizando las reacciones adversas, a la vez que se mejoraría el grado de aceptación por parte de los pacientes y se reducirían los costes asociados al tratamiento de la DMAE neovascular.

La presente tesis doctoral se divide en dos secciones principales en concordancia con las dos enfermedades oculares previamente descritas. La primera sección se centra en el desarrollo y caracterización de hidrogeles oculares de cisteamina para el tratamiento de la cistinosis y consta de dos capítulos. La segunda sección incluye los estudios relacionados con las inyecciones intravítreas en la DMAE, incluyendo los cuatro capítulos restantes.

El **primer capítulo** comprende el desarrollo de dos tipos diferentes de hidrogeles oculares que contienen cisteamina, uno preparado con el polímero ácido hialurónico y el otro es un hidrogel sensible a iones compuesto de goma gellan y carragenato kappa. Ambos hidrogeles incorporan un 0,55 % de cisteamina. El hidrogel sensible a iones está compuesto por un 0,2 % de polímeros (88 %) de goma gellan y 12 % de carragenato kappa) disueltos en agua. En cambio, un 0,4 % de hialuronato sódico se disolvió en BSS (Balance Salt Solution) para la preparación del hidrogel hialurónico.

Para caracterizar galénicamente ambos hidrogeles se han realizado diferentes ensayos. Se realizó un estudio de liberación *in vitro* utilizando células de difusión de Franz, obteniendo una cinética de liberación de orden cero en las primeras cuatro horas para ambos hidrogeles. La tasa de liberación de cisteamina fue de 0,75 $mg \cdot cm^{-2} \cdot h^{-1}$ para el hidrogel hialurónico y de 0,45 $mg \cdot cm^{-2} \cdot h^{-1}$ para el hidrogel sensible a iones. Se encontraron diferencias significativas en la cantidad de cisteamina liberada entre ambos hidrogeles. Además, se realizó un estudio similar utilizando córneas bovinas *ex vivo* para evaluar la permeación transcorneal. A las cinco horas, el 0,09 % de la dosis de cisteamina fue capaz de atravesar la córnea a partir de la solución control. En cambio, el paso transcorneal a partir del hidrogel hialurónico fue del 0,45 % y a partir del hidrogel sensible a iones, del 0,40 %. Se encontraron diferencias significativas entre los hidrogeles y la solución control, aunque no entre ambos hidrogeles.

La evaluación *in vivo* del tiempo de permanencia sobre la superficie ocular se realizó en ratas Sprague-Dawley mediante medidas cualitativas directas (utilizando el colorante azul tripán para visualizar el hidrogel en la superficie ocular) y mediante medidas cuantitativas. El ensayo

cuantitativo se realizó mediante la utilización pionera de técnicas de imagen molecular con microPET y por lo tanto fue necesario radiomarcar los hidrogeles con ^{18}F-FDG. La prueba cualitativa demostró que ambas formulaciones presentaban un alto tiempo de permanencia en la superficie ocular. En lo que respecta al estudio microPET, las formulaciones evaluadas presentaron una intensa señal radioactiva en los primeros momentos después de la instilación. El uso de la metodología microPET permitió cuantificar la cantidad de hidrogel que permanecía sobre la superficie ocular. De esta manera, una hora después de la instilación, el 83,5 % del hidrogel sensible a iones permanecía sobre la superficie ocular, mientras que el 48,2 % del hidrogel hialurónico y sólo el 16,7 % de la solución de control. El tiempo de vida media fue de 0,99 h en el caso del hidrogel hialurónico, 1,27 h para el hidrogel sensible a iones, y 0,31 h para la solución control.

Por último, se realizaron ensayos de seguridad oftálmica. Para ello, se llevó a cabo un ensayo de citotoxicidad de la cisteamina sobre la viabilidad celular de los queratocitos mediante la vigilancia en tiempo real. Este demostró que la cisteamina inducía la muerte celular gradual a lo largo del tiempo. Por otra parte, se realizó el ensayo HET-CAM para estimar la posible irritación ocular que podrías causar los hidrogeles, el cual demostró la ausencia de daños en los vasos sanguíneos tras la aplicación de ambos hidrogeles.

Los diferentes ensayos realizados muestran que estas formulaciones pueden controlar la liberación de cisteamina a lo largo del tiempo, presentan un alto tiempo de retención en la superficie ocular, pueden actuar como promotores de la absorción corneal y no muestran signos de irritación en el ensayo HET-CAM. Estos resultados demuestran que las formulaciones desarrolladas son adecuadas para la administración ocular tópica de cisteamina y para su futura elaboración como formulación magistral en los Servicios de Farmacia Hospitalaria.

El **capítulo 2** describe el estudio de la estabilidad del hidrogel ocular de ácido hialurónico que contiene cisteamina, el cual ha sido previamente caracterizado a nivel galénico y de seguridad en el capítulo anterior. Se evaluó el efecto del conservante EDTA y la refrigeración como agentes estabilizadores. Se determinaron diferentes parámetros fisicoquímicos, como la osmolalidad, el pH y la concentración de cisteamina, y también ensayos descriptivos, como los ensayos de transparencia y microbiológicos para verificar la esterilidad.

Los resultados mostraron que todas las condiciones evaluadas presentaron una buena estabilidad durante el período de estudio de 30 días, ya que la transparencia, la esterilidad, la osmolalidad, el pH y la concentración de cisteamina se mantuvieron prácticamente constantes sin diferencias estadísticamente significativas entre los valores iniciales y finales. Aunque la adición de EDTA como agente conservante mostró un ligero aumento de la osmolalidad y una ligera disminución del pH sin afectar a la estabilidad de la cisteamina, su adición no mostró un efecto beneficioso sustancial sobre la formulación que no lo contenía.

Por lo tanto, la recomendación general para la conservación de los hidrogeles de cisteamina de ácido hialurónico es el almacenamiento refrigerado para prevenir el crecimiento microbiológico no existiendo la necesidad de adicionar conservantes.

El **capítulo 3** contiene una revisión bibliográfica que describe sistemas de liberación sostenida de anticuerpos antiangiogénicos intravítreos, así como la farmacocinética de los mismos. Este capítulo es introductorio de los capítulos 4, 5 y 6 en los cuales se desarrollará la parte experimental relativa a estos dos campos.

La mayoría de los estudios se centran en el comportamiento de la liberación *in vitro* de los sistemas desarrollados, pero la información proporcionada sobre la bioactividad de los anticuerpos, la biocompatibilidad o la estabilidad *in vivo* es a veces escasa. Los sistemas de liberación de anticuerpos anti-VEGF incluyen sistemas como hidrogeles, liposomas, micropartículas, nanopartículas e implantes. Los hidrogeles presentan la ventaja de que pueden ser fácilmente inyectados en la cavidad vítrea a través de una aguja de pequeño calibre. Además, los hidrogeles termosensibles presentan una estructura no viscosa al ser inyectados, que posteriormente, se transforma *in situ* en una estructura tipo gel. Sin embargo, la difusión de los anti-VEGF a través de la estructura del gel es relativamente rápida, lo que limita su utilidad como formulaciones de larga liberación. Tanto las micropartículas como las nanopartículas han sido testadas como sistemas de administración de fármacos intravítreos. Las micropartículas presentan un mayor tamaño, permiten cargas de fármaco mayores y podrían tener tiempos de liberación más largos. Sin embargo, pueden provocar visión borrosa debido a los efectos de dispersión de la luz dentro del humor vítreo. Por el contrario, las nanopartículas presentan la ventaja de una posible penetración en la retina. Ambos tipos de

partículas presentan efecto *burst*, que puede controlarse mediante su inclusión en hidrogeles. En comparación con otros sistemas, los implantes presentan tiempos de liberación más largos, ya que normalmente presentan una liberación del fármaco de varias semanas a meses y además permiten una alta carga de cantidad de fármaco. Son los sistemas de liberación prolongada más prometedores en la actualidad, aunque todavía se encuentran en las primeras etapas de desarrollo para los anticuerpos anti-VEGF.

Por otro lado, como el desarrollo de sistemas de liberación de fármaco se basa en análisis farmacocinéticos *in vivo* para evaluar la liberación prolongada del fármaco, en esta revisión también se ha abordado toda la información relativa a la farmacocinética intravítrea de los anti-VEGF en las diferentes especies animales. Se han observado diferencias considerables entre los distintos estudios preclínicos en los parámetros farmacocinéticos calculados. Además, se encontraron diferencias entre los diferentes anticuerpos anti-VEGF. En este sentido, el tiempo de vida media en humor vítreo en conejos (el animal más evaluado en los estudios de farmacocinética) es en promedio de 4,94 días para el bevacizumab (150 kDa), 2,83 días para el ranibizumab (48 kDa) y 4,58 días para aflibercept (115 kDa), lo que demuestra la relación directa entre la vida media intravítrea y el peso molecular de los anticuerpos.

El **capítulo 4** tiene por objeto la optimización de la técnica de tomografía por emisión de positrones (PET – Positron Emission Tomography) como un instrumento no invasivo para el análisis de la farmacocinética intravítrea de radiotrazadores inyectados en ojos de ratas. El perfil farmacocinético de inyecciones intravítreas de moléculas marcadas con 18-Flúor (^{18}F) se evaluó en ratas Sprague-Dawley adultas utilizando un escáner para animales pequeños de PET/tomografía computarizada. Se estudiaron diferentes condiciones: tres moléculas radiomarcadas con ^{18}F (^{18}F-FDG, ^{18}F-NaF y ^{18}F-Colina), tres volúmenes de inyección intravítrea (7, 4 y 2 µL) y la ausencia o presencia de inflamación ocular (uveítis inducida por lipopolisacárido (LPS)).

Los trazadores ^{18}F-FDG y ^{18}F-Colina se ajustaron a un modelo de dos compartimentos con un aclaramiento bifásico desde el humor vítreo. El promedio del tiempo vida media intravítrea obtenido para estas moléculas radiomarcadas fue de 13,99 minutos para la ^{18}F-FDG y de 35,18 minutos para la ^{18}F-Colina para la fase inicial de eliminación rápida (α), y de 214,2 minutos y

1351 minutos, respectivamente, para la fase de eliminación lenta (β). El ^{18}F-Na se ajustó a un modelo farmacocinético monocompartimental, y el tiempo de vida media intravítrea fue de 113,2 minutos. La comparación del área bajo la curva entre 0 y 360 minutos (AUC_0^{360}) entre las tres moléculas radiomarcadas mostró que la ^{18}F-Colina permanece significativamente más tiempo en el ojo que la ^{18}F-FDG y la ^{18}F-NaF.

No se encontraron diferencias significativas entre los distintos volúmenes de inyección intravítrea (2, 4 y 7 µL) para los radiocompuestos ^{18}F-Na y ^{18}F-FDG, aunque se observó un colapso vascular transitorio en los vasos retinianos después de la administración de 7 µL. La inflamación causada por la uveítis inducida provocó un aumento del aclaramiento intravítreo, ya que los ojos con uveítis presentaron un AUC_0^{360} más pequeño que los ojos sanos.

En conclusión, los estudios farmacocinéticos intravítreos basados en el uso de imágenes microPET pueden tener un potencial interés como herramientas no invasivas en animales pequeños para el desarrollo de fármacos oftálmicos. Los resultados mostraron que existen diferencias farmacocinéticas significativas entre las moléculas radiomarcadas estudiadas, pero no entre los volúmenes inyectados. Por lo tanto, el peso molecular y las propiedades fisicoquímicas juegan un papel clave en la eliminación desde el humor vítreo. La presencia o ausencia de uveítis fue un factor importante en el aclaramiento intravítreo, ya que la eliminación del fármaco se incrementó claramente cuando esta condición se encontraba presente.

El **capítulo 5** se basa en la metodología PET, previamente caracterizada, para estudiar la farmacocinética de la inyección intravítrea de los anticuerpos anti-VEGF bevacizumab y aflibercept en ratas. Para ello, ambos anticuerpos fueron radiomarcados con el radiotrazador zirconio-89 (^{89}Zr).

Ambos anticuerpos fueron radiomarcados con zirconio-89 con una actividad específica máxima de 15 Mbq/mg para el bevacizumab y 10 Mbq/mg para el aflibercept. Se inyectaron cuatro microlitros de anticuerpo marcado con ^{89}Zr (1-1,2 Mbq) en el humor vítreo de las ratas. Se realizó una adquisición con el microPET inmediatamente después de la inyección y a diferentes tiempos durante 12 días, y además se obtuvieron muestras de sangre a través de la vena de la cola.

El radiomarcaje se realizó con éxito con una pureza radioquímica tras la ultrafiltración superior al 95 % para ambos agentes. Los niveles oculares de ambos anticuerpos mostraron una fase inicial de rápida disminución durante las primeras horas posteriores a la administración, seguida de una fase de disminución gradual. Las curvas oculares de ambos anticuerpos se ajustaron a un modelo de dos compartimentos en el que se encontró un tiempo de vida media de eliminación intraocular de 16,44 h para el ^{89}Zr-bevacizumab y de 4,51 h para el ^{89}Zr-aflibercept, considerando la fase alfa como la fase de eliminación. El aclaramiento ocular fue de 49,35 µL·día^{-1} para el ^{89}Zr-bevacizumab y de 176,72 µL·día^{-1} para el ^{89}Zr-aflibercept. En cuanto a la fase beta, se observó un tiempo de vida media de 3,23 días para el ^{89}Zr-bevacizumab y de 4,69 días para el ^{89}Zr-aflibercept. El área bajo la curva ocular de actividad-tiempo fue ligeramente superior para el ^{89}Zr-bevacizumab (175,25 % actividad·día) que para el ^{89}Zr-aflibercept (138,37 % actividad·día).

En cuanto a la concentración sanguínea, según el ajuste a un modelo monocompartimental con absorción de primer orden, el ^{89}Zr-bevacizumab mostró un tiempo de vida media en sangre de 7,08 días, mientras que el ^{89}Zr-aflibercept de 3,18 días. El ^{89}Zr-aflibercept alcanzó una concentración sanguínea máxima del 23,82 % de la dosis intravítrea inyectada a las 8,24 h y el ^{89}Zr-bevacizumab alcanzó el 19,42 % a las 27,36 h posteriores a la inyección. En cuanto a la distribución sistémica, se observó una gran intensidad de señal radioactiva correspondiente al ^{89}Zr-aflibercept y al ^{89}Zr-bevacizumab en el corazón (básicamente debido a la radioactividad en la sangre) durante los primeros tiempos y que luego disminuye. Ambos anticuerpos también se observaron en el hígado.

Como conclusión, este estudio muestra por primera vez la farmacocinética ocular y sanguínea del aflibercept y el bevacizumab inyectados por vía intravítrea en ratas. Además, presenta los parámetros farmacocinéticos calculados en base a imágenes secuenciales del mismo animal a lo largo del tiempo.

El **capítulo 6** consiste en el desarrollo de implantes a base de quitosano para modular la liberación intravítrea de aflibercept con el objetivo de optimizar el tratamiento de la DMAE. El objetivo de este estudio es evaluar quitosanos de diferente peso molecular (PM) como formadores de la matriz del gel para la formación de los implantes, así como la influencia de

varias modificaciones del método de preparación en los implantes finales. La matriz de gel consistió en una mezcla de quitosano (10 %) y aflibercept (10 mg/mL), que posteriormente fue utilizada para la formación de los implantes mediante la impresión por extrusión semisólida. Luego los implantes fueron reticulados con TPP al 2 %. Finalmente, los implantes fueron liofilizados.

Los implantes preparados mediante impresión por extrusión semisólida presentaron unas dimensiones medias de 10 mm x 2,5 mm justo después de ser impresos, excepto los implantes de quitosano de PM medio, que sufrieron una dilatación considerable y fueron descartados. Además, los implantes de quitosano de PM alto se eligieron para los siguientes estudios debido a la mayor facilidad de procesamiento de la matriz del gel. El aumento del tiempo de reticulación en la solución de TPP de 10 a 60 minutos produjo implantes más pequeños, más compactos y con una superficie más lisa. En cuanto a la modificación del método de congelación a la utilización de nitrógeno líquido, los implantes preparados por este último procedimiento mostraron un tamaño ligeramente superior.

El comportamiento de hinchamiento de los implantes se caracterizó por un incremento inicial rápido y alto en los valores de índice de hinchamiento. Los índices de hinchamiento finales fueron considerablemente altos, al menos del 350 %, excepto para los implantes reticulados durante 60 min, los cuales presentaron los valores de índice de hinchamiento más bajos (260 %). Por lo tanto, se observó que el aumento del tiempo de reticulación tuvo un impacto importante en la capacidad de hinchamiento.

Los ensayos de liberación mostraron que los implantes de alto PM siguieron un mecanismo mixto de liberación controlada por difusión e hinchamiento. Esto es debido a que el exponente n del ajuste al modelo de Korsmeyer-Peppas fue de aproximadamente 0,5 para los implantes congelados a − 80 °C (que mostraron un mecanismo de liberación más próximo a una liberación controlada por difusión) y alrededor de 0,8 para los implantes congelados en nitrógeno líquido (en los que el mecanismo de liberación de aflibercept estaba considerablemente influido por el hinchamiento).

Los estudios preliminares realizados muestran que los implantes preparados con quitosano de alto peso molecular, con un tiempo de reticulación con TPP de 60 min y congelados

mediante su inmersión en nitrógeno líquido presentaron las mejores características de todos los implantes propuestos. Esto implantes liofilizados presentaron un tamaño menor (7.00 x 1.87 mm), un bajo grado de hinchamiento y el mejor comportamiento en cuanto a la liberación se refiere. Estos fueron capaces de liberar aflibercept de manera controlada durante al menos 21 días mostrando un bajo efecto *burst* (alrededor del 20 % a las 24 h) y un alto porcentaje de aflibercept liberado (90 %) con respecto a la cantidad de fármaco inicialmente cargada en el implante.

En **conclusión**, en esta tesis doctoral se han desarrollado formulaciones a base de hidrogeles conteniendo cisteamina de gran potencial para el tratamiento de la cistinosis ocular. El hidrogel basado en el polímero de ácido hialurónico ha sido ampliamente caracterizado y su preparación se ha trasladado a los Servicios de Farmacia Hospitalaria.

Por otra parte, en lo que respecta al estudio de las inyecciones intravítreas en la DMAE, esta tesis doctoral ha demostrado la utilidad de la metodología PET para el estudio de la farmacocinética intravítrea en ratas, que posteriormente ha sido utilizada para la evaluación de la farmacocinética ocular tras la administración intravítrea de aflibercept y bevacizumab. Además, se han desarrollado implantes intravítreos a base de quitosano conteniendo aflibercept que permiten una liberación retardada del mismo.

INDEX

Objectives and organisation

USC
UNIVERSIDADE
DE SANTIAGO
DE COMPOSTELA

OBJECTIVES AND ORGANISATION

STATEMENT OF THE PROBLEM

Ocular diseases require specialised routes of drug administration for their treatment due to the singular and complex characteristics of the eye. Drug delivery to the different parts of eye is one of the most challenging tasks for pharmacists, since ocular surface diseases suffer from high clearance decreasing the drug bioavailability whereas posterior segment diseases need to overcome ocular barriers by invasive repetitive intravitreal injections. These two common limitations are portrayed in the difficulties in the treatment of ocular cystinosis and age-related macular degeneration, respectively.

The current treatment for the corneal deposits of cystine crystals in ocular cystinosis disease is an ophthalmic solution of cysteamine hydrochloride, which has been demonstrated to be effective in the elimination of these crystals. However, these eye drops need to be instilled every awaken hour in order to achieve maximum efficacy. Moreover, the eye drops are quickly drained from the ocular surface due to the continuous tear replacement. All these limitations make patient compliance to the treatment very difficult, mainly in children and teenagers. In order to increase the bioavailability of the eye drops, decrease disease progression and prolong the dosing interval, it is desirable to increase the residence time of the cysteamine ocular formulation on the ocular surface. This is the reason why hydrogels containing cysteamine represent a viable alternative to the standard solutions.

On the other hand, retinal diseases such as AMD are difficult to treat due to the anatomical characteristics of the eye that hinders drug access to the target site. Such is the case that a special route of administration is needed to achieve adequate drug levels in the retina, the intravitreal injection. However, AMD treatment consist of anti-VEGF antibodies whose

commercial medications are just solutions without any controlled drug release mechanism. The limited knowledge of the anti-VEGF intravitreal pharmacokinetics due to the lack of non-invasive methods of evaluation makes that injection intervals are based on clinical outcomes rather than pharmacokinetic studies. Therefore, anti-VEFG intravitreal injections need to be administered every one or two months by an ophthalmologist. Repeated intravitreal injections entail inherent adverse complications such as endophthalmitis and retinal detachment. Moreover, the high costs of these treatments and the high AMD incidence make AMD to present a high health impact. The development of drug delivery systems containing the anti-VEGF antibodies would allow increasing the dosing intervals, which subsequently would improve patient compliance, reducing the number of visits to the ophthalmologist and decreasing the treatment costs.

OBJECTIVES

Having in mind these premises, this thesis has stablished as general objective the improvement of the drug treatment for the two aforementioned diseases, ocular cystinosis and age-related macular degeneration.

Specific objectives are listed below.

1. Development of a cysteamine ophthalmic formulation intended for the topical treatment of ocular cystinosis.
   1.1. Design, optimisation, and characterisation of a hydrogel-based topical ocular formulation containing cysteamine with higher ocular residence.
   1.2. Characterise the stability of the developed formulation and translate its preparation to hospital pharmacy departments.
2. Evaluation of the intravitreal route for the administration of anti-VEGF antibodies in age-related macular degeneration.
   2.1. Feasibility of the use of Positron Emission Tomography as a non-invasive tool to study intravitreal pharmacokinetics.
   2.2. Evaluation of the pharmacokinetics of intravitreally injected anti-VEGF agents in rat eyes.

2.3. Design and development of an intravitreal implant intended for AMD treatment.

ORGANISATION

Based on the formulated objectives, this doctoral thesis is presented as a compendium of five original research works and one review article.

This doctoral thesis has been organised to comply with the regulation of the International Doctorate School at the University of Santiago de Compostela (Spain) regarding thesis structure, languages, and ethical and intellectual properties.

The present doctoral thesis is divided in two main sections in correspondence with the two ocular diseases addressed. The first section focuses on the development and characterisation of ocular cysteamine hydrogels for the treatment of cystinosis. It is divided in two chapters.

Chapter 1 comprises the development of two different types of ocular hydrogels containing cysteamine, one made from hyaluronic acid polymer and the other is an ion sensitive hydrogel composed of gellan gum and kappa carrageenan. Moreover, an extensive *in vitro* and *in vivo* characterisation have been performed of both hydrogels.

Chapter 2 is a stability study of the hyaluronan hydrogel, which has been previously characterised in the former chapter, in different preservation conditions during a follow-up of 30 days. Moreover, the effect of the preservative EDTA and refrigeration were assessed as stabilising agents.

The second section of the present thesis comprises the studies related to intravitreal injections in AMD. It consists of four chapters, from Chapter 3 to 6.

Chapter 3 contains a bibliographic review which acts as an introduction to the following chapters 4, 5 and 6. It describes the drug delivery systems developed regarding intravitreal anti-VEGF drugs, which include systems as hydrogels, liposomes, microparticles, nanoparticles or implants. It focuses on evaluating the prolonged drug release time of anti-VEGF drugs through these devices, mainly through *in vitro* release tests and some through *in vivo* pharmacokinetic analyses. Moreover, it incorporates an analysis of anti-VEGF intravitreal

pharmacokinetics in different animal species, which would be of great interest for the pharmacokinetic evaluation that will be performed in chapter 5.

Chapter 4 is aimed at assessing the feasibility of the analysis of the intravitreal pharmacokinetics of radiotracers injected into rat eyes using Positron Emission Tomography as a non-invasive tool. Different fluorinated radiotracers were used to determine factors affecting the vitreous clearance and to stablish an adequate intravitreal injection volume in rats.

Chapter 5 is based on the PET methodology for the study of intravitreal pharmacokinetics described in the previous chapter. The aim of this chapter is to study the ocular and blood pharmacokinetics following the intravitreal injection of the anti-VEGF antibodies bevacizumab and aflibercept in rats. For that purpose, both antibodies were radiolabelled to the radiotracer zirconium-89 in order to visualise them via PET.

Finally, **chapter 6** describes the preliminary study of developing intravitreal implants containing aflibercept. Different molecular weight chitosans and different methods of preparations were tested. Swelling and *in vitro* release was assessed for the aflibercept-loaded implants.

All the research has been done between the PARAQUASIL Research Group at the Department of Pharmacology, Pharmacy and Pharmaceutical (Faculty of Pharmacy, University of Santiago de Compostela (USC), Santiago de Compostela, Spain) and the Clinical Pharmacology Group from the Health Research Institute of Santiago de Compostela (IDIS) (University Clinical Hospital of Santiago de Compostela, Santiago de Compostela, Spain). Moreover, molecular imaging (presented in chapters 1, 4 and 5) was performed in close collaboration with the Molecular Imaging Group (UNIME) of the Health Research Institute of Santiago de Compostela (IDIS) (University Clinical Hospital of Santiago de Compostela, Santiago de Compostela, Spain). In addition, antibody radiolabelling to zirconium-89 was feasible due to the collaboration with the Department of Nuclear Medicine and Molecular Imaging of the University Medical Center Groningen (University of Groningen, Groningen, The Netherlands) through a 3-month-stay.

Introduction

USC
UNIVERSIDADE
DE SANTIAGO
DE COMPOSTELA

INTRODUCTION

DRUG DELIVERY TO SPECIFIC COMPARTMENTS OF THE EYE

Eye diseases affect the quality of life of hundreds of millions of people over the world (1). Blindness and visual impairment have important and long-lasting consequences on all aspects of life, including daily personal activities, interacting with the community, school and work opportunities and the ability to access public services. The eye is a unique organ due to its complex anatomy, physiology, and biochemistry because it comprises highly different structures with specific physiological functions (2,3). It presents a great number of defence mechanisms for protection against external hazards, which also represent an impediment for the ocular administration of medications; therefore, making drug delivery to the eye as one of the most challenging tasks for pharmacists (4).

Until 50 years ago, the drugs used in ophthalmology were adapted from other fields. Therefore, ophthalmic treatments relied on the pharmaceutical compounding performed at the hospital pharmacy departments in order to provide adequate medications to the patients. Luckily, drug development for ocular diseases has taken great strides in the last decades providing new drugs primarily designed for ocular administration (5), although some treatments still depend on the pharmaceutical compounding (6,7). However, in these cases, ophthalmic compounded formulations are devoid of adequate galenic development due to the lack of appropriate vehicles, extensive characterisation and stability studies. Therefore, there is a need of improving the quality of the ocular compounded formulations prepared at the hospital level. On the other hand, mostly all the commercial ophthalmic medications lack of controlled release systems which make them less effective than they could be (8). Although some progress has been done regarding ocular drug delivery systems, there is room for

improvement even with the faced challenges that need to be accounted for due to the complex nature of the eye (9).

The eye can be divided in two major parts, anterior and posterior segments, which are separated by the posterior surface of the lens (Figure 1). This classification is actually adapted for the ocular drug delivery as the method and route of administration is highly dependable on the part of the eye segment (10). The anterior segment is composed of the cornea, the aqueous humour, the iris and the lens. The posterior segment comprises the back two-thirds of the eye, including the vitreous humour, the retina, the choroid and the optic nerve (4).

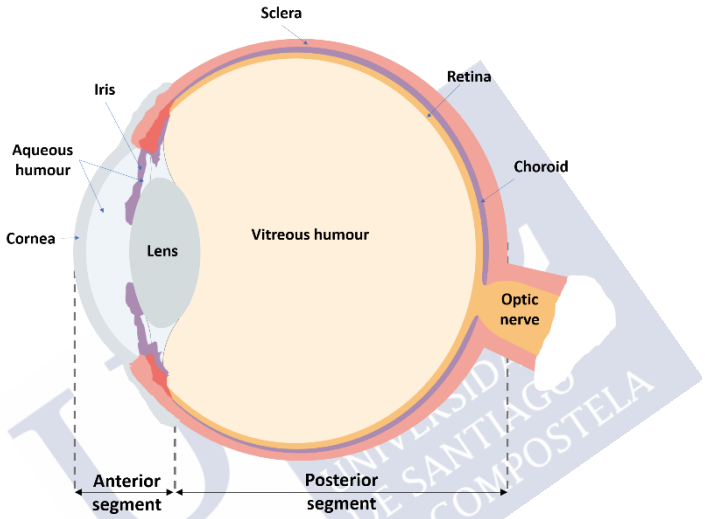

Figure 1. An eye model representing the anterior and posterior segment.

Anterior segment delivery

The singular and complex characteristics of this organ make necessary to use specialised routes of administration adapted to the ocular anatomy itself (10). For the therapeutic management of the diseases affecting the anterior segment of the eye, the ocular topical route of administration is the most preferable one (5). Various reasons account for this: convenience of administration, non-invasiveness, self-administration, patient compliance, relatively high ratio of ocular to systemic drug levels and cost-effectiveness (5,9,11). The most commonly used ophthalmic dosage forms for topical instillation are solution-based eye drops, which account for approximately 90 % of drug administered through this route (11,12). However, it encounters several drawbacks. It is estimated that less than 5-10 % of the topically

instilled drug dose in the eye is absorbed (13,14). This low bioavailability is attributed primarily to physiological protective mechanisms such as nasolacrimal drainage, reflex blinking and tear turn over (15), even though anatomical barriers, such as the permeability of the corneal epithelium, and the inherent properties of the drug molecules also play an important part (5). This rapid drainage from the precorneal surface significantly lowers ocular retention time which produces a rapid reduction in drug concentration, thereby decreasing drug absorption and needing repeated frequent instillations (12).

Therefore, one factor that has a prime influence on the amount of drug which would penetrate the cornea is the time during which it is in contact with this part of the eye. Hence, using drug delivery systems with prolonged ocular drug residence time in the precorneal area would ultimately improve ocular bioavailability (5,10). One of the approaches to extend bioavailability of ophthalmic drugs is to use viscosity-enhancing polymers, which would resist lacrimal drainage and increase the residence time of the drug on the ocular surface (10).

This strategy would be especially beneficial for ocular cystinosis treatment. Cystinosis is a systemic metabolic disorder which also affects the cornea. Ocular cystinosis is characterised by the presence of cystine crystals in the cornea which are treated by the instillation of cysteamine eye drops. Topical administration of cysteamine for long treatment periods has demonstrated to be effective in decreasing the cystine crystals (16–18). Due to the low bioavailability of the current cysteamine formulations, the eye drops must be administered every awaken hour in order to achieve maximum benefit (16). Because of this frequent usage, compliance with the use of these eye drops is a major issue in cystinosis patients. Considering these data, there is a need of reducing the frequency of administration to provide some relief to patients. In order to do so, one approach would be including cysteamine in adapted drug release systems with increased precorneal residence time which might lead to a more effective treatment.

Posterior segment delivery

Posterior segment eye diseases account for most cases of irreversible blindness worldwide (19). The standard route of administration to treat these diseases in clinical practice is the

intravitreal injection of drugs, although topic and systemic administration have also been addressed with limited results. It has been demonstrated that these both routes do not provide adequate concentrations of drugs in the posterior segment due to various physiological factors (10,20). Topical ocular administration of eye drops is the chosen route for the treatment of anterior segment diseases. However, due to the low ocular retention on the ocular surface of the majority of the ophthalmic medicines and to a much greater extent to the poor drug penetration to the posterior segment of the eye (21), topical ocular route is not a desirable route of administration for retina diseases. Successful systemic administration to treat retinal pathologies is prevented from the very low drug bioavailability, normally less than 2 % (22). This low bioavailability is caused by the difficulty of accessing the ocular compartments due to the presence of physiological barriers, specifically the blood retinal barrier (BRB) (22,23). Moreover, it makes necessary to administer very high drug doses in order to achieve a therapeutic concentration in the posterior segment of the eye, which produces a high systemic exposure which is related to systemic adverse effects (10,23–25).

Other approaches have been proposed for accessing the posterior segment such as periocular (which includes subconjunctival, sub-Tenon's, peribulbar, retro bulbar and posterior juxtascleral injection), suprachoroidal and subretinal route of administration (Figure 2). The medicines administered by these routes are delivered to different tissues and layers of the eye. Hence, these procedures of injection have the drawback of the drug needing to cross several barriers to access the site of action, which might result in infra-therapeutic drug levels at the target site. On the contrary, they possess the features of being less painful and safer compared to intravitreal injections (10).

Intravitreal administration directly delivers the drug in the proximity to the site of action, where there are none or a few physiological barriers to overcome. Specifically, it deposits the drug in the vitreous humour through a pars plana injection. Intravitreal injection offers local and direct delivery of drugs, bypassing ocular barriers and minimising drug diffusion in order to provide a very high bioavailability in the posterior segment (10,26). Moreover, it reduces systemic exposure to the drug with the consequently minimal systemic adverse effects, and decreases drug delivery to other off-target sites (10,27).

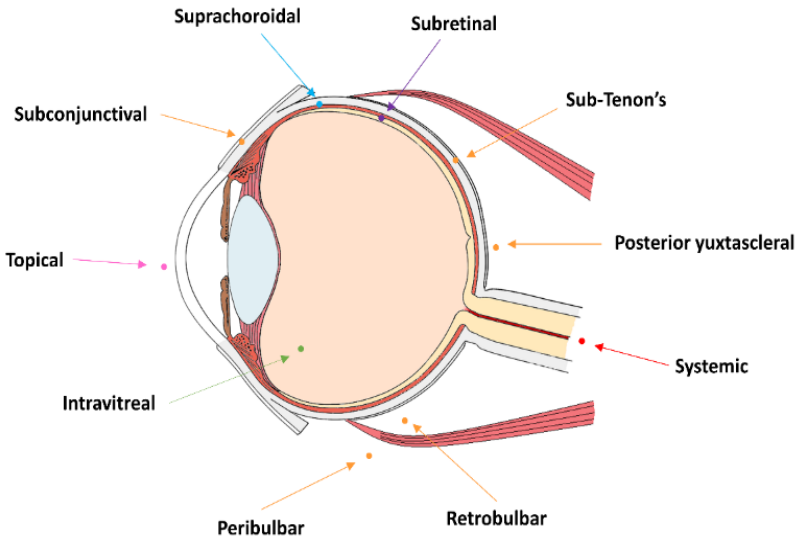

Figure 2. Scheme of the different routes of drug administration to the posterior segment. Dots symbolize the injection site of each route.

Even though intravitreal injection is preferred for drug administration to the posterior segment, it presents several limitations. The main one is that is a very invasive route of administration with associate discomfort for the patient. Although the incidence of side effects inherent to the intravitreal injection is low, the severity of these complications is relatively high. These adverse effects include endophthalmitis, retinal detachment, inflammation and vitreous haemorrhage. On the other hand, most posterior segment disorders require repetitive injections (26), which aggravates the apprehension and distress of the patients associated with inserting needles into the eye (28). In addition, the chance of occurrence of these adverse effects increases with the number of intravitreal injections (27).

All these difficulties make sustained release drug delivery systems for intravitreal injection very desirable because they would offer therapeutic concentrations in the posterior segment for prolonged periods. Consequently, they can avoid frequent administration of drugs minimising repetitive injections with the decreased risk of side effects. Moreover, reducing the number of intravitreal injections would improve patient acceptability and decrease health care costs (10,27).

A posterior segment disease affecting the retina is age-related macular degeneration (AMD), which ranks third among the global causes of visual impairment with a blindness prevalence

of 8.7 %, although it is the primary cause of visual deficiency in industrialized countries (29). The most common form of AMD is the neovascular or wet form. Its standard treatment is the intravitreal injection of anti-VEGF antibodies, which share the same problems as described above. One possible strategy to minimize these drawbacks would be the design of drug delivery systems containing the anti-VEGF drugs currently available. This would permit to obtain a long-lasting delivery of these anti-VEGF antibodies, decreasing the number of intravitreal injections and the invasiveness. Consequently, anti-VEGF drug delivery systems would reduce the number of visits to the ophthalmologist and decrease the treatment costs, which eventually would improve the effective clinical administration in the current therapy for wet AMD.

CYSTINOSIS

Cystinosis is a rare lysosomal storage disorder that follows an autosomal recessive inheritance pattern (30). The estimated incidence is 1 in 100,000 live births (30). This metabolic disorder is characterized by the accumulation of the amino acid cystine in lysosomes due to defective cystine efflux from the lysosome. Cystine has low solubility in water, leading to the formation of intra-lysosomal crystals and damage to various tissues and organs, including the cornea (31).

Cystinosis is caused by a defective transporter, called cystinosin, which transports cystine from inside the lysosome to the exterior (32–34). In 1995 the gene responsible for the cystinosis was discovered, CTNS gene (chromosome 17p13, 12 exons, 23 kb), which encodes 367 amino acids that form the cystinosin (31,35). More than 100 different mutations have been found in patients with cystinosis. However, half of the cases in Europe and the United States are caused by a 57.2 kb deletion (36).

Although is not clear how the intra-lysosomal crystals of cystine produce cellular damage, they can be found in all the organs and tissues of patients with cystinosis, especially in kidney, cornea, liver, spleen, brain and gut. The earliest manifestation of cystinosis is renal dysfunction leading to end-stage renal disease.

The ocular manifestations of the disease are due to the accumulation of cystine crystal deposits in the cornea, which are a pathognomonic sign of cystinosis (37). They start forming during childhood and from 16 months of age onward they can be observed through a slit lamp. Patients are initially asymptomatic; however, ocular symptoms appear due to the accumulation of corneal cystine crystals over time (38). The main symptom described by cystinosis patients is photophobia followed by blepharospasm (39).

Cystinosis presents two types of phenotypes depending on severity of illness and time of appearance, i.e., nephropathic and non-nephropathic cystinosis, although all present ocular symptoms. Infantile nephropathic cystinosis is the most common and severe form of this diseases, accounting for 95 % of cystinosis cases. Juvenile or intermediate nephropathic cystinosis is characterised by a slower progression of symptoms. Ocular or non-nephropathic cystinosis is characterized by an adult onset with only ocular manifestations (40,41).

Ocular treatment: cysteamine

The standard treatment of cystinosis is cysteamine, also called mercaptamine or 2-aminoethanethiol (42). Cysteamine was introduced as a possible therapeutic agent for cystinosis in 1976 and remains the only available treatment (43). Although cysteamine does not cure cystinosis, it has revolutionized patient management and prognosis. It has been shown to slow disease progression and can reduce the amount of intracellular cystine by more than 90 %. Cysteamine therapy should be started as soon as the diagnosis is made and should be continued for the lifetime of the patient. Patients with poor adherence to treatment or with a late beginning do not achieve such beneficial outcomes (44). Cysteamine treatment causes a considerable depletion of cystine crystals in the lysosomes. Once cysteamine is inside de lysosome, it reacts with cystine, breaking the disulphide bond in the cystine in order to form cysteine and a cysteine-cysteamine complex (Figure 3). Contrary to cystine, cysteine can escape from the lysosome through a cysteine transporter and the complex uses a cationic amino acid transporter (45). This transporter has recently been identified as protein PQLC2, a heptahelical PQ-loop protein whose mechanism of action is still not well understood (46).

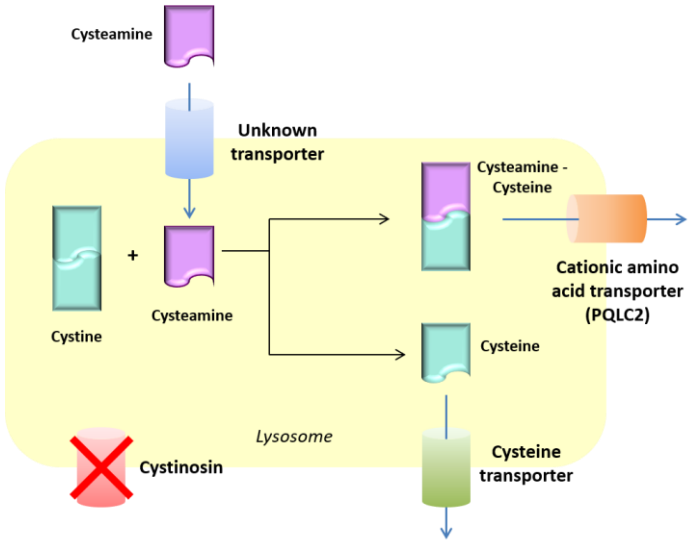

Figure 3. Mechanism of action of cysteamine in the lysosomes.

Oral cysteamine does not reach the cornea due to the lack of corneal vascularization. Therefore, topical ocular application of cysteamine is needed in order to treat ocular cystinosis symptoms. Safety and effectiveness of ocular cysteamine hydrochloride was demonstrated in the 1980s (16,47,48). However, ocular administration of cysteamine presents two problems. On the one hand, effectiveness relies on a steady cysteamine concentration on the ocular surface, so ocular instillation every hour during waking hours is needed in order to achieve a reduction in cystine crystals. On the other hand, cysteamine is prone to oxidation to its dimer at room temperature, cystamine, which has proved to not be effective in cystine depletion (49) (Figure 4).

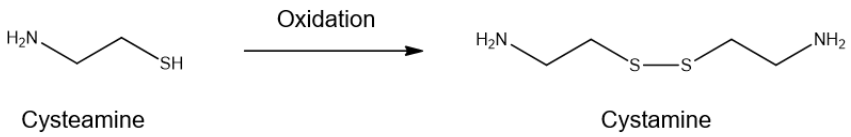

Figure 4. Oxidation of cysteamine to its dimer cystamine.

Cysteamine ocular formulations

To our knowledge, Cystaran® (Sigma-Tau Pharmaceuticals) was the first available commercial ophthalmic product for the treatment of corneal cystine crystals and it is only approved by the FDA (50). Although Cystaran® has proven to be effective in depleting the corneal cystine crystals, it needs to be instilled into the ocular surface at least 6-10 times per day to achieve

the maximum benefit, complicating patient's adherence to the treatment. Even with a high therapeutic compliance, this formulation is rapidly drained from the ocular surface since it is just a 0.44 % solution of cysteamine hydrochloride in saline with the preservative benzalkonium chloride (50,51). In this aspect, Cystadrops® (0.55 % cysteamine gel, Orphan Europe) enhances the dosage regimen by incorporating sodium carboxymethyl cellulose, which provides a high viscosity to the formulation and allows a dosage of just 4 times per day (52). Although it has obtained the European marketing authorization (53), it has no public financing in Spain (54).

Unfortunately, both commercial cysteamine eye drops are not available at present in most countries due to rare nature of the disease. Therefore, most patients depend on cysteamine ocular solutions prepared at the hospital pharmacies as pharmaceutical compounded formulations in order to gain access to cystinosis ocular treatment (55). These eye drops have been used since the 80's, even when no commercial formulation existed, and have been considered as a valid alternative (55). Moreover, nowadays, its relatively low cost of preparation compared to acquiring commercial solutions has led to some hospitals no approving their purchase due to economic reasons.

The topical ophthalmic cystinosis treatment manufactured at hospital pharmacy departments is a solution of 0.55 % cysteamine hydrochloride eye drops (56,57). However, this approach is limited by the short retention time in corneal surface and consequently the need of instillation every wakening hour to obtain a sustainable benefit (58).

Cysteamine delivery systems under investigation

Some studies have focused on the development of systems which will delay the delivery of cysteamine in order to minimise its frequency of administration. In order to achieve this, hydrogels with different types of polymers were developed, such as hydroxypropylmethyl cellulose (59), hydroxyethyl cellulose (60), carbomer 934 (60,61) and sodium hyaluronan (60,62), as well as cysteamine loaded contact lenses (63). Although they had characterised their formulations, they all lack *in vivo* studies to show the permanence of the gels on the

ocular surface, even when this is an important aspect as the purpose of the study itself is to extend the retention time of the cysteamine.

Cysteamine quantification

The analysis of compounds with thiol groups, as the cysteamine, has always been of extremely complication due to the susceptibility of this group to oxidation before or during its analysis and also because of the lack of a chromophore structure to its detection (64,65). Moreover, the low molecular weight of the cysteamine (77.15 g/mol) complicates its detection.

Some methods have been reported for the measurement of cysteamine. One of the first methods used is the iodometric titration (59,66), which is also used to determine the purity of the cysteamine hydrochloride commercial product. UV-vis spectrophotometry was also used for the determination of the cysteamine in the range of 211-240 nm. However, by this method both cysteamine and its oxidative product cystamine are quantified at the same time (63). In another method, a cystamine-phenylalanine conjugate is synthetized and then measured at 254 nm using a UV spectrophotometer. In this case, the process is quite long and complex (61). Gas spectrophotometry (67,68) was also carried out using pre-column derivatization to form N-alcoxy-carbonyl derivatives.

Reverse phase high performance liquid chromatography (RP-HPLC) systems were also performed for the quantification of cysteamine, but the lack of a chromophore forces to use a pre-column derivatization. Waters® AccQFluor Reagent (6-aminoquinolyl-N-hydrozysuccinimidyl carbamate, ACQ) is a pre-column derivatization reagent that is used for the analysis of amino acids and related compounds (69) and that has been used for the determination of cysteamine with no promising results (65). Another derivatization agent that has been used is 2-chloro-1-methylquinolinium tetrafluoroborate (CMQT), which reacts both with thiol groups and cysteamine, but presents the inconvenience that needs to be synthesized before each analysis (65,70). Another approach used to facilitate the quantification of cysteamine by RE-HPLC is using sodium 1-heptanesulfonate as an ion-pairing agent, which presents the advantage of simultaneously determine both cysteamine and cystamine (71).

Therefore, there is not a standardised method of quantification of cysteamine and most of the methods which were used are complex, not discriminating and/or not viable.

Stability of cysteamine formulations

The stability of a compounded formulation is defined as the amount of time during which a product maintains, within very specific limits, the properties and characteristics that it possessed at the time of manufacture, throughout storage, and during use (72). Stability studies determine how the quality of a drug varies over time under the influence of a number of factors and use this information to provide recommendations on its expiration date and storage conditions.

The instability of cysteamine formulations has been a constantly concern in the preparation at hospital pharmacies. In general, stability studies present relevant technical and economic challenges for hospital pharmacy departments, and in the case of cysteamine eye drops, most hospitals do not carry out them due to the difficulties of cysteamine quantification mentioned above (64,65).

However, the stability of cysteamine formulations manufactured at hospital departments is de high importance as the cysteamine itself is prone to oxidation boosted by oxygen and room temperature (49). In the case of the commercial eye drops, stability studies are required in order to obtain the pertinent authorisation. In this way, Cystaran® vials need to be stored in the freezer until usage and then after opening refrigerated for up to one week (50). In the case of Cystadrops®, it needs to be stored refrigerated before opening, but afterwards it could be kept at room temperature below 25 °C for seven days (73).

AGE-RELATED MACULAR DEGENERATION

Age-Related Macular Degeneration (AMD) is the leading cause of severe irreversible visual impairment among people over the age of 65 years old in developed countries. Based on a recent meta-analysis, global prevalence of any type of AMD within an age of 45-85 years old was 8.7 % in 2017 (74). It is expected to double its prevalence in the next few decades, with an estimate of 280 million people affected by 2040 (75,76).

AMD is classified based on disease progression (77). The hallmark of AMD is drusen, which are deposits of extracellular material between Bruch's membrane and retinal pigment epithelium. Early AMD is characterised by the presence of small or intermediate drusen and by mild retinal pigment epithelium (RPE) abnormalities. Intermediate AMD is characterised by multiple intermediate drusen or at least one large druse. Advanced AMD is defined by the presence of either geographic atrophy or choroidal neovascular maculopathy (78,79). Advanced AMD can be divided in two categories depending on whether choroidal neovascularization is present or not: non-neovascular, non-exudative or dry AMD, and neovascular, exudative or wet AMD. Choroidal neovascularisation refers to the abnormal growth of blood vessels in the choroid which leak into the retina through a break in the Bruch's membrane (78,80). The proliferation of abnormal blood vessels is stimulated by vascular endothelial growth factor (VEGF). Blood and protein leakage damage the photoreceptors in the macula, which ultimately produce loss of central visual acuity characterised by blind spots in the centre of the visual field. Advanced dry AMD is defined by geographic atrophy which results in a gradual degeneration of the cells of the retina that also causes a severe loss of vision (50,51).

Although 80 % of AMD patients present the non-neovascular form of the disease, the neovascular form is responsible for more than 90 % of severe vision loss cases related to AMD (79). The disease almost always begins as a non-neovascular form of AMD and it may progress to the neovascular form in one or both eyes (77).

AMD pathogenesis is not fully understood, although is considered to be a multifactorial interaction among metabolic, functional, genetic, and environmental factors (81,82). AMD is a degenerative disease which has aging as major risk factor. Other risk factors include smoking, dietary habits, obesity and environmental factors like being exposed to certain drugs (83–85). Moreover, AMD has a high genetic component, with a lot of genes involved, which has been estimated at 45-75 % (86). Genes related to AMD development are implicated in immune response and inflammation, metabolism and lipid transport, extracellular matrix and cell adhesion, angiogenesis and cellular survival and response to stress (87).

AMD treatment

Although dry AMD is the most prevalent type of AMD, nowadays no treatment to slow or reverse dry AMD progression has been approved (88). Most treatment research has focused on wet AMD since it is the one that causes most cases of severe vision loss (88). Moreover, wet AMD has a huge impact on patient quality of life and imposes substantial burdens on healthcare systems.

Management of wet AMD has significantly advanced in recent years. Some treatments have been tested for wet AMD in the past, such as laser photocoagulation and photodynamic eye therapy with verteporfin, but at present the standard treatment consists of the intravitreal injection of anti-VEGF antibodies (89).

Intravitreal anti-VEGF agents

Vascular endothelial growth factor comprises a family of five members in mammals: VEGF-A, VEGF-B, VEGF-C, VEGF-D and PlGF (placental growth factor). VEGF-A is the most important and potent stimulator of angiogenesis. It presents several isoforms with different biological activities, but VEGF-A_{165} is the predominant isoform and the most active in neovascularisation. VEGF factors stimulate cellular responses by binding to tyrosine kinase receptors (VEGFR). VEGF-A binds to VEGFR1 and VEGFR2, although is thought to produce the primarily pro-angiogenic activity by its binding to VEGFR2 (90).

The aim of intravitreal anti-VEGF antibodies is to inhibit angiogenesis by blocking free VEGF factor in the ocular environment, thereby preventing binding of VEGF-A to its receptors VEGFR-1 and VEGFR-2. Up to date, four anti-VEGF inhibitors have been widely used in clinical practice for the treatment of AMD: pegaptanib (withdrawn), bevacizumab, ranibizumab and aflibercept (Figure 5, Table 1). Pegaptanib (Macugen®, Pfizer) was the first anti-VEGF drug approved for wet AMD treatment by the FDA in 2004 (91) and the EMA in 2006 (92). It is a RNA aptamer that specifically binds to the VEGF-165 isoform (81). This medicine is now withdrawn from use in the European Union (92).

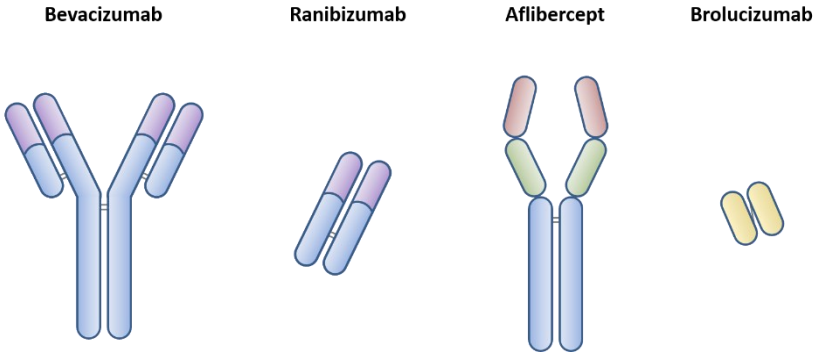

Figure 5. Representation of the antibody structure of bevacizumab, ranibizumab, aflibercept and brolucizumab.

Bevacizumab (Avastin®, Roche) is a recombinant humanised monoclonal IgG1 antibody developed for systemic administration. It is currently only approved for metastatic colorectal cancer, cervical/ovarian/fallopian tube cancers, glioblastoma, non-small cell lung cancer, and metastatic renal cell carcinoma (93). However, it is widely used off-label intravitreally to treat VEGF-mediated diseases due to its lower cost. In addition, the possibility of splitting up the vial in the pharmacy departments reduces the cost of the treatment in comparison with the other two drugs that do have the indication (ranibizumab and aflibercept) (94,95). For that reason, although bevacizumab is not authorised for the treatment of AMD, the European Court of Justice has justified its reimbursement by national healthcare insurances (96).

Ranibizumab (Lucentis®, Genentech-Roche/Novartis) was first approved by the FDA in 2006 (97) and the EMA in 2007 (98) based on the results of two clinical trials (ANCHOR and MARINE) (99,100). It is a recombinant humanised IgG1 monoclonal Fab fragment obtained from the same parent antibody as bevacizumab. It presents affinity for all subtypes of VEGF-A (101). Studies comparing bevacizumab and ranibizumab showed that visual acuity outcomes were similar between both anti-VEGF agents under several different dosing strategies (102).

Aflibercept (Eylea®, Bayer) was approved by the FDA in 2011 (103) and by the EMA in 2012 (104). It is a recombinant protein created by fusing the second Ig domain of human VEGFR1 with the third Ig domain of human VEGFR2, which is in turn fused to the constant region of human IgG1. It binds to VEGF-A, VEGF-B and PlGF (105). VIEW1 and VIEW2 clinical trials reported non-inferior outcomes in eyes treated with aflibercept against ranibizumab and

suggested that aflibercept could reduce the burden of monthly monitoring as it is use in bimonthly regimen (106).

Recently, a new anti-VEGF agent has been approved for the treatment of AMD, brolucizumab (Beovu®, Novartis), which received the marketing authorisation in July 2019 by the FDA (107) and in February 2020 by the EMA (108). Brolucizumab is a humanised monoclonal single chain Fv (scFv) antibody fragment with a molecular weight of 26 kDa which binds with high affinity to VEGF-A isoforms (109).

Table 1. Properties of anti-VEGF antibodies for AMD (108–110).

Property	Bevacizumab	Ranibizumab	Aflibercept	Brolucizumab
Class	Monoclonal antibody	Antibody fragment (Fab)	Fusion protein	Antibody fragment (scFv)
MW (kDa)	149	48	115	26
Clinical dose (mg)	1.25	0.5	2	6
Net charge	Negative	Negative	Slightly positive	-
Binding target	VEGF-A	VEGF-A	VEGF-A, VEGF-B, PIGF	VEGF-A
K_D for $VEGF_{165}$ (pM)	58	46	0.49	-

MW = molecular weight; K_D = equilibrium dissociation constant.

A systematic review found that intravitreal aflibercept, bevacizumab and ranibizumab have comparable effects on visual acuity and similar rates of adverse effects (113). However, some studies have reported a small benefit of aflibercept over the other two, but more research is needed to demonstrate the advantage of aflibercept (113). Compounded bevacizumab presents a cost-effectiveness advantage over the other two antibodies (113–115), but it involves safety concerns due to the compounding and using of a not intended intravitreal formulation.

Anti-VEGF antibodies are administered as single intravitreal injections of 1.25 mg/50 µL bevacizumab, 0.5 mg/50 µL ranibizumab (101), 2 mg/50 µL aflibercept (105) and 6 mg/50 µL brolucizumab (109). Treatment intervals are different for each drug, although they all are initiated with a predetermined interval until maximum visual acuity is achieved and/or are no signs of disease activity. Subsequently, after three months, monitoring and treatment

intervals should be determined by the ophthalmologist and should be based on disease activity. Initial treatment intervals are one injection per month for ranibizumab, aflibercept and brolucizumab. Aflibercept interval is then extended to two months or further (101,105). Brolucizumab injection interval can be extended to every two or three months depending on disease activity (109). Because bevacizumab has no marketed authorisation for intravitreal injection, there is no standard regimen, but the most practised schedule is an initial interval of one and a half months (116).

Despite the promising efficacy in improving the vision for AMD patients, intravitreal injections of anti-VEGF agents carry some complications. Ocular adverse effects following intravitreal injections of anti-VEGF antibodies include infectious endophthalmitis, intraocular inflammation, rhegmatogenous retinal detachment, intraocular pressure elevation and ocular haemorrhage (117–119). Although rates of significant ocular secondary effects are relatively low, they are devastating and sight-threatening complications that need to be addressed. Moreover, the necessity of repeated and long-term intravitreal injections increases the possibility of ocular adverse effects (117).

Systemic adverse effects have also been reported due to anti-VEGF levels detected in the systemic circulation following intravitreal anti-VEGF therapy, with the subsequently suppression of systemic VEGF levels (117). Several systemic adverse events caused by intravitreal anti-VEGF injection have been reported such as cardiovascular effects (thrombosis, haemorrhage, hypertension, proteinuria), cerebrovascular accidents, myocardial infarction, transient ischemic attacks, deep vein thrombosis, pulmonary embolism and thrombophlebitis. However, the incidence of these numerous adverse reactions is very low (120).

Anti-VEGF drug pharmacokinetics

Available pharmacokinetic data on intravitreally injected anti-VEGF antibodies is still limited despite being the standard treatment of AMD (121). Intravitreal pharmacokinetics faces several challenges, being the most remarkable the needing of extracting invasive vitreous samples in order to obtain direct pharmacokinetic data in the vitreous humour. Therefore,

some studies rely on aqueous humour or even serum samples drug concentration to estimate intravitreal pharmacokinetics (121).

Pharmacokinetics of intravitreally injected anti-VEGF antibodies has been studied in several animal models and in humans, finding remarkable interspecies differences (89). However, complete data is missing, particularly in humans, due to the complexity of performing this type of studies (121). Moreover, considerable differences have been seen among the different preclinical studies in the pharmacokinetic parameters calculated. A comprehensive review of all pharmacokinetic studies regarding intravitreal injection of anti-VEGF antibodies have been compiled elsewhere (121). Thus, this thesis has focused on the summary of all these works in order to provide a general information regarding vitreous humour, aqueous humour and serum half-lives in different species of the three main intravitreal anti-VEGF antibodies.

Pharmacokinetic studies have shown that all intravitreal anti-VEGF antibodies leave the ocular tissues in order to reach the blood circulation (122). The passage of the intravitreal drugs to the systemic circulation is conditioned by their vitreous humour distribution, mainly regulated by diffusion and convection, and their ocular clearance. Diffusion through the vitreous humour depends on its intrinsic characteristics and the physiochemical properties of the drug. The vitreous humour is a transparent gel-like structure composed of hyaluronic acid, collagen and water (98 %). The diffusion of large molecular-weight molecules such as the anti-VEGF antibodies can be limited by the vitreous meshwork (123). Moreover, the vitreous humour is negatively charged mainly through the hyaluronic acid (124,125), so cationic molecules could show restrictive diffusion due to electrostatically interactions (126,127), such as aflibercept, which is considered to have a mild positive charge (112). On the contrary, ranibizumab and bevacizumab are negatively charge compounds (111).

Surgical eye procedures can have an impact on drug pharmacokinetics. The effect of vitrectomy (removal of the vitreous humour) has been studied in animal models obtaining an intravitreal drug half-life reduction due to increased drug diffusion (128), including the anti-VEGF antibodies (129–131). However, the relevance of these differences regarding dosing schedules is not clear (132,133). Moreover, this outcome is higher when the vitrectomy is performed in combination with a lensectomy (removal of the lens) (128).

Elimination from the ocular compartments to the systemic blood flow can follow two different routes of elimination: anterior and posterior clearance (Figure 6). Anterior route implies the entry of the drug to the aqueous humour chamber in which they are removed by the trabecular and uveoscleral outflow (134). This route of elimination is accessible to all drugs, particularly to hydrophilic and large molecules (135–138). Posterior clearance comprises the permeation through the retina and the subsequently clearance by the choroidal blood flow. Retina permeation implies that this route is mainly accessible to small and lipophilic compounds since they can easily cross the retina (139). Various studies have shown that anti-VEGF drugs are mainly cleared by the anterior route (140–144), being the impact of the posterior elimination very small (145–147).

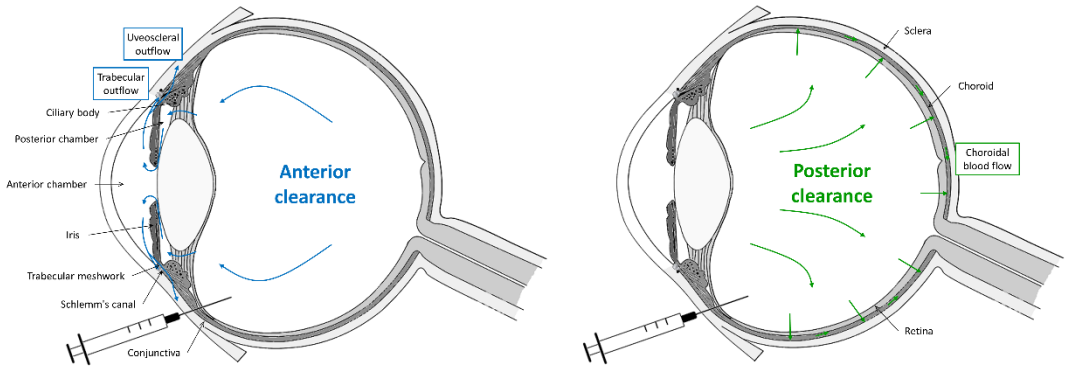

Figure 6. Schematic representation of the anterior and posterior clearance from the vitreous humour.

Anti-VEGF drug delivery systems under investigation

Clinically used intravitreal anti-VEGF antibodies are simple solutions with excipients. For that reason, patients require to undergo intravitreal injections every one or two months. Minimising repeated intravitreal injections of anti-VEGF agents will decrease the risk of adverse effects while decreasing the economic burden of AMD (148). Because of that, the development of drug delivery systems is very attractive although it faces great challenges.

Although there is no doubt about the invaluable benefits that extended release delivery systems of anti-VEGF antibodies would provide, until date none have been reached a stage of development enough to achieve the commercial state (149). Due to the high effort that the

scientific community has been recently made with the aim of developing prolonged release delivery systems containing anti-VEGF agents, an extensive review regarding the anti-VEGF drug delivery systems under investigation up to date has been put up.

As a brief overview, drug delivery systems for anti-VEGF drugs include systems as hydrogels, liposomes, microparticles, nanoparticles or implants. Hydrogels can be injected into the vitreous body through a small needle. In situ thermosensitive hydrogels are non-viscous upon injection and after injected into the vitreous, they form a gel-like structure. However, diffusion through the gel structure is relatively fast, limiting is usefulness as long release formulations. Both microparticles and nanoparticles have been tested as intravitreal drug delivery systems. Microparticles are larger in size, can afford higher loadings and could have extended release times. However, they can lead to blurred vision due to light scattering effects inside the vitreous body. On the contrary, nanoparticles present the advantage of potential retinal penetration. Both present burst release, which may be overcome by including them in hydrogels. In comparison with other systems, implants present the longest release times, as normally they release the drug from several weeks to months and permit high drug loading. They are the most promising prolonged release systems at present, although there are still in early stages of development for anti-VEGF antibodies.

CONCLUDING REMARKS

Treatment of ocular pathologies requires using specialised routes of administration due to the high complexity of the eye, which is a very protected and isolated organ. Consequently, ocular treatments present great challenges, because on the one hand the treatment of ocular surface diseases implies a high clearance with low drug bioavailability. On the other hand, posterior segment diseases require repetitive invasive injections to overcome various barriers to reach the target site. These difficulties are exemplified in the treatment of ocular cystinosis and age-related macular degeneration, respectively, the two pathologies in which this thesis is focused. In such cases, the study of pharmacokinetics and dosage forms is the critical importance to enhance the current available treatments due to the necessity of addressing these problems in a very specific way.

REFERENCES

1. Vision impairment and blindness [Internet]. World Health Organization. [cited 2020 Jan 31]. Available from: https://www.who.int/news-room/fact-sheets/detail/blindness-and-visual-impairment
2. Boddu SHS, Menees AL, Ray A, Mitra AK. A brief overview of ocular anatomy and physiology. In: Treatise on Ocular Drug Delivery. Bentham Science Publishers; 2013.
3. Stjernschantz J, Astin M. Anatomy and physiology of the eye. Physiological aspects of ocular drug therapy. In: Biopharmaceutics of Ocular Drug Delivery. CRC Press; 2019.
4. Addo E, Bamiro OA, Siwale R. Anatomy of the eye and common diseases affecting the eye. In: Ocular Drug Delivery: Advances, Challenges and Applications. Springer; 2016.
5. Reddy IK, Ganesan MG. Ocular therapeutics and drug delivery: an overview. In: Ocular Therapeutics and Drug Delivery. CRC Press; 1995.
6. Fernández-Ferreiro A, González-Barcia M, Otero Espinar FJ, Blanco Méndez J, Lamas MJ. Retos en la formulación magistral oftálmica. Farmacia Hospitalaria. 2016 Feb;40(1):1–2.
7. Fernández-Ferreiro A. Formulación magistral oftálmica antiinfecciosa. Sociedad Española de Farmacia Hospitalaria; 2019.
8. Thassu D, Holt K, Chader GJ. Nanoparticle-based therapeutics: an overview. In: Ocular Drug Delivery Systems: Barriers and Application of Nanoparticulate Systems. CRC Press; 2012.
9. Bamiro OA, Ubale RV, Addo RT. Background of ocular drug delivery. In: Ocular Drug Delivery: Advances, Challenges and Applications. Springer; 2016.
10. Bennet L. Drug delivery to specific compartments of the eye. In: Ocular Drug Delivery: Advances, Challenges and Applications. Springer; 2016.
11. Kwatra D, Vadlapatla RK, Khurana V, Pal D, Mitra AK. Routes of ocular drug delivery - conventional vs novel routes. In: Treatise on Ocular Drug Delivery. Bentham Science Publishers; 2013.
12. Renukuntla J, Shah SJ, Patel M, Vadlapudi AD, Mitra AK. Drug delivery to anterior segment of the eye. In: Treatise on Ocular Drug Delivery. Bentham Science Publishers; 2013.
13. Urtti A, Salminen L. Minimizing systemic absorption of topically administered ophthalmic drugs. Surv Ophthalmol. 1993 Jun;37(6):435–56.
14. Gaudana R, Ananthula HK, Parenky A, Mitra AK. Ocular drug delivery. AAPS J. 2010 Sep;12(3):348–60.
15. Agrahari V, Mandal A, Agrahari V, Trinh HM, Joseph M, Ray A, et al. A comprehensive insight on ocular pharmacokinetics. Drug Deliv Transl Res. 2016;6(6):735–54.
16. Kaiser-Kupfer MI, Gazzo MA, Datiles MB, Caruso RC, Kuehl EM, Gahl WA. A randomized placebo-controlled trial of cysteamine eye drops in nephropathic cystinosis. Arch Ophthalmol. 1990 May;108(5):689–93.

17. Kaiser-Kupfer MI, Fujikawa L, Kuwabara T, Jain S, Gahl WA. Removal of corneal crystals by topical cysteamine in nephropathic cystinosis. N Engl J Med. 1987 Mar 26;316(13):775–9.

18. MacDonald IM, Noel LP, Mintsioulis G, Clarke WN. The effect of topical cysteamine drops on reducing crystal formation within the cornea of patients affected by nephropathic cystinosis. J Pediatr Ophthalmol Strabismus. 1990 Oct;27(5):272–4.

19. Geroski DH, Edelhauser HF. Drug delivery for posterior segment eye disease. Invest Ophthalmol Vis Sci. 2000 Apr;41(5):961–4.

20. López-Cabezas C, Muner DS, Massa MR, Mensa Pueyo JM. Antibiotics in endophthalmitis: microbiological and pharmacokinetic considerations. Curr Clin Pharmacol. 2010 Feb;5(1):47–54.

21. Del Amo EM, Rimpelä A-K, Heikkinen E, Kari OK, Ramsay E, Lajunen T, et al. Pharmacokinetic aspects of retinal drug delivery. Prog Retin Eye Res. 2017 Mar;57:134–85.

22. Gaudana R, Ananthula HK, Parenky A, Mitra AK. Ocular drug delivery. AAPS J. 2010 Sep;12(3):348–60.

23. Vadlapudi AD, CholKAr K, Dasari SR, Mitra AK. Ocular drug delivery. Drug Delivery Burlington MA: Jones & Bartlett Learning. 2015;219–263.

24. Thrimawithana TR, Young S, Bunt CR, Green C, Alany RG. Drug delivery to the posterior segment of the eye. Drug Discov Today. 2011 Mar;16(5–6):270–7.

25. Mitra AK, Anand BS, Duvvuri S. Drug delivery to the eye. New York: Academic Press. 2006;307–51.

26. Gaudana RJ, Barot M, Patel A, Khurana V, Mitra AK. Barriers for posterior segment ocular drug delivery. In: Treatise on Ocular Drug Delivery. Bentham Science Publishers; 2013.

27. Marsh DA. Selection of Drug Delivery Approaches for the Back of the Eye: Opportunities and Unmet Needs. In: Drug Product Development for the Back of the Eye. Springer Science & Business Media; 2011. p. 125–58.

28. Shahar J, Avery RL, Heilweil G, Barak A, Zemel E, Lewis GP, et al. Electrophysiologic and retinal penetration studies following intravitreal injection of bevacizumab (Avastin). Retina (Philadelphia, Pa). 2006 Mar;26(3):262–9.

29. WHO | Priority eye diseases [Internet]. World Health Organization. [cited 2019 Aug 26]. Available from: http://www.who.int/blindness/causes/priority/en/

30. Gahl WA, Thoene JG, Schneider JA. Cystinosis. New England Journal of Medicine. 2002 Jul 11;347(2):111–21.

31. Town M, Jean G, Cherqui S, Attard M, Forestier L, Whitmore SA, et al. A novel gene encoding an integral membrane protein is mutated in nephropathic cystinosis. Nat Genet. 1998 Apr;18(4):319–24.

32. Gahl WA, Bashan N, Tietze F, Bernardini I, Schulman JD. Cystine transport is defective in isolated leukocyte lysosomes from patients with cystinosis. Science. 1982 Sep 24;217(4566):1263–5.

33. Gahl WA, Tietze F, Bashan N, Steinherz R, Schulman JD. Defective cystine exodus from isolated lysosome-rich fractions of cystinotic leucocytes. J Biol Chem. 1982 Aug 25;257(16):9570–5.

34. Jonas AJ, Smith ML, Schneider JA. ATP-dependent lysosomal cystine efflux is defective in cystinosis. J Biol Chem. 1982 Nov 25;257(22):13185–8.

35. Linkage of the gene for cystinosis to markers on the short arm of chromosome 17. The Cystinosis Collaborative Research Group. Nat Genet. 1995 Jun;10(2):246–8.

36. Goodyer P. The History of Cystinosis: Lessons for Clinical Management. International Journal of Nephrology. 2011;2011:1–6.

37. Burki E. Ueber die Cystinkrankheit im Kleinkindesalter unter besonderer Berücksichtigung des Augenbefundes [About the Cystinosis in infancy with special reference to eye findings]. Ophthalmologica. 1941;101:331–342.

38. Gahl WA, Kuehl EM, Iwata F, Lindblad A, Kaiser-Kupfer MI. Corneal crystals in nephropathic cystinosis: natural history and treatment with cysteamine eyedrops. Mol Genet Metab. 2000 Oct;71(1–2):100–20.

39. Shams F, Livingstone I, Oladiwura D, Ramaesh K. Treatment of corneal cystine crystal accumulation in patients with cystinosis. Clin Ophthalmol. 2014 Oct 10;8:2077–84.

40. Gahl WA, Thoene JG, Schneider JA. Cystinosis. N Engl J Med. 2002 Jul 11;347(2):111–21.

41. Elmonem MA, Veys KR, Soliman NA, van Dyck M, van den Heuvel LP, Levtchenko E. Cystinosis: a review. Orphanet J Rare Dis. 2016;11:47.

42. Pubchem. Cysteamine (C2H7NS) [Internet]. [cited 2017 Jun 22]. Available from: https://pubchem.ncbi.nlm.nih.gov/compound/2-Aminoethanethiol

43. Thoene JG, Oshima RG, Crawhall JC, Olson DL, Schneider JA. Cystinosis. Intracellular cystine depletion by aminothiols in vitro and in vivo. J Clin Invest. 1976 Jul;58(1):180–9.

44. Brodin-Sartorius A, Tête M-J, Niaudet P, Antignac C, Guest G, Ottolenghi C, et al. Cysteamine therapy delays the progression of nephropathic cystinosis in late adolescents and adults. Kidney Int. 2012 Jan;81(2):179–89.

45. Martine Besouw RM. Cysteamine: An old drug with new potential. Drug Discov Today. 2013;18(15).

46. Jézégou A, Llinares E, Anne C, Kieffer-Jaquinod S, O'Regan S, Aupetit J, et al. Heptahelical protein PQLC2 is a lysosomal cationic amino acid exporter underlying the action of cysteamine in cystinosis therapy. Proc Natl Acad Sci U S A. 2012 Dec 11;109(50):E3434–43.

47. Kaiser-Kupfer MI, Caruso RC, Minkler DS, Gahl WA. Long-term ocular manifestations in nephropathic cystinosis. Arch Ophthalmol. 1986 May;104(5):706–11.

48. Cysteamine Eye Drops to Treat Corneal Crystals in Cystinosis. Clinical Trial. [Internet]. Clinicaltrials.gov (A service of the U.S. National Institutes of Health). [cited 2016 May 6]. Available from: https://clinicaltrials.gov

49. Iwata F, Kuehl EM, Reed GF, McCain LM, Gahl WA, Kaiser-Kupfer MI. A randomized clinical trial of topical cysteamine disulfide (cystamine) versus free thiol (cysteamine) in the treatment of corneal cystine crystals in cystinosis. Mol Genet Metab. 1998 Aug;64(4):237–42.

50. Food and Drug Administration. Cystaran®. Prescribing information [Internet]. 2016 [cited 2016 May 3]. Available from: www.sigmatau.com

51. Veys KR, Elmonem MA, Arcolino FO, van den Heuvel L, Levtchenko E. Nephropathic cystinosis: an update. Curr Opin Pediatr. 2017 Jan 18;

52. Liang H, Labbé A, Le Mouhaër J, Plisson C, Baudouin C. A New Viscous Cysteamine Eye Drops Treatment for Ophthalmic Cystinosis: An Open-Label Randomized Comparative Phase III Pivotal Study. Invest Ophthalmol Vis Sci. 2017 Apr 1;58(4):2275–83.

53. European Medicines Agency. CHMP summary of positive opinion for Cystadrops [Internet]. 2017 [cited 2017 Feb 1]. Available from: http://www.ema.europa.eu/ema/index.jsp?curl=pages/medicines/human/medicines/003769/smops/Positive/human_smop_001034.jsp&mid=WC0b01ac058001d127

54. García-Hernández. Informe de Posicionamiento Terapéutico de mercaptamina clorhidrato (Cystadrops®) en el tratamiento del depósito de cristales de cistina corneales producidos en cistinosis [Internet]. 2019 [cited 2020 Mar 20]. Available from: https://www.aemps.gob.es/medicamentos-de-uso-humano/informes-de-posicionamiento-terapeutico/

55. Reda A, Van Schepdael A, Adams E, Paul P, Devolder D, Elmonem MA, et al. Effect of Storage Conditions on Stability of Ophthalmological Compounded Cysteamine Eye Drops. JIMD Rep. 2017 Dec 7;42:47–51.

56. National Eye Institute. Cysteamine Eye Drops to Treat Corneal Crystals in Cystinosis. Clinical Trial. [Internet]. 2016 May [cited 2016 May 6]. Available from: https://clinicaltrials.gov

57. Kaiser-Kupfer MI, Gazzo MA, Datiles MB, Caruso RC, Kuehl EM, Gahl WA. A randomized placebo-controlled trial of cysteamine eye drops in nephropathic cystinosis. Arch Ophthalmol. 1990 May;108(5):689–93.

58. Ribeiro MVMR, Ribeiro LEF, Ribeiro ÊAN, Ferreira CV, Barbosa FT, Ribeiro MVMR, et al. Adherence assessment of eye drops in patients with glaucoma using 8 item Morisky Score: a cross sectional study. Revista Brasileira de Oftalmologia. 2016 Dec;75(6):432–7.

59. Bozdağ S, Gümüş K, Gümüş O, Unlü N. Formulation and in vitro evaluation of cysteamine hydrochloride viscous solutions for the treatment of corneal cystinosis. Eur J Pharm Biopharm. 2008 Sep;70(1):260–9.

60. McKenzie B, Kay G, Matthews KH, Knott R, Cairns D. Preformulation of cysteamine gels for treatment of the ophthalmic complications in cystinosis. Int J Pharm. 2016 Dec 30;515(1–2):575–82.

61. Buchan B, Kay G, Heneghan A, Matthews KH, Cairns D. Gel formulations for treatment of the ophthalmic complications in cystinosis. Int J Pharm. 2010 Jun 15;392(1–2):192–7.

62. McKenzie B, Kay G, Matthews KH, Knott RM, Cairns D. The hen's egg chorioallantoic membrane (HET-CAM) test to predict the ophthalmic irritation potential of a cysteamine-containing gel: Quantification using Photoshop® and ImageJ. Int J Pharm. 2015 Jul 25;490(1–2):1–8.

63. Hsu K-H, Fentzke RC, Chauhan A. Feasibility of corneal drug delivery of cysteamine using vitamin E modified silicone hydrogel contact lenses. Eur J Pharm Biopharm. 2013 Nov;85(3 Pt A):531–40.

64. Guan X, Hoffman B, Dwivedi C, Matthees DP. A simultaneous liquid chromatography/mass spectrometric assay of glutathione, cysteine, homocysteine and their disulfides in biological samples. J Pharm Biomed Anal. 2003 Feb 26;31(2):251–61.

65. Lawal B. Development of a cysteamine in situ gelling system for the treatment of corneal crystals in cystinosis [Internet]. 2008 [cited 2016 Feb 3]. Available from: https://cystinosis.org/images/research/updates/CRN_Research_UpdateB.pdf

66. Chanakira A, Chikwana E, Peyton DH, Simoyi RH. Oxyhalogen-sulfur chemistry kinetics and mechanism of the oxidation of cysteamine by acidic iodate and iodine. Can J Chem. 2006 Jan 1;84(1):49–57.

67. Kataoka H, Tanaka H, Makita M. Determination of total cysteamine in urine and plasma samples by gas chromatography with flame photometric detection. J Chromatogr B, Biomed Appl. 1994 Jul 1;657(1):9–13.

68. Kataoka H, Imamura Y, Tanaka H, Makita M. Determination of cysteamine and cystamine by gas chromatography with flame photometric detection. J Pharm Biomed Anal. 1993 Oct;11(10):963–9.

69. Cohen SA, Michaud DP. Synthesis of a fluorescent derivatizing reagent, 6-aminoquinolyl-N-hydroxysuccinimidyl carbamate, and its application for the analysis of hydrolysate amino acids via high-performance liquid chromatography. Anal Biochem. 1993 Jun;211(2):279–87.

70. Bald E, Chwatko G, Głowacki R, Kuśmierek K. Analysis of plasma thiols by high-performance liquid chromatography with ultraviolet detection. J Chromatogr A. 2004 Apr 2;1032(1–2):109–15.

71. Kim Y, Na DH. Simultaneous Determination of Cysteamine and Cystamine in Cosmetics by Ion-Pairing Reversed-Phase High-Performance Liquid Chromatography. Toxicol Res. 2019 Apr;35(2):161–5.

72. United States Pharmacopeia and National Formulary (USP 37-NF 32). 2013.

73. Cystadrops® 0,55 eye drops solution. Summary of product characteristics. 2015.

74. Jonas JB, Cheung CMG, Panda-Jonas S. Updates on the Epidemiology of Age-Related Macular Degeneration. Asia Pac J Ophthalmol (Phila). 2017 Dec;6(6):493–7.

75. Pascolini D, Mariotti SP. Global estimates of visual impairment: 2010. Br J Ophthalmol. 2012 May;96(5):614–8.

76. Wong WL, Su X, Li X, Cheung CMG, Klein R, Cheng C-Y, et al. Global prevalence of age-related macular degeneration and disease burden projection for 2020 and 2040: a systematic review and meta-analysis. Lancet Glob Health. 2014 Feb;2(2):e106-116.

77. Ferris FL, Wilkinson CP, Bird A, Chakravarthy U, Chew E, Csaky K, et al. Clinical classification of age-related macular degeneration. Ophthalmology. 2013 Apr;120(4):844–51.

78. Maroñas O, García-Quintanilla L, Luaces-Rodríguez A, Fernández-Ferreiro A, Latorre-Pellicer A, Abraldes MJ, et al. Anti-VEGF treatment and response in Age-related Macular Degeneration: Disease´s susceptibility, pharmacogenetics and pharmacokinetics. Curr Med Chem. 2019 10;

79. American Academy of Ophthalmology Retina/Vitreous Panel. Preferred Practice Pattern®Guidelines. Age-Related Macular Degeneration [Internet]. American Academy of Ophthalmology; 2015. Available from: www.aao.org/ppp

80. Information NC for B, Pike USNL of M 8600 R, MD B, Usa 20894. Age-related macular degeneration (AMD): Overview [Internet]. Institute for Quality and Efficiency in Health Care (IQWiG); 2018 [cited 2020 Jan 7]. Available from: https://www.ncbi.nlm.nih.gov/books/NBK315804/

81. Al-Zamil WM, Yassin SA. Recent developments in age-related macular degeneration: a review. Clin Interv Aging. 2017;12:1313–30.

82. Rohrer B, Frazer-Abel A, Leonard A, Ratnapriya R, Ward T, Pietraszkiewicz A, et al. Association of age-related macular degeneration with complement activation products, smoking, and single nucleotide polymorphisms in South Carolinians of European and African descent. Mol Vis. 2019;25:79–92.

83. Haddad S, Chen CA, Santangelo SL, Seddon JM. The genetics of age-related macular degeneration: a review of progress to date. Surv Ophthalmol. 2006 Aug;51(4):316–63.

84. Klein R, Cruickshanks KJ, Nash SD, Krantz EM, Nieto FJ, Huang GH, et al. The prevalence of age-related macular degeneration and associated risk factors. Arch Ophthalmol. 2010 Jun;128(6):750–8.

85. Sobrin L, Seddon JM. Nature and nurture- genes and environment- predict onset and progression of macular degeneration. Prog Retin Eye Res. 2014 May;40:1–15.

86. Seddon JM, Cote J, Page WF, Aggen SH, Neale MC. The US twin study of age-related macular degeneration: relative roles of genetic and environmental influences. Arch Ophthalmol. 2005 Mar;123(3):321–7.

87. Fritsche LG, Fariss RN, Stambolian D, Abecasis GR, Curcio CA, Swaroop A. Age-related macular degeneration: genetics and biology coming together. Annu Rev Genomics Hum Genet. 2014;15:151–71.

88. Gil-Martínez M, Santos-Ramos P, Fernández-Rodríguez M, Abraldes MJ, Rodríguez-Cid MJ, Santiago-Varela M, et al. Pharmacological advances in the treatment of age-related macular degeneration. Curr Med Chem. 2019 26;

89. Fogli S, Del Re M, Rofi E, Posarelli C, Figus M, Danesi R. Clinical pharmacology of intravitreal anti-VEGF drugs. Eye (Lond). 2018;32(6):1010–20.

90. Melincovici CS, Boşca AB, Şuşman S, Mărginean M, Mihu C, Istrate M, et al. Vascular endothelial growth factor (VEGF) - key factor in normal and pathological angiogenesis. Rom J Morphol Embryol. 2018;59(2):455–67.

91. Drug Approval Package: Macugen (Pegaptanib Sodium) [Internet]. [cited 2019 Sep 23]. Available from: https://www.accessdata.fda.gov/drugsatfda_docs/nda/2004/21-756_Macugen.cfm

92. Macugen [Internet]. European Medicines Agency. 2018 [cited 2019 Sep 23]. Available from: https://www.ema.europa.eu/en/medicines/human/EPAR/macugen

93. Avastin: European Public Assessment Report - Product Information [Internet]. European Medicines Agency. 2018 [cited 2020 Jan 9]. Available from: https://www.ema.europa.eu/en/medicines/human/EPAR/avastin

94. Empeslidis T, Storey M, Giannopoulos T, Konidaris V, Tranos PG, Panagiotou ES, et al. How Successful is Switching from Bevacizumab or Ranibizumab to Aflibercept in Age-Related Macular Degeneration? A Systematic Overview. Adv Ther. 2019 May 17;

95. Pershing S, Talwar N, Armenti ST, Grubbs J, Rosenthal JM, Dedania VS, et al. Use of Bevacizumab and Ranibizumab for Wet Age-Related Macular Degeneration: Influence of CATT Results and Introduction of Aflibercept. Am J Ophthalmol. 2019 May 14;

96. Reimbursement by a national healthcare insurance system of a medicinal product for a use not covered by its marketing authorisation (off-label use) [Internet]. 2018. Available from: http://curia.europa.eu/juris/document/document.jsf?docid=207947&text=&dir=&doclang=EN&part=1&occ=first&mode=DOC&pageIndex=0&cid=137655

97. Drug Approval Package: Lucentis (Ranibizumab) [Internet]. [cited 2020 Jan 9]. Available from: https://www.accessdata.fda.gov/drugsatfda_docs/nda/2006/125156s0000_LucentisTOC.cfm

98. Lucentis [Internet]. European Medicines Agency. 2018 [cited 2020 Jan 9]. Available from: https://www.ema.europa.eu/en/medicines/human/EPAR/lucentis

99. Brown DM, Michels M, Kaiser PK, Heier JS, Sy JP, Ianchulev T, et al. Ranibizumab versus verteporfin photodynamic therapy for neovascular age-related macular degeneration: Two-year results of the ANCHOR study. Ophthalmology. 2009 Jan;116(1):57-65.e5.

100. Rosenfeld PJ, Brown DM, Heier JS, Boyer DS, Kaiser PK, Chung CY, et al. Ranibizumab for neovascular age-related macular degeneration. N Engl J Med. 2006 Oct 5;355(14):1419–31.

101. Lucentis: European Public Assessment Report - Product Information [Internet]. European Medicines Agency. 2018 [cited 2020 Jan 9]. Available from: https://www.ema.europa.eu/en/medicines/human/EPAR/lucentis

102. Comparison of Age-related Macular Degeneration Treatments Trials (CATT) Research Group, Maguire MG, Martin DF, Ying G-S, Jaffe GJ, Daniel E, et al. Five-Year Outcomes with Anti-Vascular Endothelial Growth Factor Treatment of Neovascular Age-Related Macular Degeneration: The Comparison of Age-Related Macular Degeneration Treatments Trials. Ophthalmology. 2016;123(8):1751–61.

103. Drug Approval Package: Eylea (Aflibercept) [Internet]. [cited 2020 Jan 9]. Available from: https://www.accessdata.fda.gov/drugsatfda_docs/nda/2011/125387s0000TOC.cfm

104. Eylea [Internet]. European Medicines Agency. 2018 [cited 2020 Jan 9]. Available from: https://www.ema.europa.eu/en/medicines/human/EPAR/eylea

105. Eylea: European Public Assessment Report - Product Information [Internet]. European Medicines Agency. 2018 [cited 2020 Jan 9]. Available from: https://www.ema.europa.eu/en/medicines/human/EPAR/eylea

106. Heier JS, Brown DM, Chong V, Korobelnik J-F, Kaiser PK, Nguyen QD, et al. Intravitreal aflibercept (VEGF trap-eye) in wet age-related macular degeneration. Ophthalmology. 2012 Dec;119(12):2537–48.

107. Drug Approval Package: Beovu (brolucizumab-dbll) [Internet]. [cited 2020 Mar 19]. Available from: https://www.accessdata.fda.gov/drugsatfda_docs/nda/2019/761125_Orig1_toc.cfm

108. Beovu [Internet]. European Medicines Agency. 2019 [cited 2020 Mar 19]. Available from: https://www.ema.europa.eu/en/medicines/human/EPAR/beovu

109. Beovu: European Public Assessment Report - Product Information [Internet]. European Medicines Agency. 2019 [cited 2020 Mar 19]. Available from: https://www.ema.europa.eu/en/medicines/human/EPAR/beovu

110. Papadopoulos N, Martin J, Ruan Q, Rafique A, Rosconi MP, Shi E, et al. Binding and neutralization of vascular endothelial growth factor (VEGF) and related ligands by VEGF Trap, ranibizumab and bevacizumab. Angiogenesis. 2012 Jun;15(2):171–85.

111. Li SK, Liddell MR, Wen H. Effective electrophoretic mobilities and charges of anti-VEGF proteins determined by capillary zone electrophoresis. J Pharm Biomed Anal. 2011 Jun 1;55(3):603–7.

112. Holash J, Davis S, Papadopoulos N, Croll SD, Ho L, Russell M, et al. VEGF-Trap: a VEGF blocker with potent antitumor effects. Proc Natl Acad Sci USA. 2002 Aug 20;99(17):11393–8.

113. Low A, Kansagara D, Freeman M, Fu R, Bhavsar K, Faridi A, et al. Comparative Clinical and Economic Effectiveness of Anti-vascular Endothelial Growth Factor Agents [Internet]. Washington (DC): Department of Veterans Affairs (US); 2017 [cited 2018 May 15]. (VA Evidence-based Synthesis Program Reports). Available from: http://www.ncbi.nlm.nih.gov/books/NBK476461/

114. Patel JJ, Mendes MAS, Bounthavong M, Christopher MLD, Boggie D, Morreale AP. Cost-utility analysis of bevacizumab versus ranibizumab in neovascular age-related macular degeneration using a Markov model. J Eval Clin Pract. 2012 Apr;18(2):247–55.

115. Stein JD, Newman-Casey PA, Mrinalini T, Lee PP, Hutton DW. Cost-effectiveness of bevacizumab and ranibizumab for newly diagnosed neovascular macular degeneration. Ophthalmology. 2014 Apr;121(4):936–45.

116. Jyothi S, Chowdhury H, Elagouz M, Sivaprasad S. Intravitreal bevacizumab (Avastin) for age-related macular degeneration: a critical analysis of literature. Eye (Lond). 2010 May;24(5):816–24.

117. Falavarjani KG, Nguyen QD. Adverse events and complications associated with intravitreal injection of anti-VEGF agents: a review of literature. Eye (Lond). 2013 Jul;27(7):787–94.

118. Williams D, Argáez C. Acute, Sustained, Intraocular Pressure increases following Anti-Vascular Endothelial Growth Factor Treatment for Retinal Conditions: A Review of Clinical Evidence and Guidelines [Internet]. Ottawa (ON): Canadian Agency for Drugs and Technologies in Health; 2019 [cited 2020 Jan 15]. (CADTH Rapid Response Reports). Available from: http://www.ncbi.nlm.nih.gov/books/NBK545133/

119. Bracha P, Moore NA, Ciulla TA, WuDunn D, Cantor LB. The acute and chronic effects of intravitreal anti-vascular endothelial growth factor injections on intraocular pressure: A review. Surv Ophthalmol. 2018 Jun;63(3):281–95.

120. Semeraro F, Morescalchi F, Parmeggiani F, Arcidiacono B, Costagliola C. Systemic adverse drug reactions secondary to anti-VEGF intravitreal injection in patients with neovascular age-related macular degeneration. Curr Vasc Pharmacol. 2011 Sep;9(5):629–46.

121. García-Quintanilla L, Luaces-Rodríguez A, Gil-Martínez M, Mondelo-García C, Maroñas O, Mangas-Sanjuan V, et al. Pharmacokinetics of Intravitreal Anti-VEGF Drugs in Age-Related Macular Degeneration. Pharmaceutics. 2019 Jul 31;11(8).

122. Semeraro F, Morescalchi F, Duse S, Gambicorti E, Cancarini A, Costagliola C. Pharmacokinetic and Pharmacodynamic Properties of Anti-VEGF Drugs After Intravitreal Injection. Curr Drug Metab. 2015;16(7):572–84.

123. Laude A, Tan LE, Wilson CG, Lascaratos G, Elashry M, Aslam T, et al. Intravitreal therapy for neovascular age-related macular degeneration and inter-individual variations in vitreous pharmacokinetics. Prog Retin Eye Res. 2010 Nov;29(6):466–75.

124. Lee B, Litt M, Buchsbaum G. Rheology of the vitreous body: part 3. Concentration of electrolytes, collagen and hyaluronic acid. Biorheology. 1994 Aug;31(4):339–51.

125. Xu Q, Boylan NJ, Suk JS, Wang Y-Y, Nance EA, Yang J-C, et al. Nanoparticle diffusion in, and microrheology of, the bovine vitreous ex vivo. J Control Release. 2013 Apr 10;167(1):76–84.

126. Xu Q, Boylan NJ, Suk JS, Wang Y-Y, Nance EA, Yang J-C, et al. Nanoparticle diffusion in, and microrheology of, the bovine vitreous ex vivo. J Control Release. 2013 Apr 10;167(1):76–84.

127. Käsdorf BT, Arends F, Lieleg O. Diffusion Regulation in the Vitreous Humor. Biophysical Journal. 2015 Nov 17;109(10):2171–81.

128. Edington M, Connolly J, Chong NV. Pharmacokinetics of intravitreal anti-VEGF drugs in vitrectomized versus non-vitrectomized eyes. Expert Opin Drug Metab Toxicol. 2017 Dec;13(12):1217–24.

129. Christoforidis JB, Williams MM, Wang J, Jiang A, Pratt C, Abdel-Rasoul M, et al. Anatomic and pharmacokinetic properties of intravitreal bevacizumab and ranibizumab after vitrectomy and lensectomy. Retina (Philadelphia, Pa). 2013 May;33(5):946–52.

130. Kakinoki M, Sawada O, Sawada T, Saishin Y, Kawamura H, Ohji M. Effect of vitrectomy on aqueous VEGF concentration and pharmacokinetics of bevacizumab in macaque monkeys. Invest Ophthalmol Vis Sci. 2012 Aug 24;53(9):5877–80.

131. Niwa Y, Kakinoki M, Sawada T, Wang X, Ohji M. Ranibizumab and Aflibercept: Intraocular Pharmacokinetics and Their Effects on Aqueous VEGF Level in Vitrectomized and Nonvitrectomized Macaque Eyes. Invest Ophthalmol Vis Sci. 2015 Oct;56(11):6501–5.

132. Edington M, Connolly J, Chong NV. Pharmacokinetics of intravitreal anti-VEGF drugs in vitrectomized versus non-vitrectomized eyes. Expert Opin Drug Metab Toxicol. 2017 Dec;13(12):1217–24.

133. Kakinoki M, Sawada O, Sawada T, Saishin Y, Kawamura H, Ohji M. Effect of vitrectomy on aqueous VEGF concentration and pharmacokinetics of bevacizumab in macaque monkeys. Invest Ophthalmol Vis Sci. 2012 Aug 24;53(9):5877–80.

134. Cunha-Vaz JG. The blood–retinal barriers system. Basic concept sand clinical evaluation. Experimental eye research. 78th ed. 2004 Mar;715–21.

135. Wilson CG, Tan LE, Mains J. Principles of Retinal Drug Delivery from Within the Vitreous. In: Drug Product Development for the Back of the Eye. Springer Science & Business Media; 2011. p. 125–58.

136. Maurice D. Review: practical issues in intravitreal drug delivery. J Ocul Pharmacol Ther. 2001 Aug;17(4):393–401.

137. Maurice DM, Mishima. Ocular Pharmacokinetics. In: Pharmacology of the Eye. Springer Science & Business Media; 2012. p. 19–116.

138. Dias CS, Mitra AK. Vitreal elimination kinetics of large molecular weight FITC-labeled dextrans in albino rabbits using a novel microsampling technique. J Pharm Sci. 2000 May;89(5):572–8.

139. Durairaj C, Shah JC, Senapati S, Kompella UB. Prediction of vitreal half-life based on drug physicochemical properties: quantitative structure-pharmacokinetic relationships (QSPKR). Pharm Res. 2009 May;26(5):1236–60.

140. Bakri SJ, Snyder MR, Reid JM, Pulido JS, Ezzat MK, Singh RJ. Pharmacokinetics of intravitreal ranibizumab (Lucentis). Ophthalmology. 2007 Dec;114(12):2179–82.

141. Gaudreault J, Fei D, Beyer JC, Ryan A, Rangell L, Shiu V, et al. Pharmacokinetics and retinal distribution of ranibizumab, a humanized antibody fragment directed against VEGF-A, following intravitreal administration in rabbits. Retina (Philadelphia, Pa). 2007 Dec;27(9):1260–6.

142. Krohne TU, Eter N, Holz FG, Meyer CH. Intraocular pharmacokinetics of bevacizumab after a single intravitreal injection in humans. Am J Ophthalmol. 2008 Oct;146(4):508–12.

143. Gal-Or O, Dotan A, Dachbash M, Tal K, Nisgav Y, Weinberger D, et al. Bevacizumab clearance through the iridocorneal angle following intravitreal injection in a rat model. Exp Eye Res. 2016;145:412–6.

144. Krohne TU, Liu Z, Holz FG, Meyer CH. Intraocular pharmacokinetics of ranibizumab following a single intravitreal injection in humans. Am J Ophthalmol. 2012 Oct;154(4):682-686.e2.

145. Heiduschka P, Fietz H, Hofmeister S, Schultheiss S, Mack AF, Peters S, et al. Penetration of bevacizumab through the retina after intravitreal injection in the monkey. Invest Ophthalmol Vis Sci. 2007 Jun;48(6):2814–23.

146. Nomoto H, Shiraga F, Kuno N, Kimura E, Fujii S, Shinomiya K, et al. Pharmacokinetics of bevacizumab after topical, subconjunctival, and intravitreal administration in rabbits. Invest Ophthalmol Vis Sci. 2009 Oct;50(10):4807–13.

147. Rimpelä A-K, Kiiski I, Deng F, Kidron H, Urtti A. Pharmacokinetic Simulations of Intravitreal Biologicals: Aspects of Drug Delivery to the Posterior and Anterior Segments. Pharmaceutics [Internet]. 2018 Dec 30 [cited 2019 Nov 27];11(1). Available from: https://www.ncbi.nlm.nih.gov/pmc/articles/PMC6359489/

148. Okada M, Kandasamy R, Chong EW, McGuiness M, Guymer RH. The Treat-and-Extend Injection Regimen Versus Alternate Dosing Strategies in Age-related Macular Degeneration: A Systematic Review and Meta-analysis. Am J Ophthalmol. 2018 Aug;192:184–97.

149. Subrizi A, del Amo EM, Korzhikov-Vlakh V, Tennikova T, Ruponen M, Urtti A. Design principles of ocular drug delivery systems: importance of drug payload, release rate, and material properties. Drug Discovery Today [Internet]. 2019 Feb 7 [cited 2019 Jul 2]; Available from: http://www.sciencedirect.com/science/article/pii/S1359644618303994

Chapter 1. Cysteamine polysaccharide hydrogels: study of extended ocular delivery and biopermanence time by PET imaging

USC
UNIVERSIDADE
DE SANTIAGO
DE COMPOSTELA

1. CYSTEAMINE POLYSACCHARIDE HYDROGELS: STUDY OF EXTENDED OCULAR DELIVERY AND BIOPERMANENCE TIME BY PET IMAGING

1.1. INTRODUCTION

Cystinosis is a rare autosomal recessive disease in which cystine crystals accumulate within the lysosomes due to mutations in the CTNS gene. This gene encodes the carrier protein cystinosin that transports cystine out of the lysosome (1,2). Although renal disease prevails in premature forms of cystinosis, all forms of the disease can result in pigmented retinopathy and deposition of cystine crystals within the eye with the consequent photophobia and visual impairment (3,4).

Cysteamine is the most effective drug in the treatment for cystinosis, a cystine-depleting drug that acts in the lysosomes and converts cystine into a form that can be easily removed from them (5,6). Despite oral cysteamine (Cystagon®) has revolutionized the management and prognosis of the patients with cystinosis, orally administered cysteamine cannot reach the cornea. Therefore, it remains necessary to instil cysteamine into the ocular surface in order to eliminate the cystine crystals from the cornea (1).

To our knowledge, Cystaran® is the only available commercial ophthalmic product for the treatment of corneal cystine crystals and it is only approved by the FDA (7). Although Cystaran® has proven to be effective in depleting the corneal cystine crystals, it needs to be instilled into the ocular surface at least 6-10 times per day to achieve the maximum benefit, complicating patient's adherence to the treatment. Even with a high therapeutic compliance, this formulation is rapidly drained from the ocular surface since it is just a solution of cysteamine hydrochloride in saline with the preservative benzalkonium chloride (8). In this aspect, Cystadrops® enhances the dosage regimen by incorporating sodium carboxymethyl

cellulose, which provides a high viscosity to the formulation and which allows a dosage of just 4 times per day (9). It has recently obtained the European marketing authorization (10).

In fact, a substantial number of ophthalmic drugs have not been commercialized due to economic reasons or stability, leaving a significant number of patients in a precarious situation and forcing ophthalmologists to try alternative channels, as in the case of ocular cystinosis treatment. At a hospital level, the use of pharmaceutical compounded eye drops has increased in order to fill this therapeutic vacuum (11,12). Nowadays, the topical ophthalmic cystinosis treatment manufactured at hospital pharmacy departments is a solution of 0.55% cysteamine hydrochloride eye drops (CSS) (13) (14). However, this approach is limited by the short retention time in corneal surface and consequently the need of instillation every hour to obtain a sustainable benefit (15).

The development of new drug delivery systems which can help to overcome the high ocular clearance of conventional eye drops has been a hot topic in ophthalmology research (16). The increase of patient's compliance and the establishment of appropriate dosing schedules are key factors for improving the treatment of many ophthalmic pathologies (17).

Other studies have focused on the development of systems which will delay the delivery of cysteamine in order to minimise its frequency of administration. In order to achieve this, hydrogels with different types of polymers were developed, such as hydroxypropylmethyl cellulose (18), hydroxyethyl cellulose (19), carbomer 934 (19,20) and sodium hyaluronan (19,21), as well as cysteamine loaded contact lenses (22). Although they had characterised their formulations, they all lack *in vivo* studies to show the permanence of the gels on the ocular surface, even when this is an important aspect as the purpose of the study itself is to extend the retention time of the cysteamine.

In this regard, this work is aimed at developing cysteamine ophthalmic formulations with mucoadhesive hydrogels, which can potentially improve the current pharmaceutical compounds prepared at hospital pharmacies. For this, we have performed *in vitro* (characterisation of the hydrogels, drug release and cell toxicity assays), *ex vivo* (transcorneal permeation and HET-CAM assay) and *in vivo* (biopermanence time measured directly and by Positron Emission Tomography) assays. We have selected two different polysaccharide

hydrogels to formulate cysteamine: an in situ ion sensitive hydrogel previously developed by our group for the controlled ocular release of antifungal drugs (23) and a mucoadhesive hydrogel based on hyaluronic acid that has been proposed by McKenzie et al. for the ocular release of cysteamine (19).

1.2. MATERIALS AND METHODS

1.2.1. Cysteamine incorporated into hydrogels

1.2.1.1. Cysteamine hydrogels preparation

Two hydrogels were chosen for the incorporation of 0.55 % cysteamine (BioXtra, Sigma-Aldrich).

The Ion Sensitive Hydrogel (ISH) is composed of 88 % deacylated gellan gum (GG) (Kelcogel® CG-LA provided by CP Kelco®) (molecular weight 1.5-2.5·10^6 Da (24)) and 12 % kappa carrageenan (CK) (Genugel® carrageenan GC-130 provided by CP Kelco®) (molecular weight 3.5-8.0·10^5 Da (24)) and it is prepared with an overall total polymer concentration of 0.2 % (w/v). For the preparation, the cysteamine was dissolved in deionized water, the polymers were added, and the solution was heated at 65 °C. Then, the hydrogel was left to cool down.

On the other hand, the hyaluronic acid based mucoadhesive hydrogel is composed of 0.4 % Hyaluronic Acid (HAH) and was prepared by dissolving the cysteamine in the required amount of BSS (Balance Salt Solution, Sterile Irrigating Solution, Alcon®) under stirring. Then, sodium hyaluronate (Acofarma, Spain) (molecular weight 1.5-2.0·10^6 Da) was added under continuous stirring until its complete dissolution.

1.2.1.2. Quantification of cysteamine by UPLC–MS/MS

Quantification of cysteamine by UPLC–MS/MS was performed by using a modified version of the method proposed by Guan et al. (25). This method requires the derivatization of the cysteamine using the Ellman's reagent (dithionitrobenzoic acid) (Sigma-Aldrich) (Figure 1.1). For this, we prepared a saturated solution of the Ellman's reagent: 29.6 mg of the product was

dissolved in 0.018 M NaOH (VWR®). For the calibration curve, a solution of 1 mg/mL of cysteamine was prepared in ultrapure water. A series of consecutive dilutions were prepared and afterwards 50 mL of each dilution was mixed with 100 mL of Ellman's reagent and 100 mL of PBS. The final concentrations used for the standard curve were from 100 to 0.10 mg/mL. All the standards were analysed just after the addition of the Ellman's reagent.

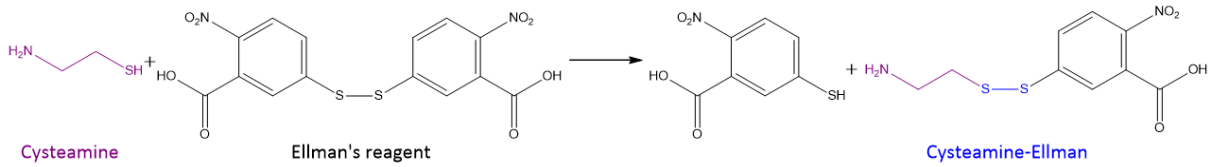

Figure 1.1. Scheme of precolumn derivatization of the cysteamine with Ellman's reagent for the determination of cysteamine by UPLC-MS/MS.

The resultant solutions were analysed by ultra-performance liquid chromatography-tandem mass spectrometer (UPLC–MS/ MS), using an ACQUITY UPLC H-Class System (Waters®) with Xevo TQD Tandem Mass spectrometer (Waters®). The data were collected with the program Masslynx v4.1 and processed with TargetLynzTM Application Manager. We employed an Acquity BEH C18 column (2.1 50 mm, 1.7 mm, Waters®) at a temperature of 40 °C. The mobile phases were 0.1 % formic acid (Sigma-Aldrich) in ultrapure water (MilliQ®, Merck-Millipore) (phase A) and acetonitrile (suitable for UPLC–Ms instruments, VWR®) (phase B). The flow rate was maintained constant at 0.4 mL/min and a gradient elution was used. The gradient started with 100 % of phase A, then linearly changed to a solution of 40 % A – 60 % B at 2.20 min, maintaining it until 2.60 min and then returning to the initial conditions 3 min. The injection volume was 10 mL, and the temperature in the injector was 10 °C in order to minimise sample evaporation. The MS employed positive ion electrospray ionization and the results were obtained by multiple reaction monitoring (MRM). Collision energies and cone source potentials were optimized for each transition using IntelliStart® software (Waters®, Czech Republic).

The values of the optimized MRM transitions, cone voltage, and collision energy for the complex cysteamine-Ellman were 275.97 > 275.92 *m/z*, 72 v and 4 v respectively for the ion transition. The desolvation temperature and the source temperature were 600 °C and 146 °C

respectively, and the nitrogen flow was 1100 mL/ h, cone gas of 80 L/h and capillary voltage of 3.2 kV.

1.2.1.3. *In vitro* release studies

The cysteamine release was estimated by using Franz diffusion cells with visking dialysis membranes (molecular weight cut-off of 12-14 kDa) (Medicell Membranes Ltd). The surface area for diffusion was 0.785 cm^2 (26). 1 mL of each formulation containing 5.5 mg of cysteamine was placed in the upper compartment, adding 300 mL of Simulated Lacrimal Fluid (SLF), which was prepared as previously detailed by Ceulemans et al. (27). Sink conditions were maintained in the receptor compartment, which was filled with 6 mL of Phosphate Buffer Saline (PBS). During the experiment, the cell compartments were placed in an incubating orbital mini shaker (VWR®) where they were continuously homogenized by orbital shaking at 200 rpm and 36 °C. Serial sampling was performed at different times. Each experiment was repeated three times.

For the determination of the samples, ultra-performance liquid chromatography – tandem mass spectrometer (UPLC–MS/MS) was used. Release data were fitted to the zero-order kinetics using GraphPad Prism 6.01 (2014; GraphPad Software, Inc., San Diego, CA, USA). Statistical comparison of the slopes was made by extra sum of square F test for $\alpha < 0.05$, using GraphPad Prism 6.01 software.

1.2.2. *In vivo* evaluation of the biopermanence time on the ocular surface

These studies were carried out on male Sprague-Dawley rats with an average weight of 350 g supplied by the animal facility at the University of Santiago Compostela (Spain). The animals were kept in individual cages with free access to food and water on a room under controlled temperature (22 ± 1 °C) and humidity (60 ± 5 %) and with day-night cycles regulated by artificial light (12/12 h). The animals were treated according to the guidelines for laboratory animals (28,29). Experiments were approved by the Galician Network Committee for Ethics Research following the Spanish and European Union (EU) rules (86/609/CEE, 2003/65/CE, 2010/63/ EU, RD 1201/2005 and RD53/2013).

1.2.2.1. Qualitative direct measures

For direct ocular examination, 0.04 % Trypan Blue was incorporated in both formulations. Previously to the instillation, a pseudo-anaesthesia was induced to take pictures (Integrated Standalone Digital Camera Olympus SZ-Stereomicroscope for STN) at different times to observe the presence/absence of hydrogels on the rat's ocular surface.

2.2.2. Quantitative PET measures

The Positron Emission Tomography (PET) and Computerized Tomography (CT) procedures for conducting the radiolabelling of hydrogels and the quantitative ocular permanence study are described in our previous works (30). Briefly, PET and CT images were acquired using the Albira PET/CT Preclinical Imaging System (Bruker Biospin, Woodbridge, Connecticut, United States). Anaesthetized animals were positioned into the imaging bed, and 7.5 mL of radiotracer solution or 7.5 mL hydrogel labelled with ^{18}F-fluorodeoxyglucose (^{18}F-FDG) were instilled into the conjunctival sac eye using a micropipette. The administered radiotracer dose was approximately 0.4 MBq. After the instillation, single frames of 10 min at different times were acquired. Three animals (6 eyes) were tested for each hydrogel. Different Regions of Interest (ROIs) were manually drawn containing the signal on each eye. The ROIs were replicated on the different frames over time, and the results were corrected for radioactive decay. Afterwards, graphical representations of radioactivity versus time were obtained.

Fitting of the remaining formulation vs time to a mono-exponential decay equation using a single compartmental model was performed using pKSolver (31). Non-Compartmental Analysis was also performed calculating the mean residence time (MRT) and the total area under the curve (AUC) of the percentage remaining of hydrogel vs time.

1.2.3. *Ex vivo* transcorneal permeation

Ex vivo transcorneal permeation was evaluated using bovine corneas. Bovine eyes were obtained during the first hour after animal's death and transported following the bovine corneal opacity and permeability test protocol (32). Once received, the corneas were isolated with 2-3 mm of surrounding sclera, washed with an isotonic saline solution, and placed on

Franz diffusion cells in a way that the epithelial surface faced the upper compartment. The receptor chamber was filled (6 mL) with PBS and 1 mL of each formulation containing 5.5 mg of cysteamine was placed in the upper compartment, adding 300 mL of SLF. During the experiment, cells were continuously homogenised using an incubating orbital shaker (VWR1) at 200 rpm and 36 °C. Serial sampling was performed at different times. Each experiment was repeated three times. For the determination of the samples, ultraperformance liquid chromatography – tandem mass spectrometer (UPLC–MS/MS) was used.

Apparent corneal permeability (P_{app}) was calculated according to the equation:

$$P_{app} = \frac{\delta Q/\delta t}{A \cdot C_0}$$

where δQ/δt is the flux of cysteamine across corneal tissues in the linear portion of the representation, A is the corneal surface (in this study 0.785 cm^2) and C_0 the initial drug concentration at the epithelial side.

Analysis of the Variance (ANOVA) was used to compare the permeated cysteamine from the formulations at each time and significant differences in the flux were analysed by P value (twotailed) testing calculated with GraphPad Prism 6.01 (2014; GraphPad Software, Inc., San Diego, CA, USA).

1.2.4. Ocular safety studies

1.2.4.1. Cytotoxicity assay of cysteamine

The influence of the cysteamine on the cell viability of primary human corneal keratocytes (KCH) was studied by using the xCELLigence Real-Time Cell Analyzer System (RTCA) (ACEA Biosciences, San Diego, CA) for real-time monitoring. The collection and characterization of the cells as well as the methodology of the study has been described in detail in our previous works (33,34).

Cell index (CI) (35) was used to represent the number of cells based on the measured electric impedance. Three thousand cells per well (16 wells E-plates) were incubated for 24 h. Subsequently, the original culture medium (Modified Eagle's Medium/Ham F-12

supplemented with bovine fetal serum at 10 %, with 2 mM L-glutamine and antibiotics) was aspirated and different concentrations of cysteamine (0.26, 0.50, 0.60, and 0.79 mg/mL) were added to different wells. The obtained data were represented as dose response curves versus time and Normalized Cell Index (NCI) (36). NCI is defined by the following equation: $NCI = CI_{(t)} / CI_{(t \text{ of the dose})}$; in which $CI_{(t)}$ is CI at time 't', and $CI_{(t \text{ of the dose})}$ is CI at the time when the cysteamine was added.

1.2.4.2. Ocular irritation assay of the hydrogels with cysteamine

Hen's Egg Test Chorioallantoic Membrane (HET-CAM) was used to study the acute ocular irritation using the methodology described in our previous work (37). A volume of 0.3 mL of both hydrogels with cysteamine was tested. Three eggs were used for each compound. Blood vessels were observed for 300 s with a stereomicroscope (Olympus SZ-STN), looking for episodes of bleeding, coagulation and partial lysis. The irritation index (IS) was determined as described in the Protocol INVITTOX 96 (38).

1.3. RESULTS

1.3.1. Cysteamine incorporated into hydrogels

1.3.1.1. *In vitro* release studies

The release of cysteamine from both HAH and ISH hydrogels is shown in Figure 1.2. Results suggest a zero-order release kinetics process in the first four hours (determination coefficients R^2 of 0.9891 and 0.9875 for HAH and ISH, respectively), where the amount of released cysteamine increases linearly with time. The cysteamine release rate, calculated from the slope after linear fitting of the release data, was 0.75 for HAH and 0.45 $mg \cdot cm^{-2} \cdot h^{-1}$ for ISH. Statistical analysis shows significant differences ($\alpha < 0.05$) in the slopes between hydrogels. At 24 h, the cysteamine released is only slightly higher than that obtained at 4 h, suggesting that the equilibrium between the donor and receptor compartments is reached. Significant differences for the cysteamine released at 24 h were observed between hydrogels for $\alpha < 0.05$.

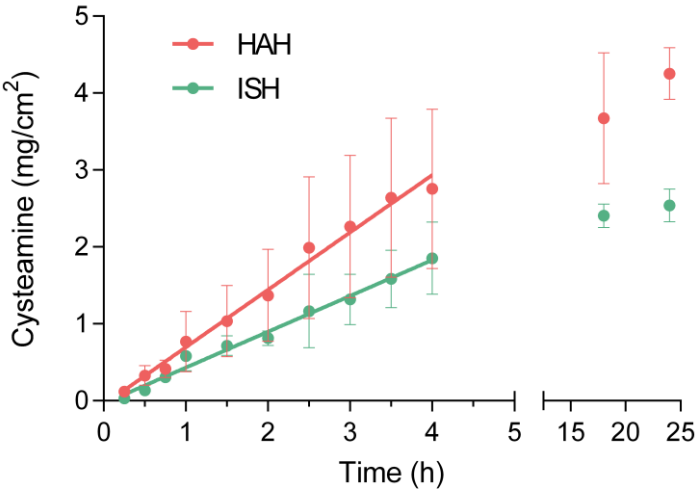

Figure 1.2. Release kinetics of cysteamine from hydrogels (HAH and ISH). Data until 4 hours were fitted to a zero-order kinetics obtaining determination coefficients R^2 of 0.9891 and 0.9875 for HAH and ISH, respectively.

1.3.2. *In vivo* evaluation of the biopermanence time on the ocular surface

1.3.2.1. Qualitative direct measures

The images obtained by direct examination of the hydrogels containing Trypan Blue in the eye surface shows that both cysteamine hydrogels remain throughout all the observation period. Both formulations showed high permanence times on the ocular surface, being observable for at least eight hours (Figure 1.3).

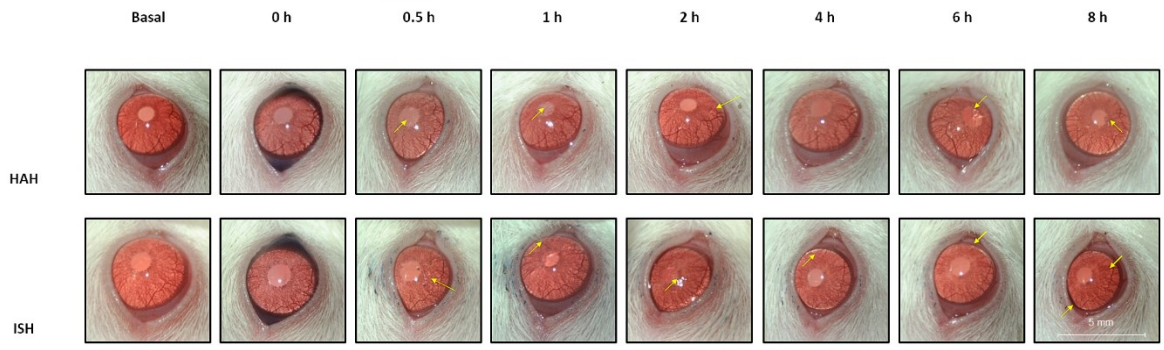

Figure 1.3. *In vivo* qualitative direct biopermanence showing the presence of both hydrogels (HAH and ISH) on the ocular surface in rats until 8 hours.

1.3.2.2. Quantitative PET measures

The biopermanence of the ^{18}F-FDG-labelled hydrogels was calculated by using small-animal PET imaging in rats and compared to a solution of ^{18}F-FDG in saline form (CSS). Figure 1.4 shows the clearance of the formulations from the eye. A strong signal at early times after instillation was observed for both formulations. It can be observed that after 1 h of contact, 83.5 % of the ISH remains in the ocular surface, while 48.2 % of HAH and only 16.7 % of CSS remains. Data were fitted to a mono-exponential model dependent on time, as it can be seen in Figure 1.4, and the pharmacokinetic parameters obtained by the fitting to the mono-compartment model are shown in Table 1.1. We obtained an average half-life time and a mean permanence time of 0.99 ± 0.18 and 1.43 ± 0.26 h in the case of the HAH, 1.27 ± 0.47 and 1.85 ± 0.68 h for the ISH and 0.31 ± 0.10 and 0.45 ± 0.14 h for the CSS. The labelling of the hydrogels was considered as optimum since the ^{18}F-FDG remain in both hydrogels was above 95 % at 4 h post-preparation.

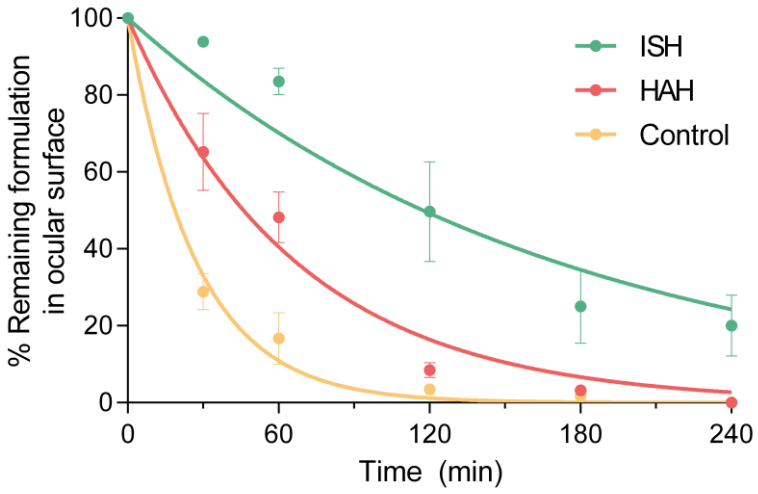

Figure 1.4. Clearance rate of the hydrogels (HAH and ISH) from the ocular surface determined by PET.

Table 1.1. Parameters obtained by the fitting of the % formulation remaining on ocular surface obtained by PET imaging to a mono-compartmental model.

Formulation	$t_{1/2}$ (h)	AUC_0^∞ (mg/mL·h)	MRT (h)
HAH	0.99 ± 0.18	497.3 ± 75.7	1.43 ± 0.26
ISH	1.27 ± 0.47	644.9 ± 220.9	1.85 ± 0.68
CSS	0.31 ± 0.10	159.9 ± 48.8	0.45 ± 0.14

Figure 1.5 shows the axial and sagittal views of the registered PET/CT images of the animal head after the administration of the HAH hydrogel and 2 h post-instillation. CT images show the bone structure of the head and PET images show the distribution of the labelled hydrogel. Initially, all the hydrogel is located on the eye surface. After 2 h, the concentration on the eye is still significant, indicating a high retention time on the ocular surface. Also, the radiotracer signal is detected in the nasolacrimal duct and in the nasal cavity due to the clearance of part of the hydrogel from the lacrimal sac into the nasal cavity.

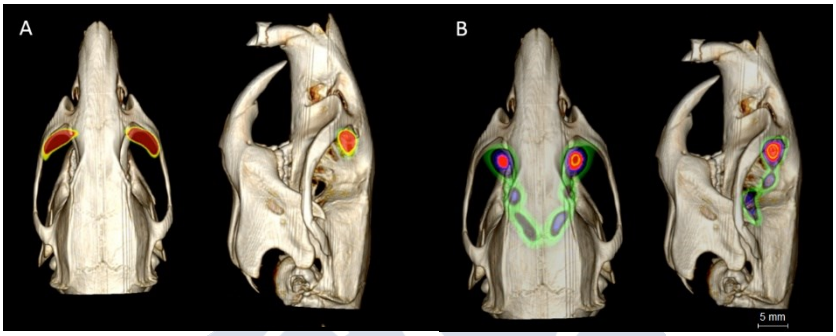

Figure 1.5. Axial (left) and sagittal (right) fusion PET-TAC images of the rat's head. A) HAH 10 minutes post-administration. B) HAH 2 hours post-administration.

1.3.3. *Ex vivo* transcorneal permeation

Figure 1.6 shows the transcorneal permeation profiles of cysteamine hydrogels and CSS. The apparent permeability coefficient and the percentage of the dose of cysteamine permeated at 5 h are showed in Table 1.2. Results indicate that only 0.09 % of the cysteamine was able to permeate during 5 h from the CSS. On the other hand, there was a more complete permeation from HAH (0.45 %) and from ISH (0.40 %). Cysteamine Papp increases in both hydrogels compared to the solution and the higher value was obtained with the HAH. P test shows significant differences in the P_{app} among all treatments ($\alpha < 0.01$).

Table 1.2. Parameters obtained by *ex vivo* transcorneal permeation assay.

Formulation	P_{app} x 10^{-7} (cm/s)	% permeation at 5 h
HAH	3.19 ± 0.27	0.45 ± 0.040
ISH	2.36 ± 0.32	0.40 ± 0.210
CSS	0.39 ± 0.20	0.09 ± 0.001

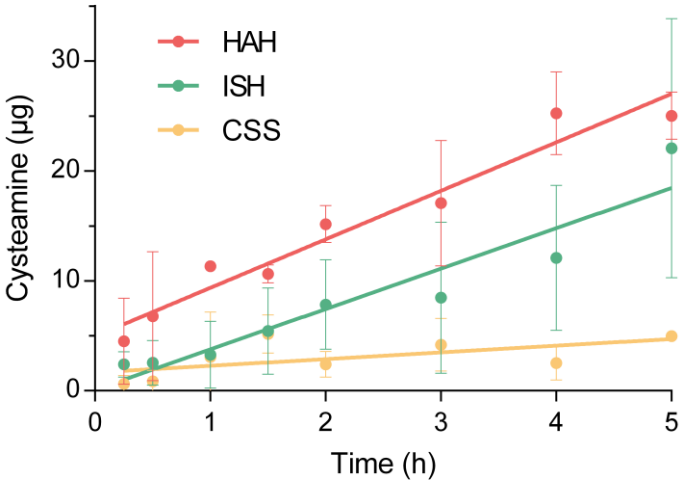

Figure 1.6. Permeation of cysteamine (µg) through the cornea from the cysteamine hydrogels (HAH and ISH) and solution (CSS).

Two-way analysis of variance (ANOVA) shows significant differences on the cysteamine permeated through the cornea from the hydrogels and the solution for all the times studied ($\alpha < 0.05$). Significant statistically differences between hydrogels were observed only in the first hour ($\alpha < 0.05$).

1.3.4. Ocular safety studies

1.3.4.1. Cytotoxicity assay of cysteamine

NCI values obtained from the real-time monitoring are shown in Figure 1.7. Cysteamine induced a gradual cell death over time. At the initial time of contact, keratocytes present

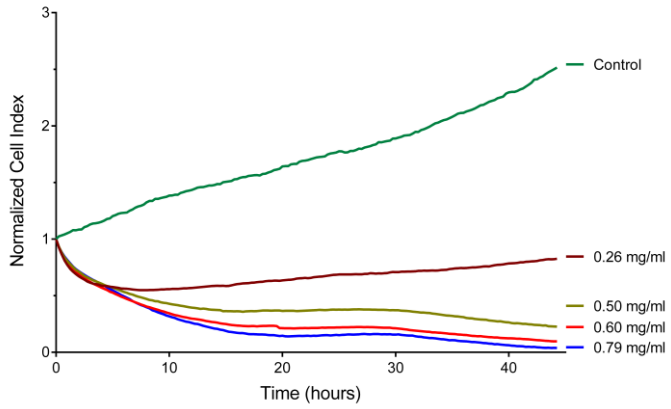

Figure 1.7. Cytotoxicity assay results of cysteamine using the xCELLigence Real-Time Cell Analyzer System.

similar toxic sensitivity for all cysteamine concentrations tested; however, at prolonged times, cysteamine is more toxic at higher concentrations. It can even eliminate the complete population of keratocytes with the highest concentrations tested at prolonged times.

1.3.4.2. Ocular irritation assay of the hydrogels with cysteamine

The results show the absence of damage on the blood vessels after the addition of both cysteamine hydrogels after 5 min of contact (IS = 0). The images of the intact blood vessels after the addition of the hydrogels can be observed in Figure 1.8.

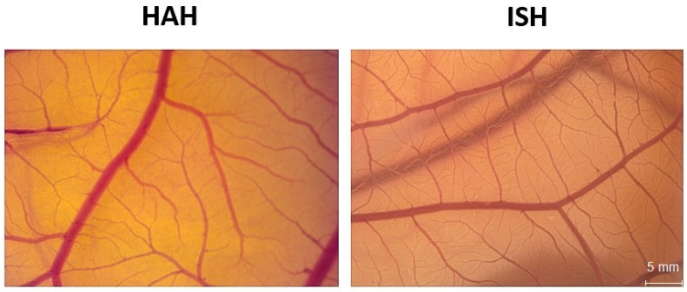

Figure 1.8. CAM's pictures of both formulations (HAH and ISH) after 5 minutes of contact.

1.4. DISCUSSION

The principal vehicles used for the elaboration of topic ophthalmic formulations at hospital pharmacy departments are saline solution and balanced saline solution (BSS); however, these present many limitations, especially due to their low retention time on the ocular surface. For this reason, the development of new ophthalmic topical vehicles of improved ocular permanence could have an important impact in the enhancement of drug efficacy. In our case, the development of cysteamine eye drops with high ocular surface permanence would cause an improvement on patient compliance and therapeutic efficacy (39).

Cysteamine hyaluronic acid-based hydrogels were elaborated at a concentration of 0.4 % sodium hyaluronate since it is a common concentration used in eye drops for dry eye treatment. This concentration was higher than the 0.3 % used by McKenzie in their study (19). Both the hyaluronic acid and the ion sensitive hydrogel show a pseudoplastic behaviour at low shear rate (see Figure 1.1 supplementary) becoming to newtonian at shear rates higher than

1 rad/s. On the other hand, the formulation with an ion sensitive hydrogel, composed of GG and KC, at similar polysaccharide concentration than the ones developed in our previous work (23), significantly increases its viscosity after the incorporation of the cysteamine (see Figure 1.2 supplementary).

The final hydrogel was too viscous for their application into the eye. The gelation of the polymer could have been produced by the electrostatic interactions between the negatively charged carboxylic acid and sulphate residues of the polysaccharides and the positively charged quaternary ammonium group of the cysteamine. For this reason, the concentration of polymers was optimized to obtain a formulation with an adequate viscosity for the ocular use; 0.2 % of total concentration of polymers (88 % GG and 12 % KC).

One of the first challenges in the development of new cysteamine eye drops is the difficulty to find an adequate analytical method to determine the cysteamine concentrations in the formulations and also in the media used from *in vitro* and *ex vivo* tests. On the other hand, it is convenient to point out that the analysis of compounds with thiol groups as cysteamine has always entailed complications due to the susceptibility of this group to oxidation before or during its analysis and also because of the lack of a chromophore structure for its detection (25,40). In order to avoid these problems, we have developed a method based in the pre-column derivatization of cysteamine using Ellman's reagent in combination with a UPLC–MS/MS equipment that provides a highly selective and sensitive method for the analysis of cysteamine derivative. Ellman's reagent is a commercially available reagent that provides an easy way of derivatization of the cysteamine. In Figure 1.1, we have included a scheme of the formation of the cysteamine derivative using this reagent. The Ellman's reagent has been employed by other authors for the determination of cysteamine by UV–vis spectrophotometry (19). Regarding other methods for cysteamine quantification (18,20,41–43), our method provides a higher efficacy and shorter times of analysis, needing only 3 min per sample.

The *in vitro* release studies using vertical Franz cells show that both ISH and HAH can effectively control the release of cysteamine over time, showing a zero-order kinetics during the first four hours. Compared to the data from 0.3 % hyaluronic acid hydrogels from

McKenzie's study (19), the release of cysteamine is significantly slower in our system. These differences may be attributed to the differences in the procedure used to evaluate the release rate. We have used the same membrane (12000-14000 Da) but in vertical Franz cell systems incorporating 1 mL of formulation versus 7 mL of the gel tied in a rod shape tubing membrane. The effective area of diffusion in the Franz cell system was 0.785 cm^2 in comparison with the 8.58 cm^2 of the cylinder, the receptor volume was 6 mL vs 50 mL and finally the stirring system was slow oscillation vs magnetic stirring.

The zero-order kinetics obtained from our systems suggest the interaction of the cysteamine with the polysaccharide network that controls the release process. After 24 h, the release percentage of cysteamine was 60.7 % and 36.3 % for HAH and ISH, respectively. The lower release rate and fraction release from ISH suggest a strong interaction of the cysteamine with the gellan gum or the κ-carrageenan, higher than with hyaluronic acid. Cysteamine is positively charged at physiological pH and can electrostatically interact with negatively charged polysaccharides forming supramolecular complexes. Hyaluronic acid and gellan gum have carboxylic acid radicals and κ-carrageenan has sulphate radicals that can interact with cysteamine. The stronger interaction between cysteamine and sulphate radicals compared to carboxilates may be the cause of the slower release and fraction release at 24 h of the ISH. In the case of HAH at 24 h, the concentration is near the equilibrium concentration of the free cysteamine between the donor and receptor compartments considering their volume. Nevertheless, the proportion of cysteamine released from ISH is significantly lower than from HAH, indicating that part of the cysteamine is bound to the hydrogel at this time.

To date, several methodologies have been proposed to carry out a biopermanence study for ophthalmic formulations (44,45). In this work, we used a novel methodology based on Positron Emission Tomography (PET) for evaluating the biopermanence of these hydrogels (30). The introduction of new imaging techniques has improved many aspects of both the therapeutic-diagnostic ophthalmic procedures and the development of eye formulations and ophthalmic drugs. Previous works have shown the presence or absence of ophthalmic formulations in the eye only with qualitative measures, without providing pharmacokinetic profiles. Direct examination of the gel containing Trypan Blue (Figure 1.3) qualitatively

determine the increase of permanence time of hydrogels compared to a solution. Also, PET/CT images (Figure 1.5) confirm the high retention time of the hydrogel. Nevertheless, PET studies allow to quantitatively analyse the pharmacokinetic profile of the ophthalmic formulations and to calculate the elimination constant, the half-live and the zero and first moment pharmacokinetic parameters AUC_0^{∞} and MRT. All the pharmacokinetic parameters indicate a significant increase in the ocular retention time of the hydrogels compared to the CSS acquisitions. The hydrogels have a mean retention time in the ocular surface four/five times higher than the CSS. The results from the ocular biopermanence assays show us that both hydrogels are mucoadhesive compounds and have an adequate consistence to remain on the ocular surface for a long time. Finally, the results indicate that the ocular retention time was slightly higher for ISH. This better permanence time can be attributed to the ability of gellan gum and κ-carrageenan to in situ gel in the presence of the tear ions, which results in the formation of a more compact and resistant hydrogel (37).

The combination of the results from the release study and the high retention time of the hydrogels in the ocular surface suggest the interesting potential of these formulations for the controlled release of cysteamine in the eye. These two properties of the cysteamine hydrogels might lead to an increase in the bioavailability and consequently an increase in the time of duration of action, decreasing the frequency of administration. For this, it is mandatory that cysteamine permeates into the cornea and reaches the lysosomes of the corneal cells where cystine crystals accumulate (3). Hence, in order to verify that the hydrogels were able to allow the penetration of the cysteamine into the cornea, the *ex vivo* transcorneal study was performed. The results show that both hydrogels allowed a higher permeation of cysteamine through the cornea than the solution, obtaining values of apparent corneal permeability one order of magnitude higher with the hydrogels. These results indicate that the polysaccharides used could behave as corneal absorption promoters.

There are various mechanisms to enhance the corneal absorption. One of them is the opening of tight junctions, which has been proved to be caused by some polysaccharides at the ocular level, such as chitosan (46,47). Hyaluronic acid has been also reported as a penetration enhancer in the nasal (48,49), buccal, vaginal and intestinal mucosa (50). In accordance with

Sandri et al. (50), hyaluronic acid, specially varieties with low molecular weight (202 kDa), exhibited penetration enhancement properties comparable with or even better than chitosan hydrochloride, depending on the substrate. Also, transepithelial electrical resistance experiments performed using Caco-2 cell monolayers indicate that an opening of the tight junctions was produced by hyaluronic acid. Our results also indicate that the hyaluronic acid presents penetration enhancement properties, as its penetration through bovine corneas was observed to be higher compared to a solution of cysteamine. Therefore, we concluded that the cysteamine can cross the bovine cornea, which means that the cysteamine is able to be released from the hydrogels and to enter the corneal stroma, and also that the hydrogels enhance the diffusion of the cysteamine through the cornea in comparison with a solution of cysteamine.

In order to improve the safety of patients receiving topical ocular treatment, it is essential to estimate the cytotoxicity and the potential of causing irritation of any compound that would come in contact with the eye. The HET-CAM is an alternative method to determine ocular irritation using the chorioallantoic membrane of fertile chicken eggs. It has shown a good predictability for the determination of *in vivo* non-irritant substances (51). In our experiment, the hydrogels have not shown any type of damage in the vessels; thus, we can suppose that the formulations tested would not present acute irritant effects *in vivo*.

Additionally, cytotoxicity assays have been carried out to study the real-time interaction between cysteamine and keratocytes corneal cells. For this purpose, the RTCA system was used. This is a novel technique with several advantages over the classical methods, as it does not interfere with dyes, is non-invasive, does not require a single time point measurement and does not require the use of labels (33). Furthermore, it is a high-throughput technique that allows acquisition of multiple data and representation of these data in a dynamic real-time manner (34). We have observed a gradual destruction of keratocytes when cysteamine is in contact and that this is time and concentration dependent. It has been previously described the cytotoxic effect of cysteamine at 10^{-4} to 10^{-3} M concentrations (52). The cysteamine toxicity is related to the capacity of the thiols to generate H_2O_2 in an oxidation reaction catalysed by transition metals that kill cells by apoptosis. Nevertheless, *in vivo*,

cysteamine stimulates the synthesis of intracellular glutathione that protects the cells against peroxides and could limit the effects of cysteamine-derived H_2O_2 (53). However, no serious adverse events of cysteamine eye drops are related in other works (18,54).

1.5. CONCLUSION

Independent research on rare diseases is of great importance nowadays, and although rare, it should not be forgotten. The development of useful formulations at a hospital pharmacy department is feasible when the commercial product cannot be obtained or when it is ineffective, being able to elaborate these formulations as a pharmaceutical compounding. Our results indicate that both hydrogels HAH and ISH have a high potential as vehicles for the ocular administration of cysteamine. The hydrogels have demonstrated a prolonged retention time in the ocular surface, an adequate cysteamine controlled release and to be safe. *In vivo* bioavailability cysteamine studies must be developed to confirm the potential of this systems.

1.6. REFERENCES

1. Gahl WA, Thoene JG, Schneider JA. Cystinosis. N Engl J Med. 2002 Jul 11;347(2):111–21.
2. Shams F, Livingstone I, Oladiwura D, Ramaesh K. Treatment of corneal cystine crystal accumulation in patients with cystinosis. Clin Ophthalmol Auckl NZ. 2014 Oct 10;8:2077–84.
3. Gahl WA, Kuehl EM, Iwata F, Lindblad A, Kaiser-Kupfer MI. Corneal crystals in nephropathic cystinosis: natural history and treatment with cysteamine eyedrops. Mol Genet Metab. 2000 Oct;71(1–2):100–20.
4. Nesterova G, Gahl WA. Cystinosis: the evolution of a treatable disease. Pediatr Nephrol Berl Ger. 2013 Jan;28(1):51–9.
5. Martine Besouw RM. Cysteamine: An old drug with new potential. Drug Discov Today. 2013;18(15).
6. Jézégou A, Llinares E, Anne C, Kieffer-Jaquinod S, O'Regan S, Aupetit J, et al. Heptahelical protein PQLC2 is a lysosomal cationic amino acid exporter underlying the action of cysteamine in cystinosis therapy. Proc Natl Acad Sci U S A. 2012 Dec 11;109(50):E3434–43.
7. Food and Drug Administration. Cystaran®. Prescribing information [Internet]. 2016 [cited 2016 May 3]. Available from: www.sigmatau.com
8. Veys KR, Elmonem MA, Arcolino FO, van den Heuvel L, Levtchenko E. Nephropathic cystinosis: an update. Curr Opin Pediatr. 2017 Jan 18;

9. Liang H, Labbé A, Le Mouhaër J, Plisson C, Baudouin C. A New Viscous Cysteamine Eye Drops Treatment for Ophthalmic Cystinosis: An Open-Label Randomized Comparative Phase III Pivotal Study. Invest Ophthalmol Vis Sci. 2017 Apr 1;58(4):2275–83.

10. European Medicines Agency. CHMP summary of positive opinion for Cystadrops [Internet]. 2017 [cited 2017 Feb 1]. Available from: http://www.ema.europa.eu/ema/index.jsp?curl=pages/medicines/human/medicines/003769/smops/Positive/human_smop_001034.jsp&mid=WC0b01ac058001d127

11. Fernández-Ferreiro A, González Barcia M, Blanco Mendez J, Lamas MJ, Otero Espinar FJ. Optimization Ophthalmic Topical Antifungal Treatment. Fungal Genomics Biol [Internet]. 2016 Jan 8 [cited 2017 Apr 24]; Available from: https://www.omicsgroup.org/journals/optimization-ophthalmic-topical-antifungal-treatment-2165-8056-1000e119.php?aid=66109

12. Fernández-Ferreiro A, González-Barcia M, Otero Espinar FJ, Blanco Méndez J, Lamas MJ. Ophthalmic formulations new goals. Farm Hosp Órgano Of Expr Científica Soc Esp Farm Hosp. 2016 Feb;40(1):1–2.

13. National Eye Institute. Cysteamine Eye Drops to Treat Corneal Crystals in Cystinosis. Clinical Trial. [Internet]. 2016 May [cited 2016 May 6]. Available from: https://clinicaltrials.gov

14. Kaiser-Kupfer MI, Gazzo MA, Datiles MB, Caruso RC, Kuehl EM, Gahl WA. A randomized placebo-controlled trial of cysteamine eye drops in nephropathic cystinosis. Arch Ophthalmol Chic Ill 1960. 1990 May;108(5):689–93.

15. Ribeiro MVMR, Ribeiro LEF, Ribeiro ÊAN, Ferreira CV, Barbosa FT, Ribeiro MVMR, et al. Adherence assessment of eye drops in patients with glaucoma using 8 item Morisky Score: a cross sectional study. Rev Bras Oftalmol. 2016 Dec;75(6):432–7.

16. Almeida H, Amaral MH, Lobão P, Lobo JMS. In situ gelling systems: a strategy to improve the bioavailability of ophthalmic pharmaceutical formulations. Drug Discov Today. 2014 Apr;19(4):400–12.

17. Patel A, Cholkar K, Agrahari V, Mitra AK. Ocular drug delivery systems: An overview. World J Pharmacol. 2013;2(2):47–64.

18. Bozdağ S, Gümüş K, Gümüş O, Unlü N. Formulation and in vitro evaluation of cysteamine hydrochloride viscous solutions for the treatment of corneal cystinosis. Eur J Pharm Biopharm Off J Arbeitsgemeinschaft Für Pharm Verfahrenstechnik EV. 2008 Sep;70(1):260–9.

19. McKenzie B, Kay G, Matthews KH, Knott R, Cairns D. Preformulation of cysteamine gels for treatment of the ophthalmic complications in cystinosis. Int J Pharm. 2016 Dec 30;515(1–2):575–82.

20. Buchan B, Kay G, Heneghan A, Matthews KH, Cairns D. Gel formulations for treatment of the ophthalmic complications in cystinosis. Int J Pharm. 2010 Jun 15;392(1–2):192–7.

21. McKenzie B, Kay G, Matthews KH, Knott RM, Cairns D. The hen's egg chorioallantoic membrane (HET-CAM) test to predict the ophthalmic irritation potential of a cysteamine-

containing gel: Quantification using Photoshop® and ImageJ. Int J Pharm. 2015 Jul 25;490(1–2):1–8.

22. Hsu K-H, Fentzke RC, Chauhan A. Feasibility of corneal drug delivery of cysteamine using vitamin E modified silicone hydrogel contact lenses. Eur J Pharm Biopharm Off J Arbeitsgemeinschaft Für Pharm Verfahrenstechnik EV. 2013 Nov;85(3 Pt A):531–40.

23. Fernández-Ferreiro A, González Barcia M, Gil-Martínez M, Vieites-Prado A, Lema I, Argibay B, et al. In vitro and in vivo ocular safety and eye surface permanence determination by direct and Magnetic Resonance Imaging of ion-sensitive hydrogels based on gellan gum and kappa-carrageenan. Eur J Pharm Biopharm. 2015 Jun 14;

24. De Silva DA. Characterization of single network and interpenetrating network hydrogels of natural and synthetic polymerss, Doctor of Philosophy thesis, School of Chemistry [Internet]. [Australia]: University of Wollongong; 2013 [cited 2017 Feb 6]. Available from: http://ro.uow.edu.au/theses/4042

25. Guan X, Hoffman B, Dwivedi C, Matthees DP. A simultaneous liquid chromatography/mass spectrometric assay of glutathione, cysteine, homocysteine and their disulfides in biological samples. J Pharm Biomed Anal. 2003 Feb 26;31(2):251–61.

26. Baranowski P, aw, Karolewicz B, ena, Gajda M, Pluta J. Ophthalmic Drug Dosage Forms: Characterisation and Research Methods. Sci World J. 2014 Mar 18;2014.

27. Ceulemans J, Ludwig A. Optimisation of carbomer viscous eye drops: an in vitro experimental design approach using rheological techniques. Eur J Pharm Biopharm Off J Arbeitsgemeinschaft Für Pharm Verfahrenstechnik EV. 2002 Jul;54(1):41–50.

28. The Association for Research in Vision and Ophthalmology. Statement for the Use of Animals in Ophthalmic and Visual Research [Internet]. 2014. Available from: http://www.arvo.org/About_ARVO/Policies/Statement_for_the_Use_of_Animals_in_Ophthalmic_and_Visual_Research/

29. National Research Council (US) Committee for the Update of the Guide for the Care and Use of Laboratory Animals. Guide for the Care and Use of Laboratory Animals [Internet]. 8th ed. Washington (DC): National Academies Press (US); 2011 [cited 2014 Nov 28]. (The National Academies Collection: Reports funded by National Institutes of Health). Available from: http://www.ncbi.nlm.nih.gov/books/NBK54050/

30. Fernández-Ferreiro A, Silva-Rodríguez J, Otero-Espinar FJ, González-Barcia M, Lamas MJ, Ruibal A, et al. Positron Emission Tomography for the Development and Characterization of Corneal Permanence of Ophthalmic Pharmaceutical Formulations. Invest Ophthalmol Vis Sci. 2017 Feb 1;58(2):772–80.

31. Zhang Y, Huo M, Zhou J, Xie S. PKSolver: An add-in program for pharmacokinetic and pharmacodynamic data analysis in Microsoft Excel. Comput Methods Programs Biomed. 2010 Sep;99(3):306–14.

32. OECD. Test No. 437: Bovine Corneal Opacity and Permeability Test Method for Identifying Ocular Corrosives and Severe Irritants [Internet]. Paris: Organisation for

Economic Co-operation and Development; 2009 [cited 2014 Jan 28]. Available from: http://www.oecd-ilibrary.org/content/book/9789264076303-en

33. Fernández-Ferreiro A, González-Barcia M, Gil-Martínez M, Santiago Varela M, Pardo M, Blanco-Méndez J, et al. Evaluation of the in vitro ocular toxicity of the fortified antibiotic eye drops prepared at the Hospital Pharmacy Departments. Farm Hosp Organo Of Expresion Cient Soc Espanola Farm Hosp. 2016 Sep 1;40(5):352–70.

34. Fernández-Ferreiro A, Santiago-Varela M, Gil-Martínez M, Parada TG-C, Pardo M, González-Barcia M, et al. Ocular safety comparison of non-steroidal anti-inflammatory eye drops used in pseudophakic cystoid macular edema prevention. Int J Pharm. 2015 Nov 30;495(2):680–91.

35. Xing JZ, Zhu L, Gabos S, Xie L. Microelectronic cell sensor assay for detection of cytotoxicity and prediction of acute toxicity. Toxicol In Vitro. 2006 Sep;20(6):995–1004.

36. Atienza JM, Zhu J, Wang X, Xu X, Abassi Y. Dynamic Monitoring of Cell Adhesion and Spreading on Microelectronic Sensor Arrays. J Biomol Screen. 2005 Dec 1;10(8):795–805.

37. Fernández-Ferreiro A, Fernández Bargiela N, Varela MS, Martínez MG, Pardo M, Piñeiro Ces A, et al. Cyclodextrin-polysaccharide-based, in situ-gelled system for ocular antifungal delivery. Beilstein J Org Chem. 2014;10:2903–11.

38. Hen's Egg Test on the Chorioallantoic Membrane (HET-CAM) INVITTOX n° 96 [Internet]. [cited 2014 Jan 27]. Available from: http://www.vitrotox.com/uploadfile/UploadFile/2008121382926916.pdf

39. Thompson AC, Thompson MO, Young DL, Lin RC, Sanislo SR, Moshfeghi DM, et al. Barriers to Follow-Up and Strategies to Improve Adherence to Appointments for Care of Chronic Eye Diseases. Investig Opthalmology Vis Sci. 2015 Jul 8;56(8):4324.

40. Lawal B. Development of a cysteamine in situ gelling system for the treatment of corneal crystals in cystinosis [Internet]. 2008 [cited 2016 Feb 3]. Available from: https://cystinosis.org/images/research/updates/CRN_Research_UpdateB.pdf

41. Chanakira A, Chikwana E, Peyton DH, Simoyi RH. Oxyhalogen-sulfur chemistry kinetics and mechanism of the oxidation of cysteamine by acidic iodate and iodine. Can J Chem. 2006 Jan 1;84(1):49–57.

42. Pescina S, Carra F, Padula C, Santi P, Nicoli S. Effect of pH and penetration enhancers on cysteamine stability and trans-corneal transport. Eur J Pharm Biopharm Off J Arbeitsgemeinschaft Pharm Verfahrenstechnik EV. 2016 Oct;107:171–9.

43. Kataoka H, Imamura Y, Tanaka H, Makita M. Determination of cysteamine and cystamine by gas chromatography with flame photometric detection. J Pharm Biomed Anal. 1993 Oct;11(10):963–9.

44. Fernández-Ferreiro A, Silva J, Otero-Espinar FJ, González-Barcia M, Lamas MJ, Ruibal A, et al. In vivo eye surface residence determination by high-resolution scintigraphy of a novel ion-sensitive hydrogel based on gellan gum and kappa-carrageenan. Eur J Pharm Biopharm. 2017 Feb 9;

45. Eter N. Molecular imaging in the eye. Br J Ophthalmol. 2010 Nov;94(11):1420–6.

46. Zambito Y, Di Colo G. Polysaccharides as Excipients for Ocular Topical Formulations. In: Pignatello R, editor. Biomaterials Applications for Nanomedicine. InTech; 2011. p. 253–80.

47. Kim NJ, Harris A, Elghouche A, Gama W, Siesky B. Ocular Permeation Enhancers. In: Pathak YV, Sutariya V, Hirani AA, editors. Nano-Biomaterials For Ophthalmic Drug Delivery. Springer International Publishing; 2016.

48. Morimoto K, Yamaguchi H, Iwakura Y, Morisaka K, Ohashi Y, Nakai Y. Effects of viscous hyaluronate-sodium solutions on the nasal absorption of vasopressin and an analogue. Pharm Res. 1991 Apr;8(4):471–4.

49. Rydén L, Edman P. Effect of polymers and microspheres on the nasal absorption of insulin in rats. Int J Pharm. 1992 Jun 30;83(1):1–10.

50. Sandri G, Rossi S, Ferrari F, Bonferoni MC, Zerrouk N, Caramella C. Mucoadhesive and penetration enhancement properties of three grades of hyaluronic acid using porcine buccal and vaginal tissue, Caco-2 cell lines, and rat jejunum. J Pharm Pharmacol. 2004 Sep;56(9):1083–90.

51. Scheel J, Kleber M, Kreutz J, Lehringer E, Mehling A, Reisinger K, et al. Eye irritation potential: usefulness of the HET-CAM under the Globally Harmonized System of classification and labeling of chemicals (GHS). Regul Toxicol Pharmacol RTP. 2011 Apr;59(3):471–92.

52. Jeitner TM, Lawrence DA. Mechanisms for the cytotoxicity of cysteamine. Toxicol Sci Off J Soc Toxicol. 2001 Sep;63(1):57–64.

53. Meier T, Issels RD. Promotion of cyst(e)ine uptake. Methods Enzymol. 1995;252:103–12.

54. Labbé A, Baudouin C, Deschênes G, Loirat C, Charbit M, Guest G, et al. A new gel formulation of topical cysteamine for the treatment of corneal cystine crystals in cystinosis: the Cystadrops OCT-1 study. Mol Genet Metab. 2014 Mar;111(3):314–20.

1.7. SUPPLEMENTARY MATERIAL

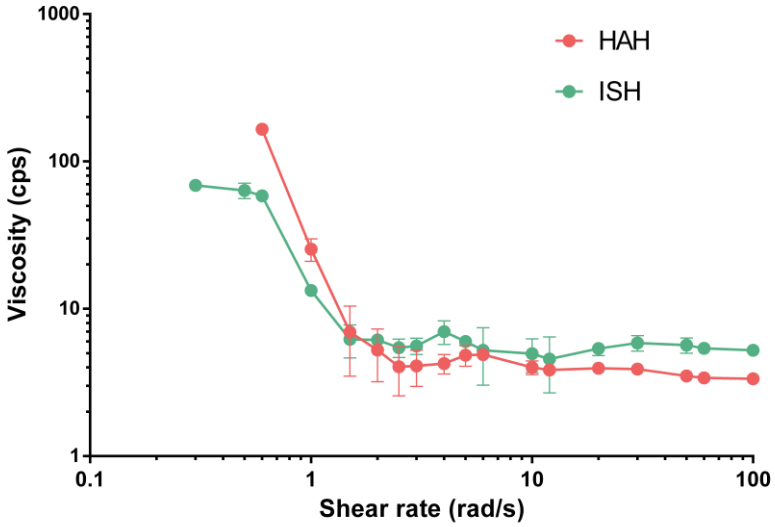

Figure 1.1 supplementary. Viscosity curves of the hydrogels without cysteamine. Viscosity measurements were performed in a rotational viscometer Fungilab Smart Series (Fungilab, Barcelona) at 25 °C.

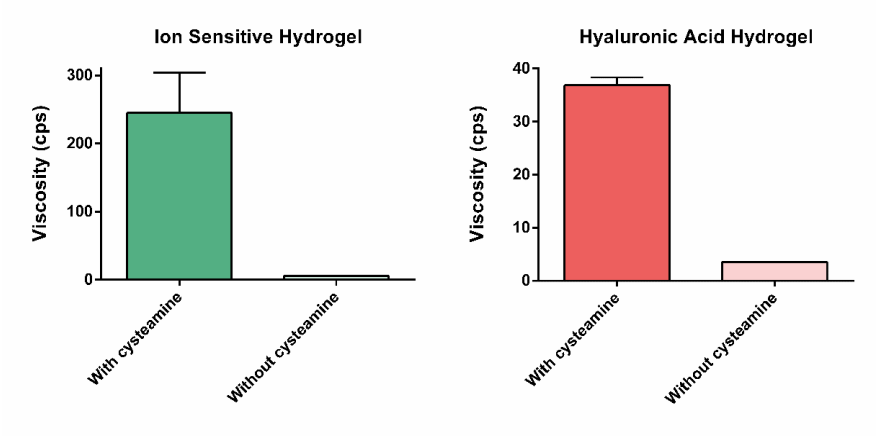

Figure 1.2 supplementary. Effect of the addition of cysteamine on the viscosity of hydrogels. Viscosity measurements were performed in a rotational viscometer Fungilab Smart Series (Fungilab, Barcelona) at a shear rate of 50 rad/s and 25 °C.

USC
UNIVERSIDADE
DE SANTIAGO
DE COMPOSTELA

Chapter 2. Stability study of a hyaluronan-based hydrogel containing cysteamine for ocular cystinosis

USC
UNIVERSIDADE
DE SANTIAGO
DE COMPOSTELA

2. STABILITY STUDY OF A HYALURONAN-BASED HYDROGEL CONTAINING CYSTEAMINE FOR OCULAR CYSTINOSIS

2.1. INTRODUCTION

Cystinosis is a rare lysosomal storage disorder that follows an autosomal recessive inheritance pattern (1). This metabolic disorder is characterized by the accumulation of the amino acid cystine in lysosomes due to defective cystine transportation from the interior to the exterior of the lysosome (2,3). Cystine has low solubility in water, leading to the formation of intralysosomal crystals and damage to various tissues and organs, including the cornea. As described by Burki in the 1940s, the ocular manifestations of the disease are due to the accumulation of cystine crystals in the ocular surface (4). These crystals can be observed with a slit lamp and are a pathognomonic sign of cystinosis. They begin to form during infancy and from 16 months of age onward they can be observed through a slit lamp. Patients are initially asymptomatic. Due to the accumulation of corneal cystine crystals over time, ocular symptoms do not appear until approximately 10 years of age (5).

The specific treatment of cystinosis is cysteamine, also called mercaptamine or 2-aminoethanethiol, which is an aminothiol with chemical formula $HSCH_2CH_2NH_2$ (6). Cysteamine was introduced as a possible therapeutic agent for cystinosis in 1976 and remains the only available treatment (7). Although cysteamine does not cure cystinosis, it has revolutionized patient management and prognosis. It has been shown to slow disease progression and can reduce the amount of intracellular cystine by more than 90 %. Cysteamine therapy should be started as soon as the diagnosis is made and should be continued for the lifetime of the patient. Patients with poor adherence to treatment or begin it later do not achieve such beneficial outcomes (8).

Oral cysteamine is administered in the form of cysteamine bitartrate but does not reach the cornea due to the lack of corneal vascularization. Thus, a topical ocular application was developed, whose safety and effectiveness had already been demonstrated in the 1980s (9–11). Currently, there are two available ophthalmic formulations of cysteamine hydrochloride: Cystaran® (Sigma Tau Pharmaceuticals Inc.), an FDA-approved medication, which must be instilled from 6 to 12 times a day (12); and Cystadrops® (Orphan Europe, Paris, France), which has a higher viscosity and increased ocular permanence (13,14). Cystadrops is currently in Phase III trials; however, the European Medicines Agency has recently allowed it to be marketed as an orphan drug to facilitate access (15).

Access to foreign and/or orphan drugs can sometimes be delayed by the obligatory procedures and approvals required for their use. In addition, the sometimes-exorbitant price of these drugs can hamper access (16). In order to facilitate the treatment of ocular cystinosis, cysteamine eye drops as a compounded formulation are commonly prepared in hospital pharmacy services.

Two major problems are associated with these formulations. Firstly, cysteamine eye drops must be instilled every hour while the patient is awake to reduce the amount of corneal crystals. To optimise the formulation and avoid these difficult dosage schedules, our group developed a bioadhesive cysteamine hydrogel with high ocular permanence, which could be prepared by hospital pharmacy services (17,18). Secondly, there is a lack of studies on the stability of cysteamine formulations. The analysis of compounds with thiol groups has always proved difficult, owing to their susceptibility to oxidisation and the lack of a structural chromophore needed for their detection (19,20). Furthermore, the low molecular weight of cysteamine (MW = 77.15 g/mol) hinders its direct detection by mass detectors. Thus, the methods used to determine these types of compounds usually derivatize the cysteamine molecule before quantification (21).

The objective of this article was to determine the stability of a bioadhesive ophthalmic cysteamine hydrogel under different storage conditions.

2.2. MATERIALS AND METHODS

2.2.1. Preparation of 0.55 % ophthalmic cysteamine hydrogel

The preparation of the hydrogel is performed in 2 stages. Firstly, a sufficient quantity of cysteamine (BioXtra, Sigma-Aldrich) is gradually added to Balanced Salt Solution Alcon® and magnetically stirred over a period of 5 minutes to achieve a concentration of 0.55 %. While continuing to stir, hyaluronic acid (Acofarma®) is then added to achieve a final concentration of 0.4 %.

Secondly, the resulting hydrogel is vacuum filtered using a 0.22-µm membrane filter (Stericup® Merck Millipore ExpressTM PLUS 0.22 µm) and poured into 15-mL type-1 amber glass containers, adding 10 mL of hydrogel to each container. The remaining volume is filled with nitrogen gas, and the containers are closed. The entire process is performed under aseptic conditions using a horizontal laminar flow hood

2.2.2. Preservation conditions and study variables

The formulas were divided into 2 batches: those without preservatives and those with preservatives. The latter batches were prepared by adding 0.01 % Ethylene Diamine Tetraacetic Acid (EDTA) while dissolving the cysteamine. Half of the batches with and without preservatives were stored for 30 days at 22 °C (room temperature) and the other batches were stored at 4 °C (refrigerated). In the rest of this article, these formulations are referred to as HA (room temperature without EDTA), HAE (room temperature with EDTA), HN (refrigerated without EDTA), and HNE (refrigerated with EDTA).

Osmolality, pH, and cysteamine concentrations were assessed. Descriptive tests were based on transparency measurements, and microbiological tests were based on sterility testing.

All samples were allowed to reach and stay at room temperature for a minimum of 30 minutes to avoid measurement errors due to temperature variations. All tests were performed in triplicate and were conducted on days 0, 7, 14, and 30 after the preparation of the hydrogels.

2.2.3. Descriptive tests

The transparency of the samples was determined by measuring transmittance in the visible light range (380-780 nm) using a UV-VIS spectrophotometer (model 8452 Diode Array Spectrophotometer, Hewlett Packard). A blank was made with distilled water, the different formulations were placed in quartz cuvettes, and then transmittance was measured, thus obtaining a graph representing the percentage of transmitted light as a function of wavelength.

2.2.3.1. Physicochemical tests

2.2.3.1.1. *Determination of osmolality and pH*

Osmolality was measured using a vapour pressure osmometer (VAPRO 5520). 10 µL of each formulation was deposited on a disk of Whatman filter paper on the chamber. pH was determined using a Crison microph2001® pH-metre.

2.2.3.1.2. *Quantification of cysteamine*

A saturated solution of Ellman's reagent (5,5'-dithiobis-(2-nitrobenzoic acid)) was prepared as a derivatizing agent (22) (Figure 2.1), by dissolving 29.6 mg of the powder in 10 mL of 0.018 M aqueous NaOH. Subsequently, the solution was filtered through a 0.45 µm filter.

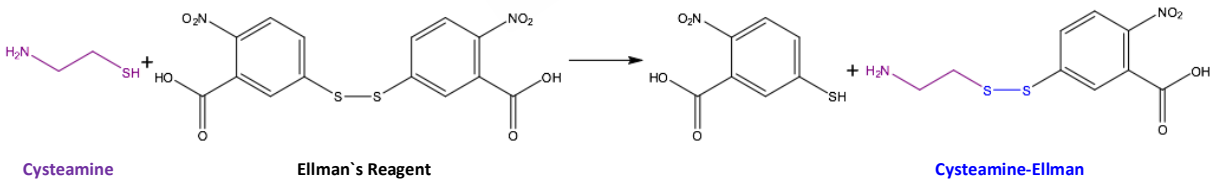

Figure 2.1. Cysteamine derivatization using Ellman´s reagent.

To quantify cysteamine, a 1:1000 dilution of the formulation was prepared. 100 µL of Ellman's reagent and 100 µL of purified water were added to this diluted sample. The resulting solution was analysed using an ultra-performance liquid chromatography-tandem mass spectrometer (UPLC–MS/MS) method. Measurements were taken using an Acquity UPLC® H-Class system (Waters® Milford, Massachusetts) coupled to a Xevo TQD mass spectrometer (Waters®). Data

were collected using Mass lynx v4.1 software and processed using Target LynxTM Application Manager chromatographic software. Chromatographic separation was conducted at 40 °C using an Acquity BEH C18 column (2.1 mm x 50 mm; particle size 1.7 µm) (Waters®). The mobile phase solvents used were a 0.1 % formic acid solution in water (MilliQ®) (Phase A) and acetonitrile (Phase B). A gradient with constant flow rate of 0.4 mL/min was used. The gradient was started at 100 % phase A, changing linearly to a 40 % A – 60 % B composition at 2.2 minutes, maintaining the composition until the 2.60-minute mark, and then returned to initial conditions at 3 minutes. The autosampler was set to 10 °C and 10 µL of each sample was injected. Total run time was 3 minutes, which included equilibration of the chromatographic system prior to sample injection. Mass spectrometry data were obtained using the multiple reaction monitoring (MRM) mode through positive electrospray ionization. Quantification was achieved by means of the transitions of the precursor ion at m/z 313 and the 196.85 fragment ion using a desolvation gas flow rate of 1.1 L/h, cone gas flow rate of 80 L/h, and a capillary voltage of 3.2 kV. Desolvation and source temperatures were 600 °C and 146 °C, respectively.

2.2.3.1.3. *Microbiological tests*

Each of the hydrogels was analysed on the aforementioned days to determine microbiological stability. 1 mL of each of the hydrogels was added to plates containing blood agar, sabouraud agar, and fluid thioglycolate medium. The samples were cultured at 37 °C for 48 hours, 15 days, and 10 days, respectively. At the end of each incubation period, the samples were inspected for any signs of microbiological growth.

2.2.4. Allowed variation range and statistical analysis

The Pharmaceutical Codex was used to establish the expiry date of the formulation, which was set (23) when there was a 10 % reduction of active ingredients compared to the initial concentration. Changes in pH and osmolality were considered unacceptable if their values exceeded the acceptance criteria for ophthalmic applications. Microbiological stability was considered acceptable providing no microbial growth was detected in the cultured samples. Finally, the product was considered unacceptable in the absence of complete transparency on descriptive tests.

The results of the different preservation conditions were compared by multivariate analysis of variance using Graph Pad Prism® v.6.01 software (2014; GraphPad Software, Inc., San Diego, CA, USA).

2.3. RESULTS

2.3.1. Descriptive and physicochemical tests

All the formulations were completely transparent and no decrease in transparency was observed over the study period. No signal was observed in the visible range, demonstrating the transparency of the sample (Figure 2.2).

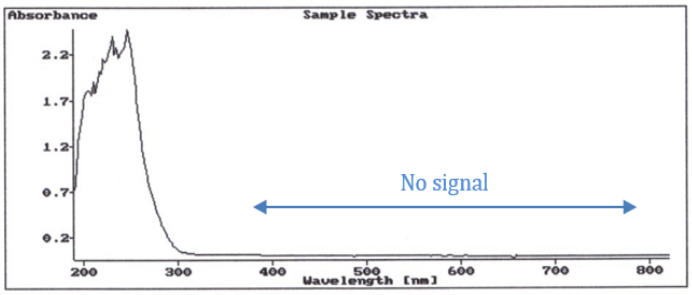

Figure 2.2. Graph obtained by determining the transparency of one of the formulations, showing negligible absorbance in the visible light spectrum (380-780 nm).

Figure 2.3 shows variations in osmolality of the cysteamine hydrogel under all four preservation conditions over time. Osmolality values of all formulations remained between 90 % and 100 % of the initial values over the study period. Under the different study conditions, no statistically significant differences were observed among the formulations, although those containing EDTA showed slightly higher values (427 ± 8.96 mOsm/Kg vs 410 ± 9.48 mOsm/Kg).

However, as shown in Figure 2.4, neither the addition of EDTA to the hydrogel nor storage temperature influenced the pH values of the hydrogel over the study period. Under all the conditions tested, no statistically significant differences were observed between the initial and final pH, except for a slight decrease in pH in the EDTA formulations (6.29 vs 6.44).

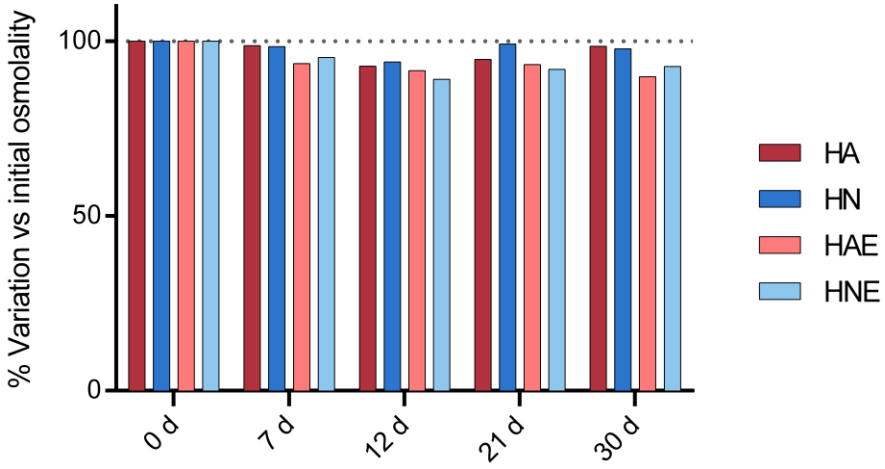

Figure 2.4. Percentage change in osmolality (mOsm/Kg) (mean ± SD) of cysteamine hydrogel over 30 days under the four different storage conditions. HA, room temperature without EDTA; HAE, room temperature with EDTA; HN, refrigerated without EDTA; HNE, refrigerated with EDTA.

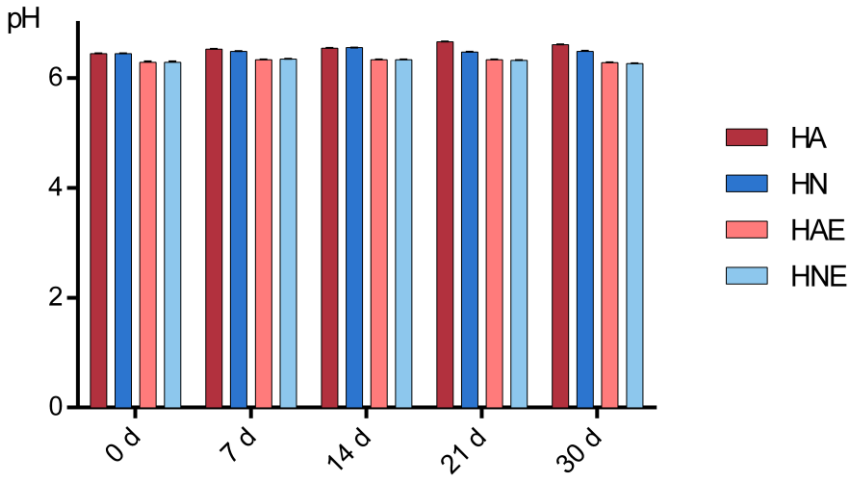

Figure 2.3. Change in pH (mean ± SD) of cysteamine hydrogel over 30 days under the four different storage conditions. HA, room temperature without EDTA; HAE, room temperature with EDTA; HN, refrigerated without EDTA; HNE, refrigerated with EDTA.

2.3.2. Concentration of cysteamine

A narrow, symmetrical, and well-defined chromatographic peak was obtained with an elution time of 0.33 minutes. Figure 2.5 shows an example chromatogram of the derivatised cysteamine obtained using the UPLC–MS/MS method.

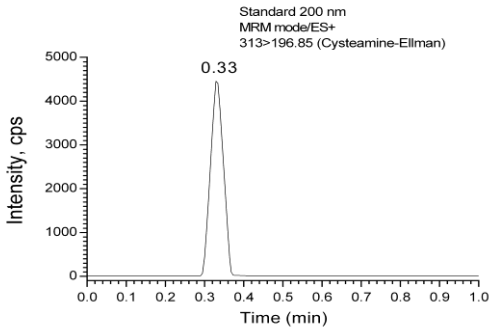

Figure 2.5. Example of chromatogram obtained for cysteamine derivatized with Ellman´s reagent, using the UPLC-MS/MS method.

The UPLC–MS/MS determination method employed is highly specific because it combines the efficiency of chromatographic separation and the high selectivity of a tandem mass detector to select the chemical structure to be determined. Using this method, the derivatised product was separated from any compounds that may have formed from cysteamine degradation.

Figure 2.6 shows variations in cysteamine concentrations over time under the four different storage conditions. Cysteamine concentrations did not fall below 90 % at any point during the study period. Nevertheless, it should be noted that a wide range of concentration values was observed at different time points during the storage period. Some samples had percentages of more than 100 % of the initial concentration. This variability was caused by the high viscosity of hydrogels, which makes it difficult to obtain reproducible volumetric samples by aspiration.

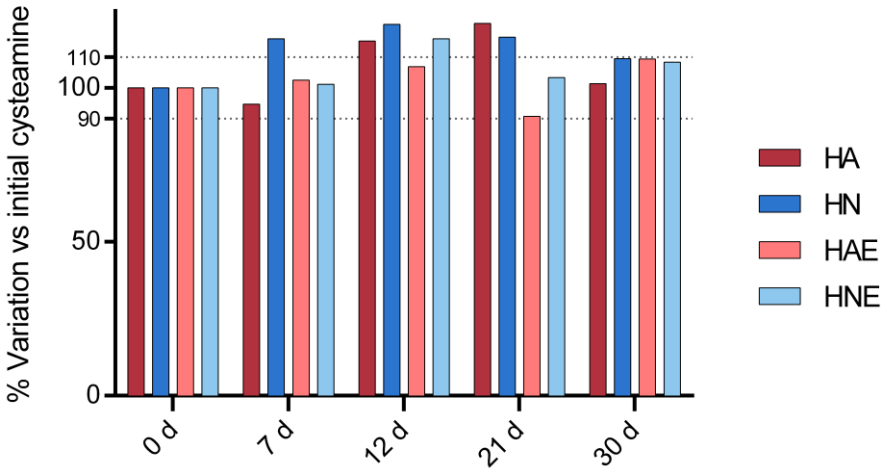

Figure 2.6. Percentage of change in cysteamine concentrations over 30 days. HA, room temperature without EDTA; HAE, room temperature with EDTA; HN, refrigerated without EDTA; HNE, refrigerated with EDTA.

2.3.3. Microbiological stability

Adequate storage of samples was maintained under all study conditions, and no microbial growth was observed in any of the hydrogels during the storage period.

2.4. DISCUSSION

Difficult dosage schedules are the major challenge to the use of ophthalmic compounded formulations of cysteamine hydrochloride because they require hourly instillations to reduce the amount of corneal crystals. A preclinical study has shown that the biopermanence of the hydrogel under study is similar to that of Cystadrops® (18). Quantitative PET biopermanence studies have shown that cysteamine hydrogel with hyaluronic acid has a 60-minute half-life, which is much higher than the 18-minute half-life of cysteamine eye drops typically prepared by hospital pharmacy services. In addition, more cysteamine reaches the stroma after administration of this hydrogel than reaches it with eye drops, and there are statistically significant differences in transcorneal permeation values between the two media. This hydrogel formulation achieves a controlled release of cysteamine over time and can be prepared by pharmacy services for patients with ocular cystinosis (17). Two preparation methods are presented in the supplementary materials.

Stability studies are a relevant technical and economic challenge for hospital pharmacy services and are becoming more frequent to guarantee the quality of the prepared drugs (24). The present study investigated the stability of cysteamine hydrogel with hyaluronic acid and showed that its properties were unchanged in a variety of storage conditions over the study period. Other authors have shown that at room temperature cysteamine oxidises into its cystamine dimer, which is ineffective for the removal of corneal cystine crystals (25). For this reason, nitrogen was used to remove environmental oxygen before sealing the containers.

The choice of EDTA as a preservative was based on previous publications, which have shown it to be the most suitable preservative for use in cysteamine formulations. The lowest possible concentration of EDTA was chosen to minimize potential toxicity on the corneal epithelium (20,26–28). Other preservatives, such as benzalkonium chloride, were ruled out after an unfavourable benefit-risk assessment by ophthalmologists. This decision was based on their

potential epithelial toxicity, which would be higher during the chronic use of the hydrogel under study (29).

According to the United States Pharmacopoeia, the stability of a compounded formulation is defined as the amount of time during which a product maintains, within very specific limits, the properties and characteristics that it possessed at the time of manufacture, throughout storage, and during use (30). Stability studies determine how the quality of a drug varies over time under the influence of a number of factors and use this information to provide recommendations on its expiration date and storage conditions. Over the study period, the pH and osmolality of the hydrogels remained practically constant, with no statistically significant differences ($\alpha < 0.001$) between the initial and final values under all storage conditions. The addition of EDTA to the formulation led to a slight increase in osmolality and a decrease in pH without affecting the stability of cysteamine. All the measures applied showed that transparency was 100 %. Cysteamine hydrogel with hyaluronic acid maintained its properties for 30 days after preparation. However, because the addition of EDTA did not improve stability and the use of benzalkonium chloride as a preservative was discarded, it is recommended that the hydrogel should be stored in a refrigerator to prevent microbiological growth and as an alternative method to sealing the containers with nitrogen (31).

2.5. CONCLUSION

The properties of cysteamine hydrogel have been described in previous studies and the results of this stability study show that the use of cysteamine hydrogel may increase therapeutic benefit in patients with ocular cystinosis. In addition, this formulation may be an effective alternative to those not marketed in Spain, but which are available for importation. The cost of imported formulations is €37,728/y/patient, whereas the estimated cost of producing the formulation is €1,080/y/patient.

The authors conducted a survey using the mailing list of the Spanish Society of Hospital Pharmacy (SEFH) and estimated that there are currently 39 patients under treatment with ocular topical cysteamine in Spain. Thus, the cost of this drug acquired through the Access to Medicines not Authorized in Spain process would be €1,

471,392/y. The use of cysteamine hydrogel prepared in hospital pharmacy services would provide patients with better access to treatment and achieve significant savings for the Spanish National Health System.

2.6. REFERENCES

1. Gahl WA, Thoene JG, Schneider JA. Cystinosis. N Engl J Med. 2002 Jul 11;347(2):111–21.
2. Linkage of the gene for cystinosis to markers on the short arm of chromosome 17. The Cystinosis Collaborative Research Group. Nat Genet. 1995 Jun;10(2):246–8.
3. Town M, Jean G, Cherqui S, Attard M, Forestier L, Whitmore SA, et al. A novel gene encoding an integral membrane protein is mutated in nephropathic cystinosis. Nat Genet. 1998 Apr;18(4):319–24.
4. Burki E. Ueber die Cystinkrankheit im Kleinkindesalter unter besonderer Berücksichtigung des Augenbefundes [About the Cystinosis in infancy with special reference to eye findings]. Ophthalmologica. 1941;101:331–342.
5. Gahl WA, Kuehl EM, Iwata F, Lindblad A, Kaiser-Kupfer MI. Corneal crystals in nephropathic cystinosis: natural history and treatment with cysteamine eyedrops. Mol Genet Metab. 2000 Oct;71(1–2):100–20.
6. Pubchem. Cysteamine (C2H7NS) [Internet]. [cited 2017 Jun 22]. Available from: https://pubchem.ncbi.nlm.nih.gov/compound/2-Aminoethanethiol
7. Thoene JG, Oshima RG, Crawhall JC, Olson DL, Schneider JA. Cystinosis. Intracellular cystine depletion by aminothiols in vitro and in vivo. J Clin Invest. 1976 Jul;58(1):180–9.
8. Brodin-Sartorius A, Tête M-J, Niaudet P, Antignac C, Guest G, Ottolenghi C, et al. Cysteamine therapy delays the progression of nephropathic cystinosis in late adolescents and adults. Kidney Int. 2012 Jan;81(2):179–89.
9. Kaiser-Kupfer MI, Caruso RC, Minkler DS, Gahl WA. Long-term ocular manifestations in nephropathic cystinosis. Arch Ophthalmol Chic Ill 1960. 1986 May;104(5):706–11.
10. Cysteamine Eye Drops to Treat Corneal Crystals in Cystinosis. Clinical Trial. [Internet]. Clinicaltrials.gov (A service of the U.S. National Institutes of Health). [cited 2016 May 6]. Available from: https://clinicaltrials.gov
11. Kaiser-Kupfer MI, Gazzo MA, Datiles MB, Caruso RC, Kuehl EM, Gahl WA. A randomized placebo-controlled trial of cysteamine eye drops in nephropathic cystinosis. Arch Ophthalmol Chic Ill 1960. 1990 May;108(5):689–93.
12. Cystaran®. Prescribing information [Internet]. 2016 [cited 2016 May 3]. Available from: www.sigmatau.com
13. Cystadrops® 0,55% eye drops solution. Summary of product characteristics. 2015.
14. Cystadrops® 0,55% collyre en solutions. Protocole d'utilisation therapeutique et de recueil d'informations. Autorisation temporaire d'utilisation dite de cohorte. 2013.

15. Cysteamine Hydrochloride for nephropathic Cystinosis, open-label Phase III pivotal study (CYSTADROPS CHOC study) [Internet]. Clinical Trials Register. 2016 [cited 2016 Jun 18]. Available from: www.clinicaltrialsregister.eu

16. Velásquez G. El acceso global a los medicamentos en el contexto internacional actual. Biomédica. 2011 Jun;31(2):162–3.

17. Luaces-Rodríguez A, Díaz-Tomé V, González-Barcia M, Silva-Rodríguez J, Herranz M, Gil-Martínez M, et al. Cysteamine polysaccharide hydrogels: study of extended ocular delivery and biopermanence time by PET imaging. Int J Pharm [Internet]. Available from: http://www.sciencedirect.com/science/article/pii/S0378517317305689

18. Fernández Ferreiro A, Luaces-Rodriguez A, González Barcia M, Otero Espinar FJ, Lamas MJ. Evaluación de la biopermanencia ocular in vivo de tres formulaciones oftálmicas de cisteamina clorhidrato. Farm Hosp. 2016 Apr 10;61 Congreso SEFH.

19. Guan X, Hoffman B, Dwivedi C, Matthees DP. A simultaneous liquid chromatography/mass spectrometric assay of glutathione, cysteine, homocysteine and their disulfides in biological samples. J Pharm Biomed Anal. 2003 Feb 26;31(2):251–61.

20. Lawal B. Development of a cysteamine in situ gelling system for the treatment of corneal crystals in cystinosis [Internet]. 2008 [cited 2016 Feb 3]. Available from: https://cystinosis.org/images/research/updates/CRN_Research_UpdateB.pdf

21. Qi B-L, Liu P, Wang Q-Y, Cai W-J, Yuan B-F, Feng Y-Q. Derivatization for liquid chromatography-mass spectrometry. TrAC Trends Anal Chem. 2014 Jul 1;59:121–32.

22. Ellman GL. Tissue sulfhydryl groups. Arch Biochem Biophys. 1959 May;82(1):70–7.

23. Royal Pharmaceutical Society of Great Britain Dept of Pharmaceutical. The Pharmaceutical Codex: Principles and Practice of Pharmaceutics. Twelfth Edition. London: Pharmaceutical Press; 1994. 1117 p.

24. Barrueco N, Escobar Rodríguez I, García Díaz B, Gil Alegre ME, López Lunar E, Ventura Valares MG. Estabilidad de medicamentos en la práctica clínica: de la seguridad a la eficiencia. Farm Hosp. 2013 Jun;37(3):175–7.

25. Iwata F, Kuehl EM, Reed GF, McCain LM, Gahl WA, Kaiser-Kupfer MI. A randomized clinical trial of topical cysteamine disulfide (cystamine) versus free thiol (cysteamine) in the treatment of corneal cystine crystals in cystinosis. Mol Genet Metab. 1998 Aug;64(4):237–42.

26. Herreros JMA. Preparación de medicamentos y formulación magistral para oftalmología. Ediciones Díaz de Santos; 2003. 164 p.

27. Fernández MA, Atienza JM, Vayo CÁ del. Formulación en farmacia pediátrica. A. Madrid Vicente; 2011. 273 p.

28. Asociación de Formulistas de Andalucia [Internet]. 2016 [cited 2016 May 28]. Available from: http://www.formulistasdeandalucia.es/noticia.php?id=264

29. Rosin LM, Bell NP. Preservative toxicity in glaucoma medication: clinical evaluation of benzalkonium chloride-free 0.5% timolol eye drops. Clin Ophthalmol Auckl NZ. 2013;7:2131–5.

30. Convention USP. Farmacopea de los Estados Unidos de América, USP 37, 2014: Formulario nacional, NF 32. United States Pharmacopeia; 2013. book.

31. Practical Pharmaceutics - An International Guideline for the | Yvonne Bouwman | Springer [Internet]. [cited 2017 Jun 22]. Available from: http://www.springer.com/gp/book/9783319158136

USC
UNIVERSIDADE
DE SANTIAGO
DE COMPOSTELA

Chapter 3. Intravitreal anti-VEGF drug delivery systems for age-related macular degeneration

USC
UNIVERSIDADE
DE SANTIAGO
DE COMPOSTELA

3. INTRAVITREAL ANTI-VEGF DRUG DELIVERY SYSTEMS FOR AGE-RELATED MACULAR DEGENERATION

3.1. INTRODUCTION

Age-related macular degeneration (AMD) is the most common cause of vision loss in elderly people in developed countries and the estimated global prevalence is projected to be 288 million in 2040 (1). AMD is a common acquired degenerative disease characterised by the presence of drusen deposits affecting the interface between the retinal pigmented epithelium and Bruch's membrane (2). AMD has been divided into two major subtypes: non-neovascular or dry AMD and wet or exudative AMD (w-AMD). w-AMD is characterised by the development of choroidal neovascularisation and causes most of the cases of severe vision loss. For this reason, most of the pharmacological research have been done in the field of w-AMD (3). Anti-vascular endothelial growth factor (anti-VEGF) therapy is the gold standard treatment of w-AMD (4). Nowadays, in clinical practice, three anti-VEGF agents are commonly used (bevacizumab, aflibercept and ranibizumab) (5). These drugs are injected intravitreally and block the growth of abnormal blood vessels in the choroid improving visual acuity (6). Ranibizumab (Lucentis®, Genentech, Inc.) and aflibercept (Eylea®, Bayer AG) are also approved for the treatment of choroidal neovascularisation (CNV), diabetic macular oedema (DME) and macular oedema secondary to retinal vein occlusion (branch RVO or central RVO) (7,8).

Normally, in order to achieve a sustained therapeutic drug concentration in the vitreous, administration frequency should be based on the half-life of the drug ($t_{1/2}$), but the information on anti-VEGF ocular pharmacokinetics is very limited. In this sense, the frequency of administration of anti-VEGF drugs plays a key role, being currently not homogenised in clinical practice and coexisting different administration schedules (9).

Decreasing the number of visits to the ophthalmologist and the number of intravitreal injections is one of the priority goals in AMD research (6). Research of intravitreal drug delivery systems (DDSs) stems from the need to minimise repeated intravitreal injections of anti-VEGF antibodies, which thereof will decrease the risk of adverse effects and will optimise the public economic expense that these patients require. Although various strategies for the intravitreal delivery of anti-VEGF macromolecules are currently under development, most of them are in very early stages of research, some of them reaching preclinical studies and just a few clinical trials (10).

The design of novel intravitreal DDSs presents great challenges. On the one hand, the systems should be in the micro/nano scale as they need to ft inside the vitreous chamber, while simultaneously allowing high dose loading in order to obtain effective monoclonal antibody (mAb) concentrations during extended periods of time. Moreover, a hurdle in the development of antibody release formulations is maintaining the antibody stability and bioactivity for a long-time during storage and *in vivo* release (11).

In the following sections, different long release formulations developed as well as preclinical pharmacokinetics studies available of intravitreal anti-VEGF antibodies used in AMD will be discussed.

3.2. DRUG DELIVERY SYSTEMS (DDSS)

Although the variability of DDSs intended for intravitreal administration has raised in the last decade and it continues increasing, the main DDSs studied for intravitreal anti-VEGF antibodies are hydrogels, liposomes, particulate systems (microparticles (MPs) and nanoparticles (NPs)), implants and the combination of two of the aforementioned systems (composite systems) (Figure 3.1).

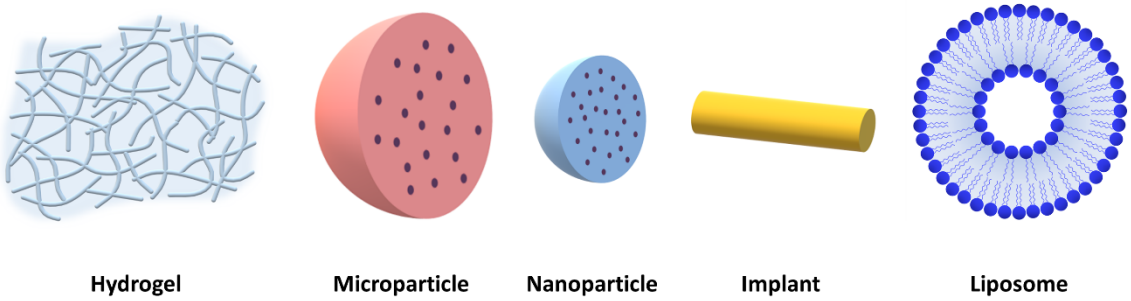

Figure 3.1. Types of drug delivery systems intended for intravitreal sustained delivery of anti-VEGF antibodies.

3.2.1. Hydrogels

Hydrogels are networks of polymer chains that have the property of extensive swelling with water, which they retain within its structure. Their porosity and high-water content make hydrogels suitable for encapsulation of water-soluble drugs, such as biomacromolecules since they are processed at room temperature and organic solvents are rarely needed (12,13).

Hydrogels can be classified as biodegradable and non-biodegradable (14). The main advantage of using biodegradable hydrogels is that just the initial intravitreal injection is needed for the implantation of the DDS, and after that they are completely degraded after a certain period of time in the body. Moreover, compared to the non-bioerodible hydrogels, biodegradable hydrogels do not require surgical removal, which decreases the probability of associated complications (14). Biodegradable hydrogel drug release follows a diffusion-controlled release at initial times and then diffusion and degradation co-exist as mechanisms for drug release (15).

Biodegradable hydrogels can be designed from natural or synthetic polymers (12,13). The most used synthetic polymers intended for intraocular administration are poly(ethylene glycol) (PEG), poly(lactic acid-co-glycolic acid) (PLGA), poly-ε-caprolactone (PCL) and mixtures of these and with others. Natural polymers include hyaluronic acid (HA), chitosan, alginate, dextrans and silk polymers, which present the advantage of minimal toxicity due to their high compatibility (14). However, their disadvantage is considerably shorter drug release compared to synthetic hydrogels, which limits their use as long-term sustained DDSs (15).

All the DDSs developed in this field have used bevacizumab as drug loaded within the hydrogel, with no data regarding inclusion of ranibizumab nor aflibercept in any type of hydrogels (Table 3.1). Considering the substantial benefits of biodegradable hydrogels for the intraocular use, most authors have attempted to create biodegradable hydrogels.

Table 3.1. Bevacizumab-loaded hydrogels intended for intravitreal injection.

Temperature sensitivity	**Polymers**				***In vitro* release test**				**Ref.**
	Composition	Origin	Biodegradability	Conc. (w/v)	% BR	Time BR	% CR	Time CR	
Thermosensitive	ESHU	Synthetic	Biodegradable	15 %	10-35 %	0 h	95-100 %	17 w	(16,17)
				20 %	10-20 %	0 h	85-95 %	17 w	
	mPEG-PLGA-BOX	Synthetic	Biodegradable	20 %	*		55 %	30 d	(15)
				35 %	*		65 %	30 d	
	PLGA-PEG-PLGA	Synthetic	Biodegradable	20 %	15 %	6 h	18 %	14 d	(18)
	PEOz-PCL-PEOz	Synthetic		20 %	*		80 %	20 d	(19)
	PNIPAm-PEG DA	Synthetic	Non-biodegradable		60 %	5 d	88 %	28 d	(20)
	Glycol Chitosan/ Oxidised Alginate	Natural	Biodegradable	0.8/0.5-2 %	30 %	4 h	100 %	3 d	(21)
Non-thermosensitive	PEG-Mal / PEG-SH	Synthetic	Biodegradable	10/7.5 %	20 %	1 d	70 %	14 d	(22)
	HA-VS / Dex-SH	Natural	Partially biodegradable		40 %	1 d	60 %	90 d	(23)
	Silk fibroin	Natural	Biodegradable	2 %		7 d	40 %	91 d	(24)

BR = burst release; CR = final cumulative release
* No burst release found

3.2.1.1. Thermosensitive hydrogels

Hydrogels which have a spontaneous sol-gel phase transition with temperature elevation are referred to as thermosensitive hydrogels. Ideally, the material should be in solution phase at room temperature and form a physical gel when placed at 35-37 °C (physiological temperature) (25).

In recent years, copolymers of hydrophilic biocompatible PEG with biodegradable and biocompatible substances have been gaining attention as promising thermosensitive biomaterials in ocular drug development (25). The main advantages of PEG hydrogels are their biocompatibility, non-toxicity, hydrophilicity, tuneable degradability and its easiness of mixing with other polymers (14).

In order to take advantage of these characteristics, Park et al. designed a thermoresponsive hydrogel formed by the polymer poly(ethylene glycol)-poly-(serinol hexamethylene urethane) (ESHU). Their experiments *in vitro* showed that bevacizumab release was sustained without reaching plateau during the 17-week observation period and showed good cytocompatibility with ocular cells. Higher drug loading and higher polymer concentration resulted in lower initial burst release effect and a more rigid hydrogel (16). *In vivo* experiments in New Zealand white rabbits demonstrated that after intravitreal administration of 1.25 mg bevacizumab in 15 % ESHU (in a volume of 50 µL), bevacizumab concentration in the aqueous humour was 4.7-fold higher compared to the control and was maintained for 9 weeks (17). This study showed for the first time the *in vivo* release of bevacizumab from thermoresponsive hydrogels demonstrating the viability of these hydrogels as DDSs for antibodies.

PEG can be also part of amphiphilic gels (hydrophilic and hydrophobic), such as the thermosensitive gel prepared by Hu et al. which consists of block copolymers of methoxy-poly(ethylene glycol)-blockpoly (lactic-co-glycolic acid) synthesised with ring-opening polymerisation, and cross-linked with 2,2-bis (2-oxazoline) (mPEG-PLGABOX). *In vitro* experiments showed that the release of bevacizumab from 20 % (w/w) and 25 % (w/w) mPEG-PLGA-BOX hydrogels lasted up to a month, with no significant burst effect. In addition, at day 30 the total cumulative release of bevacizumab from these hydrogels were 55 % and 65 %, respectively (15). Despite their promising results, further studies would be needed to analyse the potential *in vivo* effects.

Xie et al. also employed PEG to synthesise their thermoresponsive gel formed by poly(lactic acid-co-glycolic acid)-poly(ethylene glycol)-poly(lactic acid-co-glycolic acid) (PLGA-PEG-PLGA). In this case, *in vitro* studies revealed an initial burst release of bevacizumab (15 % released in the first 6 h) followed by a slowly released phase for up to 14 days. Regarding *in vivo* studies, 1.5 µL of the hydrogel (18.75 µg bevacizumab, 20 % (w/v) PLGA-PEG-PLGA) were intravitreally administered to Sprague-Dawley rats. One day after injection, bevacizumab concentrations in the vitreous humour reached 56.56 µg/mL and 59.31 µg/mL for bevacizumab aqueous solution and the bevacizumab/hydrogel, respectively. At 4 weeks after drug administration, bevacizumab concentration in the vitreous humour was 0.03 µg/mL in animals injected with

the bevacizumab-loaded hydrogel, while no drug was detected in the vitreous humour of animals injected with bevacizumab aqueous solution (18). As it has been shown, minor differences were detected by the authors between bevacizumab release from aqueous solution and hydrogel so these results should be interpreted cautiously.

Using other polymers, Wang et al. created a biodegradable hydrogel consisting of the triblock polymer poly(2-ethyl-2-oxazoline)-b-poly(ε-caprolactone)-b-poly(2-ethyl-2-oxazoline) (PEOz-PCL-PEOz). This hydrogel showed that bevacizumab was *in vitro* released at a constant rate of 40 µg/day for 11 days without an initial burst effect and that 80 % of the loaded bevacizumab was released in 20 days (19). Nevertheless, therapeutic concentrations were not achieved at initial times with this hydrogel.

Other authors have evaluated the potential usefulness of preparing non-biodegradable hydrogels. A thermoresponsive poly(N-isopropylacrylamide) cross-linked with poly(ethylene glycol) diacrylate (PNIPAm-PEG DA) hydrogel have been prepared by the group of Awwad et al. *In vitro* studies showed a bimodal release profile formed by a first burst phase (60 % of bevacizumab cleared after 5 days) followed by a slower prolonged release phase until day 28 (20). However, they have not addressed in animal models the consequences of injecting non-biodegradable polymers.

Natural polymers have also been used as potential intravitreal hydrogels. Xu et al. synthesised composite polysaccharides cross-linked hydrogels (homogeneously mixing different amounts of oxidised alginate and glycol chitosan water solution). They performed several *in vitro* studies which demonstrated that 30 % of bevacizumab was released from hydrogels within the first 4 h, while nearly 100 % of bevacizumab was released in 3 days (21). This short release time demonstrates the typical more rapid release of hydrogels formed with natural polymers.

3.2.1.2. Non-thermosensitive hydrogels

Yu et al. elaborated another type of gels which also contain PEG but its gelation behaviour is less affected by temperature changes. These authors prepared an in situ covalently cross-linked PEG hydrogel via thiol-maleimide reaction using 4-arm PEG-Mal and 4-arm PEG-SH. According to the *in vitro* studies, an increase in cross-linking density in these gels produces a

decrease in the release rate of bevacizumab. For that reason, the slowest release was achieved by the hydrogel with the highest cross-linking density (7.5 % (w/v) 4-arm PEG-SH solution) with approximately 20 % bevacizumab released within one day and nearly 70 % bevacizumab released in the following 14 days (22). In this sense, the most interesting characteristic of this hydrogel is that its gelling time, pore size, swelling ratio and mechanical properties can be controlled by modulating the concentration of 4-arm PEG-SH.

In this sense, a vinylsulfone functionalised hyaluronic acid (HA-VS) and thiolated dextran in situ hydrogel (formed by catalyst-free chemical crosslinking) was synthesised including bevacizumab. *In vitro* test showed around a 40 % burst release within the first day and a final cumulative release of 60 % at day 90. They tested the developed hydrogel in New Zealand white rabbits (volume injection of 40 µL), demonstrating that the bevacizumab concentration in the vitreous was at a therapeutically relevant level (around 50 µg/mL) at 6 months after injection and about 107-fold higher compared to a bevacizumab solution. Moreover, authors claim that protein stability is not compromised as there are no hydrophobic interactions between the antibody and the polymer (23).

Regarding natural polymers, Lovett et al. synthesised a hydrogel based on silk fibroin. They tested a standard dose (1.25 mg bevacizumab) and a high dose (5.0 mg bevacizumab) in hydrogel formulations. Both types of hydrogels showed a high burst release until day 7 and a cumulative final release of 40 % and 62 % after 91 days, respectively. The standard dose control fell below the limit of quantitation after 30 days. These hydrogels were intravitreally injected in Dutch-belted rabbits (50 µL/eye), finding vitreous half-lives of 10 days for the high dose hydrogel and 13.1 days for the standard dose, which were significantly higher compared to the standard dose control (4.32 days). Considering these results at 90 days for the hydrogels and 30 days for the control, the authors conclude that these gel formulations can provide therapeutic levels of bevacizumab for at least three times longer than using the solution dosage (24). However, some mild inflammation has been found in the vitreous and cornea in the rabbits following hydrogel injection, which could compromise their good release results.

3.2.2. Liposomes

Liposomes consist of one or more outer lipid bilayers ranging in size from 0.01 to 1 µm. They are composed of phospholipids and cholesterol and present an aqueous internal compartment. They have many features such as biocompatibility, biodegradability, amphipathic nature and the ability to increase half-life of the encapsulated drugs, which make them a very useful DDS (26,27).

Abrishami et al. proposed nanoliposomes encapsulating bevacizumab for intravitreal administration prepared by a dehydration-rehydration method. These nanoliposomes were composed by a phospholipid (egg phosphatidylcholine) and cholesterol in a 1:1 M ratio, which were dissolved in a minimum amount of methanol:chloroform (2:1). They obtained multilamellar vesicles with an EE % of 45.5 % which were posteriorly tested in New Zealand albino rabbits (1.25 mg bevacizumab injected). After 42 days, concentration of liposomal bevacizumab was more than 5-fold higher compared to bevacizumab solution. In addition, area under the drug concentration time curve for liposomal bevacizumab was 1.5-fold higher (28).

The use of bevacizumab-loaded multivesicular liposomes (BevMVLs) prepared by double emulsification method (W/O/W) constitutes another form to prolong the release of anti-VEGF agents in the eye. In this sense, Mu et al. prepared these vehicles by adding bevacizumab into a lipid mixture solution (containing 1,2-dioleoyl-sn-glycero-3-phosphocholine, 1,2 dipalmitoyl-sn-glycero-3-phosphoglycerol, cholesterol and triolein) with a volume ratio of 1:1, obtaining an EE % of 80.65 %. Regarding the *in vitro* release profile, the initial burst release was lower than 30 % and at day 13 approximately 90 % bevacizumab was released. After intravitreal administration in New Zealand albino rabbits (0.25 mg bevacizumab/10 µL), bevacizumab-loaded multivesicular liposomes showed a 2-fold higher half-life both in the vitreous (8.84 d) and aqueous humour (8.26 d) compared to bevacizumab solution (4.45 d and 4.23 d, respectively). Final concentrations were 0.34 µg/mL and < 0.01 µg/mL at day 56, respectively. The area under the drug concentration of bevacizumab-loaded multivesicular liposomes was 2-fold greater than bevacizumab solution, both in the vitreous humour and aqueous humour (29).

3.2.3. Particulate systems

Nanosized and microsized particles can be used as DDSs for intravitreal administration as they permit to extend half-life in the vitreous humour, since they release the drug in a more controlled manner and are less affected by the vitreous clearance mechanisms (30).

Based on their size, polymeric particulates can be classified as NPs if the diameter is between 1 and 1000 nm and as MPs if the size is between 1 and 1000 µm (31,32). Most of the NPs developed present a particle size between 20 and 500 nm.

Both NPs and MPs can be divided into two subtypes according to their structure: nano/microcapsules for reservoir structures or nano/microspheres for matrix structures. The drug is dispersed in the matrix polymer in the nano/microspheres whereas the nano/microcapsules follow a core-shell structure, where the core is composed of the drug surrounded by a polymeric layer (Figure 3.2).

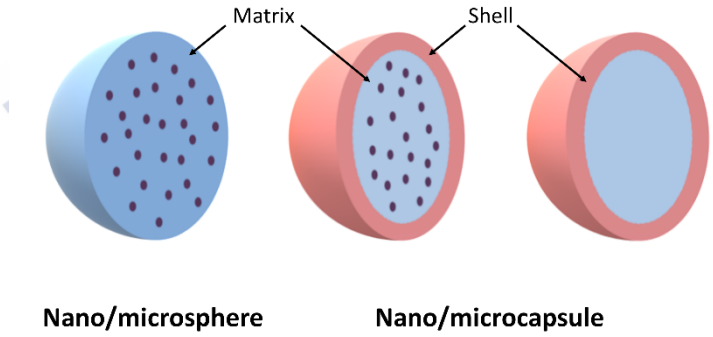

Figure 3.2. Two different structures of nano/microparticles: nano/microspheres (matrix) and nano/microcapsules (core-shell).

Although NPs and MPs seem to prolong their residence time in the vitreous humour, the correlation between the particle size and its vitreous half-life has not been properly defined (33,34). The work performed by Xu et al. in fresh *ex vivo* bovine vitreous concluded that surface charge was a decisive factor in the NPs' behaviour in the vitreous. They claimed that positive-charged NPs at the vitreous pH were immobilised in contrast to negative-charge ones, which freely diffused. On the contrary, in the case of MPs, the size is a more important factor as they found steric hindrance through the gel-like structure of the vitreous (21).

A study showed that NPs with a particle size lower than 200 nm were able to penetrate the retina of rabbits whereas MPs 2 µm in size were maintained within the vitreous humour (35). Therefore, although there is evidence of the introduction and retention of NPs in the retina, it needs still to be addressed whether it would offer substantial benefits to retinal diseases compared to MPs (34). Nevertheless, it is considered that the release time provided by NPs is shorter compared to the MPs (36). Therefore, their usefulness lies in their retina penetration characteristics and cell internalisation (36).

In order to be able to inject the NPs/MPs with a needle and without performing a surgical incision, the NPs/MPs need to be suspended in a compatible medium. In this sense, parameters as syringeability and injectability are of great importance for the development of intravitreal formulations (33). However, this issue is not always addressed by researchers.

Polymeric NPs or MPs can be prepared using various natural or synthetic materials, which should be compatible and inert. Regarding anti-VEGF drugs, our review showed that the most addressed polymer is PLGA, which have been used for the preparation of either NPs or MPs. Chitosan-based NPs have also been investigated for bevacizumab. However, these studies are just focused on the development of the NPs/MPs and their characterisation, some of them going as far as to test the DDSs on animal models, but none of them have reached a clinical stage.

3.2.3.1. PLGA nanoparticles and microparticles

PLGA is a widely used biodegradable polymer in the field of controlled release systems of proteins (37). It is one of the most popular biodegradable polymers due to its favourable degradation properties, its clinical experience, its sustained delivery of drugs and the various possibilities to form different DDSs (37). It is a biocompatible polymer approved by the US Food and Drug Administration (FDA) and the European Medicine Agency (EMA).

Both NPs and MPs made from PLGA have been explored as delivery systems for macromolecules, although none of them have reached its commercialisation (38). Despite the general advantages of PLGA particles, there are still some issues to account for: the instability of the antibodies through the process of NP/MP preparation, which involves conditions such

as using organic solvents, sonication, high temperature, high pressure… This may lead to a decrease in the antibody bioactivity through denaturation or aggregation of the mAbs (39).

The poly(D,L-lactide-co-glycolide) used in the studies significantly differs among the MPs/NPs prepared with this polymer. The most used PLGA presents a free carboxylic acid as an end-group and a PLA:PGA ratio of 50:50 (40–44), which has considered to exhibit the fastest degradation (37), although some had used a ratio of 75:25 (45).

There are various techniques to fabricate PLGA NPs/MPs, being the modified double-emulsion solvent evaporation the most common method. This strategy permits to encapsulate hydrophilic compounds such as antibodies and to obtain particles with a composition of water-in-oil-in-water (W/O/W). One of its advantages is the possibility of controlling the particle size until a certain point, which is the reason why either NPs or MPs can be obtained through this method. However, it presents the inconveniences of polydispersity on the particle size, batch-to-batch variance and the instability mentioned above (38). This technique has produced particles encapsulating anti-VEGF antibodies with, in general, encapsulation efficiencies (EE %) higher than 80 % for NPs (41,43,46,47) and MPs (44,45).

Another method for the preparation of PLGA NPs/MPs is via solid-in-oil-in-water (S/O/W) (40,44), but the EE % is normally considerably lower compared to the W/O/W NPs/MPs for the anti-VEGF encapsulation. One problem of this method is the need of converting the commercial solutions of the anti-VEGF antibodies to the solid form, mainly through a lyophilisation process. A variation of this method is the solid-in-oil-in-hydrophilic oil (S/O/hO) used by Ye et al. (48).

The differences in the PLGA used, the method followed, the particle size obtained, the encapsulation efficiency and the antibody employed make that the *in vitro* release tests show completely different results from the different NPs/MPs prepared with anti-VEGF antibodies and impossible to compare (Table 3.2). However, most of the studies followed the general triphasic release profile of PLGA NPs/MPs, which consists of an initial burst release phase, followed by a sustained release phase and a final third rapid release phase (49,50) (Figure 3.3). The burst release is considered to be caused by the release and dissolution of the proteins adhered to the particle surface. During the second phase, an almost constant drug release

rate is obtained, which must be owed to the diffusion of the antibodies through the polymeric network by small pores. The third phase is normally related to the degradation of the PLGA, either way by bulk erosion or surface erosion (33,49,50).

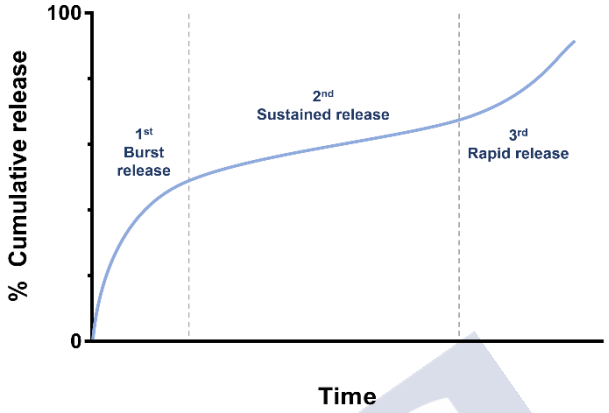

Figure 3.3. Typical triphasic release profile of PLGA nano/microparticles: initial burst release phase, intermediate sustained release phase and final rapid release phase.

Table 3.2. Bevacizumab-, ranibizumab- and aflibercept-loaded PLGA nanoparticles and microparticles intended for intravitreal injection.

Antibody	Method	Particle size	EE %	*In vitro* release test				*In vivo* PK studies			Ref.
				% BR	Time BR	% CR	Time CR	Species	T_{max}	$t_{1/2}$	
Bevacizumab	W/O/W	299.8 nm	82 %			20 %	7 d				(43)
	W/O/W	90 nm	80 %	40 %	2 h	90 %	21 d	Mice	6 d	8.65 d	(51)
	W/O/W	190 nm	84 %			10 %	3 d	Rabbit	7 d	8.42 d	(41,42)
	W/O/W	0.2-1 µm	90 %	*		47 %	91 d				(47)
	S/O/W	819 nm									(40)
	S/O/W	14 µm	35 %	9 %	1 h	76 %	50 d				(52)
	S/O/hO		49 %					Rabbit	3 d	10.2 d	(48)
Ranibizumab	W/O/W	20 µm	89 %	60 %	3 d	100 %	45 d				(45)
	W/O/W	209 nm	40 %	66 %	1 d	75 %	7 d				(44)
	W/O/W	112 µm	83 %	35 %	1 d	39 %	7 d				(44)
	S/O/W	70 µm	22 %	23 %	1 d	48 %	15 d				(44)
	Coaxial electrospray	2.36 µm	70 %								(46)
Aflibercept	W/O/W	243.13 nm	76 %	20 %	2 h	74 %	7 d				(53)

BR = burst release; CR = final cumulative release; EE % = encapsulation efficiency
* No burst release found

3.2.3.1.1. *PLGA nanoparticles*

The preparation of bevacizumab-loaded PLGA NPs via W/O/W emulsion technique has been investigated by several authors obtaining discrepant release results (41–43,51). Varshochian et al. have previously studied the protective effect of various stabilisers (sugars, amino acids, surfactants, polyvinyl alcohol (PVA), PEGs, proteins) in the preparation of bevacizumab-loaded PLGA NPs formulated by W/O/W. They concluded that interfacial adsorption of the bevacizumab was the most destabilising factor in the double emulsion method and that the addition of appropriate concentrations of albumin could decrease bevacizumab instability. *In vitro* release tests showed that less than 10 % of bevacizumab was released after 21 days and the conditions used were inappropriate compared to employing vitreous fluid, which showed a better release profile. The *ex vivo* release study in rabbit vitreous humour revealed an initial burst release of 10 % of the encapsulated bevacizumab and a final 40 % released after 6 weeks. Moreover, the last samples of the release tests showed aggregation and enlargement of the NPs (42).

The same authors performed an animal pharmacokinetic study in New Zealand albino rabbit eyes (1 mg bevacizumab/eye). The noncompartmental analysis showed an increased vitreal half-life by 1.6-fold of the PLGA NPs (8.42 days) versus an injection of free bevacizumab (5.19 days). Moreover, the maximum bevacizumab was obtained 7 days post-injection versus the control which was immediately following the intravitreal injection (41).

The main outcome of the study conducted by Sousa et al. is that they proved that freeze-drying process promoted nanoparticle aggregation and increased particle size compared to fresh NPs. Moreover, they found that PLGA NPs with bevacizumab exhibited a pH-dependent *in vitro* release profile, since the bevacizumab released percentage increased when increasing the pH. The released bevacizumab from their NPs was less than 20 % at 7 days at physiological pH (43).

Comparing these results to the release test performed by Zhang et al., they obtained that 40 % of the loaded bevacizumab was released during the first two hours and another 40 % following the next 7 days, They performed an *in vivo* pharmacokinetic study in mice (0.01 mg bevacizumab/eye) where they obtained a T_{max} of 7 days and a vitreous $t_{1/2}$ of 8.65 days for the

NPs, and a T_{max} immediately after intravitreal injection and a $t_{1/2}$ of 4.96 days for the bevacizumab control (51).

Solid-in-oil-in-water emulsion was also assessed as a method for the fabrication of bevacizumab-loaded PLGA NPs. NPs of 819 nm were obtained which produced a reduction in the choroidal neovascularisation (CNV) area on experimentally induced CNV rat models, suggesting that bevacizumab active antiangiogenic properties were maintained (40).

Ranibizumab and aflibercept were also tested as potential encapsulated drugs into PLGA particles. Chua et al. prepared ranibizumab-loaded PLGA MPs and NPs. Regarding the NPs, they obtained a rather low EE % and a high burst release of 66 % during the first day (44), which depicts the uselessness of this formulation as a long release system.

Only one study analysed the encapsulation of aflibercept in either NPs or MPs. Kelly et al. followed the double-emulsion diffusion method to obtain aflibercept-loaded PLGA NPs with a relatively high EE % of 75.76 % and with an *in vitro* release of 74.49 % at 7 days (53).

3.2.3.1.2. *PLGA microparticles*

Two different types of polymers were investigated in the Li et al. study for the preparation of bevacizumab MPs by a double-emulsion methodology: PLGA (50:50) and a diblock polymer of PEG(1000)-b-PLA(5000) (PEGLA15), which is more hydrophilic than the PLGA. PEGLA15 MPs presented a higher particle size (2-10 µm) than the PLGA ones (0.2-1 µm), although they both showed an EE % above 90 %. *In vitro* release study showed that only 47 % of bevacizumab was released from the PLGA MPs at 91 days in contrast to the 62 % released from the PEGLA15 MPs. Moreover, they tested two concentration of the loaded bevacizumab into the PLGA MPs, showing that the particles lost uniformity with increasing the bevacizumab loading from 1.6 % to 13 % bevacizumab/PLGA ratio (47).

Another study that used a mixture of PLGA and other polymer is the one carried out by Liu et al. They prepared freeze-dried dextran particles containing bevacizumab which were included into poly(lactide-co-glycolide)/poly(cyclohexane-1,4-diyl acetone dimethylene ketal (PLGA/PCADK) microspheres using a S/O/W emulsification method. The use of the polyketal

PCADK is justified by the authors because this polymer produces a smaller pH decrease through degradation compared to PLGA. Moreover, including bevacizumab into dextran particles could decrease the exposure of the antibody to the water-oil interface. PLGA/PCADK microspheres containing 20 % of PCADK showed an EE % of 35.32 % and a particle size of 13.70 µm. *In vitro* release test showed a minimal initial burst release (9.3 % in 1 h) and a steady sustained release behaviour with a cumulative release of 75.7 % at 50 days. In comparison with the same microparticles prepared by W/O/W method, a considerably decrease of the initial burst release was observed. The *in vivo* study performed in rabbits, injecting a dose of 0.4 mg bevacizumab, showed a higher AUC from the PLGA/PCADK microparticles compared to bevacizumab solution and PLGA MPs (52).

Bevacizumab was also encapsulated into PLGA MPs via a novel technique, solids-in-oil-in-hydrophilic oil (S/O/hO) method. In contrast to the more used S/O/W method, the external phase in this one is composed of 1 % PVA, propenyl alcohol and 5 % NaCl. The MPs showed an EE % of 49 % and an $t_{1/2}$ in the vitreous humour of 10.2 days in rabbit eyes (1.25 mg bevacizumab injected), which is considerably higher than the bevacizumab solution used as control (3.91 days). However, neither the bioactivity of bevacizumab after encapsulation nor the particle size was characterised. Moreover, it remains unclear the advantages of such system compared to the S/O/W or W/OW method (48).

Chua et al. prepared ranibizumab-loaded PLGA MPs and NPs. They compared two methods for the preparation of the MPs: via W/O/W and S/O/W emulsions. The S/O/W MPs showed a lower EE % of 22 % compared to the W/O/W (83 %) since the incorporation of solid antibody into a MPs is more difficult. However, S/O/W MPs showed a lower burst release of 23 % compared to the W/O/W MPs of 35 %, which can be attributed to the relatively smooth surface morphology of the S/O/W MPs. Differences in particle size were also obtained (W/O/W MPs 112 µm vs S/O/W MPs 70 µm). Regarding the bioactivity of the released ranibizumab, less than 60 % of the ranibizumab released from the W/O/W MPs was active in comparison to more than 80 % from the S/O/W MPs, calculating bioactive ranibizumab/total ranibizumab measured by ELISA and micro-BCA, respectively (44).

W/O/W double emulsion technique was also used in the study of Zhang et al. to prepare ranibizumab MPs. They obtained a similar EE % (89 %) although a rather smaller particle size (20 µm) and slower release rate (approximately 80 % of release ranibizumab within 3 weeks) (45). Another study investigated the preparation of ranibizumab PLGA MP through coaxial electrospray (CES). They obtained core-shell structured MPs with a diameter of 2.36 µm and an EE % of 70 % (46).

3.2.3.2. Chitosan nanoparticles

Some other polymers have also been utilised as sustained release vehicles in the preparation of NPs, such as chitosan and its derivatives. Chitosan is a widely used natural polymer in the pharmaceutical field due to its biocompatibility and biodegradability. It has been used for the preparation of NPs in different areas, but its mucoadhesivity has made it extremely suitable for the mucosal route, although some NPs intended for ocular delivery have also been investigated (54,55).

Lu et al. have developed bevacizumab-chitosan NPs by an emulsification evaporation method. They tested the intravitreally injected NPs in a model of diabetic rat obtaining that the encapsulated bevacizumab effectively inhibited VEGF expression and presented a longer duration of action compared to the control (56).

One of the main disadvantages of using chitosan is its low solubility at physiological pH, being only soluble in dilute acidic solution. Therefore, one group carried out the synthesis of a new polymer of chitosan grafted PEG methacrylate (CS-g-PEGMA) with an improved solubility in aqueous solutions. They used this polymer to prepare NPs loaded with bevacizumab by the methodology of double cross-linking (ionic followed by covalent) in reverse emulsion (W/O), obtaining particles of 500 nm in size with an EE % of 39 %. Moreover, the *in vitro* release test indicated that bevacizumab was released in an almost linear manner, apart from the burst released observed at the first 30 min, and at 25 days almost all the loaded bevacizumab was released. They also tested their NPs in rabbit models of inflammation and central retinal vein occlusion, where they obtained a moderate efficacy, and in models of diabetes with a higher efficiency (57).

3.2.3.3. Other nanoparticles

Some efforts have been made in the development of NPs of other origins. Mesoporous silica NPs (MSNs) have gained some interest in drug delivery due to their advantageous features as biocompatibility, mechanical and chemical properties, possibility of controlling parameters as morphology, pore size and volume (58,59). MSNs are solid NPs with numerous mesopores which enables drug loading (60).

MSNs have been prepared by soft template method and surface modified with NH2- and PEG-modification where bevacizumab was encapsulated via nanocasting strategy. They obtained NPs of 150 nm with an EE % of 79.2 %. More than 35 % of bevacizumab was released in the first two days, but with a burst release in the first 1-10 h. About 35 % of bevacizumab was released in the next 5 days (sustained release) with a subsequent slow release up to 28 days. Bevacizumab solution achieved almost 100 % release at 4 days (61). They tested the developed NPs in mice by injecting 0.01 mg bevacizumab intravitreally. MSNs reached a maximum concentration at 7 days post-injection and a vitreous half-life of 8.76 days vs 5.31 days of the solution of bevacizumab. Moreover, concerns have been raised about the safety and toxicity of the MSNs (58), although these authors proved that their MSNs had no toxicity effects on endothelial cell function *in vitro* and mouse retina function *in vivo* (61). Another issue would be the accumulation of these MSNs in the eye after successive intravitreal injections, which has not been addressed.

3.2.4. Implants

Intravitreal implants are solid devices which can be surgically implanted or injected in the vitreous humour (26). Nowadays, there are several implants on the market which prolong the release of drugs such as dexamethasone (Ozurdex®), fluocinolone (Iluvien®, Retisert®) and ganciclovir (Vitrasert®). Regarding implants under clinical investigation, NT-503 cell line is an Encapsulated Cellular Delivery System implanted into the vitreous cavity which produces VEGF antagonists and release them into the retina. It needs to be implanted once every 12 weeks (62). This device was assessed in both phase I and II clinical trials, and although the procedure seems well-tolerated, the Phase II trial was stopped early due to lack of reproducible long-

term efficacy (63). However, no implants carrying anti-VEGF antibodies have reached the market.

It is necessary to take into account that the size of implants is a critical point. Implants have to be large enough to guarantee an adequate protein loading, but they must be also small enough to ft inside the vitreous body. In comparison with other DDSs, implants present the longest release time, as normally they release the drug from several weeks to months, and permit high drug loading (64).

Polymer-based implants can also be made of biodegradable or nonbiodegradable polymers. Non-biodegradable implants need to be removed surgically from the eye after drug depletion as the materials will not be cleared, with the corresponding inconvenience to the patient (12,64). Therefore, biodegradable implants present more promising results.

Regarding preclinical research, Lance et al. created an implant formed by two circular poly(caprolactone) nanoporous thin films of 10 mm in diameter sealed at the perimeter and containing between them a 3-mm-diameter pellet of ranibizumab (payload was 177-189 µg per device). *In vitro* studies resulted in a biphasic release of ranibizumab: a burst release in the first five weeks followed by a gradually diminishing second release phase up to week 16. At that time, 62.8 % of the initial payload has been released from the device. The device was administered intravitreally in New Zealand white rabbits and ranibizumab was detectable in the vitreous up to 12 weeks (65).

For their part, Vollrath et al. elaborated solid lipid implants by twin-screw extrusion using low melting triglyceride H12 and high melting triglyceride Dynasan D118 for intravitreal administration of ranibizumab. The devices were 1.5 mm in diameter, 15 mm in length and 30.7 mg in weight. Release profiles were obtained from an implant formulation consisting of 45 % H12, 45 % D118 and 10 % protein lyophilisate resulting in 1.53 mg of ranibizumab per implant. *In vitro* studies showed a triphasic release behaviour with no burst effect: during the first phase (0-28 days) 53 % of ranibizumab was released, the second phase (28-110 days) showed an almost linear release with 34 % of protein liberation and in the third phase (110-126 days), only small amounts were released. Finally, at 126 days, 90 % of ranibizumab was released (66).

On the other hand, Burgalassi et al. obtained bevacizumab-loaded matrices by freeze-drying based on hydroxypropylmethyl cellulose (HPMC) or PVA. The matrices presented a diameter of 2.9 mm and a length of 11.5 mm. *In vitro* studies revealed that the quantity of drug released after 96 h was 1.855 % for HPMC and 3.533 % for PVA matrices. Therefore, both matrices demonstrated to prolong the release of bevacizumab, but HPMC was selected for following *in vivo* studies for its higher viscosity after rehydration. HPMC loaded with 0.625 mg of bevacizumab was administered intravitreally to New Zealand albino rabbits. Vitreous concentrations were 199.23 ng/mL at 2 weeks and 4.72 ng/mL at 12 weeks. According to their results, it would be possible using freeze-dried matrices as bevacizumab delivery system to the posterior segment of the eye (67).

3.2.5. Composite systems

Among the DDSs developed for intravitreal administration (hydrogels, NPs, liposomes, MPs, implants…), there is still the possibility of combining two or more of these DDSs in order to obtain formulations which present the main advantages of both. For anti-VEGF drugs, embedding MPs in a hydrogel or incorporating NPs in MPs/implants have been investigated as potential platforms of drug delivery (Figure 3.4).

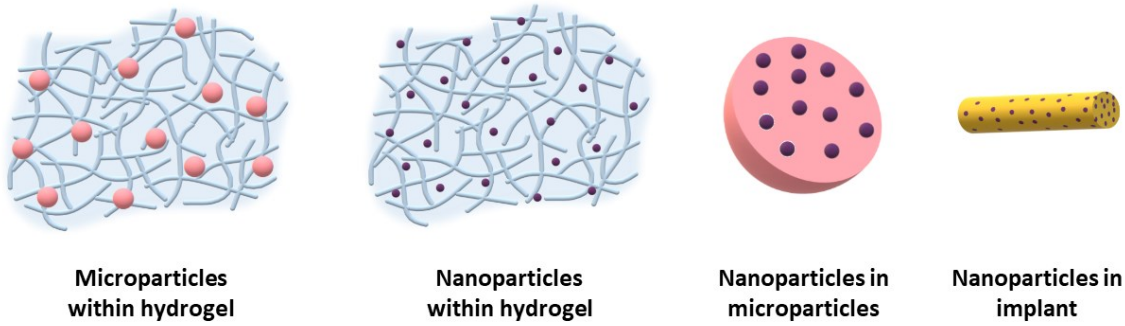

Figure 3.4. Composite system approaches for intravitreal anti-VEGF drugs.

3.2.5.1. Microparticles within hydrogel

Incorporating MPs within a hydrogel meshwork stems from the problems that intravitreal MPs entail. The main disadvantage of polymeric MPs is the initial burst release effect. This issue may be overcome by the inclusion of the MPs within the hydrogel, which will act as a diffusion

barrier of anti-VEGF antibodies. Moreover, the hydrogel would provide a more controlled and extended release compared to the MPs alone (68,69).

Concerns have been raised whether MPs can migrate from the vitreous chamber to the aqueous chamber and from there access the trabecular meshwork where they could become lodged. Therefore, the inclusion of the MPs within a hydrogel would decrease the possibility of this complication to occur (68).

Osswald et al. (70,71) have developed a DDS composed of PLGA MPs suspended within a hydrogel based on thermoresponsive poly(N-isopropylacrylamide) (PNIPAAm). They encapsulated both ranibizumab and aflibercept in the MPs. One of the concerns of this type of DDSs is the injectability that they checked and concluded that their DDS remained injectable through a 28 G needle at room temperature. Ranibizumab-loaded microspheres embedded in the hydrogel matrix resulted in twice EE % (89.5 %) than aflibercept-loaded microspheres (44.6 %) even when they were prepared in the same conditions, which could be attributed to the different molecular weight. However, they both presented similar particle size (7.5-8 µm).

Suspending the MPs within the hydrogel had as the main outcome a significantly reduction in the typical initial burst release of PLGA MPs and a steady extension of the anti-VEGF drugs release. The initial burst release was reduced by 58 % for ranibizumab and by 76 % for aflibercept proving that the hydrogel was acting as a diffusion barrier. After 7 days, the steadied state was achieved where 0.153 µg/day of ranibizumab and 0.065 µg/day of aflibercept were released for more than 6 months. However, some drug remained trapped within the hydrogel (25 % for ranibizumab and 32 % for aflibercept) after complete degradation of the MPs (70).

They have also assessed the efficacy of the ranibizumab and aflibercept mentioned DDSs in reducing the lesions on a laser-induced rat model of choroidal neovascularisation (Osswald et al., 2017). In addition, they tested their aflibercept-loaded MP-hydrogel in a non-human primate model concluding that aflibercept was released at a sustained manner and remained bioactive (Kang-Mieler et al., 2018). This study was one of the first ones to obtain an anti-VEGF antibody release up to six-months *in vitro* through a DDS. However, the use of PNIPAAm hydrogel has the drawback of being non-degradable, which holds its clinical relevance.

Therefore, the same group has continued researching to obtain a biodegradable hydrogel composed of poly(ethylene glycol)-co-(L-lactic acid) diacrylate/N-isopropylacrylamide (PEGPLLA-DA/NIPAAm) (72,73).

For ranibizumab, after testing different concentrations of PEGPLLA-DA (1, 2, and 3 mM) for a MP loading of 10 mg/mL, they obtained a lower EE % (45.67 %) compared to the previous study (89.5 %). The DDS with a 3 mM concentration showed an initial burst release of 21.13 %, a release rate of 0.04 µg/day at the steady state and a higher final release amount (78.52 %) at 6 months (Liu et al., 2019b). The developed DDS in the same described conditions (loading 10 mg/mL and polymer 3 mM) but including aflibercept instead of ranibizumab showed different results: a higher EE % (70.98 %), a higher burst release (38.62 %), a higher release rate at steady state (0.07 %) and a lower final release amount of aflibercept (70.02 %) (73).

3.2.5.2. Nanoparticles in microparticles

NPs in MPs systems have centred their attention on the improvement of the beyond characterised PLGA MPs. One limitation of the PLGA MPs is the instability associated to the contact of the anti-VEGF drug to the organic phase in the W/O/W method. Therefore, it has been hypothesised that including the VEGF inhibitors into non-PLGA NPs would prevent its poor protein stability meanwhile maintaining the main advantages of PLGA MPs. Moreover, the combination of both DDSs will extend the release time of the drug.

Elsaid et al. have prepared chitosan-N-acetyl-L-cysteine (CNAC) NPs incorporated into PLGA MPs containing ranibizumab. Both chitosan-based NPs and PLGA MPs have already been revised in the previous sections. The modification of chitosan with acetylcysteine have been chosen because the disulphide bonds of the cysteine residues could potentially form bonds with ranibizumab and therefore enhance the interactions NP-ranibizumab, which they have confirmed later by FT-IR (74).

CNAC NPs showed a particle size of 25.7 nm and the PLGA MP containing them a size of 3 µm. The EE % in the composite system was 69 %. It showed the typical tri-phase release profile of PLGA MPs, but with the initial burst released significantly reduced (only around 5 %), a steady

state released up to 4 months and a complete release at 6 months. The released ranibizumab maintained its structural integrity and *in vitro* activity through a cell migration assay. Therefore, these authors have considerably improved the release profile of PLGA MPs by the incorporation of CNAC NPs while maintaining the EE % and decreasing its particle size. These benefits may be attributed to the modification of the chitosan by acetylcysteine and its interaction with ranibizumab (74).

Yandrapu et al. design a DDS using supercritical fluid pressure quench technology in which bevacizumab-coated PLA NPs were encapsulated inside porous PLGA MPs (NPinPMP). They followed the widely used emulsion solvent evaporation method for both the preparation of the PLA-NPs and the PLGA-MPs, which has a main drawback of utilising organic solvents which are considered to cause protein instability. However, these authors followed a different approach, they first prepared the blank PLA-NPs and PLGA-MPs. Then, the NPs were coated with bevacizumab by lyophilization and further mixed with the already prepared blank MPs at a Bevacizumab/NP:MP ratio of 10 % (w/w). Afterwards, the mixture was exposed to SC-CO_2 to porosify the PLGA MPs. This exposure increased the MP size by 7-fold (final particle size 11.6 µm), although no EE % was provided. *In vitro* release study showed 81 % of cumulative total release at 4 months but with an initial burst release of 21 % during the first day. Bevacizumab maintained its VEGF-165 binding activity through all the study time. Prolonged release up to 2 months was obtained when the NPinPMPs were intravitreally injected into rat eyes. In conclusion, these authors provided a DDS with two main advantages to the PLGA MPs already tested elsewhere: avoidance of the contact of antibody to organic solvents and extension of the *in vitro* release (75).

3.2.5.3. Nanoparticles in implants

Once again, the inclusion of NPs in an implant has the aim of extending the release of intravitreal anti-VEGF drugs. Bevacizumab-loaded chitosan NPs were prepared by ionic gelation method and inserted in the matrix of hyaluronic acid and zinc sulphate. They performed statistical analysis based on design of experiments to optimise the chitosan NPs, obtaining a particle size of 78.5 nm and an EE % of 67.6 %. The incorporation of the NPs to the implants produced yellowish white implants with diameter of 7.49 mm and thickness of 1.67

mm. The NPs seemed to be homogenously distributed in the implant matrix and surface. The NPs-loaded implant released more than 40 % of bevacizumab in 20 days in a relatively slow manner and from 20 to 60 days a sustained release profile was observed with a final cumulative release of 46.70 % (76).

3.3. INTRAVITREAL PHARMACOKINETICS

In previous sections, the drug release profile of the DDSs developed with anti-VEGF drugs have been described. Normally, these *in vitro* assays are detailed adequately in the studies, however, the parameters obtained are not sufficient to determine *in vivo* behaviour, and ocular pharmacokinetic (PK) studies on animals should be carried out (77). *In vivo* studies are necessary to determine the drug concentration in the vitreous, which allows to determine the half-life of the drug ($t_{1/2}$) and therefore its frequency of administration.

However, intravitreal pharmacokinetic studies are extremely difficult to perform due to the invasiveness of taking vitreous samples. On the other hand, the differences in the methods of determination, in the samples analysed, in the time points taken and in the compartmental analysis, etc., make it difficult to have standardised values for each anti-VEGF antibody. Moreover, different animal models have been used to study PK behaviour of anti-VEGF drugs after intravitreal injection, varying the results among them. By last, most of the human studies calculate a serum half-life, or even, an aqueous half-life, which could be an indirect estimate of the half-life of the antibodies in the vitreous humour (9).

All these factors entail important hurdles in the progress of intravitreal DDSs development. In this way, if intravitreal pharmacokinetics of the commercial solutions is not well characterised, it will be difficult to obtain comparative data with the developed DDSs. In order to clarify and compile the available information in this field, the main studies published on anti-VEGF intravitreal pharmacokinetics are presented in Table 3.3 and Figure 3.5.

Table 3.3. Vitreous humour, aqueous humour and serum half-lives (days) of bevacizumab, ranibizumab and aflibercept in different animal species (mice, rabbits, monkeys, humans). Data is shown as mean ± standard deviation.

Antibody	Animal	Half-lives (days)			Ref
		Vitreous humour	Aqueous humour	Serum	
Bevacizumab	Mice	5.14 ± 0.25	5.03 ± 0.13	*	(51,58)
	Rabbit	4.94 ± 1.21	5.11 ± 1.04	8.09 ± 3.27	(29,41,48,78–85)
	Monkey	3.6	2.8	9.1 ± 4.53	(86–88)
	Human	5.8 ± 1.27	9.79 ± 1.92	15 ± 5.23	(89–94)
Ranibizumab	Rabbit	2.83 ± 0.06	2.92 ± 0.11	*	(80,81,95–97)
	Monkey	3.1 ± 0.73	2.49 ± 0.17	2.84 ± 0.67	(86,98,99)
	Human	*	7.19	2.94 ± 4.04	(91,92,100,101)
Aflibercept	Rabbit	4.58	*	*	(102)
	Monkey	2.44	2.22	*	(86,99)
	Human	*	11	11.4	(91,92,103)

* Data not available

The vitreous half-life on rabbits (most studied animal in PK studies) is on average 4.94 days for bevacizumab, 2.83 days for ranibizumab and 4.58 days for aflibercept. Although the relation between the antibody intravitreal half-life and the molecular weight is not always clear, in this case, it follows the general rule that the intravitreal half-life of macromolecules has a direct correlation with the molecular weight. In this way, bevacizumab (MW = 150 kDa) presents the higher vitreous half-life of the three antibodies, followed by aflibercept (MW = 115 kDa) which has a slightly lower $t_{1/2}$, and ranibizumab (MW = 48 kDa) with the lowest one (104).

The differences found among species should be also noted. Taking as example the vitreous half-lives of bevacizumab because it is the one that has most intravitreal PK data. The rabbit presents a mean vitreous $t_{1/2}$ almost equal to mice (4.94 vs 5.14 days) and similar, although slightly lower, to human (5.8 days) (Table 3.3, Figure 3.5). On the contrary, vitreous $t_{1/2}$ in monkeys (3.6 days) is considerably lower compared to rabbits. However, it should be mention than only one study analysed the vitreous half-life on monkeys, so this assumption has to be taken with caution. However, these relations among species may not be the same for all the

antibodies. In this way, ranibizumab seems to present a similar or slightly higher half-life in monkeys (3.1 days) compared to rabbits (2.83 days) (Table 3.3, Figure 3.5).

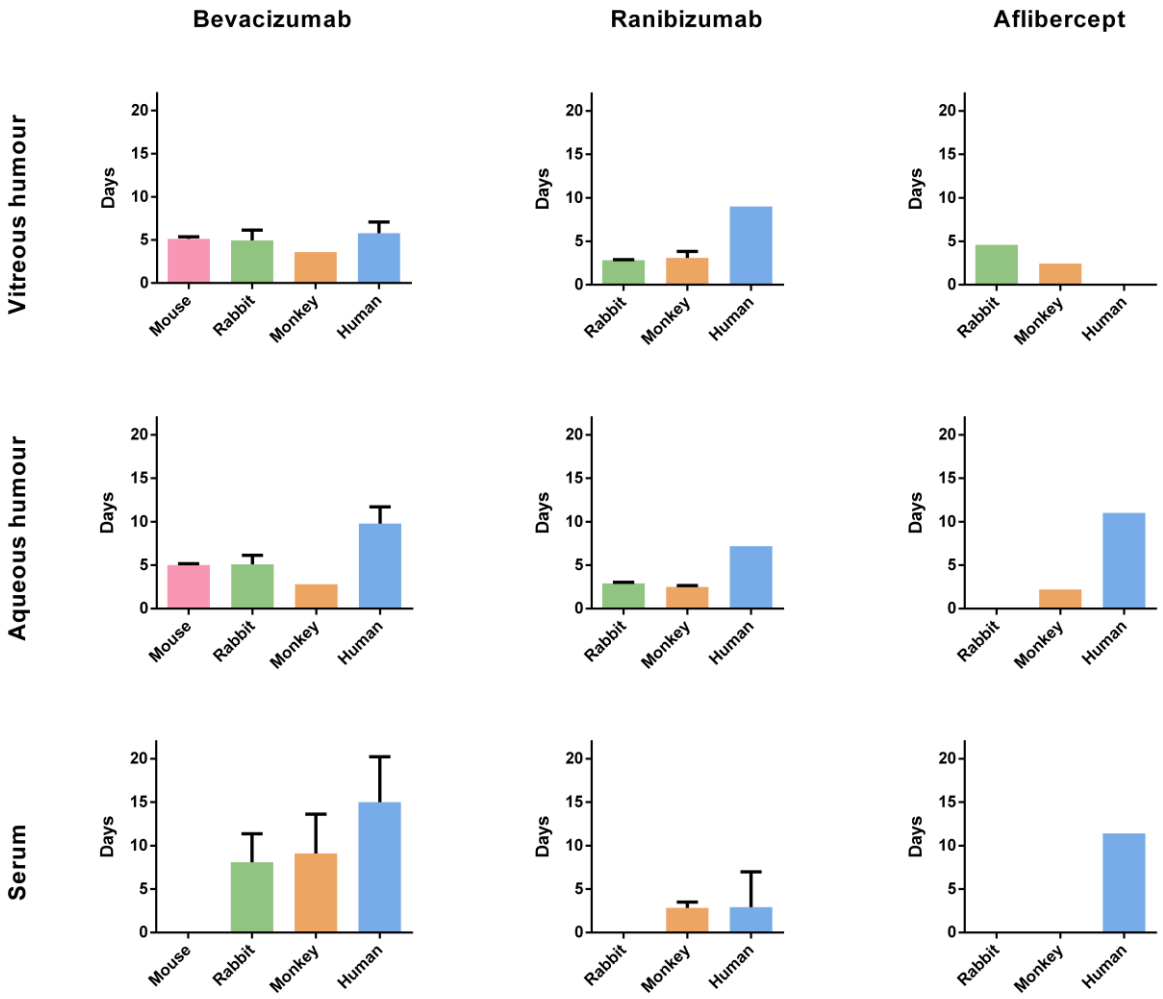

Figure 3.5. Comparison of vitreous, aqueous and serum half-lives (days) of bevacizumab, ranibizumab and aflibercept in mice, rabbits, monkeys, and humans.

Finally, it should be pointed out the differences that can be found in the bibliography depending on the type of the samples analysed. It should be considered that the majority of the human studies have been performed in blood samples (indirect measurement) whereas in preclinical research is where most vitreous samples are analysed. The existence of studies which provide longitudinal measures by non-invasive techniques (molecular imaging) with indirect blood samples could offer a tool to study in a precise manner this relation.

3.4. CONCLUSION

In this review we have summarised the DDSs developed up to date regarding intravitreal anti-VEGF drugs. Clinically used intravitreal anti-VEGF antibodies are simple solutions with excipients. For that reason, patients require to undergo intravitreal injections every one or two months. Therefore, sustained drug delivery of these drugs is highly attractive, but also presents a great challenge. Extending the delivery of anti-VEGF drugs would have a positive effect both on patient compliance and on the economic burden. DDSs should allow high drug loading while maintaining a small size and preserving the bioactivity of the antibodies upon release. Several types of DDSs have been studied for intravitreal administration, such as hydrogels, liposomes, microparticles, nanoparticles, implants… Hydrogels can be injected into the vitreous body through a small needle. In situ thermosensitive hydrogels are really attractive due to the fact that they are non-viscous upon injection and after injected into the vitreous they form a gel-like structure. However, diffusion through the gel structure is relatively fast, limiting is usefulness as long release formulations. Both microparticles and nanoparticles have been tested as intravitreal DDSs. Microparticles are larger in size, can afford higher loadings and could have extended release times. However, they can lead to blurred vision due to light scattering effects inside the vitreous body. On the contrary, nanoparticles present the advantage of potential retinal penetration. Both present burst release, which may be overcome by including them in hydrogels. In comparison with other DDSs, implants present the longest release times, as normally they release the drug from several weeks to months, and permit high drug loading. They are the most promising DDSs at present, although there are still in early stages of development for anti-VEGF antibodies. On the other hand, DDS development relies on pharmacokinetic analyses to evaluate the extended drug release. Further research is needed in general through this direction, but hopefully in the next years effective DDSs will be available for the delivery of intravitreal VEGF inhibitors.

3.5. REFERENCES

1. Wong WL, Su X, Li X, Cheung CMG, Klein R, Cheng C-Y, et al. Global prevalence of age-related macular degeneration and disease burden projection for 2020 and 2040: a systematic review and meta-analysis. Lancet Glob Health. 2014 Feb;2(2):e106-116.
2. Al-Zamil WM, Yassin SA. Recent developments in age-related macular degeneration: a review. Clin Interv Aging. 2017 Aug 22;12:1313–30.
3. Garrity ST, Sarraf D, Freund KB, Sadda SR. Multimodal Imaging of Nonneovascular Age-Related Macular Degeneration. Invest Ophthalmol Vis Sci. 2018 Mar 20;59(4):AMD48–64.
4. Comparison of Age-related Macular Degeneration Treatments Trials (CATT) Research Group, Maguire MG, Martin DF, Ying G-S, Jaffe GJ, Daniel E, et al. Five-Year Outcomes with Anti-Vascular Endothelial Growth Factor Treatment of Neovascular Age-Related Macular Degeneration: The Comparison of Age-Related Macular Degeneration Treatments Trials. Ophthalmology. 2016;123(8):1751–61.
5. Gil-Martínez M, Santos-Ramos P, Fernández-Rodríguez M, Abraldes MJ, Rodríguez-Cid MJ, Santiago-Varela M, et al. Pharmacological advances in the treatment of age-related macular degeneration. Curr Med Chem. 2019 26;
6. Okada M, Kandasamy R, Chong EW, McGuiness M, Guymer RH. The Treat-and-Extend Injection Regimen Versus Alternate Dosing Strategies in Age-related Macular Degeneration: A Systematic Review and Meta-analysis. Am J Ophthalmol. 2018 Aug;192:184–97.
7. Eylea: EPAR - Product Information [Internet]. 2019 [cited 2019 Sep 24]. Available from: https://www.ema.europa.eu/en/documents/product-information/eylea-epar-product-information_en.pdf
8. Lucentis: EPAR - Product Information [Internet]. 2019 [cited 2019 Sep 24]. Available from: https://www.ema.europa.eu/en/documents/product-information/lucentis-epar-product-information_en.pdf
9. García-Quintanilla L, Luaces-Rodríguez A, Gil-Martínez M, Mondelo-García C, Maroñas O, Mangas-Sanjuan V, et al. Pharmacokinetics of Intravitreal Anti-VEGF Drugs in Age-Related Macular Degeneration. Pharmaceutics. 2019 Jul 31;11(8).
10. Subrizi A, del Amo EM, Korzhikov-Vlakh V, Tennikova T, Ruponen M, Urtti A. Design principles of ocular drug delivery systems: importance of drug payload, release rate, and material properties. Drug Discov Today [Internet]. 2019 Feb 7 [cited 2019 Jul 2]; Available from: http://www.sciencedirect.com/science/article/pii/S1359644618303994
11. Delplace V, Ortin-Martinez A, Tsai ELS, Amin AN, Wallace V, Shoichet MS. Controlled release strategy designed for intravitreal protein delivery to the retina. J Controlled Release. 2019 Jan 10;293:10–20.

12. Agrahari V, Agrahari V, Mandal A, Pal D, Mitra AK. How are we improving the delivery to back of the eye? Advances and challenges of novel therapeutic approaches. Expert Opin Drug Deliv. 2017;14(10):1145–62.

13. Ahmed EM. Hydrogel: Preparation, characterization, and applications: A review. J Adv Res. 2015 Mar;6(2):105–21.

14. Anwary M, Kumar P, du Toit LC, Choonara YE, Pillay V. Polymeric, injectable, intravitreal hydrogel devices for posterior segment applications and interventions. Artif Cells Nanomedicine Biotechnol. 2018;46(sup2):1074–81.

15. Hu C-C, Chaw J-R, Chen C-F, Liu H-W. Controlled release bevacizumab in thermoresponsive hydrogel found to inhibit angiogenesis. Biomed Mater Eng. 2014;24(6):1941–50.

16. Park D, Shah V, Rauck BM, Friberg TR, Wang Y. An anti-angiogenic reverse thermal gel as a drug-delivery system for age-related wet macular degeneration. Macromol Biosci. 2013 Apr;13(4):464–9.

17. Rauck BM, Friberg TR, Medina Mendez CA, Park D, Shah V, Bilonick RA, et al. Biocompatible reverse thermal gel sustains the release of intravitreal bevacizumab in vivo. Invest Ophthalmol Vis Sci. 2014 Jan 23;55(1):469–76.

18. Xie B, Jin L, Luo Z, Yu J, Shi S, Zhang Z, et al. An injectable thermosensitive polymeric hydrogel for sustained release of Avastin® to treat posterior segment disease. Int J Pharm. 2015 Jul;490(1–2):375–83.

19. Wang C-H, Hwang Y-S, Chiang P-R, Shen C-R, Hong W-H, Hsiue G-H. Extended release of bevacizumab by thermosensitive biodegradable and biocompatible hydrogel. Biomacromolecules. 2012 Jan 9;13(1):40–8.

20. Awwad S, Al-Shohani A, Khaw PT, Brocchini S. Comparative Study of In Situ Loaded Antibody and PEG-Fab NIPAAM Gels. Macromol Biosci. 2018;18(2).

21. Xu Q, Boylan NJ, Suk JS, Wang Y-Y, Nance EA, Yang J-C, et al. Nanoparticle diffusion in, and microrheology of, the bovine vitreous ex vivo. J Control Release Off J Control Release Soc. 2013 Apr 10;167(1):76–84.

22. Yu J, Xu X, Yao F, Luo Z, Jin L, Xie B, et al. In situ covalently cross-linked PEG hydrogel for ocular drug delivery applications. Int J Pharm. 2014 Aug;470(1–2):151–7.

23. Yu Y, Lau LCM, Lo AC-Y, Chau Y. Injectable Chemically Crosslinked Hydrogel for the Controlled Release of Bevacizumab in Vitreous: A 6-Month In Vivo Study. Transl Vis Sci Technol. 2015 Mar;4(2):5.

24. Lovett ML, Wang X, Yucel T, York L, Keirstead M, Haggerty L, et al. Silk hydrogels for sustained ocular delivery of anti-vascular endothelial growth factor (anti-VEGF) therapeutics. Eur J Pharm Biopharm. 2015 Sep;95:271–8.

25. Nguyen MK, Lee DS. Injectable Biodegradable Hydrogels. Macromol Biosci. 2010 Jun 9;10(6):563–79.

26. Gote V, Sikder S, Sicotte J, Pal D. Ocular Drug Delivery: Present Innovations and Future Challenges. J Pharmacol Exp Ther. 2019 May 9;jpet.119.256933.

27. Madni A, Sarfraz M, Rehman M, Ahmad M, Akhtar N, Ahmad S, et al. Liposomal Drug Delivery: A Versatile Platform for Challenging Clinical Applications. J Pharm Pharm Sci. 2014 Aug 26;17(3):401.

28. Abrishami M, Zarei-Ghanavati S, Soroush D, Rouhbakhsh M, Jaafari MR, Malaekeh-Nikouei B. Preparation, characterization, and in vivo evaluation of nanoliposomes-encapsulated bevacizumab (avastin) for intravitreal administration. Retina Phila Pa. 2009 May;29(5):699–703.

29. Mu H, Wang Y, Chu Y, Jiang Y, Hua H, Chu L, et al. Multivesicular liposomes for sustained release of bevacizumab in treating laser-induced choroidal neovascularization. Drug Deliv. 2018 Jan;25(1):1372–83.

30. Joseph M, Trinh HM, Cholkar K, Pal D, Mitra AK. Recent perspectives on the delivery of biologics to back of the eye. Expert Opin Drug Deliv. 2017 May;14(5):631–45.

31. Herrero-Vanrell R, Bravo-Osuna I, Andrés-Guerrero V, Vicario-de-la-Torre M, Molina-Martínez IT. The potential of using biodegradable microspheres in retinal diseases and other intraocular pathologies. Prog Retin Eye Res. 2014 Sep;42:27–43.

32. Iyer S, Radwan AE, Hafezi-Moghadam A, Malyala P, Amiji M. Long-acting intraocular Delivery strategies for biological therapy of age-related macular degeneration. J Control Release Off J Control Release Soc. 2019 Feb 28;296:140–9.

33. Gavini E, Bonferoni MC, Rassu G, Obinu A, Ferrari F, Giunchedi P. Biodegradable Microspheres as Intravitreal Delivery Systems for Prolonged Drug Release. What is their Eminence in the Nanoparticle Era? Curr Drug Deliv. 2018;15(7):930–40.

34. Thakur SS, Barnett NL, Donaldson MJ, Parekh HS. Intravitreal drug delivery in retinal disease: are we out of our depth? Expert Opin Drug Deliv. 2014 Oct;11(10):1575–90.

35. Sakurai E, Ozeki H, Kunou N, Ogura Y. Effect of particle size of polymeric nanospheres on intravitreal kinetics. Ophthalmic Res. 2001 Feb;33(1):31–6.

36. Huang X, Chau Y. Intravitreal nanoparticles for retinal delivery. Drug Discov Today. 2019 May 16;

37. Makadia HK, Siegel SJ. Poly Lactic-co-Glycolic Acid (PLGA) as Biodegradable Controlled Drug Delivery Carrier. Polymers. 2011 Sep 1;3(3):1377–97.

38. Ding D, Zhu Q. Recent advances of PLGA micro/nanoparticles for the delivery of biomacromolecular therapeutics. Mater Sci Eng C Mater Biol Appl. 2018 Nov 1;92:1041–60.

39. van de Weert M, Hennink WE, Jiskoot W. Protein instability in poly(lactic-co-glycolic acid) microparticles. Pharm Res. 2000 Oct;17(10):1159–67.

40. Pan CK, Durairaj C, Kompella UB, Agwu O, Oliver SCN, Quiroz-Mercado H, et al. Comparison of long-acting bevacizumab formulations in the treatment of choroidal

neovascularization in a rat model. J Ocul Pharmacol Ther Off J Assoc Ocul Pharmacol Ther. 2011 Jun;27(3):219–24.

41. Varshochian R, Riazi-Esfahani M, Jeddi-Tehrani M, Mahmoudi A-R, Aghazadeh S, Mahbod M, et al. Albuminated PLGA nanoparticles containing bevacizumab intended for ocular neovascularization treatment. J Biomed Mater Res A. 2015 Oct;103(10):3148–56.

42. Varshochian R, Jeddi-Tehrani M, Mahmoudi AR, Khoshayand MR, Atyabi F, Sabzevari A, et al. The protective effect of albumin on bevacizumab activity and stability in PLGA nanoparticles intended for retinal and choroidal neovascularization treatments. Eur J Pharm Sci. 2013 Nov;50(3–4):341–52.

43. Sousa F, Cruz A, Fonte P, Pinto IM, Neves-Petersen MT, Sarmento B. A new paradigm for antiangiogenic therapy through controlled release of bevacizumab from PLGA nanoparticles. Sci Rep. 2017 16;7(1):3736.

44. Chua HY, Lui YS, Bhuthalingam R, Agrawal R, Wong T, Preiser PR, et al. One-step solid-oil-water emulsion for sustained bioactive ranibizumab release. Expert Opin Drug Deliv. 2018;15(12):1143–56.

45. Tanetsugu Y, Tagami T, Terukina T, Ogawa T, Ohta M, Ozeki T. Development of a Sustainable Release System for a Ranibizumab Biosimilar Using Poly(lactic-co-glycolic acid) Biodegradable Polymer-Based Microparticles as a Platform. Biol Pharm Bull. 2017;40(2):145–50.

46. Zhang L, Si T, Fischer AJ, Letson A, Yuan S, Roberts CJ, et al. Coaxial Electrospray of Ranibizumab-Loaded Microparticles for Sustained Release of Anti-VEGF Therapies. Jablonski MM, editor. PLOS ONE. 2015 Aug 14;10(8):e0135608.

47. Li F, Hurley B, Liu Y, Leonard B, Griffith M. Controlled release of bevacizumab through nanospheres for extended treatment of age-related macular degeneration. Open Ophthalmol J. 2012;6:54–8.

48. Ye Z, Ji Y-L, Ma X, Wen J-G, Wei W, Huang S-M. Pharmacokinetics and distributions of bevacizumab by intravitreal injection of bevacizumab-PLGA microspheres in rabbits. Int J Ophthalmol. 2015;8(4):653–8.

49. Gasmi H, Siepmann F, Hamoudi MC, Danede F, Verin J, Willart J-F, et al. Towards a better understanding of the different release phases from PLGA microparticles: Dexamethasone-loaded systems. Int J Pharm. 2016 Nov 30;514(1):189–99.

50. Fredenberg S, Wahlgren M, Reslow M, Axelsson A. The mechanisms of drug release in poly(lactic-co-glycolic acid)-based drug delivery systems--a review. Int J Pharm. 2011 Aug 30;415(1–2):34–52.

51. Zhang X-P, Sun J-G, Yao J, Shan K, Liu B-H, Yao M-D, et al. Effect of nanoencapsulation using poly (lactide-co-glycolide) (PLGA) on anti-angiogenic activity of bevacizumab for ocular angiogenesis therapy. Biomed Pharmacother. 2018 Nov;107:1056–63.

52. Liu J, Li S, Li G, Li X, Yu C, Fu Z, et al. Highly bioactive, bevacizumab-loaded, sustained-release PLGA/PCADK microspheres for intravitreal therapy in ocular diseases. Int J Pharm. 2019 May 30;563:228–36.

53. Kelly SJ, Hirani A, Shahidadpury V, Solanki A, Halasz K, Varghese Gupta S, et al. Aflibercept Nanoformulation Inhibits VEGF Expression in Ocular In Vitro Model: A Preliminary Report. Biomedicines. 2018 Sep 11;6(3).

54. Mohammed MA, Syeda JTM, Wasan KM, Wasan EK. An Overview of Chitosan Nanoparticles and Its Application in Non-Parenteral Drug Delivery. Pharmaceutics. 2017 Nov 20;9(4).

55. Naskar S, Koutsu K, Sharma S. Chitosan-based nanoparticles as drug delivery systems: a review on two decades of research. J Drug Target. 2019 Apr;27(4):379–93.

56. Lu Y, Zhou N, Huang X, Cheng J-W, Li F-Q, Wei R-L, et al. Effect of intravitreal injection of bevacizumab-chitosan nanoparticles on retina of diabetic rats. Int J Ophthalmol. 2014;7(1):1–7.

57. Savin C-L, Popa M, Delaite C, Costuleanu M, Costin D, Peptu CA. Chitosan grafted-poly(ethylene glycol) methacrylate nanoparticles as carrier for controlled release of bevacizumab. Mater Sci Eng C. 2019 May;98:843–60.

58. Narayan R, Nayak UY, Raichur AM, Garg S. Mesoporous Silica Nanoparticles: A Comprehensive Review on Synthesis and Recent Advances. Pharmaceutics. 2018 Aug 6;10(3).

59. Slowing II, Trewyn BG, Giri S, Lin VS-Y. Mesoporous Silica Nanoparticles for Drug Delivery and Biosensing Applications. Adv Funct Mater. 2007;17(8):1225–36.

60. Tang F, Li L, Chen D. Mesoporous silica nanoparticles: synthesis, biocompatibility and drug delivery. Adv Mater Deerfield Beach Fla. 2012 Mar 22;24(12):1504–34.

61. Sun J-G, Jiang Q, Zhang X-P, Shan K, Liu B-H, Zhao C, et al. Mesoporous silica nanoparticles as a delivery system for improving antiangiogenic therapy. Int J Nanomedicine. 2019;14:1489–501.

62. Najafabadi HS, Daftarian N, Ahmadieh H, Soheili Z-S. Pharmacologic Treatment of Wet Type Age-related Macular Degeneration; Current and Evolving Therapies. Arch Iran Med. 2017;20(8):525–37.

63. Adamson P, Wilde T, Dobrzynski E, Sychterz C, Polsky R, Kurali E, et al. Single ocular injection of a sustained-release anti -VEGF delivers 6 months pharmacokinetics and efficacy in a primate laser CNV model. J Controlled Release. 2016 Dec;244:1–13.

64. Lee SS, Hughes P, Ross AD, Robinson MR. Biodegradable implants for sustained drug release in the eye. Pharm Res. 2010 Oct;27(10):2043–53.

65. Lance KD, Bernards DA, Ciaccio NA, Good SD, Mendes TS, Kudisch M, et al. In vivo and in vitro sustained release of ranibizumab from a nanoporous thin-film device. Drug Deliv Transl Res. 2016;6(6):771–80.

66. Vollrath M, Engert J, Winter G. Long-term release and stability of pharmaceutical proteins delivered from solid lipid implants. Eur J Pharm Biopharm Off J Arbeitsgemeinschaft Pharm Verfahrenstechnik EV. 2017 Aug;117:244–55.

67. Burgalassi S, Monti D, Nicosia N, Tampucci S, Terreni E, Vento A, et al. Freeze-dried matrices for ocular administration of bevacizumab: a comparison between subconjunctival and intravitreal administration in rabbits. Drug Deliv Transl Res. 2018 Jun;8(3):461–72.

68. Osswald CR, Kang-Mieler JJ. Controlled and Extended Release of a Model Protein from a Microsphere-Hydrogel Drug Delivery System. Ann Biomed Eng. 2015 Nov;43(11):2609–17.

69. DeFail AJ, Chu CR, Izzo N, Marra KG. Controlled release of bioactive TGF-beta 1 from microspheres embedded within biodegradable hydrogels. Biomaterials. 2006 Mar;27(8):1579–85.

70. Osswald CR, Kang-Mieler JJ. Controlled and Extended In Vitro Release of Bioactive Anti-Vascular Endothelial Growth Factors from a Microsphere-Hydrogel Drug Delivery System. Curr Eye Res. 2016 Sep;41(9):1216–22.

71. Osswald CR, Guthrie MJ, Avila A, Valio JA, Mieler WF, Kang-Mieler JJ. In Vivo Efficacy of an Injectable Microsphere-Hydrogel Ocular Drug Delivery System. Curr Eye Res. 2017 Sep 2;42(9):1293–301.

72. Liu W, Borrell MA, Venerus DC, Mieler WF, Kang-Mieler JJ. Characterization of Biodegradable Microsphere-Hydrogel Ocular Drug Delivery System for Controlled and Extended Release of Ranibizumab. Transl Vis Sci Technol. 2019 Jan;8(1):12.

73. Liu W, Lee B-S, Mieler WF, Kang-Mieler JJ. Biodegradable Microsphere-Hydrogel Ocular Drug Delivery System for Controlled and Extended Release of Bioactive Aflibercept In Vitro. Curr Eye Res. 2019 Mar 4;44(3):264–74.

74. Elsaid N, Jackson TL, Elsaid Z, Alqathama A, Somavarapu S. PLGA Microparticles Entrapping Chitosan-Based Nanoparticles for the Ocular Delivery of Ranibizumab. Mol Pharm. 2016 Sep 6;13(9):2923–40.

75. Yandrapu SK, Upadhyay AK, Petrash JM, Kompella UB. Nanoparticles in porous microparticles prepared by supercritical infusion and pressure quench technology for sustained delivery of bevacizumab. Mol Pharm. 2013 Dec 2;10(12):4676–86.

76. Badiee P, Varshochian R, Rafiee-Tehrani M, Abedin Dorkoosh F, Khoshayand MR, Dinarvand R. Ocular implant containing bevacizumab-loaded chitosan nanoparticles intended for choroidal neovascularization treatment. J Biomed Mater Res A. 2018 Aug;106(8):2261–71.

77. Stein S, Auel T, Kempin W, Bogdahn M, Weitschies W, Seidlitz A. Influence of the test method on in vitro drug release from intravitreal model implants containing dexamethasone or fluorescein sodium in poly (d,l-lactide-co-glycolide) or polycaprolactone. Eur J Pharm Biopharm Off J Arbeitsgemeinschaft Pharm Verfahrenstechnik EV. 2018 Jun;127:270–8.

78. Bakri SJ, Snyder MR, Reid JM, Pulido JS, Singh RJ. Pharmacokinetics of intravitreal bevacizumab (Avastin). Ophthalmology. 2007 May;114(5):855–9.

79. Nomoto H, Shiraga F, Kuno N, Kimura E, Fujii S, Shinomiya K, et al. Pharmacokinetics of bevacizumab after topical, subconjunctival, and intravitreal administration in rabbits. Invest Ophthalmol Vis Sci. 2009 Oct;50(10):4807–13.

80. Christoforidis JB, Carlton MM, Knopp MV, Hinkle GH. PET/CT imaging of I-124-radiolabeled bevacizumab and ranibizumab after intravitreal injection in a rabbit model. Invest Ophthalmol Vis Sci. 2011 Jul 29;52(8):5899–903.

81. Christoforidis JB, Williams MM, Wang J, Jiang A, Pratt C, Abdel-Rasoul M, et al. Anatomic and pharmacokinetic properties of intravitreal bevacizumab and ranibizumab after vitrectomy and lensectomy. Retina Phila Pa. 2013 May;33(5):946–52.

82. Christoforidis JB, Xie Z, Jiang A, Wang J, Pratt C, Gemensky-Metzler A, et al. Serum levels of intravitreal bevacizumab after vitrectomy, lensectomy and non-surgical controls. Curr Eye Res. 2013 Jul;38(7):761–6.

83. Sinapis CI, Routsias JG, Sinapis AI, Sinapis DI, Agrogiannis GD, Pantopoulou A, et al. Pharmacokinetics of intravitreal bevacizumab (Avastin®) in rabbits. Clin Ophthalmol Auckl NZ. 2011;5:697–704.

84. Ahn J, Kim H, Woo SJ, Park JH, Park S, Hwang DJ, et al. Pharmacokinetics of intravitreally injected bevacizumab in vitrectomized eyes. J Ocul Pharmacol Ther Off J Assoc Ocul Pharmacol Ther. 2013 Sep;29(7):612–8.

85. Liu X, Ye J, Zhang Y, Liu Q, Bai R, Yuan W, et al. Ocular Biodistribution of ^{89}Zr-Bevacizumab in New Zealand Rabbits Determined Using PET/MRI: A Feasibility Study. Iran J Radiol [Internet]. 2019 Apr [cited 2019 May 28];16(2). Available from: http://ijr.tums.ac.ir/en/articles/68697.html

86. Christoforidis JB, Briley K, Binzel K, Bhatia P, Wei L, Kumar K, et al. Systemic Biodistribution and Intravitreal Pharmacokinetic Properties of Bevacizumab, Ranibizumab, and Aflibercept in a Nonhuman Primate Model. Invest Ophthalmol Vis Sci. 2017 01;58(13):5636–45.

87. Miyake T, Sawada O, Kakinoki M, Sawada T, Kawamura H, Ogasawara K, et al. Pharmacokinetics of bevacizumab and its effect on vascular endothelial growth factor after intravitreal injection of bevacizumab in macaque eyes. Invest Ophthalmol Vis Sci. 2010 Mar;51(3):1606–8.

88. Kakinoki M, Sawada O, Sawada T, Saishin Y, Kawamura H, Ohji M. Effect of vitrectomy on aqueous VEGF concentration and pharmacokinetics of bevacizumab in macaque monkeys. Invest Ophthalmol Vis Sci. 2012 Aug 24;53(9):5877–80.

89. Zhu Q, Ziemssen F, Henke-Fahle S, Tatar O, Szurman P, Aisenbrey S, et al. Vitreous levels of bevacizumab and vascular endothelial growth factor-A in patients with choroidal neovascularization. Ophthalmology. 2008 Oct;115(10):1750–5, 1755.e1.

90. Moisseiev E, Waisbourd M, Ben-Artsi E, Levinger E, Barak A, Daniels T, et al. Pharmacokinetics of bevacizumab after topical and intravitreal administration in human eyes. Graefes Arch Clin Exp Ophthalmol Albrecht Von Graefes Arch Klin Exp Ophthalmol. 2014 Feb;252(2):331–7.

91. Avery RL, Castellarin AA, Steinle NC, Dhoot DS, Pieramici DJ, See R, et al. Systemic pharmacokinetics following intravitreal injections of ranibizumab, bevacizumab or aflibercept in patients with neovascular AMD. Br J Ophthalmol. 2014 Dec;98(12):1636–41.

92. Avery RL, Castellarin AA, Steinle NC, Dhoot DS, Pieramici DJ, See R, et al. Systemic pharmacokinetics and pharmacodynamics of intravitreal aflibercept, bevacizumab, and ranibizumab. Retina Phila Pa. 2017 Oct;37(10):1847–58.

93. Meyer CH, Krohne TU, Holz FG. Intraocular pharmacokinetics after a single intravitreal injection of 1.5 mg versus 3.0 mg of bevacizumab in humans. Retina Phila Pa. 2011 Oct;31(9):1877–84.

94. Krohne TU, Eter N, Holz FG, Meyer CH. Intraocular pharmacokinetics of bevacizumab after a single intravitreal injection in humans. Am J Ophthalmol. 2008 Oct;146(4):508–12.

95. Bakri SJ, Snyder MR, Reid JM, Pulido JS, Ezzat MK, Singh RJ. Pharmacokinetics of intravitreal ranibizumab (Lucentis). Ophthalmology. 2007 Dec;114(12):2179–82.

96. Gaudreault J, Fei D, Beyer JC, Ryan A, Rangell L, Shiu V, et al. Pharmacokinetics and retinal distribution of ranibizumab, a humanized antibody fragment directed against VEGF-A, following intravitreal administration in rabbits. Retina Phila Pa. 2007 Dec;27(9):1260–6.

97. Ahn SJ, Ahn J, Park S, Kim H, Hwang DJ, Park JH, et al. Intraocular pharmacokinetics of ranibizumab in vitrectomized versus nonvitrectomized eyes. Invest Ophthalmol Vis Sci. 2014 Jan 29;55(1):567–73.

98. Gaudreault J, Fei D, Rusit J, Suboc P, Shiu V. Preclinical pharmacokinetics of Ranibizumab (rhuFabV2) after a single intravitreal administration. Invest Ophthalmol Vis Sci. 2005 Feb;46(2):726–33.

99. Niwa Y, Kakinoki M, Sawada T, Wang X, Ohji M. Ranibizumab and Aflibercept: Intraocular Pharmacokinetics and Their Effects on Aqueous VEGF Level in Vitrectomized and Nonvitrectomized Macaque Eyes. Invest Ophthalmol Vis Sci. 2015 Oct;56(11):6501–5.

100. Krohne TU, Liu Z, Holz FG, Meyer CH. Intraocular pharmacokinetics of ranibizumab following a single intravitreal injection in humans. Am J Ophthalmol. 2012 Oct;154(4):682-686.e2.

101. Xu L, Lu T, Tuomi L, Jumbe N, Lu J, Eppler S, et al. Pharmacokinetics of ranibizumab in patients with neovascular age-related macular degeneration: a population approach. Invest Ophthalmol Vis Sci. 2013 Mar 5;54(3):1616–24.

102. Christoforidis JB, Williams MM, Kothandaraman S, Kumar K, Epitropoulos FJ, Knopp MV. Pharmacokinetic properties of intravitreal I-124-aflibercept in a rabbit model using PET/CT. Curr Eye Res. 2012 Dec;37(12):1171–4.

103. Do DV, Rhoades W, Nguyen QD. Pharmacokinetic study of intravitreal aflibercept in humans with neovascular age-related macular degeneration. Retina Phila Pa. 2019 May 27;

104. Lau CML, Yu Y, Jahanmir G, Chau Y. Controlled release technology for anti-angiogenesis treatment of posterior eye diseases: Current status and challenges. Adv Drug Deliv Rev. 2018 15;126:145–61.

USC
UNIVERSIDADE
DE SANTIAGO
DE COMPOSTELA

Chapter 4. Preclinical PET study of intravitreal injections

USC
UNIVERSIDADE
DE SANTIAGO
DE COMPOSTELA

4. PRECLINICAL PET STUDY OF INTRAVITREAL INJECTIONS

4.1. INTRODUCTION

To date, most topical and systemic drugs have not achieved adequate therapeutic levels in the vitreous, mainly owing to the existence of different physiological barriers (1). On one hand, topically instilled drugs are diluted by the tear film, thus causing significant drug loss in the lachrymal flow, (2) and furthermore their physicochemical characteristics must be adequate to cross the cornea (3). On the other hand, the blood–retinal barrier (BRB), which comprises the retinal pigment epithelium and the tightly sealed walls of the retinal capillaries, complicates the arrival of systemic drugs to the vitreous (4). For these reasons, intravitreal administration has become an effective way to deliver drugs to the vitreous cavity, allowing high drug concentrations (5).

To achieve a sustained therapeutic drug concentration in the vitreous, the frequency of administration should be based on the half-life of the drug ($t_{1/2}$). Regarding this question, several *in vitro* models have been proposed for the study of intravitreal pharmacokinetics, which consider all aspects of the ocular anatomy and physiology (6–9). However, one aspect that should be taken into consideration in the *in vitro* pharmacokinetic studies is the absence of convection (10–13), even though the principal mechanism of transport through the vitreous is diffusion, and convection does not play a relevant role in the kinetics of small molecules. Other issues such as protein binding, melanin binding, drug metabolism, or active transport are usually not taken into account in the *in vitro* studies (8,14). On the other hand, *in vivo* classical pharmacokinetic studies of intravitreal injections are limited because invasive techniques are involved (15,16).

In recent years, molecular imaging techniques have become a turning point for the development and pharmacokinetic study of new drugs. These techniques involve non-invasive procedures in order to significantly decrease the number of animals used by increasing the number of measurements on each animal (17,18). In particular for the field of intravitreal drugs, single photon emission computed tomography and magnetic resonance image (MRI) have been the most commonly used imaging techniques, mainly to study pharmacokinetics (14,19) and the release of drugs from implants and liposomes (20–22).

However, in pharmacokinetic studies performed with MRI, the molecules used for the labelling of the drug usually have very high molecular weight, which can alter the properties of the original drug (21).

The use of positron emission tomography (PET) has made it possible to label drugs with small b-emitting radioisotopes (23). Current integrated PET/computed tomography (CT) scanners allow visualization of radiolabelled molecules by using a direct and non-invasive methodology, and the follow-up of the same subject over time to determine the pharmacokinetic properties of intravitreal injections (24–26).

Different radionuclides can be used to elaborate radiotracers for PET scanning. The most commonly used radionuclides are typically isotopes with short half-lives such as ^{11}C, ^{13}N, ^{15}O, ^{18}F, ^{68}Ga, ^{82}Rb, or with longer half-lives such as ^{124}I or ^{89}Zr. ^{18}F is one of the most widely used because it is easily produced with a cyclotron, its positron energy of emission is 0.64 MeV, it is safe for patients, and it allows to obtain images with high resolution. Moreover, its half-life is long enough to be able to produce commercially manufactured fluorinated radiotracers at off-site locations and to be shipped to imaging services. In practice, ^{18}F radionuclide is linked to different molecules to achieve selective transport and distribution (27).

Drug clearance in the vitreous can be influenced by various factors that include molecular weight, physicochemical properties of the drug, surgical procedure, injected volumes, and presence of ocular inflammation (1). Also, the mechanisms of membrane transport and plasmatic clearance can highly influence the distribution and elimination of drugs after intravitreal administration. For this reason, fluorodeoxyglucose (^{18}F-FDG), ^{18}F-choline (^{18}F-Choline), and ^{18}F-sodium fluoride (^{18}F-NaF) were selected in our study because of their

different molecular weight, polarity, and transport mechanism across biological membranes. The aim of the present work was to study the effect of some of these factors on the vitreous clearance by using dedicated PET/CT imaging techniques for *in vivo* studies in rats.

4.2. MATERIALS AND METHODS

Our work was designed as an experimental study in rats scanned in a dedicated PET/CT system after intravitreal injections of different radiolabelled molecules, different volumes, and absence/presence of inflammatory eye disease (uveitis).

4.2.1. Animals

This study was carried out on male adult Sprague-Dawley rats with an average weight of 300 g, supplied by the animal facility of the University of Santiago de Compostela (Santiago de Compostela, Spain). During the experiments, the animals were kept in individual cages with free access to food and water in a room under controlled temperature (22 ± 1 °C) and humidity (60 ± 5 %) and with day–night cycles regulated by artificial light (12/12 hours). The animals were treated as indicated in the ARVO Statement for the Use of Animals in Ophthalmic and Vision Research and according to the guidelines for laboratory animals (28,29). Experiments were approved by the Galician Network Committee for Ethical Research and followed the Spanish and European Union (EU) rules (86/609/CEE, 2003/ 65/CE, 2010/63/EU, RD 1201/2005, and RD53/2013).

4.2.2. Intravitreal injection procedure

Intravitreal injection was performed according to the procedure described previously by Chiu et al. (30). Firstly, the animals were placed in a gas chamber containing 2 % isoflurane in oxygen. When unconscious, the animals were removed from the chamber but kept under anaesthesia with a mask (1.5 % isoflurane in oxygen). The procedure was initiated by applying one drop of topical anaesthesia (Colircusí Anestésico Doble®: tetracaine 1 mg/mL and oxybuprocaine 4 mg/mL) on the eye followed by mydriatic eye drops (phenylephrine 100 mg/mL [Colircusí Fenilefrina®] and tropicamide 10 mg/mL [Colircusí Tropicamide®]) to

visualize the eye fundus. Thereafter, radiolabelled molecules were injected into the vitreous through the pars plana by using a Hamilton syringe with a 34 G needle. The injection procedure was performed with a surgical microscope (Takagi OM-5 220-2; Takagi, Tokyo, Japan). Pictures of the procedure were taken by means of a digital camera (Nikon D-200; Nikon, Tokyo, Japan) attached to the microscope. Eyes with lens damage, or with significant bleeding when the intravitreal injection was made, were discarded from the study.

4.2.3. Experiments

The experiments were carried out by using intravitreal injections with three radiolabelled molecules and three different injection volumes, in healthy eyes and in eyes with lipopolysaccharide (LPS)–induced uveitis.

4.2.3.1. Effect of the type of injected radiolabelled molecules

Three different molecules were labelled with ^{18}F to evaluate the intravitreal pharmacokinetics. The radiolabelled molecules to be injected were ^{18}F-NaF, ^{18}F-FDG, and ^{18}F-Choline, with molecular weights of 41, 182, and 122 g/mol, respectively (Figure 4.1).

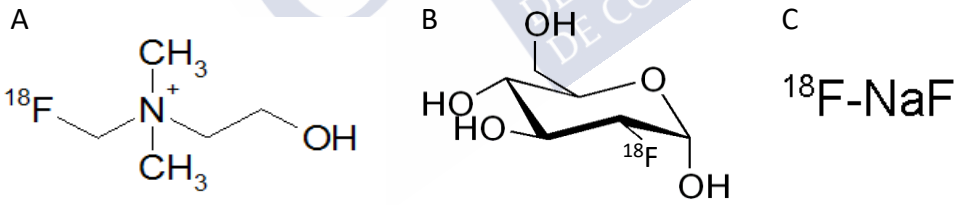

Figure 4.1. Chemical structure of (A) ^{18}F-Choline, (B) ^{18}F-FDG, and (C) ^{18}F-NaF.

The radioisotope ^{18}F was obtained from the nuclear reaction ^{18}O (proton, neutron) carried out in our PET Trace 800 cyclotron, according to the method described by Saha (31). The radiosynthesis of ^{18}F-Na was made with a carbonate-type anion-exchange resin column, in such a way that the ^{18}F is retained into the column and it is recovered as ^{18}F-sodium fluoride by elution with potassium carbonate solution. ^{18}F-FDG and ^{18}F-Choline were produced on a TRACERlab MX synthesizer (GE Healthcare, Waukesah, WI, USA) by using cassettes and reagent kits from ABX (Advanced Biochemical Compounds, Radeberg, Germany). The nucleophilic substitution standard method was used in the case of ^{18}F-FDG and for the

reaction of ^{18}F-fluoromethyl triflate with dimethylethanolamine on a Sep-Pak column used in the case of ^{18}F-Choline (32,33).

All procedures to obtain radiolabelled molecules were performed under good-manufacturing-practice conditions following the specific standards of European Pharmacopoeia (34). The purity and stability quality control requirements were undertaken via high-pressure liquid chromatography/ion chromatography (930 Compact IC Flex con; Metrohm AG, Herisau, Switzerland) and thin layer chromatography. Osmolality (mOsm/kg) and pH were determined with a vapor pressure osmometer (VAPRO 5520; ELITECH Group, Paris, France) and a pH meter (WTW inoLab; WTW, Weilheim, Germany).

4.2.3.2. Effect of the injected volumes

The effect of the injected volume on the intravitreal pharmacokinetics of the abovementioned molecules was evaluated by using three different volumes: 2, 4, and 7 µL.

4.2.3.3. Effect of the presence of inflammation

Intravitreal pharmacokinetics was assessed in a uveitis animal model previously used by our group (33) and then compared to the intravitreal pharmacokinetics in healthy eyes. To induce uveitis, rats were inoculated into the right posterior paw with 1 mg/kg *Escherichia coli* LPS diluted in 0.1 mL phosphate buffered saline by using a BD Micro-Fine syringe (BD, Oxford, UK) with 30 G needles. The presence of uveitis was assessed by direct inspection of the eye, using the surgical microscope. The animals were kept under such conditions for 24 hours. To reduce the number of animals, the influence of volume and presence or absence of uveitis were examined only for ^{18}F-NaF (mono-exponential kinetics) and ^{18}F-FDG (biexponential kinetics). Four animals (eight eyes) were used in each condition studied.

4.2.4. Data acquisition and analysis

4.2.4.1. PET data acquisition

After the intravitreal injections of 1 MBq in each eye for all experimental conditions, dynamic PET acquisition was carried out to generate eight images of 15 minutes' duration for the first 1.5 hours. Afterwards, single PET images were obtained at 4 and 6 hours after drug administration. PET and CT images were acquired by using an Albira PET/CT Preclinical Imaging System (Bruker Biospin, Woodbridge, CT, USA). Animals were kept under anaesthesia with a mask (1.5 % isoflurane in oxygen). Respiration frequency and body temperature were monitored during the anaesthesia period. The PET subsystem comprises three rings of eight compact modules based on monolithic crystals coupled to multianode photomultiplier tubes, forming an octagon with an axial field of view (FOV) of 40 mm per ring and a transaxial FOV of 80 mm in diameter. The CT system comprises a commercially available microfocus x-ray tube and a CsI scintillator 2D pixelated flat panel x-ray detector. Scatter and random coincidences were corrected by using the protocols implemented in the scanner. Attenuation correction was not performed. Images were reconstructed by using the maximum likelihood expectation maximization algorithm. Twelve iterations were performed with a reconstructed image pixel size of 0.4 x 0.4 x 0.4 mm^3.

4.2.4.2. PET data analysis

After reconstruction, quantitative measurements were obtained by using the Amide's Medical Image Data Examiner (35). Different regions of interest (ROIs) were manually drawn containing the signal on each eye. The ROIs were then replicated on the different temporal image frames to obtain the decrease curve of the radioisotope over time, conveniently corrected for radioactive decay.

4.2.4.3. Statistical analysis

The curves of percentage of radiotracer in the eye versus time were fitted to the mono- and bi-compartmental pharmacokinetic models by using nonlinear least squares regression

analysis. The area under the percentage of radiotracer time curve AUC_0^{360} from zero to infinity was calculated by log-trapezoidal rule. The statistical analysis of experiments was performed by using a one-way analysis of variance (ANOVA) and Tukey's multiple comparisons test. The nonlinear fitting and the statistical analysis were made by using the GraphPad Prism 6.01 software (2014; GraphPad Software, Inc., San Diego, CA, USA).

4.3. RESULTS

All radiolabelled molecules were clearly detected in the vitreous cavity at the initial time of the study and it was possible to observe how the signal decreased over time. Figure 4.2 shows the coronal views of the fused PET/CT images from the initial frame (10 minutes after the injection) to the last frame (360 minutes after the injection).

Figure 4.2. Fused image PET/CT showing the signal evolution in the rat eyes throughout time (minutes).

4.3.1. Effect of the type of radiolabelled molecules

The values measured from the ROI, containing each eye throughout time, were obtained for the three radiolabelled molecules, giving rise to significantly different kinetic curves (Figure 4.3-A).

On the one hand, the clearance curves from ^{18}F-FDG and ^{18}F-Choline tracers appeared to fit a two-compartment model with a biphasic clearance from the vitreous. The obtained average intravitreal half-lives for these radiolabelled molecules were 13.99 minutes for ^{18}F-FDG and 35.18 minutes for ^{18}F-Choline for the initial rapid elimination phase (α), and 214.2 minutes and 1351 minutes, respectively, for the slow elimination phase (β). Table 4.1 shows the pharmacokinetic parameters obtained by fitting the data to a bicompartmental model.

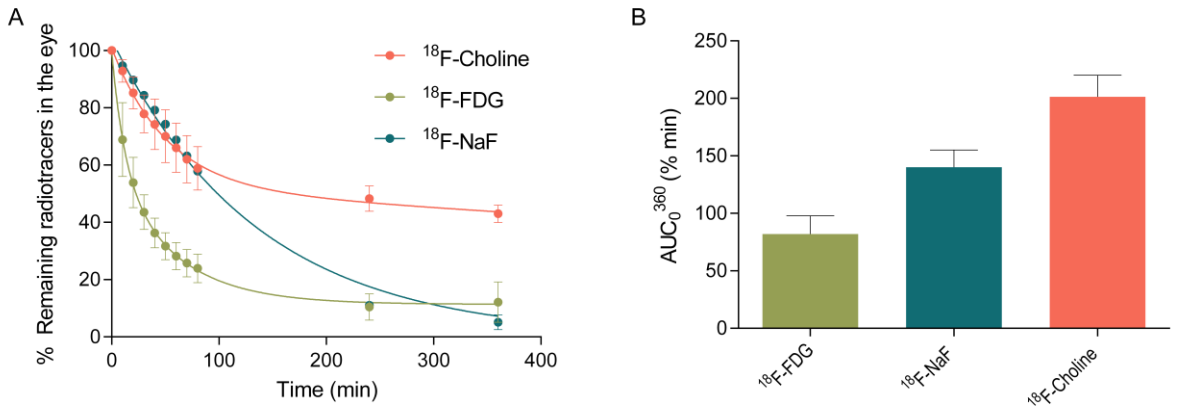

Figure 4.3. Influence of the drug type on its intravitreal release (mean ± SD, n = 8). A) Intravitreal pharmacokinetic profile of ^{18}F-FDG, ^{18}F-NaF and ^{18}F-Choline after intravitreal injection of 7 µL. B) Representation of AUC_0^{360} (% min) for all radiotracers. *One-way ANOVA analysis and Tukey multiple comparison test show significant differences among the three different compounds (α < 0.01).

Table 4.1. Pharmacokinetic parameters obtained by fitting the data to a bi-compartmental model for ^{18}F-FDG and ^{18}F-Choline.

Pharmacokinetic parameter	^{18}F-FDG				^{18}F-Choline
	2 µL #	4 µL #		7 µL #	7 µL
		Healthy*	Uveitis*		
α (min^{-1})	0.0336	0.03341	0.0416	0.0495	0.01970
$t_{1/2\alpha}$ (min)	20.65	20.75	16.66	13.99	35.18
β (min^{-1})	0.00285	0.002421	0.00218	0.00324	0.00051
$t_{1/2\beta}$ (min)	243.0	286.4	317.8	214.2	1351
AUC_0^{360} (% min)	70.13 ± 5.31	88.15 ± 7.86	70.01 ± 5.70	82.05 ± 15.67	201.3 ± 18.83
R^2	0.9958	0.9958	0.9938	0.9963	0.9971

*Statistical differences for AUC_0^{360} (% min) between healthy and uveitis eyes for α < 0.01.

No statistical differences for AUC_0^{360} (% min) were observed between different injection volumes (α n.s.).

On the other hand, the clearance curve from ^{18}F-Na showed a one-compartment pharmacokinetic model, and the average intravitreal half-life was 113.2 minutes. Table 4.2 shows the pharmacokinetic parameters obtained by fitting the data to a one-compartment pharmacokinetic model. When comparing the area under the curve between 0 and 360 minutes (AUC_0^{360}) among three radiolabelled molecules, it was observed that ^{18}F-Choline remains significantly longer in the eye than ^{18}F-FDG and ^{18}F-NaF (Figure 4.3-B).

Table 4.2. Pharmacokinetic parameters obtained by fitting the data to mono-compartmental model with ^{18}F-NaF.

Pharmacokinetics parameter	^{18}F-NaF			
	2 µL #	4 µL #		7 µL #
		Healthy**	Uveitis**	
k (min^{-1})	0.00669	0.00656	0.00805	0.00612
$t_{1/2}$ (min)	103.6	105.7	86.11	113.2
AUC_0^{360} (% min)	140.15 ± 14.93	135.23 ± 14.09	123.69 ± 21.09	137.03 ± 5.72
R^2	0.9982	0.9982	0.9952	0.9956

**No statistical differences were observed for AUC_0^{360} (% min) between healthy and uveitis eyes (α n.s.).

No statistical differences were observed for AUC_0^{360} (% min) among different injection volumes (α n.s.).

The radiolabelled molecules leave the eye and reach the systemic circulation, following different kinetic curves. Furthermore, the distribution at system level is also significantly different. Figure 4.4 shows that ^{18}F-NaF is captured by bone structures, while ^{18}F-FDG and ^{18}F-Choline are captured by internal organs.

The radiolabelled molecules used for the intravitreal injection had radiochemical purity for ^{18}F-FDG higher than 95 % with a specific activity of approximately 1000 MBq/mL. The ^{18}F-Choline had radiochemical purity higher than 95 % with a specific activity of approximately 500 MBq/mL. All radiotracers showed percentages of fluorine bound to the radiotracer that were higher than 95 % at 8 hours post synthesis. The osmolality of all radiolabelled solutions was approximately 280 ± 10 mOsm/kg with a pH around 7.4.

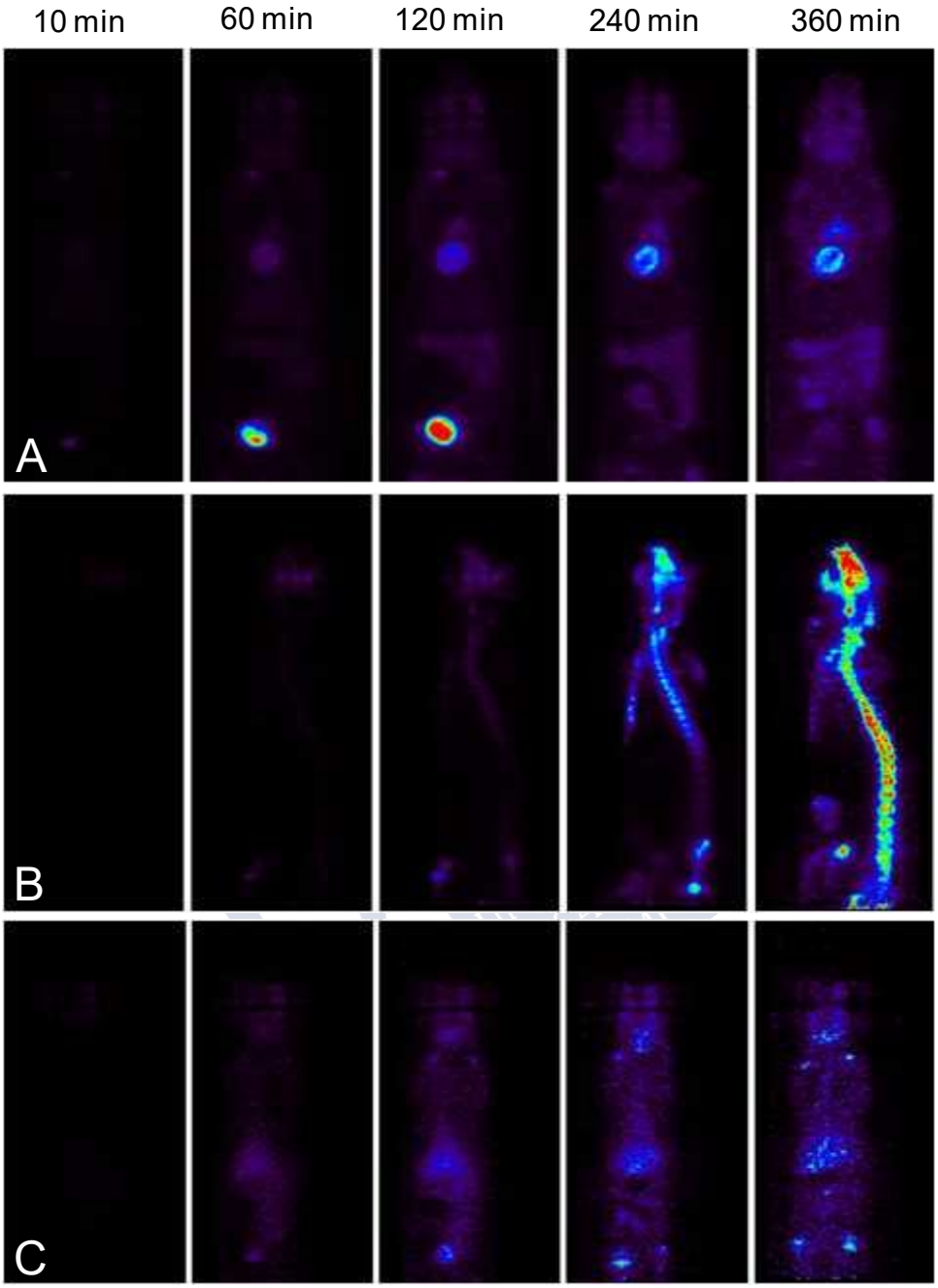

Figure 4.4. Representation of the systemic distribution of radiotracers at different times after intravitreal administration. **A)** Coronal views after injection of ^{18}F-FDG. **B)** Sagittal views after injection of ^{18}F-NaF. **C)** Coronal views after injection of and ^{18}F-Choline.

4.3.2. Effect of the injected volumes

Figure 4.5 shows no differences among the different volumes of intravitreal injections (2, 4, and 7 µL) for ^{18}F-Na and ^{18}F-FDG radioisotopes, which follow the same kinetics as previously described in Figure 4.3-A. Tables 4.1 and 4.2 show that no statistically significant differences

were found among pharmacokinetic parameters in relation to the injected volumes of both ^{18}F-FDG (Table 4.1) and ^{18}F-Na (Table 4.2). Finally, it should be noted that a transient vascular collapse in the retinal vessels was observed after administration of 7 µL, but not for 2 and 4 µL.

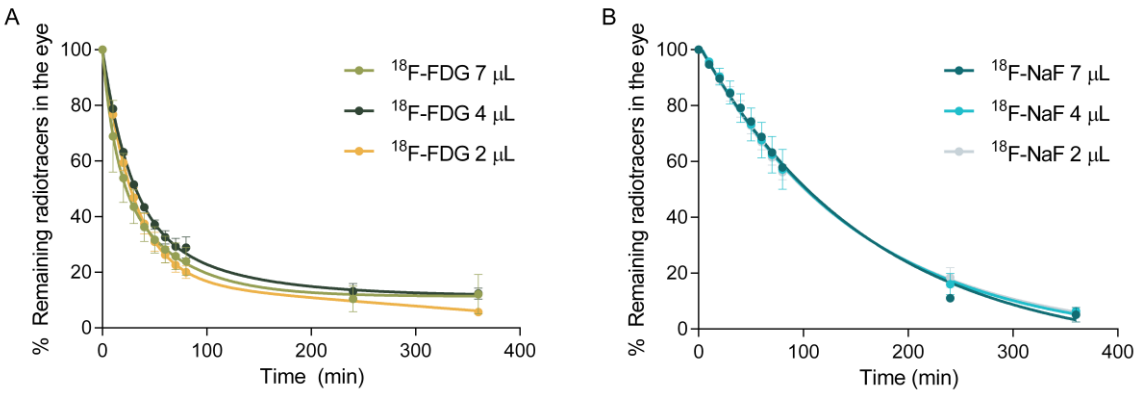

Figure 4.5. Influence of the injection volume on vitreal release (mean ± SD, n = 8). Intravitreal pharmacokinetic profile of ^{18}F-FDG (**A**) and ^{18}F-NaF (**B**) after intravitreal injection of 2, 4, and 7 µL.

4.3.3. Effect of the presence of inflammation

Figure 4.6-A shows that inflammation slightly, but with statistical significance, increased the vitreous clearance of ^{18}F-FDG. This effect was quantified by comparing the AUC_0^{360} of radiolabelled molecules in uveitis and under normal conditions. Figure 4.6-B shows that eyes with uveitis had smaller AUC_0^{360} than healthy eyes. In addition, statistically significant differences were found between the pharmacokinetic parameters in uveitis and healthy conditions for the case of ^{18}F-FDG (Table 4.1). It must be mentioned that animals receiving an LPS injection developed a fibrinous reaction in the anterior chamber of the eye, which produced a pupillary membrane and an irregular pupil after drug-induced mydriasis, caused by the adhesion of the iris to the lens (Figure 4.7). The uveitis model was successfully achieved in the same way as obtained in our previous studies (36).

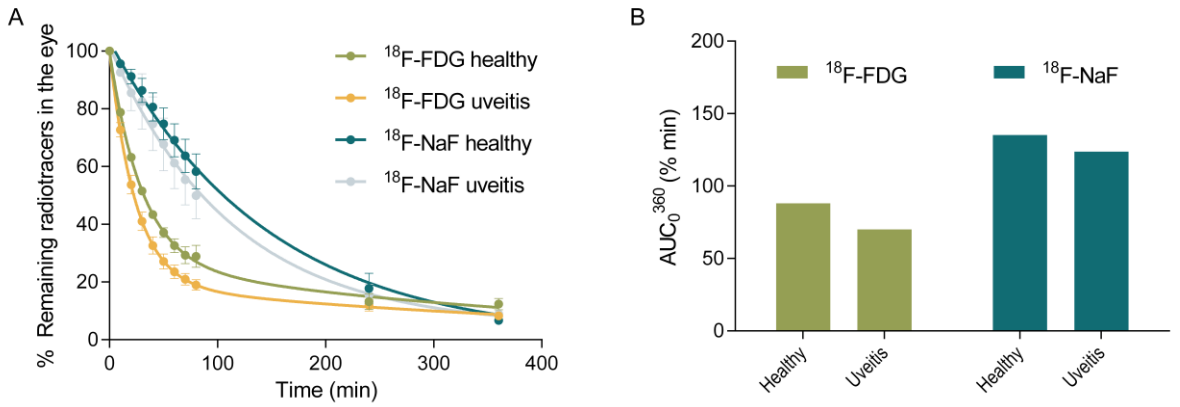

Figure 4.7. Influence of the inflammation on vitreal release (mean ± SD, n = 8). A) Intravitreal pharmacokinetic profile of ^{18}F-FDG and ^{18}F-NaF after a 7uL intravitreal injection in healthy eyes and in eyes with uveitis. B) Representation of AUC_0^{360} (% min) for ^{18}F-FDG and ^{18}F-NaF in these conditions. *Statistically significant differences between healthy and uveitis rats for $\alpha < 0.01$.

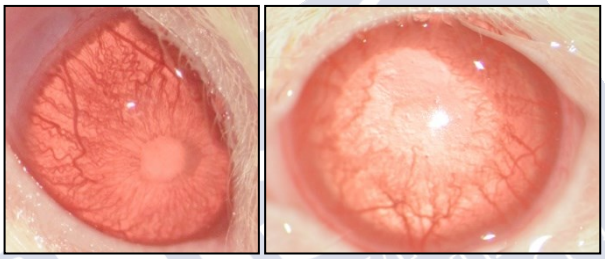

Figure 4.6. Anterior segment of two eyes 24 hours after pad injection of LPS showing signs of uveitis. **Left**: Fibrinous reaction producing a pupillary membrane. **Right**: Irregular pupil after drug induced mydriasis caused by the adhesion of the iris to the lens.

4.4. DISCUSSION

Intravitreal injections are increasingly used in a multitude of retinal ophthalmic conditions such as age-related macular degeneration (37), diabetic macular oedema (38), macular holes (39), branch and central retinal vein occlusion (40) and endophthalmitis (41). The development of new intravitreal drugs or systems that modify their release involves wide preclinical development (42) in which pharmacokinetic studies play a key role (43).

The use of small animals, such as Sprague Dawley rats, has many advantages because of their small size, the availability of research animal facilities, and multiple disease models suitable for them (44,45). However, since they have a small vitreous volume, classic pharmacokinetic studies become difficult, with *in vivo* imaging being an ideal technique, as no invasive

modalities are required to obtain experimental results (46,47). To the best of our knowledge, our work is the first study of intravitreal pharmacokinetics with PET/CT in rats. Previous intravitreal pharmacokinetic studies have required larger numbers of animals and more complex techniques to determine vitreous drug levels at different time points (48–50). In our study serial measurements were obtained at multiple time points after the intravitreal injection in the same animal. The advantage of preclinical PET/CT images in this field is very important because the technique is non-invasive, and it yields images in 3D and real time (51). PET/CT is also becoming a relevant procedure for ophthalmic research, as it has been used for diagnosis of intraocular tumours (52), neurophysiological studies (53,54) or pharmacokinetic studies with topical ophthalmic formulations (23). Although PET is a very sensitive technique, it presents some limitations related to low spatial resolution. As an example, the delineation of the vitreous area is troublesome and challenging owing to the small size of the eyeball, and therefore our measurements cannot be restricted exclusively to the vitreous area.

More than 10 % of currently used drugs contain fluorine atoms that can be labelled with ^{18}F. Moreover, the substitution of oxygen atoms or hydroxyl groups by fluorine is relatively easy with no critical changes in the properties of the molecule (55). Fluoride and oxygen have a very similar radius, whereas that of hydrogen is slightly smaller (van der Waals radii are 1.47, 1.57, and 1.20 angstroms, respectively); therefore, changing oxygen or hydrogen for fluoride does not entail substantial modifications in the molecular structure by steric impediments. Furthermore, in terms of Taft E_s parameters (56), fluoride and hydroxyl substituents have very similar characteristics (+0.78 vs +0.69); therefore, their substitution does not compromise either the structural activity of the compound or its interaction with receptors. The electronegativity of fluoride and hydrogen atoms is different (4.0 vs 2.1), hence interchanging them can substantially affect the physicochemical properties of the molecule (pKa, hydrogen bond capacity, or lipophilicity). On the contrary, fluoride and oxygen have similar values (4.0 vs 3.5), so no major changes should be expected when interchanged (55). Owing to the relatively short half-life of ^{18}F, the fluorinated radiotracers have limited use in studies of pharmacokinetics or biodistribution of drugs with long half-lives in the vitreous cavity. For these long-term studies, using other radiotracers with long half-lives such as ^{124}I (57,58) or ^{89}Zr (59) is more adequate.

Fluorinated radiotracers, as the ones used in this work, have the advantage of their low positron emission energy (the lowest of all the radiolabels used in PET). Furthermore, the greater sensitivity of modern PET technology allows the use of low radioactivity levels, so the dose received and absorbed by the animal is significantly below the dose limit (60). Additionally, during the disintegration of ^{18}F, no γ rays or α and β particles are emitted, reducing the dose received by animals and increasing safety (61). On the other hand, cytotoxicity and acute irritation of fluorinated radiotracers have been described as safe in previous reports (23). In our study, no alterations in the eye of the animals were observed after the administration of the fluorinated radiotracers.

Our findings showed significant differences among the different radiolabelled molecules we used. The reason for these differences could rest on the mechanism used for crossing the BRB. In the rat retina there are transporters for glucose and cationic amino acids, which probably are used by ^{18}F-FDG and ^{18}F-Choline to leave the vitreous cavity (62). The biexponential kinetics we observed is also common for intravitreal drugs such as bevacizumab and ranibizumab (50,63). Furthermore, it must be mentioned that hyaluronic acid, which is part of the vitreous humour, has a highly negative charge at physiological pH levels. Because of this, it could interact with positively charged molecules, such as choline, by generating polyelectrolyte complexes with low solubility (64). This is probably the reason why choline is released at a slower rate than glucose. On the other hand, our findings showed that ^{18}F-NaF is eliminated from the vitreous, following mono-exponential kinetics, which could be explained by assuming passive diffusion through the BRB because this compound diffuses freely across membranes (65). It would be similar to the release kinetics of other intravitreal drugs, such as aflibercept (15,66).

Our findings showed that the injected volume had no significant influence on vitreous drug clearance. Different studies have been carried out in human eyes (67) and in murine models (68,69) using a wide range of intravitreal injection volumes (2-20 µL), but they did not include an evaluation of their impact on the vitreous drug clearance. On the other hand, it has been pointed out that an increase of intraocular pressure could result in an increase of hydraulic flow, derived from the excess of volume introduced (10). This increase in intraocular pressure

could be the cause of the transitory collapse we observed with the administration of 7 µL. However, this process seems not to have an effect on the vitreous clearance of low-molecular-weight drugs (70,71), such as the ones we used, where all radiolabelled molecules had molecular weights below 500 Da. Finally, it has to be mentioned that the vitreous volume of a rat is smaller than that of humans (approximately 50 µL in rats versus 4.5 mL in humans) (72). This difference must be kept in mind if our results are to be translated to humans.

Our results showed an increase in the intravitreal clearance of the ^{18}F-FDG radiotracer in eyes with inflammation (uveitis) when compared to healthy eyes. On the contrary, no significant differences were observed for ^{18}F-NaF. Studies using MRI techniques have shown that inflammation in rabbit eyes, induced by LPS, can increase the permeability of BRB (73,74). On the other hand, additional studies have demonstrated that in inflammatory conditions, as in tumours, a high FDG uptake and a high GLUT-1 expression level is observed (75). Of note, ^{18}F-NaF is not affected by changes produced by the inflammatory process probably because it is freely diffusible across membranes (65). However, the increase in permeability and GLUT transporter under inflammatory conditions can increase the clearance of ^{18}F-FDG from the vitreous. Since the magnitude of the clearance changes found were small, it would be necessary to carry out additional studies to properly establish the influence of inflammation on the BRB permeability. It is possible that the severity of the inflammatory process determines the increase of BRB permeability and hence, the intravitreal clearance rate.

Finally, although the effect of inhaled anaesthesia, in particular isoflurane, on drug permeability has been extensively studied in the blood–brain barrier (BBB), no studies have shown any type of modification in the status of the BRB (76). Inhaled isoflurane in rats decreases the transfer of small hydrophilic molecules across the BBB, either by reducing the perfused capillary surface area or by a direct effect of isoflurane on the permeability of the BBB (77).

Even though BRB and BBB are thought to have similar properties owing to their similar anatomic features, some differences in the capillary endothelia at BBB and BRB have been found (78). These differences could cause a variation in the permeability across BRB compared to BBB (79), which would ultimately affect the half-life and clearance of drugs injected into

the vitreous. Therefore, we cannot assume that the observed increase in permeability through BBB would lead to a similar effect in BRB. Studies about the effect on inhaled anaesthesia on BRB permeability would be of great interest.

4.5. CONCLUSION

In summary, we demonstrated for the first time the usefulness of a PET-based methodology for the study of different factors influencing intravitreal pharmacokinetics in rats. This can be a powerful tool to develop new drugs aimed at treating ocular conditions, using intravitreal administration.

4.6. REFERENCES

1. Radhika M, Mithal K, Bawdekar A, Dave V, Jindal A, Relhan N, et al. Pharmacokinetics of intravitreal antibiotics in endophthalmitis. J Ophthalmic Inflamm Infect. 2014 Sep 10;4:22.
2. Fernández-Ferreiro A, Silva-Rodríguez J, Otero-Espinar FJ, González-Barcia M, Lamas MJ, Ruibal A, et al. In vivo eye surface residence determination by high-resolution scintigraphy of a novel ion-sensitive hydrogel based on gellan gum and kappa-carrageenan. Eur J Pharm Biopharm. 2017 May;114:317–23.
3. Fernández-Ferreiro A, González-Barcia M, Otero Espinar FJ, Blanco Méndez J, Lamas MJ. Ophthalmic formulations new goals. Farm Hosp Órgano Of Expr Científica Soc Esp Farm Hosp. 2016 Feb;40(1):1–2.
4. Gaudana R, Ananthula HK, Parenky A, Mitra AK. Ocular Drug Delivery. AAPS J. 2010 May 1;12(3):348–60.
5. Solomon SD, Lindsley K, Vedula SS, Krzystolik MG, Hawkins BS. Anti-vascular endothelial growth factor for neovascular age-related macular degeneration. Cochrane Database Syst Rev. 2014;8:CD005139.
6. Balachandran RK, Barocas VH. Computer Modeling of Drug Delivery to the Posterior Eye: Effect of Active Transport and Loss to Choroidal Blood Flow. Pharm Res. 2008 Nov 1;25(11):2685–96.
7. Awwad S, Lockwood A, Brocchini S, Khaw PT. The PK-Eye: A Novel In Vitro Ocular Flow Model for Use in Preclinical Drug Development. J Pharm Sci. 2015 Oct 1;104(10):3330–42.
8. Park J, Bungay PM, Lutz RJ, Augsburger JJ, Millard RW, Sinha Roy A, et al. Evaluation of coupled convective–diffusive transport of drugs administered by intravitreal injection and controlled release implant. J Controlled Release. 2005 Jul 20;105(3):279–95.

9. Krishnamoorthy MK, Park J, Augsburger JJ, Banerjee RK. Effect of retinal permeability, diffusivity, and aqueous humor hydrodynamics on pharmacokinetics of drugs in the eye. J Ocul Pharmacol Ther Off J Assoc Ocul Pharmacol Ther. 2008 Jun;24(3):255–67.

10. Xu J, Heys JJ, Barocas VH, Randolph TW. Permeability and diffusion in vitreous humor: implications for drug delivery. Pharm Res. 2000 Jun;17(6):664–9.

11. Gisladottir S, Loftsson T, Stefansson E. Diffusion characteristics of vitreous humour and saline solution follow the Stokes Einstein equation. Graefes Arch Clin Exp Ophthalmol Albrecht Von Graefes Arch Klin Exp Ophthalmol. 2009 Dec;247(12):1677–84.

12. Ohtori A, Tojo K. In vivo/in vitro correlation of intravitreal delivery of drugs with the help of computer simulation. Biol Pharm Bull. 1994 Feb;17(2):283–90.

13. Tojo K, Nakagawa K, Morita Y, Ohtori A. A pharmacokinetic model of intravitreal delivery of ganciclovir. Eur J Pharm Biopharm Off J Arbeitsgemeinschaft Pharm Verfahrenstechnik EV. 1999 Mar;47(2):99–104.

14. Del Amo EM, Rimpelä A-K, Heikkinen E, Kari OK, Ramsay E, Lajunen T, et al. Pharmacokinetic aspects of retinal drug delivery. Prog Retin Eye Res. 2017 Mar;57:134–85.

15. Avery RL, Castellarin AA, Steinle NC, Dhoot DS, Pieramici DJ, See R, et al. Systemic pharmacokinetics following intravitreal injections of ranibizumab, bevacizumab or aflibercept in patients with neovascular AMD. Br J Ophthalmol. 2014 Dec;98(12):1636–41.

16. Bhagat R, Zhang J, Farooq S, Li X-Y. Comparison of the Release Profile and Pharmacokinetics of Intact and Fragmented Dexamethasone Intravitreal Implants in Rabbit Eyes. J Ocul Pharmacol Ther. 2014 Dec 1;30(10):854–8.

17. Cunha L, Szigeti K, Mathé D, Metello LF. The role of molecular imaging in modern drug development. Drug Discov Today. 2014 Jul;19(7):936–48.

18. Capozzi ME, Gordon AY, Penn JS, Jayagopal A. Molecular Imaging of Retinal Disease. J Ocul Pharmacol Ther. 2013 Mar;29(2):275–86.

19. Rimpelä A-K, Schmitt M, Latonen S, Hagström M, Antopolsky M, Manzanares JA, et al. Drug Distribution to Retinal Pigment Epithelium: Studies on Melanin Binding, Cellular Kinetics, and Single Photon Emission Computed Tomography/Computed Tomography Imaging. Mol Pharm. 2016 Sep 6;13(9):2977–86.

20. Li SK, Lizak MJ, Jeong E-K. MRI in ocular drug delivery. NMR Biomed. 2008 Nov;21(9):941–56.

21. Kim H, Lizak MJ, Tansey G, Csaky KG, Robinson MR, Yuan P, et al. Study of ocular transport of drugs released from an intravitreal implant using magnetic resonance imaging. Ann Biomed Eng. 2005 Feb;33(2):150–64.

22. Molokhia SA, Jeong E-K, Higuchi WI, Li SK. Transscleral iontophoretic and intravitreal delivery of a macromolecule: study of ocular distribution in vivo and postmortem with MRI. Exp Eye Res. 2009 Mar;88(3):418–25.

23. Fernández-Ferreiro A, Silva-Rodríguez J, Otero-Espinar FJ, González-Barcia M, Lamas MJ, Ruibal A, et al. Positron Emission Tomography for the Development and Characterization of Corneal Permanence of Ophthalmic Pharmaceutical Formulations. Invest Ophthalmol Vis Sci. 2017 Feb 1;58(2):772–80.

24. Christoforidis JB, Williams MM, Kothandaraman S, Kumar K, Epitropoulos FJ, Knopp MV. Pharmacokinetic properties of intravitreal I-124-aflibercept in a rabbit model using PET/CT. Curr Eye Res. 2012 Dec;37(12):1171–4.

25. Christoforidis JB, Carlton MM, Knopp MV, Hinkle GH. PET/CT imaging of I-124-radiolabeled bevacizumab and ranibizumab after intravitreal injection in a rabbit model. Invest Ophthalmol Vis Sci. 2011 Jul;52(8):5899–903.

26. Christoforidis JB, Williams MM, Wang J, Jiang A, Pratt C, Abdel-Rasoul M, et al. Anatomic and pharmacokinetic properties of intravitreal bevacizumab and ranibizumab after vitrectomy and lensectomy. Retina Phila Pa. 2013 May;33(5):946–52.

27. Okamura N, Harada R, Furukawa K, Furumoto S, Tago T, Yanai K, et al. Advances in the development of tau PET radiotracers and their clinical applications. Ageing Res Rev. 2016 Sep;30:107–13.

28. The Association for Research in Vision and Ophthalmology. Statement for the Use of Animals in Ophthalmic and Visual Research [Internet]. 2014. Available from: http://www.arvo.org/About_ARVO/Policies/Statement_for_the_Use_of_Animals_in_Ophthalmic_and_Visual_Research/

29. National Research Council (US) Committee for the Update of the Guide for the Care and Use of Laboratory Animals. Guide for the Care and Use of Laboratory Animals [Internet]. 8th ed. Washington (DC): National Academies Press (US); 2011 [cited 2014 Nov 28]. (The National Academies Collection: Reports funded by National Institutes of Health). Available from: http://www.ncbi.nlm.nih.gov/books/NBK54050/

30. Chiu K, Chang RC-C, So K-F. Intravitreous Injection for Establishing Ocular Diseases Model. J Vis Exp JoVE [Internet]. 2007 Oct 1 [cited 2016 Dec 5];(8). Available from: http://www.ncbi.nlm.nih.gov/pmc/articles/PMC2562493/

31. Saha B. Basics of PET Imaging. Physics, Chemistry, and Regulations. Springer. 2010.

32. Yu S. Review of 18F-FDG Synthesis and Quality Control. Biomed Imaging Interv J [Internet]. 2006 Oct 1 [cited 2016 Dec 19];2(4). Available from: http://www.ncbi.nlm.nih.gov/pmc/articles/PMC3097819/

33. Vallabhajosula S. Molecular Imaging. Radiopharmaceuticals for PET and SPECT. Springer; 2009.

34. European Pharmacopoeia Commission. European Pharmacopoeia. 2016. (8ª Edition).

35. Loening AM, Gambhir SS. AMIDE: A Free Software Tool for Multimodality Medical Image Analysis. Mol Imaging. 2003 Jul 1;2(3):15353500200303132.

36. Bermudez MA, Sendon-Lago J, Seoane S, Eiro N, Gonzalez F, Saa J, et al. Anti-inflammatory effect of conditioned medium from human uterine cervical stem cells in uveitis. Exp Eye Res. 2016 Aug;149:84–92.

37. Lindsley K, Li T, Ssemanda E, Virgili G, Dickersin K. Interventions for Age-Related Macular Degeneration: Are Practice Guidelines Based on Systematic Reviews? Ophthalmology. 2016 Apr;123(4):884–97.

38. Payne JF, Wykoff CC, Clark WL, Bruce BB, Boyer DS, Brown DM. Randomized Trial of Treat and Extend Ranibizumab with and without Navigated Laser for Diabetic Macular Edema: TREX-DME 1 Year Outcomes. Ophthalmology. 2017 Jan;124(1):74–81.

39. Bennison C, Stephens S, Lescrauwaet B, Van Hout B, Jackson TL. Cost-effectiveness of ocriplasmin for the treatment of vitreomacular traction and macular hole. J Mark Access Health Policy [Internet]. 2016 Jun 23 [cited 2016 Dec 19];4. Available from: http://www.ncbi.nlm.nih.gov/pmc/articles/PMC4920942/

40. Clark WL, Boyer DS, Heier JS, Brown DM, Haller JA, Vitti R, et al. Intravitreal Aflibercept for Macular Edema Following Branch Retinal Vein Occlusion: 52-Week Results of the VIBRANT Study. Ophthalmology. 2016 Feb;123(2):330–6.

41. Joseph J, Nirmalkar K, Mathai A, Sharma S. Clinical features, microbiological profile and treatment outcome of patients with Corynebacterium endophthalmitis: review of a decade from a tertiary eye care centre in southern India. Br J Ophthalmol. 2016 Feb 1;100(2):189–94.

42. Martens TF, Remaut K, Deschout H, Engbersen JFJ, Hennink WE, van Steenbergen MJ, et al. Coating nanocarriers with hyaluronic acid facilitates intravitreal drug delivery for retinal gene therapy. J Controlled Release. 2015 Mar 28;202:83–92.

43. Adamson P, Wilde T, Dobrzynski E, Sychterz C, Polsky R, Kurali E, et al. Single ocular injection of a sustained-release anti-VEGF delivers 6 months pharmacokinetics and efficacy in a primate laser CNV model. J Controlled Release. 2016 Dec 28;244, Part A:1–13.

44. Williams D. Rabbit and rodent ophthalmology. Eur J Companion Anim Pract. 2007 Jan 12;17(3):242–52.

45. Pennesi ME, Neuringer M, Courtney RJ. Animal models of age related macular degeneration. Mol Aspects Med. 2012 Aug;33(4):487–509.

46. Willmann JK, van Bruggen N, Dinkelborg LM, Gambhir SS. Molecular imaging in drug development. Nat Rev Drug Discov. 2008 Jul;7(7):591–607.

47. Robinson MR, Baffi J, Yuan P, Sung C, Byrnes G, Cox TA, et al. Safety and pharmacokinetics of intravitreal 2-methoxyestradiol implants in normal rabbit and pharmacodynamics in a rat model of choroidal neovascularization. Exp Eye Res. 2002 Feb;74(2):309–17.

48. Gasparin F, Aguiar RG, Ioshimoto GL, Silva-Cunha A, Fialho SL, Liber AM, et al. Pharmacokinetics, electrophysiological, and morphological effects of the intravitreal injection of mycophenolic acid in rabbits. J Ocul Pharmacol Ther. 2014 Aug;30(6):502–11.

49. Park SJ, Oh J, Kim Y-K, Park JH, Park JY, Hong HK, et al. Intraocular pharmacokinetics of intravitreal vascular endothelial growth factor-Trap in a rabbit model. Eye Lond Engl. 2015 Apr;29(4):561–8.

50. Bakri SJ, Snyder MR, Reid JM, Pulido JS, Singh RJ. Pharmacokinetics of intravitreal bevacizumab (Avastin). Ophthalmology. 2007 May;114(5):855–9.

51. Kuntner C, Stout DB. Quantitative preclinical PET imaging: opportunities and challenges. Front Phys [Internet]. 2014 [cited 2016 Dec 19];2. Available from: http://journal.frontiersin.org/article/10.3389/fphy.2014.00012/abstract

52. Sek K, Wilson D, Paton K, Benard F. The role of 18F-FDG PET/CT in assessment of uveal melanoma and likelihood of primary tumour visualisation based on AJCC tumour size. J Nucl Med. 2016 May 1;57(supplement 2):409–409.

53. García-Rojas L, Adame-Ocampo G, Alexánderson E, Tovilla-Canales JL. 18-Fluorodeoxyglucose Uptake by Positron Emission Tomography in Extraocular Muscles of Patients with and without Graves' Ophthalmology. J Ophthalmol. 2013;2013:529187.

54. Wang W-F, Ishiwata K, Kiyosawa M, Kawamura K, Oda K, Matsuno K, et al. Investigation of the use of positron emission tomography for neuroreceptor imaging in rabbit eyes. Ophthalmic Res. 2004 Oct;36(5):255–63.

55. Amii H, Uneyama K. C−F Bond Activation in Organic Synthesis. Chem Rev. 2009 May 13;109(5):2119–83.

56. Chambers RD. The influence of fluorine of fluorocarbon groups on some reaction centers. In: Fluorine in Organic Chemistry. CRC Press; 2004.

57. Kuntner C, Wanek T, Hoffer M, Dangl D, Hornof M, Kvaternik H, et al. Radiosynthesis and Assessment of Ocular Pharmacokinetics of 124I-Labeled Chitosan in Rabbits Using Small-Animal PET. Mol Imaging Biol. 2011 Apr;13(2):222–6.

58. Dangl D, Hornof M, Hoffer M, Kuntner C, Wanek T, Kvaternik H. In vivo Evaluation of Ocular Residence Time of 124I-labelled Thiolated Chitosan in Rabbits Using MicroPET Technology. Invest Ophthalmol Vis Sci. 2009 Apr 28;50(13):3689–3689.

59. van Loon J, Even AJG, Aerts HJWL, Öllers M, Hoebers F, van Elmpt W, et al. PET imaging of zirconium-89 labelled cetuximab: A phase I trial in patients with head and neck and lung cancer. Radiother Oncol. 2017 Feb;122(2):267–73.

60. Ainsbury EA, Bouffler SD, Dörr W, Graw J, Muirhead CR, Edwards AA, et al. Radiation cataractogenesis: a review of recent studies. Radiat Res. 2009 Jul;172(1):1–9.

61. Peñuelas Sánchez I. PET Radiopharmaceuticals. Rev Esp Med Nucl. 2001;20(6):477–98.

62. Tombran-Tink J, Barnstable CJ. Ocular Transporters in Ophthalmic Diseases and Drug Delivery. Springer Science & Business Media; 2008. 454 p.

63. Bakri SJ, Snyder MR, Reid JM, Pulido JS, Ezzat MK, Singh RJ. Pharmacokinetics of intravitreal ranibizumab (Lucentis). Ophthalmology. 2007 Dec;114(12):2179–82.

64. Koss MJ, Hoffmann J, Nguyen N, Pfister M, Mischak H, Mullen W, et al. Proteomics of Vitreous Humor of Patients with Exudative Age-Related Macular Degeneration. PLoS ONE

[Internet]. 2014 May 14 [cited 2017 Jan 23];9(5). Available from: http://www.ncbi.nlm.nih.gov/pmc/articles/PMC4020801/

65. Czernin J, Satyamurthy N, Schiepers C. Molecular mechanisms of bone 18F-NaF deposition. J Nucl Med Off Publ Soc Nucl Med. 2010 Dec;51(12):1826–9.

66. Thai H-T, Veyrat-Follet C, Vivier N, Dubruc C, Sanderink G, Mentré F, et al. A mechanism-based model for the population pharmacokinetics of free and bound aflibercept in healthy subjects. Br J Clin Pharmacol. 2011 Sep 1;72(3):402–14.

67. Friedrich S, Saville B, Cheng YL. Drug distribution in the vitreous humor of the human eye: the effects of aphakia and changes in retinal permeability and vitreous diffusivity. J Ocul Pharmacol Ther Off J Assoc Ocul Pharmacol Ther. 1997 Oct;13(5):445–59.

68. Grant CA, Ponnazhagan S, Wang XS, Srivastava A, Li T. Evaluation of recombinant adeno-associated virus as a gene transfer vector for the retina. Curr Eye Res. 1997 Sep;16(9):949–56.

69. Li T, Davidson BL. Phenotype correction in retinal pigment epithelium in murine mucopolysaccharidosis VII by adenovirus-mediated gene transfer. Proc Natl Acad Sci U S A. 1995 Aug 15;92(17):7700–4.

70. Missel PJ. Hydraulic flow and vascular clearance influences on intravitreal drug delivery. Pharm Res. 2002 Nov;19(11):1636–47.

71. Missel PJ. Finite and infinitesimal representations of the vasculature: ocular drug clearance by vascular and hydraulic effects. Ann Biomed Eng. 2002;30(9):1128–39.

72. Basile AS, Glazier G, Lee A, Jiang L-Y, Johnson TR, Shields MJ, et al. Intravitreal concentrations of a near-infrared fluorescence-labeled biotherapeutic determined in situ using confocal scanning laser ophthalmoscopy. Invest Ophthalmol Vis Sci. 2011 Sep 1;52(9):6949–58.

73. Berkowitz BA, Roberts R, Luan H, Peysakhov J, Mao X, Thomas KA. Dynamic Contrast-Enhanced MRI Measurements of Passive Permeability through Blood Retinal Barrier in Diabetic Rats. Invest Ophthalmol Vis Sci. 2004 Jul 1;45(7):2391–8.

74. Metrikin DC, Wilson CA, Berkowitz BA, Lam MK, Wood GK, Peshock RM. Measurement of blood-retinal barrier breakdown in endotoxin-induced endophthalmitis. Invest Ophthalmol Vis Sci. 1995 Jun 1;36(7):1361–70.

75. Mochizuki T, Tsukamoto E, Kuge Y, Kanegae K, Zhao S, Hikosaka K, et al. FDG uptake and glucose transporter subtype expressions in experimental tumor and inflammation models. J Nucl Med Off Publ Soc Nucl Med. 2001 Oct;42(10):1551–5.

76. Cheng Y, He L, Prasad V, Wang S, Levy RJ. Anesthesia-Induced Neuronal Apoptosis in the Developing Retina: A Window of Opportunity. Anesth Analg. 2015 Nov;121(5):1325–35.

77. Chi OZ, Anwar M, Sinha AK, Wei HM, Klein SL, Weiss HR. Effects of isoflurane on transport across the blood-brain barrier. Anesthesiology. 1992 Mar;76(3):426–31.

78. Stewart PA, Tuor UI. Blood-eye barriers in the rat: correlation of ultrastructure with function. J Comp Neurol. 1994 Feb 22;340(4):566–76.

79. Toda R, Kawazu K, Oyabu M, Miyazaki T, Kiuchi Y. Comparison of drug permeabilities across the blood-retinal barrier, blood-aqueous humor barrier, and blood-brain barrier. J Pharm Sci. 2011 Sep;100(9):3904–11.

Chapter 5. PET study of ocular and blood pharmacokinetics of intravitreal bevacizumab and aflibercept in rats

USC
UNIVERSIDADE
DE SANTIAGO
DE COMPOSTELA

5. PET STUDY OF OCULAR AND BLOOD PHARMACOKINETICS OF INTRAVITREAL BEVACIZUMAB AND AFLIBERCEPT IN RATS

5.1. INTRODUCTION

Intravitreal injection of anti-vascular endothelial growth factor (anti-VEGF) antibodies is a common treatment for exudative age-related macular degeneration (AMD), choroidal neovascularisation (CNV), diabetic macular oedema (DME) and macular oedema secondary to central and branch retinal vein occlusion (RVO). Anti-VEGF agents block the growth of abnormal blood vessels in the choroid by blocking free VEGF factor in the ocular environment (1).

Aflibercept (Eylea®, Bayer AG) is a recombinant fusion protein consisting of portions from the extracellular domains of the human VEGF receptors 1 and 2 fused with the Fc (fragment crystallizable) portion of the human IgG1. It has been approved by the US Food and Drug Administration agency (FDA) and the European Medicines Agency (EMA) for the treatment of the aforementioned diseases (2,3). Bevacizumab (Avastin®, Roche) is a recombinant humanized monoclonal IgG1 antibody developed for systemic administration (4). It is widely used off-label intravitreally to treat VEGF-mediated diseases due to its lower cost and similar efficacy (5,6). Anti-VEGF antibodies are administered as single intravitreal injections of 1.25 mg/50 µL bevacizumab and 2 mg/50 µL aflibercept (7) in humans. Treatment is initiated with a predetermined interval until maximum visual acuity is achieved and/or there are no signs of disease activity. One injection per month and then every two months is the suggested initial treatment interval for aflibercept (7), while the most used schedule for bevacizumab is every one and half months (8). Thereon, the intervals are determined by the ophthalmologist based on disease activity. As a consequence, different administration schedules are used based on

clinical outcomes, instead of using administration intervals optimized from ocular pharmacokinetic parameters. This procedure is not currently integrated into clinical routine mainly due to the limited knowledge of the intravitreal pharmacokinetics of these drugs (9,10).

The insufficient data on intravitreal anti-VEGF pharmacokinetics stem from the hurdles that this type of studies entail. On the one hand, pharmacokinetic data in humans is scarce due to the invasiveness and impossibility of collecting vitreous samples. Therefore, most of the research has been done in preclinical settings (9,11). Current studies of intravitreal pharmacokinetics are carried out on animals sacrificed at different time points, thus collecting vitreous samples over time. However, the number of samples collected over time is limited, mainly due to the large number of animals required per each experiment. In this regard, Positron Emission Tomography (PET) represents a promising imaging tool for non-invasive evaluation of intravitreal pharmacokinetics (12). PET enables us to perform longitudinal studies in which each animal is followed over time and different serial measurements are taken from each animal. This clearly represents the advantage of reducing the number of animals used according to the 3Rs principles (13).

On the other hand, most intravitreal pharmacokinetic studies have relied on immunoassays to determine the ocular concentration of the antibodies (9). In this regard, PET also allows to indirectly evaluate the pharmacokinetic profile without causing major damage to the animals. Radiolabelling of antibodies with zirconium-89 has been extensively exploited in the area of oncology (ImmunoPET) (14,15). It is based on the conjugation of the antibody to a deferoxamine derivative and subsequently radiolabelling with zirconium-89 (^{89}Zr). In this sense, the radiolabelling of bevacizumab to ^{89}Zr has been already described (16,17), because of the fact that it has been also used in colon and breast cancer. Instead, radiolabelling of aflibercept to ^{89}Zr has not been attempted before.

Most of the animal models used for intravitreal pharmacokinetics are based on rabbits and monkeys (9,11). Conversely, rats have been widely used in efficacy studies, such as the laser-induced choroidal neovascularisation (CNV) model (18), but not in pharmacokinetics studies of intravitreal anti-VEGF drugs. Several researchers have attempted to develop intravitreal

drug delivery systems to modify the release of anti-VEGF antibodies (10), some of them using rats as a model to evaluate the pharmacokinetics of the underdeveloped drug delivery systems (18–21), even though there are not reliable pharmacokinetic studies in rats. The use of rats presents several advantages with respect to larger animals, such as the availability of research animal facilities at lower cost and multiple disease models suitable for them (22,23). On the contrary, intravitreal pharmacokinetic studies in rats are challenging, mainly due to the small size of the ocular structures. Our previous works showed that it is precisely here where PET imaging gains advantage over the classical methods (12,24).

The aim of this study is to evaluate the intraocular and blood pharmacokinetics after intravitreal injections of ^{89}Zr-labelled bevacizumab and ^{89}Zr-labelled aflibercept in Sprague-Dawley rats.

5.2. MATERIALS AND METHODS

Our work was designed as an experimental study in rats scanned in a dedicated PET/CT system after intravitreal administration of ^{89}Zr radiolabelled antibodies (bevacizumab and aflibercept).

5.2.1. Conjugation, radiolabelling and quality control

5.2.1.1. ^{89}Zr-labelling

Conjugation and labelling of the antibodies were performed as described previously by Verel et al. (25). First, the antibodies were purified from other excipients against milli-Q water using Amicon® Ultra-2 mL (NMWL 30 kDa) centrifugal filters (Merck®Millipore®). Tetrafluorphenil-N-succinyldesferrioxamine-B-Fe^{3+} (TFP-N-sucDf-Fe) (ABX®) (referred as DFO) was conjugated to the antibodies in a 2-fold molar excess. Conjugation was performed at room temperature for 30 min at pH 9.5-10 (pH adjusted with 0.1 M Na_2CO_3). After conjugation, the solution was set to pH 4.0-4.5 (pH adjusted with 0.25 M H_2SO_4), and a 50-molar excess of 25 mg/mL EDTA (ethylenediaminetetraacetic acid) was added. The solutions were incubated 30 min at 35°C.

Conjugated antibodies were again purified and stored at – 80 °C at the same concentration of the commercial solutions (25 mg/mL for bevacizumab and 40 mg/mL for aflibercept).

Frozen conjugated antibodies were thawed prior to labelling. Labelling was performed using clinical grade ^{89}Zr-oxalate dissolved in 1 M oxalic acid (BV cyclotron VU, PerkinElmer, Inc.). The ^{89}Zr-oxalate solution was first set at pH 4.0-4.5 (pH adjusted with 2 M Na_2CO_3) and then at pH 7 with HEPES buffer (4-(2-hydroxyethyl)-1-piperazineethanesulfonic acid). N-sucDf-antibodies were then added and incubated for at least 1 h at room temperature. Antibodies were labelled with a maximum specific activity of 15 Mbq/mg for bevacizumab and 10 Mbq/mg for aflibercept. After incubation, labelled antibodies were concentrated by ultrafiltration with Amicon® Ultra-0.5 mL Centrifugal Filters (Merck®Millipore®) (NMWL 100 kDa for bevacizumab and NMWL 30 kDa for aflibercept).

On the other hand, for control preparation 30 nm DFO were incubated with a 2.5 molar excess of EDTA for 30 min at 35 °C. Afterwards, 8.5 MBq of ^{89}Zr-oxalate were added and pH was adjusted to 7 (2 M Na_2CO_3). The solution was incubated for 30 min at room temperature.

5.2.1.2. Quality control

Size exclusion high performance liquid chromatography (SE-HPLC) was used to assess aggregation and fragmentation and calculated the conjugated ratio (Agilent 1260 Infinity II LC System). An Agilent Bio SEC-5, 5 µm, 300 Å, 7.8 x 150 mm column was used. The mobile phase consisted of phosphate-buffered saline ([PBS] 140 mmol/L NaCl, 9 mmol/L Na_2HPO_4, 1.3 mmol/L NaH_2PO_4; pH 5 7.4). The flow was 0.7 mL/min and the UV-detector wavelengths were set to 220, 280 and 430 nm. The ratio of conjugated TFP-N-sucDf to antibody was determined by the antibody-bound versus unbound 430 nm signal of Fe^{3+} on SE-HPLC.

Protein concentration was determined by ultraviolet-visible spectrophotometry (Shimadzu UV-mini 1240). Radiochemical purity (RCP) of labelled antibodies was assessed by trichloroacetic acid (TCA) precipitation test. TCA test was performed by mixing equal amounts of 1 % HSA (Human Serum Albumin) (Albunorm® 20 %, Octapharma) in PBS and 20 % trichloroacetic acid in milli-Q water and adding an aliquot of labelled antibody. The resultant solution was centrifuged, and the radiochemical purity was determined by separation of the

protein fraction and supernatant. The radioactivity in the fractions was measured by a well counter (Atomlab® Wipe Test Counter, Biodex®).

5.2.2. Animal studies

The study was carried out on male adult Sprague Dawley rats of 10 weeks-old with an average weight of 250-300 g, supplied by the animal facility of the University of Santiago de Compostela (Santiago de Compostela, Spain). During the experiments, the animals were kept in individual cages with free access to food and water in a room under controlled temperature (22 ± 1 °C) and humidity (60 ± 5 %) and with day–night cycles regulated by artificial light (12/12 hours). Animals were acclimatised for a week prior to the beginning of the experiments. The animals were treated as indicated in the ARVO Statement for the Use of Animals in Ophthalmic and Vision Research and according to the guidelines for laboratory animals. Experiments were approved by the Committee for Ethical Research of the Health Research Institute (IDIS) and followed the Spanish and European Union (EU) rules (86/609/CEE, 2003/ 65/CE, 2010/63/EU, RD 1201/2005, and RD53/2013). Three animals (six eyes) were used for each group (bevacizumab, aflibercept and DFO control).

5.2.2.1. Intravitreal administration

Previously to intravitreal injection, the rats were anaesthetised in a veterinary gas chamber containing 3 % isoflurane concentration in oxygen. Once unconscious, rats were removed and placed in a surface where they were kept under anaesthesia with a face mask (2.5% isoflurane).

Intravitreal injection was performed according to the procedure described in our previous article (12). Topical anaesthetic eye drops (1 mg/mL tetracaine hydrochloride, 4 mg/mL oxybuprocaine Hydrochloride; Colircusí anestésico doble®, Alcon Healthcare) were applied in both eyes followed by mydriatic eye drops (10 mg/mL cyclopentolate hydrochloride; Colircusí Ciclopléjico®, Alcon Healthcare) to visualise the eye fundus. The injection procedure was performed under a surgical microscope (Takagi OM-5 220-2; Takagi, Tokyo, Japan). Four µL of the ^{89}Zr-labelled antibody were injected into the vitreous through pars plana using a NanoFil®

syringe attached to a 35 G needle. 1-1.2 MBq of radiolabelled antibody was injected into each rat eye.

5.2.2.2. PET acquisition and analysis

The microPET acquisition was started immediately after intravitreal injection using the Albira Preclinical PET/CT System (Bruker Biospin). Animals were kept under anaesthesia with a face mask (2.5 % isoflurane/oxygen), monitoring the respiration frequency during the acquisition. Two bed position sequential acquisitions of 10 min were performed in order to cover the whole-body of the rats. Rats were scanned at different time points (initial; 2, 4, 8, 12, 24, 36 h; subsequently every day from 2 to 12 days) following the same procedure to determine the pharmacokinetic profile.

Images were reconstructed by using the maximum likelihood expectation maximization algorithm using 12 iterations. Reconstructed images were generated with a pixel size of 0.5 x 0.5 x 0.5 mm^3. Image analysis was performed using Amide's Medical Image Data Analysis Tool (26). Spherical Regions of Interest (ROIs) were manually drawn in order to encompass the total radiotracer uptake of each eye (12 x 12 x 12 mm, 904 mm^3) and they were replicated on the different temporal image frames. The mean radiotracer uptake obtained from the different ROIs were corrected for radioactive decay of ^{89}Zr (half-life of 3.3 days). The mean radiotracer uptake measured from the first frame just after intravitreal injection was considered as the reference, and the following measures from the subsequent frames were reported as percentage of this reference. The average value from both eyes of the same animal was used for the pharmacokinetic analysis.

5.2.2.3. Blood sample collection

After PET acquisition at each time point, rats were maintained anaesthetised and blood sample was obtained through the tail vein. Aliquots of known volume (between 10-200 µL) were obtained and measured in a well counter (Atomlab® Wipe Test Counter, Biodex®).

Activity from the blood samples was also corrected for radioactive decay. Theoretical rat blood volume was calculated based on body weight (Blood volume = 0.06 · Body weight + 0.77

(27,28)) each day in order to calculate total blood radioactivity. Blood activity levels after intravitreal injection were expressed in two forms as: 1) radioactivity per blood volume (Bq/µL), and 2) relative percentage of radioactivity respect to the ocular one obtained in the animal.

5.2.2.4. Pharmacokinetic analysis

Compartmental data analyses were performed using Phoenix WinNonlin (build 8.0, Certara L.P.) to calculate the pharmacokinetic parameters of the intravitreally injected radiolabelled drugs, aflibercept and bevacizumab, in eye (i.v.-bolus model) and blood (first-order absorption model) for each rat. Analyses based on blood concentration (Bq/µL of blood) were performed using a corrected injected dose according to total theoretical injected dose in both eyes and ocular activity at initial time. One- and two-compartment models were fit to the data using different weighting schemes like uniform, 1/predicted concentration and 1/(predicted concentration)^2. The model was chosen based on the best fit based on the calculated and observed concentration curve plots, the Akaike information Criterion (AIC), and smallest percentage of coefficient of variation (CV %) values.

Curves of the percentage of radiotracer uptake in the eye and blood as well as blood concentration in each rat versus time were generated using GraphPad Prism version 6.01 for Windows (2014; GraphPad Software, Inc., San Diego, CA, USA).

5.3. RESULTS

5.3.1. Conjugation, radiolabelling and quality control

The number of chelating groups per antibody was estimated to be 1.39 for N-SucDf-bevacizumab and 1.59 for N-SucDf-aflibercept. Iron removal was of 84.2 % for N-SucDf-bevacizumab and 94.3 % for N-SucDf-aflibercept. The percentage of dimers was 0.41 % and 1.20 % for the final conjugated bevacizumab and aflibercept, respectively.

The radiolabelling efficiency for ^{89}Zr-bevacizumab was 92.48 %, and the radiochemical purity after ultrafiltration was 98.49 %. In the case of ^{89}Zr-aflibercept, the radiolabelling efficiency was 93.82 %, and the radiochemical purity after ultrafiltration was 98.66 %.

5.3.2. Pharmacokinetics after intravitreal administration

5.3.2.1. Ocular levels

The percentage of remaining radioactivity in the eye (mean ± SD) versus time after intravitreal injection of ^{89}Zr-bevacizumab, ^{89}Zr-aflibercept and ^{89}Zr-DFO in rats is shown in Figure 5.1. It can be observed that both antibodies showed an initial phase of rapid decrease during the first hours post-administration followed by a phase of gradual decrease. On the contrary, ^{89}Zr-DFO control quickly declined over time practically disappearing from the ocular environment at 36 hours post-injection.

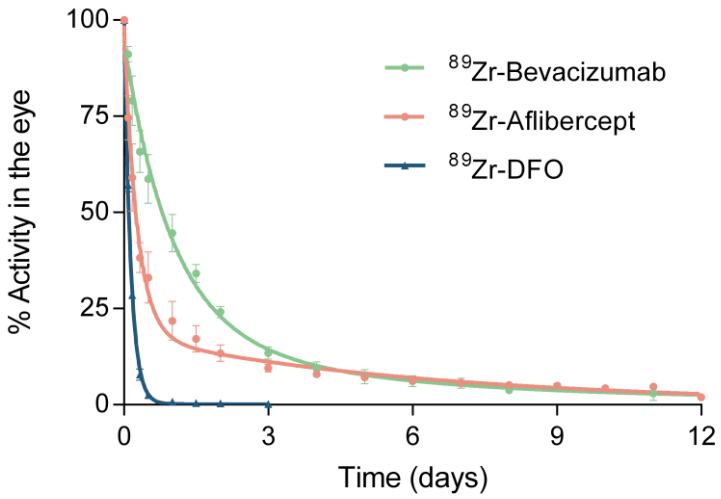

Figure 5.1. Percentage of remaining radioactivity in the eye versus time after intravitreal injection of ^{89}Zr-bevacizumab, ^{89}Zr-aflibercept and ^{89}Zr-DFO in rats. Dots and error bars represent the mean ± SD of the observed values, whereas the solid lines represent the predicted values obtained by two-compartmental analysis.

Two-compartment model with the 1/predicted concentration weighting scheme was the best fit for both antibodies based on the graphical plots of the calculated and observed concentration versus time (where calculated concentration better lie between the observed concentration points), smallest AIC value and smallest CV % values of the estimated

pharmacokinetic parameters shown in Table 5.1. The individual fittings for each animal can be found in the supplementary material.

Table 5.1. Ocular pharmacokinetic parameters (mean ± SD) for intraocular percentage of remaining activity fitted to two-compartment model with 1/predicted concentration weighting scheme after intravitreal injection of ^{89}Zr- bevacizumab and ^{89}Zr-aflibercept in rat eyes (n = 3).

Pharmacokinetic parameter	^{89}Zr-Bevacizumab	^{89}Zr-Aflibercept
α (day^{-1})	1.05 ± 0.23	3.76 ± 0.65
β (day^{-1})	0.22 ± 0.13 *	0.15 ± 0.03
$t_{1/2\alpha}$ (day)	0.68 ± 0.17	0.19 ± 0.03
$t_{1/2\beta}$ (day)	3.23 ± 0.28 *	4.69 ± 1.20
AUC_0^∞ (% activity·day)	175.25 ± 9.03 *	138.37 ± 4.77

* based on n = 2 since the terminal phase parameters for the third animal were not possible to be calculated.

Considering the alpha (or initial) phase in the ocular level profile (Figure 5.1) as the elimination phase itself, we found elimination half-life of 0.68 ± 0.17 days (16.44 ± 3.99 h) for ^{89}Zr-bevacizumab and 0.19 ± 0.03 days (4.51 ± 0.72 h) for ^{89}Zr-aflibercept. To estimate ocular clearance, we assumed that the volume of distribution (V_d) is similar to the vitreous anatomical volume of the rat, as it has been observed for rabbit and human eyes (11,29,30). According to the equation $CL = k \cdot V_d$, where k corresponds to the rate constant of elimination, clearance could be calculated. Vitreous anatomical volume of our 10-weeks-old-rats was calculated based on experimental data provided by Sha et al. (31) being of 47 µL. Therefore, ocular effective clearance, based on alpha elimination constant, was found to be 49.35 µL·day^{-1} (0.0021 mL·h^{-1}) for ^{89}Zr-bevacizumab and 176.72 µL·day^{-1} (0.0074 mL·h^{-1}) for ^{89}Zr-aflibercept. Half-lives for the beta phase were 3.23 ± 0.28 days for ^{89}Zr-bevacizumab and 4.69 ± 1.200 days for ^{89}Zr-aflibercept. Area under the ocular activity-time curve was slightly higher for ^{89}Zr-bevacizumab (175.25 ± 9.03 % activity·day) than for ^{89}Zr-aflibercept (138.37 ± 4.769 % activity·day).

Figure 5.2 shows the coronal views of the fused PET/CT images at different time points post-injection for both antibodies and the control. It is possible to observe how the ocular signal declined over time, being visually imperceptible at 11 days for ^{89}Zr-bevacizumab and ^{89}Zr-aflibercept and at 24 hours post-administration for the ^{89}Zr-DFO control.

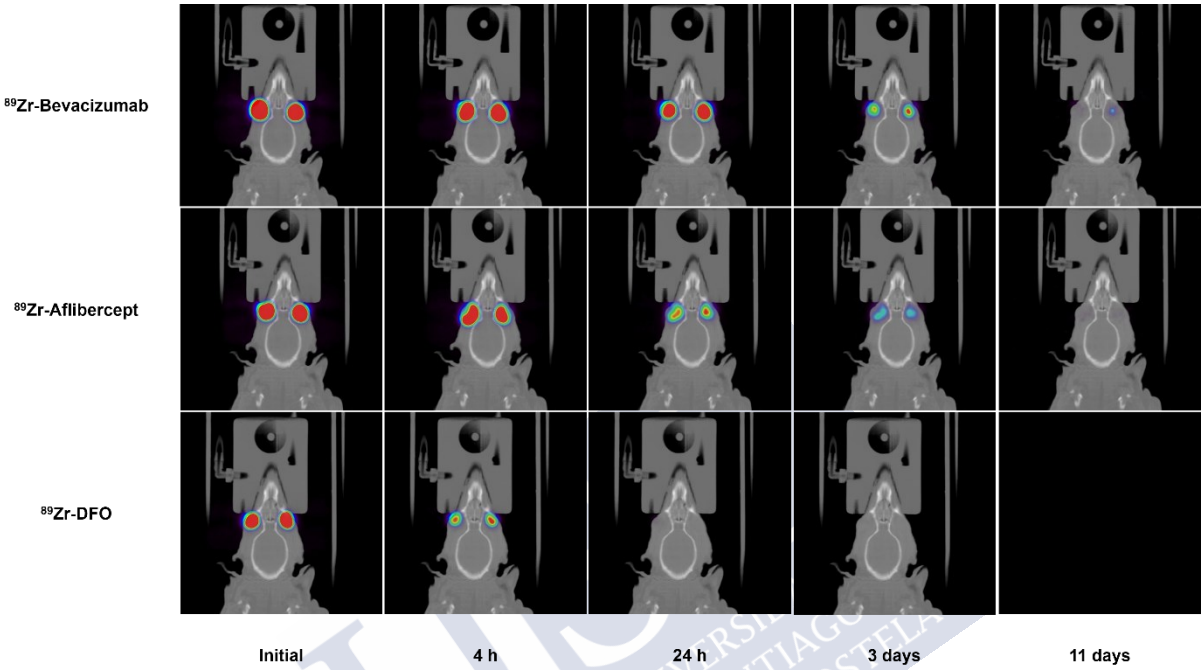

Figure 5.2. Fused PET/CT images displayed in coronal plane representing rat's head at different time points (initial, 4 h, 24 h, 3 days and 11 days) following intravitreal injection of ^{89}Zr-bevacizumab, ^{89}Zr-aflibercept and ^{89}Zr-DFO.

5.3.2.2. Systemic distribution

The blood concentration of both antibodies (Bq·µL) was fitted to the first-order absorption and one-compartment model (Figure 5.3), with the uniform weighting scheme for bevacizumab and the 1/predicted concentration weighting for aflibercept. This was the best fit, with smaller AIC and CV % values. The calculated pharmacokinetic parameters can be found in Table 5.2 (more detailed information on the individual fittings are shown in the supplementary material).

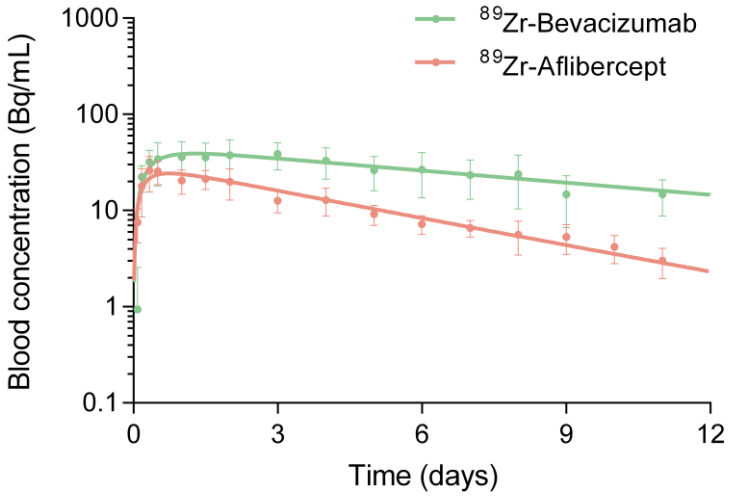

Figure 5.3. Blood concentration (Bq/µL) versus time after intravitreal injection of ^{89}Zr-aflibercept and ^{89}Zr-bevacizumab in rats. Dots and error bars represent the mean ± SD of the observed values, whereas the solid lines represent the predicted values obtained by one-compartmental analysis.

Table 5.2. Blood pharmacokinetic parameters (mean ± SD) for blood concentration data fitted to one-compartment model after intravitreal injection of ^{89}Zr-aflibercept and ^{89}Zr-bevacizumab in rat eyes (n = 3).

Pharmacokinetic parameter	^{89}Zr-Bevacizumab	^{89}Zr-Aflibercept
K_a (day^{-1})	3.89 ± 2.15	5.40 ± 3.25
k (day^{-1})	0.10 ± 0.01	0.22 ± 0.04
$t_{1/2}$ (day)	7.08 ± 0.40	3.18 ± 0.63
T_{max} (day)	1.14 ± 0.55	0.76 ± 0.42
C_{max} (Bq·µL^{-1})	39.92 ± 14.82	25.40 ± 3.40
AUC_0^∞ (Bq·µL^{-1}·day)	463.98 ± 195.24	135.51 ± 22.53
V_d (mL)	58.71 ± 2.48	83.31 ± 13.65
CL (mL·day^{-1})	5.77 ± 0.55	16.04 ± 1.37

^{89}Zr-Aflibercept presented a blood half-life of 3.18 ± 0.63 days, whereas ^{89}Zr-bevacizumab's was 7.08 ± 0.40 days. ^{89}Zr-Aflibercept maximum blood concentration was 25.40 Bq·µL^{-1} at 18.24 hours (0.76 days), which represented a 23.82 % of the intravitreal injected dose. ^{89}Zr-bevacizumab reached 39.92 Bq·µL^{-1} at 27.36 hours (1.14 days) post-injection, which corresponded to 19.42 % of the intravitreal injected dose. Area under the curve (AUC) for ^{89}Zr-

bevacizumab (463.98 ± 195.24 Bq·µL^{-1}·day) was three-and-half-fold higher than for ^{89}Zr-aflibercept (135.51 ± 22.53 Bq·µL^{-1}·day).

Figure 5.3 shows the curves of blood concentration (Bq/µL) versus time for both antibodies. Comparison of the percentage of remaining radioactivity in the eye and the blood versus time after intravitreal injection for ^{89}Zr-aflibercept and ^{89}Zr-bevacizumab in rats is presented in Figure 5.4.

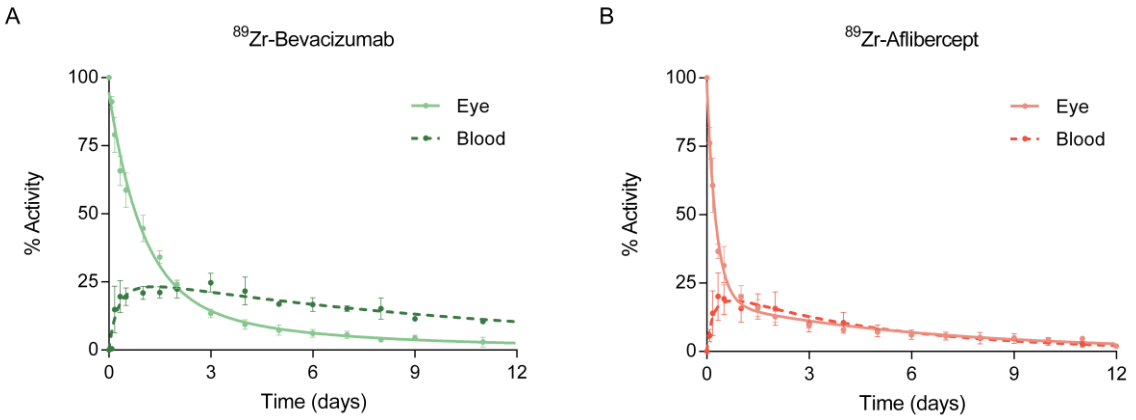

Figure 5.4. Comparison of percentage of remaining activity (mean ± SD) in the eye and the blood versus time after intravitreal injection of ^{89}Zr-bevacizumab (A) and ^{89}Zr-aflibercept (B) in rats.

Figure 5.5 shows the systemic distribution of ^{89}Zr-aflibercept, ^{89}Zr-bevacizumab and ^{89}Zr-DFO after being eliminated from the eye into the systemic circulation. It can be observed how ^{89}Zr-aflibercept and ^{89}Zr-bevacizumab signal increases in the heart (basically due to the blood signal) through the first time points and then decreases. Furthermore, ^{89}Zr-aflibercept and ^{89}Zr-bevacizumab signal could be also observed in the liver. On the other hand, ^{89}Zr-DFO was immediately detected in the kidneys and then eliminated, without significant signal in the liver.

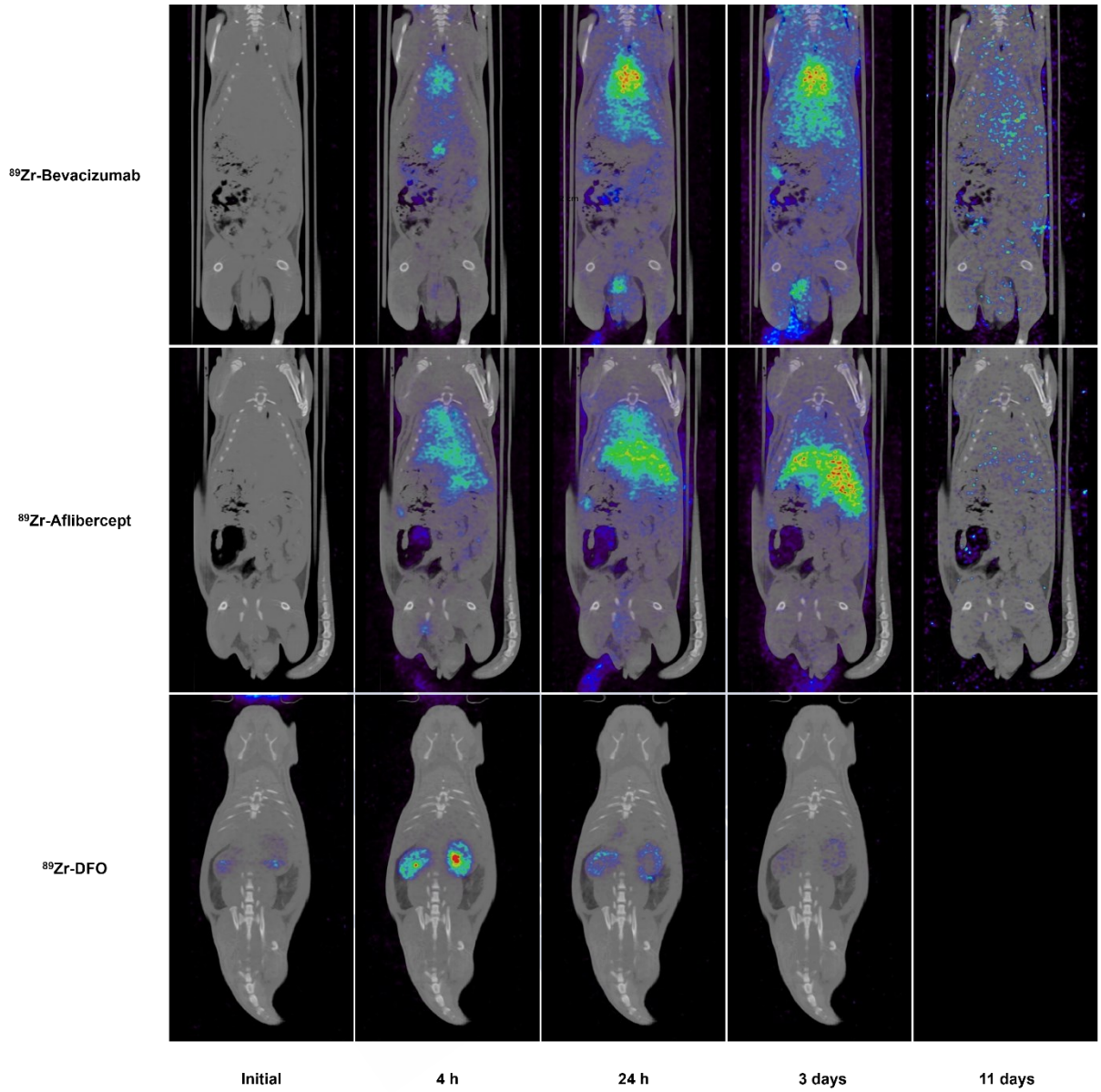

Figure 5.5. Fused PET/CT images displayed in coronal plane representing rat's body at different time points (initial, 4 h, 24 h, 3 days and 11 days) following intravitreal injection of ^{89}Zr-bevacizumab, ^{89}Zr-aflibercept and ^{89}Zr-DFO.

5.4. DISCUSSION

The evaluation of intravitreal pharmacokinetics by PET imaging methodology requires the use of stable radioactive derivatives of the antibodies being evaluated. In our case, we chose ^{89}Zr as its long half-live allows us to visualise the antibodies in the ocular cavity for up to 12 days. DFO was bound to the desired antibodies in order to act as a chelator of ^{89}Zr. As a control agent, ^{89}Zr-labelled DFO was intravitreally injected into rat eyes and the same procedure was

followed as in the case of the antibodies in order to be compared to the pharmacokinetic profiles of ^{89}Zr-bevacizumab and ^{89}Zr-aflibercept. This control confirmed that the vitreal elimination of both antibodies from the ocular cavity depended on the antibody itself and not on the DFO chelator bound to ^{89}Zr. Likewise, this was also observed in blood where ^{89}Zr-DFO concentrations were undetectable after 24 hours, thus showing that ^{89}Zr-DFO is quickly eliminated through the urine (showing high signal in kidneys at 4 hours, in Figure 5.5).

Ocular data extracted from the PET analysis fitted a two-compartment model with an initial phase of rapid decrease (alpha phase) followed by a phase of gradual decrease (beta phase) (Figure 5.1). In this last phase, it seems that ocular and blood levels are in equilibrium with a fairly similar half-live values in the eye and blood (32–34). Therefore, the initial phase (alpha phase) may represent the elimination of the antibodies from the ocular compartment into the systemic circulation, and the alpha half-life can be referred as the elimination ocular half-life.

As mentioned before, there are no data regarding intraocular pharmacokinetics of bevacizumab and aflibercept in rats. There is only an estimation of vitreous half-life for bevacizumab (0.341 days) reported based on extrapolation from serum level data in rats (35) which falls close to our experimental value of 0.68 days. In our study, the half-life of bevacizumab (149 kDa) is significantly higher than the one for aflibercept (97 kDa) of 0.19 days. This has been seen for other species (11,29) and it is due to the fact that vitreous diffusion is one factor that affects the elimination of the macromolecules from the eye, being the half-lives shorter for smaller macromolecules which diffuse more rapidly in the vitreous humour (35–37).

Additionally, blood pharmacokinetics was evaluated, finding a blood half-life of 3.18 days in rats. Regarding bevacizumab, we obtained a blood half-life of 7.08 days in rats and a T_{max} of 1.14 days, which is similar to the one obtained in serum Sprague-Dawley rats of 1 day by Chuang et al. (38). In our study, we calculated a volume of distribution of 58.71 mL for bevacizumab and 83.31 mL for aflibercept from the blood data. These higher volumes of distribution in comparison to the total blood volume indicate that part of the antibodies is redistributed to other tissues. This goes in line with what it is observed in the systemic PET/CT images (Figure 5.5), in which bevacizumab and aflibercept are also detected in the liver.

It is necessary to rely on animal sacrifice at each time point in order to obtain vitreous samples, with the inconvenience of lacking concentrations measurements from the same eye during the time course (39). For evident reason, vitreous samples cannot be analysed in patients. For that, pharmacokinetic studies in patients to evaluate anti-VEGF concentration after intravitreal administration are done from the aqueous humour (9), as it is possible to obtain several repeated aqueous humour samples in the same subject. This procedure has been also used in preclinical studies (9). Our study presents the advantage of avoiding invasive sampling and can be used for preclinical studies. One disadvantage of our study is that all ocular cavities are measured altogether, without discerning between aqueous and vitreous humour and the surrounding tissues. However, this technique allows us to determine drug levels over time in the same animal. Therefore, whereas most of the studies measuring vitreous samples by ELISA methods rely on measuring a different animal at each time point, PET methodology allows us to monitor the same animal over time, with the consequently decrease in the number of needed animals. Additionally, drug concentration declines with the same decay rate in the vitreous humour, aqueous humour and retina (40–42), so our results should represent the rate of elimination from the vitreous humour. Other studies have used the same approach to determine the ocular elimination of antibodies following intravitreal injections (30,32–34).

Pharmacokinetics following intravitreal injection has been widely studied in rabbits and monkeys whereas efficacy studies are mainly performed in rodents. Hence, one of the reasons why we have chosen rats as animal model for intravitreal pharmacokinetics is indeed several retina diseases can be modelled in rats (18). Some examples of these models are the laser or surgically induced choroidal neovascularisation (CNV) models which resemble AMD, oxygen induced retinopathy (OIR) model which represents the retinopathy of prematurity and the streptozotocin (STZ) rat model related to diabetic retinopathy (23,43,44). Therefore, rat represents a good model for further studies of the intravitreal pharmacokinetics in disease states. However, comparison among species should be made in caution due to the anatomical and physiological ocular differences between them. Rats present a larger lens and a thinner and more simplified inner limiting membrane (ILM), which could represent a less restrictive barrier to diffusion (45,46) and smaller vitreous volume, approximately 50 µL (47) than human eye. Nevertheless, valuable pharmacokinetic data can be obtained from these animals with

the right interpretation. Moreover, it has gained our attention that some intravitreal drug delivery systems containing anti-VEGF agents are being developed in rats (18–21). However, there are almost no data regarding intravitreal pharmacokinetics of anti-VEGF drugs in rats, so despite the easiness of developing these rat models and the increased use of rat for evaluating intravitreal delivery systems, there is an unmet need of knowing in depth the characteristics of those intravitreal anti-VEGF agents in this specie. Furthermore, the PET methodology presented in this work to evaluate the pharmacokinetics after intravitreal administration would present great advantages in these cases. On the one hand, it permits decreasing the number of animals per study group, which consequently makes more accessible and feasible reach the preclinical stage while at the same time makes possible to evaluate different systems. On the other hand, due to the inherit invasive nature of the intravitreal injection, the possibility of following elimination of the antibodies from the ocular environment by PET imaging considerably decrease the intrusiveness of the pharmacokinetic studies.

5.5. CONCLUSION

This study shows for the first time the ocular and blood pharmacokinetics of intravitreally injected aflibercept and bevacizumab in rats. Moreover, it presents the pharmacokinetic parameters calculated based on sequential imaging of the same animal over time.

5.6. REFERENCES

1. Hodge W, Brown A, Kymes S, Cruess A, Blackhouse G, Hopkins R, et al. Pharmacologic management of neovascular age-related macular degeneration: systematic review of economic evidence and primary economic evaluation. Can J Ophthalmol. 2010 Jun;45(3):223–30.
2. Drug Approval Package: Eylea (Aflibercept) [Internet]. [cited 2020 Jan 9]. Available from: https://www.accessdata.fda.gov/drugsatfda_docs/nda/2011/125387s0000TOC.cfm
3. Eylea [Internet]. European Medicines Agency. 2018 [cited 2020 Jan 9]. Available from: https://www.ema.europa.eu/en/medicines/human/EPAR/eylea
4. Avastin: European Public Assessment Report - Product Information [Internet]. European Medicines Agency. 2018 [cited 2020 Jan 9]. Available from: https://www.ema.europa.eu/en/medicines/human/EPAR/avastin

5. Empeslidis T, Storey M, Giannopoulos T, Konidaris V, Tranos PG, Panagiotou ES, et al. How Successful is Switching from Bevacizumab or Ranibizumab to Aflibercept in Age-Related Macular Degeneration? A Systematic Overview. Adv Ther. 2019 May 17;

6. Pershing S, Talwar N, Armenti ST, Grubbs J, Rosenthal JM, Dedania VS, et al. Use of Bevacizumab and Ranibizumab for Wet Age-Related Macular Degeneration: Influence of CATT Results and Introduction of Aflibercept. Am J Ophthalmol. 2019 May 14;

7. Eylea: European Public Assessment Report - Product Information [Internet]. European Medicines Agency. 2018 [cited 2020 Jan 9]. Available from: https://www.ema.europa.eu/en/medicines/human/EPAR/eylea

8. Jyothi S, Chowdhury H, Elagouz M, Sivaprasad S. Intravitreal bevacizumab (Avastin) for age-related macular degeneration: a critical analysis of literature. Eye (Lond). 2010 May;24(5):816–24.

9. García-Quintanilla L, Luaces-Rodríguez A, Gil-Martínez M, Mondelo-García C, Maroñas O, Mangas-Sanjuan V, et al. Pharmacokinetics of Intravitreal Anti-VEGF Drugs in Age-Related Macular Degeneration. Pharmaceutics. 2019 Jul 31;11(8).

10. Luaces-Rodríguez A, Mondelo-García C, Zarra-Ferro I, González-Barcia M, Aguiar P, Fernández-Ferreiro A, et al. Intravitreal anti-VEGF drug delivery systems for age-related macular degeneration. Int J Pharm. 2020 Jan 5;573:118767.

11. del Amo EM, Vellonen K-S, Kidron H, Urtti A. Intravitreal clearance and volume of distribution of compounds in rabbits: In silico prediction and pharmacokinetic simulations for drug development. Eur J Pharm Biopharm. 2015 Sep;95(Pt B):215–26.

12. Fernández-Ferreiro A, Luaces-Rodríguez A, Aguiar P, Pardo-Montero J, González-Barcia M, García-Varela L, et al. Preclinical PET Study of Intravitreal Injections. Invest Ophthalmol Vis Sci. 2017 Jun 1;58(7):2843–51.

13. Russell WMS, Burch RL. The principles of humane experimental technique. Methuen; 1959. 260 p.

14. van Dongen GAMS, Visser GWM, Lub-de Hooge MN, de Vries EG, Perk LR. Immuno-PET: a navigator in monoclonal antibody development and applications. Oncologist. 2007 Dec;12(12):1379–89.

15. Heskamp S, Raavé R, Boerman O, Rijpkema M, Goncalves V, Denat F. 89Zr-Immuno-Positron Emission Tomography in Oncology: State-of-the-Art 89Zr Radiochemistry. Bioconjug Chem. 2017 20;28(9):2211–23.

16. Nagengast WB, de Vries EG, Hospers GA, Mulder NH, de Jong JR, Hollema H, et al. In vivo VEGF imaging with radiolabeled bevacizumab in a human ovarian tumor xenograft. J Nucl Med. 2007 Aug;48(8):1313–9.

17. Gaykema SBM, Brouwers AH, Lub-de Hooge MN, Pleijhuis RG, Timmer-Bosscha H, Pot L, et al. 89Zr-bevacizumab PET imaging in primary breast cancer. J Nucl Med. 2013 Jul;54(7):1014–8.

18. Rowe-Rendleman CL, Durazo SA, Kompella UB, Rittenhouse KD, Di Polo A, Weiner AL, et al. Drug and Gene Delivery to the Back of the Eye: From Bench to Bedside. Invest Ophthalmol Vis Sci. 2014 Apr;55(4):2714–30.

19. Xie B, Jin L, Luo Z, Yu J, Shi S, Zhang Z, et al. An injectable thermosensitive polymeric hydrogel for sustained release of Avastin® to treat posterior segment disease. International Journal of Pharmaceutics. 2015 Jul;490(1–2):375–83.

20. Lu Y, Zhou N, Huang X, Cheng J-W, Li F-Q, Wei R-L, et al. Effect of intravitreal injection of bevacizumab-chitosan nanoparticles on retina of diabetic rats. Int J Ophthalmol. 2014;7(1):1–7.

21. Yandrapu SK, Upadhyay AK, Petrash JM, Kompella UB. Nanoparticles in porous microparticles prepared by supercritical infusion and pressure quench technology for sustained delivery of bevacizumab. Mol Pharm. 2013 Dec 2;10(12):4676–86.

22. Williams D. Rabbit and rodent ophthalmology. EJCAP. 2007 Jan 12;17(3):242–52.

23. Pennesi ME, Neuringer M, Courtney RJ. Animal models of age related macular degeneration. Mol Aspects Med. 2012 Aug;33(4):487–509.

24. Castro-Balado A, Mondelo-García C, González-Barcia M, Zarra-Ferro I, Otero-Espinar FJ, Ruibal-Morell Á, et al. Ocular Biodistribution Studies using Molecular Imaging. Pharmaceutics. 2019 May 16;11(5).

25. Verel I, Visser GWM, Boerman OC, van Eerd JEM, Finn R, Boellaard R, et al. Long-lived positron emitters zirconium-89 and iodine-124 for scouting of therapeutic radioimmunoconjugates with PET. Cancer Biother Radiopharm. 2003 Aug;18(4):655–61.

26. Loening AM, Gambhir SS. AMIDE: a free software tool for multimodality medical image analysis. Mol Imaging. 2003 Jul;2(3):131–7.

27. Lee HB, Blaufox MD. Blood volume in the rat. J Nucl Med. 1985 Jan;26(1):72–6.

28. Rodent Blood Volume Calculator from EnCor Biotechnology Inc. [Internet]. [cited 2019 Nov 20]. Available from: https://encorbio.com/protocols/Blood.htm

29. Del Amo EM, Urtti A. Rabbit as an animal model for intravitreal pharmacokinetics: Clinical predictability and quality of the published data. Exp Eye Res. 2015 Aug;137:111–24.

30. Schmitt M, Hippeläinen E, Raviña M, Arango-Gonzalez B, Antopolsky M, Vellonen K-S, et al. Intravitreal Pharmacokinetics in Mice: SPECT/CT Imaging and Scaling to Rabbits and Humans. Mol Pharm. 2019 07;16(10):4399–404.

31. Sha O, Kwong WH. Postnatal Developmental Changes of Vitreous and Lens Volumes in Sprague-Dawley Rats. NBA. 2006;4(4):183–8.

32. Christoforidis JB, Williams MM, Kothandaraman S, Kumar K, Epitropoulos FJ, Knopp MV. Pharmacokinetic properties of intravitreal I-124-aflibercept in a rabbit model using PET/CT. Curr Eye Res. 2012 Dec;37(12):1171–4.

33. Christoforidis JB, Briley K, Binzel K, Bhatia P, Wei L, Kumar K, et al. Systemic Biodistribution and Intravitreal Pharmacokinetic Properties of Bevacizumab,

Ranibizumab, and Aflibercept in a Nonhuman Primate Model. Invest Ophthalmol Vis Sci. 2017 01;58(13):5636–45.

34. Christoforidis JB, Carlton MM, Knopp MV, Hinkle GH. PET/CT imaging of I-124-radiolabeled bevacizumab and ranibizumab after intravitreal injection in a rabbit model. Invest Ophthalmol Vis Sci. 2011 Jul 29;52(8):5899–903.

35. Hutton-Smith LA, Gaffney EA, Byrne HM, Maini PK, Schwab D, Mazer NA. A Mechanistic Model of the Intravitreal Pharmacokinetics of Large Molecules and the Pharmacodynamic Suppression of Ocular Vascular Endothelial Growth Factor Levels by Ranibizumab in Patients with Neovascular Age-Related Macular Degeneration. Mol Pharm. 2016 06;13(9):2941–50.

36. Lau CML, Yu Y, Jahanmir G, Chau Y. Controlled release technology for anti-angiogenesis treatment of posterior eye diseases: Current status and challenges. Adv Drug Deliv Rev. 2018 15;126:145–61.

37. Shatz W, Hass PE, Mathieu M, Kim HS, Leach K, Zhou M, et al. Contribution of Antibody Hydrodynamic Size to Vitreal Clearance Revealed through Rabbit Studies Using a Species-Matched Fab. Mol Pharm. 2016 06;13(9):2996–3003.

38. Chuang L-H, Wu W-C, Yeung L, Wang N-K, Hwang Y-S, Chen K-J, et al. Serum concentration of bevacizumab after intravitreal injection in experimental branch retinal vein occlusion. Ophthalmic Res. 2011;45(1):31–5.

39. Miyake T, Sawada O, Kakinoki M, Sawada T, Kawamura H, Ogasawara K, et al. Pharmacokinetics of bevacizumab and its effect on vascular endothelial growth factor after intravitreal injection of bevacizumab in macaque eyes. Invest Ophthalmol Vis Sci. 2010 Mar;51(3):1606–8.

40. Gadkar K, Pastuskovas CV, Le Couter JE, Elliott JM, Zhang J, Lee CV, et al. Design and Pharmacokinetic Characterization of Novel Antibody Formats for Ocular Therapeutics. Invest Ophthalmol Vis Sci. 2015 Aug;56(9):5390–400.

41. Le KN, Gibiansky L, Good J, Davancaze T, van Lookeren Campagne M, Loyet KM, et al. A mechanistic pharmacokinetic/pharmacodynamic model of factor D inhibition in cynomolgus monkeys by lampalizumab for the treatment of geographic atrophy. J Pharmacol Exp Ther. 2015 Nov;355(2):288–96.

42. Hutton-Smith LA, Gaffney EA, Byrne HM, Maini PK, Gadkar K, Mazer NA. Ocular Pharmacokinetics of Therapeutic Antibodies Given by Intravitreal Injection: Estimation of Retinal Permeabilities Using a 3-Compartment Semi-Mechanistic Model. Mol Pharm. 2017 07;14(8):2690–6.

43. Grossniklaus HE, Kang SJ, Berglin L. Animal models of choroidal and retinal neovascularization. Prog Retin Eye Res. 2010 Nov;29(6):500–19.

44. Liu C-H, Wang Z, Sun Y, Chen J. Animal models of ocular angiogenesis: from development to pathologies. FASEB J. 2017;31(11):4665–81.

45. Kern TJ. Rabbit and rodent ophthalmology. Seminars in Avian and Exotic Pet Medicine. 1997 Jul 1;6(3):138–45.

46. Peynshaert K, Devoldere J, Minnaert A-K, De Smedt SC, Remaut K. Morphology and Composition of the Inner Limiting Membrane: Species-Specific Variations and Relevance toward Drug Delivery Research. Curr Eye Res. 2019;44(5):465–75.

47. Ahn SJ, Hong HK, Na YM, Park SJ, Ahn J, Oh J, et al. Use of Rabbit Eyes in Pharmacokinetic Studies of Intraocular Drugs. J Vis Exp [Internet]. 2016 Jul 23 [cited 2019 May 10];(113). Available from: https://www.ncbi.nlm.nih.gov/pmc/articles/PMC5091672/

5.7. SUPPLEMENTARY MATERIAL

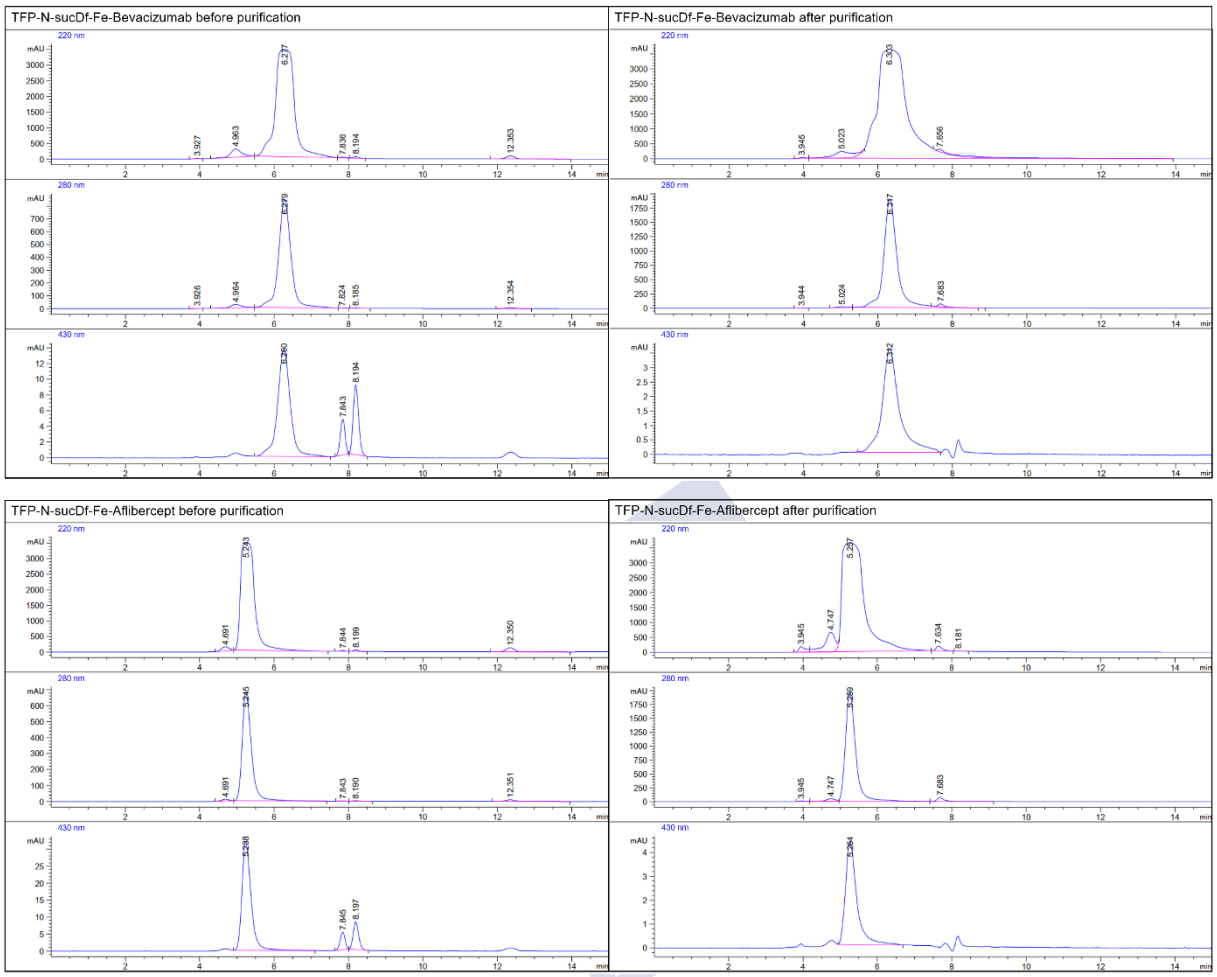

Figure 5.1 supplementary. HPLC spectra of the conjugation of bevacizumab and aflibercept to TFP-N-sucDf-Fe. Left and right spectra correspond to the antibody's samples before and after, respectively, the iron removal by EDTA incubation and purification. Each sample is shown at 220, 280 and 430 nm. 280 nm spectrum shows the dimers and antibody peaks (retention times: 4.964 and 6.279 min for bevacizumab, 4.691 and 5.245 min for aflibercept, respectively for the pre-purification samples). 430 nm spectrum shows the Fe^{3+} signal corresponded to the DFO, bound to the antibody and unbound in the pre-purification samples (6.260 and 7.843/8.194 min for bevacizumab, 5.238 and 7.845/8.197 min for aflibercept, respectively), and the remaining Fe^{3+} in the post-purification samples (6.312 min for bevacizumab and 5.264 min for aflibercept).

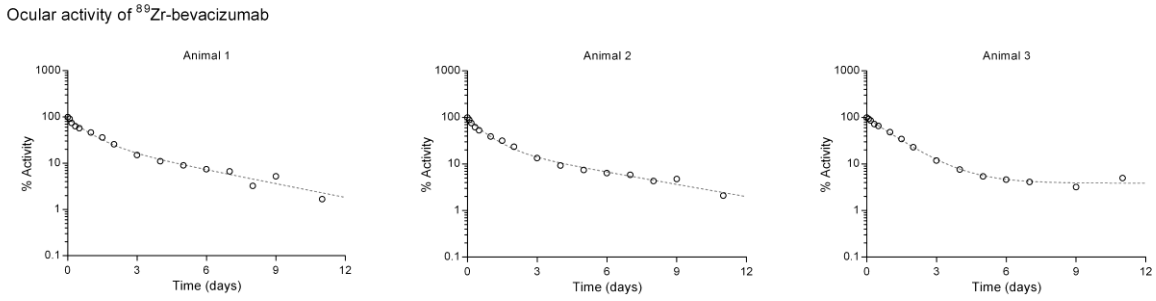

Figure 5.2 supplementary. Individual values of the percentage of remaining activity in the eye versus time after intravitreal injection of ^{89}Zr-bevacizumab in three different rats.

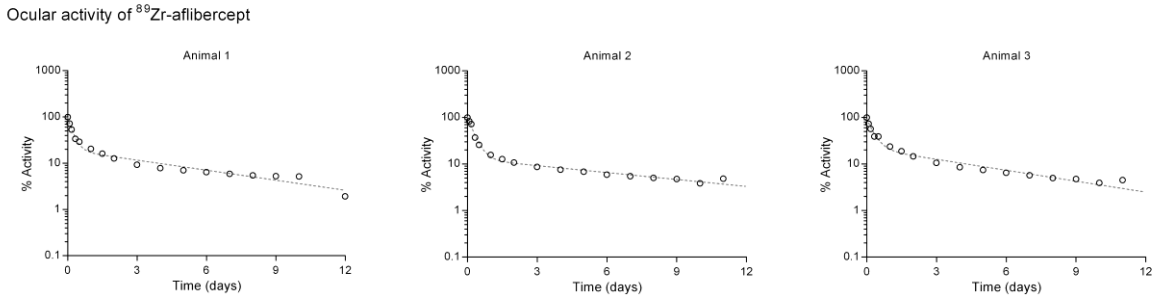

Figure 5.3 supplementary. Individual values of the percentage of remaining activity in the eye versus time after intravitreal injection of ^{89}Zr-aflibercept in three different rats.

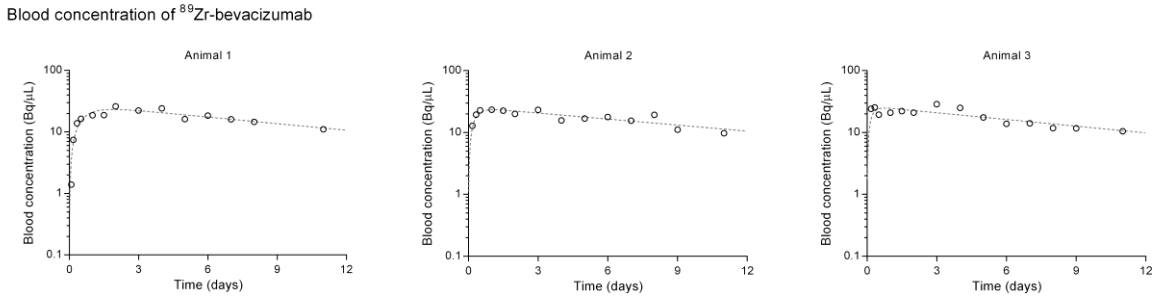

Figure 5.4 supplementary. Individual values of the blood concentration versus time after intravitreal injection of ^{89}Zr-bevacizumab in three different rats.

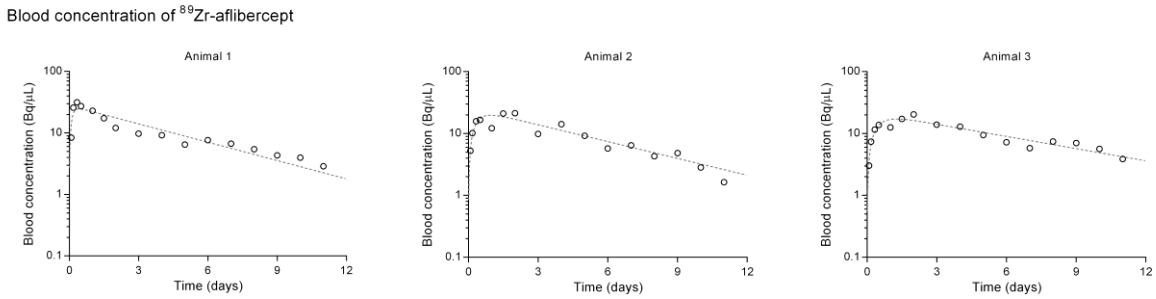

Figure 5.5 supplementary. Individual values of the blood concentration versus time after intravitreal injection of ^{89}Zr-aflibercept in three different rats.

Chapter 6. Chitosan-based intravitreal implants for extended release of aflibercept in AMD treatment

USC
UNIVERSIDADE
DE SANTIAGO
DE COMPOSTELA

6. CHITOSAN-BASED INTRAVITREAL IMPLANTS FOR EXTENDED RELEASE OF AFLIBERCEPT IN AMD TREATMENT

6.1. INTRODUCTION

Treatment of posterior segment eye diseases, such as age-related macular degeneration (AMD), diabetic retinopathy and macular oedema, is especially challenging. The most suitable route of drug delivery to the posterior segment is the intravitreal injection. Intravitreal drug injections are used to delivery high drug levels in the vitreous humour. They entail complications which include inflammation, retinal detachment, endophthalmitis and vitreous haemorrhage (1–3). Although the incidence of these adverse effects is relatively low, they might be sight-threatening (1).

AMD is the most prevalent cause of blindness in industrialised countries (4). Its exudative form is treated by the intravitreal injection of anti-vascular endothelial growth factors (anti-VEGFs) such as aflibercept, ranibizumab, brolucizumab and bevacizumab (5). Although macromolecules, such as these anti-VEGF antibodies, present a relatively long intravitreal half-life, monthly or bimonthly injections are still required to achieve visual acuity. Moreover, the need of repeated intravitreal injections increases the risk of adverse effects (1).

Therefore, drug delivery to posterior segment of the eye is the most attractive and interesting way to overcome these difficulties, although it also faces great challenges. Among the technologies being developed for intravitreal delivery of macromolecules are the intravitreal implants. Implants are solid devices that need to be surgically implanted or injected into the vitreous humour (6). Polymer-based implants are designed to allow prolonged drug levels in the vitreous humour while decreasing the number of intravitreal injections, avoiding high peak drug concentrations, decreasing systemic drug exposure as well as enhancing patient

compliance (7,8). In comparison with other intravitreal devices, implants permit high drug loading and longer release time (9).

Polymer-based implants can be composed of biodegradable or non-biodegradable polymers. Non-biodegradable implants require implantation and surgical removal after drug depletion with its related adverse effects (8,10). Biodegradable systems are normally a matrix composed of polymer and drug. They present the advantages of not eliciting foreign body reactions and not requiring posterior removal (8). Biodegradable devices are typically made of different polyesters of the poly α-hydroxy acid family, such as polyglycolic acid (PGA), polylactic acid (PLA), and especially polylactic-co-glycolic acid (PLGA) (8). PLGA has been widely used for the preparation of implants containing low molecular weight drugs. It presents the advantage that the drug release rate can be controlled by altering the polymer composition and its degradation behaviour (8). However, the implants made of these polymers encounter the potential instability of the antibodies due to the method of preparation, such as the necessity of using organic solvents to dissolve the polymers (11).

Another approach to prepare biodegradable implants is using natural polymers. Natural polymers are obtained from plants, animals or microorganisms which due to its similar composition to components of the human body produce minimal toxicity. Therefore, its great biocompatibility makes them highly suitable as drug delivery systems. The most natural polymers used in ocular therapy are cellulose, hyaluronic acid, dextrans, silk, gelatin, collagen, alginate and chitosan (12). Chitosan is a biocompatible, biodegradable and nontoxic material which is a potential candidate for drug delivery systems inside the eye (13). It is a copolymer of N-acetilglucosamine and glucosamine which is a N-deacylated derivative of the natural polymer chitin. The chitosan molecular weight and the degree of deacylation are two of the properties that affect its use as drug delivery system (14). Chitosan is positively charged in diluted acidic aqueous solutions, which makes it possible to form polyelectrolyte complexes with other anionic materials, such as tripolyphosphate (TPP), which allows to modify the mechanical characteristics of the materials prepared (15). Moreover, chitosan can be moulded into different drug delivery systems such as micro- and nanoparticles, gels, fibers, films and implants (15). Both chitosan and its degradation products have not shown any adverse effect

at the cell level (16). Therefore, due to its non-toxic behaviour and biodegradability, chitosan has been widely used in the pharmaceutical industry (14,15).

Up to date, several intravitreal implants were approved for the delivery of short organic drugs to the posterior segment of the eye, which include both biodegradable (Ozurdex® which contains dexamethasone) and non-biodegradable devices, such as Vitrasert® (ganciclovir) and Iluvien® and Retisert® (fluocinolone) (17). Further intravitreal implants are currently in clinical and preclinical settings, although devices containing anti-VEGF antibodies are still in early stages of development (9,17,18). Therefore, the present study reports the development and *in vitro* characterisation of intravitreal implants based on chitosan and containing aflibercept.

6.2. MATERIALS AND METHODS

6.2.1. Materials

Chitosans were purchased from Sigma Aldrich®: low molecular weight chitosan (MW = 50-190 kDa, >75 % deacylated), medium molecular weight chitosan (MW = 190-310 kDa, >75 % deacylated) and high molecular weight chitosan (310-375 kDa, >75 % deacylated). Sodium tripolyphosphate (TPP) was also obtained from Sigma Aldrich. Eylea® (aflibercept) commercial solution was kindly provided by the Pharmacy Department of the University Clinical Hospital of Santiago de Compostela. The remaining reagents were analytical grade.

6.2.2. Preparation of chitosan gel matrix for semisolid extrusion printing

Chitosan of different molecular weights was employed to form the matrix of the implant and tripolyphosphate (TPP) was used as crosslinker. First, aflibercept was dissolved at a concentration of 10 mg/mL in a solution of 1 % (v/v) acetic acid in milli-Q water. Then, chitosan at a concentration of 10 % (w/v) was added to the prior solution to form the gel matrix. The gel was manually homogenised and centrifuged at 5000 rpm during 10 min at room temperature. The formed gel matrix was passed to a 5 mL syringe and centrifuge again for 5 min in order to eliminate air bubbles.

6.2.3. Implant semisolid extrusion printing

For implant semisolid extrusion printing, an in-house layout was settled into a universal testing machine (Shimadzu® Autograph AGS-X), which consisted on a 1000 N load cell connected to a piston, which transferred the force to the plunger of a 5 mL syringe (Braun®). The area of application of the force was a circle of 16.45 mm of diameter, which coincides with the dimensions of the plunger flange of the syringe. The syringe contained the chitosan gel and it was supported by the barrel flange into the top surface of a container. The tip of the syringe, which presented an inner diameter of 2 mm, was immersed in a solution of 2 % tripolyphosphate (TPP). A scheme of the layout can be found in Figure 6.1.

The piston moved downwards with a compression module at 10 mm/min for 1.5 mm to produce a cylinder of approximately 10 mm of length and 2.5 mm of width. The resulted implant was cut with a surgical scalpel and left in 2 % TPP solution for 10 minutes. Trapezium X materials testing software registered a graph of force (N) versus displacement (mm) of the implant semisolid extrusion printing and calculated the parameters of energy (J), maximum force (N) and modulus of elasticity (N/mm^2).

The three different molecular weight chitosans tested produced three different MW implants: implants prepared with low MW chitosan (L-MW implants), implants prepared with medium MW chitosan (M-MW implants) and implants prepared with high MW chitosan (H-MW implants). Following implant semisolid extrusion printing, the implants were either used right away (raw implants) or freeze-dried (lyophilised implants). Lyophilisation was addressed as a method of facilitating implant handling as well as its future implantation into the vitreous cavity. For the lyophilisation, implants were frozen at − 80 °C for at least 24 h prior to lyophilisation and then were lyophilised for 24 h (Telstar® LyoQuest–85).

Once the initial evaluation of the effect of the chitosan molecular weight on the implant performance was carried out, the chitosan with better characteristics was selected for the following experiments, which resulted to be the high MW chitosan. Some modifications in the method of the semisolid extrusion printing were performed in order to evaluate the effect of these changes on the properties of the prepared implants. On the one hand, the crosslinking time was increased from 10 minutes to 60 minutes (implants H-MW-60) in order to obtain a

higher degree of crosslinking of the chitosan with TPP. On the other hand, the method of freezing the implants prior to lyophilisation was changed. Instead of freezing the implants at -80 °C in a freezer, the implants were frozen by immersion in liquid nitrogen for a few seconds and immediately lyophilised (H-MW-N). Finally, both modifications were addressed in combination (H-MW-60-N).

One-way ANOVA with Tukey test for multiple comparisons was used for the analysis of these parameters in the three different molecular weight implants prepared.

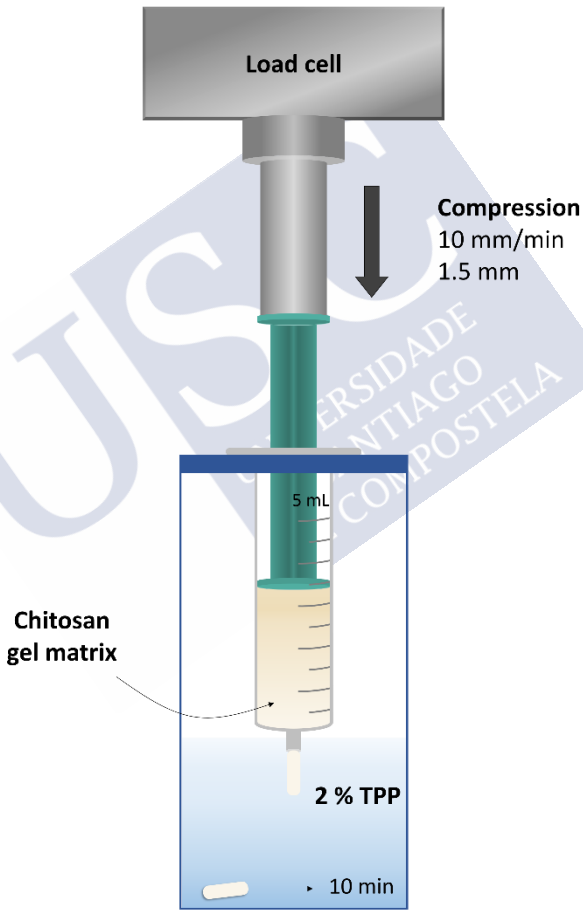

Figure 6.1. Schematic representation of the process of implant semisolid extrusion printing using an in-house layout settled into a universal testing machine.

6.2.4. Morphology

20 different implants of each batch were measured following semisolid extrusion printing (raw implants) and after freeze drying (lyophilised implants). A calliper was employed to measure the diameter and length of the implants. For uniformity of weight, implants were weight in an analytical balance. The volume of each implant was calculated based on its diameter and length according to the volume formula of a cylinder ($l \cdot \pi \cdot r^2$). One-way ANOVA with Tukey test for multiple comparisons was used for the analysis of the parameters of weight, length, diameter and volume.

Lyophilised implants were measured and weighted in the same way as the raw implants. Water loss (%) due to lyophilisation process was calculated as:

$$Water\ loss\ (\%) = \frac{W_{raw} - W_{lyophilised}}{W_{raw}} \cdot 100$$

where, W_{raw} is the weight of the raw implant and $W_{lyophilised}$ is the weight of the implant after lyophilisation.

The volume reduction due to lyophilisation process was calculated as following:

$$Volume\ reduction\ (\%) = \frac{V_{raw} - V_{lyophilised}}{V_{raw}} \cdot 100$$

where, V_{raw} is the volume of the raw implant and $V_{lyophilised}$ is the volume of the implant after lyophilisation.

6.2.5. Swelling analysis

Swelling analysis was conducted by placing lyophilised priorly weighted implants (n = 6 for each type of implant) in 1.5 mL micro-centrifuge tubes containing 1 mL PBS. Vials were maintained at 37 °C in an orbital shaker with 100 rpm stirring. At predetermined time intervals, the implants were removed, dried by filter paper and weighed. Swelling index (SI) for each implant was calculated using the following equation:

$$SI\ (\%) = \frac{W_t - W_0}{W_0} \cdot 100$$

where, W_0 is the initial weight of the lyophilised implant at the start of the experiment and W_t is the weight of the hydrated implant at time t.

Two-way ANOVA with Tukey test for multiple comparisons was used for the analysis of the swelling index at each time point among the different implants.

6.2.6. HPLC quantification

Reverse Phase High Performance Liquid Cromatography (RP-HPLC) was employed for aflibercept quantification. An Agilent® 1260 Infinity II LC Systems was used. A column specially designed to optimize the performance of monoclonal antibodies (AdvanceBio RP-mAb SB-C8, 4.6 x 100 mm, 3.5 µm, Agilent®) was used. The mobile phases were: phase A (0.1 % trifluoroacetic acid in milli-Q water) and phase B (10 % phase A, 10 % acetonitrile, 80 % n-propanol). A gradient at a flow rate of 0.8 mL/min was used, starting from 95 % A and 5 % B for 2 minutes, changing steadily in three minutes to 5 % A and 95 % B, and returning to initial conditions in one minute to continue one more minute. The column temperature was kept at 60 °C and the injection volume was 50 µL. UV-detector wavelength was set at 280 nm. For the calibration curve, different standards (2-200 µg/mL) were prepared from the commercial solution of aflibercept (Eylea®) in PBS.

6.2.7. *In vitro* aflibercept release from the implants

Lyophilised priorly weighed implants (n = 4 for each type of implant) were placed in amber-coloured vials containing 1 mL of PBS pH 7.4 as the dissolution medium. The vials were stoppered and placed in a horizontal orbital shaker at 100 rpm and 37 °C. At predetermined time intervals, 300 µL of dissolution medium was withdrawn and replaced with fresh 300 µL of pre-heated PBS. The samples were analysed by RP-HPLC to determine antibody content. Kinetic release data were fitted to different models by linear and non-linear fitting using GraphPad Prism 6.01 for Windows® (2014; GraphPad Software, Inc., San Diego, CA, USA).

6.3. RESULTS

6.3.1. Implant semisolid extrusion printing

The parameters of energy, maximum force and modulus of elasticity were calculated by the semisolid extrusion printing of the implants with the in-house layout settled into the universal testing machine. An increase in energy, maximum force and elastic modulus was observed when increasing the molecular weight of the chitosan (Table 6.1). Implants prepared with L-MW and M-MW chitosans showed similar values of energy and elastic modulus, although statistically significant differences in the parameter of maximum force ($\alpha < 0.05$). Conversely, H-MW implants showed parameters of energy, maximum force and modulus of elasticity statistically significant higher in comparison to the other two ($\alpha < 0.05$).

Table 6.1. Parameters of energy (mJ), maximum force (N) and modulus of elasticity (N/mm^2) obtained from the implant semisolid extrusion printing in a universal testing machine. Data is provided as mean ± standard deviation.

Parameter	L-MW	M-MW	H-MW
Energy (mJ)	7.336 ± 0.533	7.619 ± 0.335	9.002 ± 0.682
Maximum force (N)	8.367 ± 0.672	8.958 ± 0.487	11.317 ± 0.720
Modulus of elasticity (N/mm^2)	0.359 ± 0.061	0.369 ± 0.016	0.414 ± 0.052

6.3.2. Morphology

Table 6.2 shows the mean and standard deviation of the weight, length, diameter and calculated volume of the implants prepared with the three chitosans of different molecular weight. Both implants after printing made by L-MW and H-MW chitosans presented approximately a length of 10 mm and a diameter of 2.5 mm. No statistically significant differences were found in the diameter (α n.s.) as it was determined by the inner diameter of the printing syringe. The weight was approximately of 55 mg/implant and calculated volume was 50 µL. However, in the case of M-MW Chit, the implants suffered a small contraction in the length (5.5 %) but an important dilation in the diameter (33.6 %) when printed into the TPP solution and during the time of crosslinking, so that the final implants presented lower length and higher diameter. The weight was also considerably higher (94.52 mg). Therefore,

even though L-MW and H-MW showed a comparable morphology, the more easiness of processing the gel matrix prepared with high MW chitosan made that it was chosen as the prototype for the following studies regarding modifications in the method of preparation.

Table 6.2. Weight (mg), length (mm), diameter (mm) and volume (µL) (mean ± SD) of the implants prepared with three different molecular weight chitosans: low (L-MW), medium (M-MW) and high (H-MW); and after printing (raw) and after lyophilisation (lyop.).

Implant	State	Weight (mg)	Length (mm)	Diameter (mm)	Volume (µL)
L-MW	Raw	57.00 ± 2.55	10.10 ± 0.30	2.54 ± 0.05	51.24 ± 3.66
	Lyop.	7.61 ± 0.50	7.85 ± 0.40	2.00 ± 0.14	25.51 ± 3.64
M-MW	Raw	94.52 ± 7.84	9.45 ± 0.40	3.34 ± 0.14	82.70 ± 9.36
	Lyop.	11.29 ± 1.23	8.00 ± 0.35	2.71 ± 0.15	46.07 ± 4.82
H-MW	Raw	52.18 ± 1.67	9.84 ± 0.36	2.60 ± 0.07	51.89 ± 3.57
	Lyop.	6.50 ± 0.30	7.64 ± 0.32	1.82 ± 0.11	19.43 ± 2.30

Lyop.: lyophilised

The dimensions of the modifications in the method of preparation of the high MW implants are shown in Table 6.3. Increasing the crosslinking time in the TPP solution from 10 min to 60 min produced a smaller raw implant (statistically significant differences for $\alpha < 0.05$), presenting lower length (a 16.8 % reduction) and diameter (6.2 %), with a considerable reduction in weight (17.3 %) and volume (26.9 %).

Table 6.3. Weight (mg), length (mm), diameter (mm) and volume (µL) (mean ± SD) of the implants prepared from high molecular weight chitosan with three different modifications: increased crosslinking time to 60 min (H-MW-60), freezing in liquid nitrogen (H-MW-N) and the combination of both (H-MW-60-N); and after printing (raw) and after lyophilisation (lyop.).

Implant	State	Weight (mg)	Length (mm)	Diameter (mm)	Volume (µL)
H-MW-60	Raw	43.16 ± 1.77	8.19 ± 0.25	2.44 ± 0.10	37.92 ± 3.26
	Lyop.	7.73 ± 0.23	6.64 ± 0.19	1.88 ± 0.10	17.84 ± 2.72
H-MW-N	Raw	58.02 ± 2.82	9.49 ± 0.29	2.56 ± 0.11	47.33 ± 2.73
	Lyop.	7.86 ± 0.26	7.82 ± 0.33	1.96 ± 0.11	22.34 ± 1.83
H-MW-60-N	Raw	48.61 ± 2.33	8.21 ± 0.29	2.38 ± 0.09	35.94 ± 2.70
	Lyop.	7.57 ± 0.27	7.00 ± 0.22	1.87 ± 0.09	18.92 ± 2.04

Lyop.: lyophilised

Lyophilised implants showed a considerably reduction in weight due to the water loss by the lyophilisation process (Table 6.4). Water loss during lyophilisation was similar in the different MW implants (86-88 %) (no statistically significant differences between them, α n.s.). In the case of H-MW implants with a 60 min crosslinking, the water loss was a little lower compared to 10 min crosslinking (82.11 % vs 87.60 %) ($\alpha < 0.05$). The same occurs in the H-MW-60-N implants in comparison with H-MW-N (84.60 % vs 86.62 %) ($\alpha < 0.05$).

Table 6.4. Water loss (%) and volume reduction (%) of the different types of implants due to the lyophilisation process. Data is provided as mean ± standard deviation.

Implant	Water loss (%)	Volume reduction (%)
L-MW	86.72 ± 0.70	50.90 ± 5.39
M-MW	88.01 ± 0.41	41.92 ± 5.72
H-MW	87.60 ± 0.49	60.03 ± 4.18
H-MW-60	82.11 ± 1.01	49.58 ± 6.03
H-MW-N	86.62 ± 0.34	53.86 ± 4.11
H-MW-60-N	84.60 ± 0.41	47.79 ± 4.03

Freeze-dried implants presented in general lower length and diameter in comparison to their counterparts in all the different types. This can be observed in the percentage of volume reduction shown in Table 6.4. Volume reduction (%) was significant different ($\alpha < 0.05$) between the implants prepared with different MW chitosan: M-MW implant presented the lowest volume reduction (41.92 %), H-MW the highest one (60.03 %) and L-MW an intermediate value (50.90 %). Regarding modifications in implants prepared with high MW chitosan, they all showed a slight decrease in the volume reduction due to the lyophilisation process in comparison to the standard H-MW implants (H-MW-60: 49.58 %, H-MW-N: 53.86 %, and H-MW-60-N: 47.79 %), but similar between them.

Regarding the modification in the method of freezing to using immersion in liquid nitrogen (Table 6.3), it produced an implant with similar dimensions in comparison with the one placed in a freezer, showing no statistically significant differences between them (α n.s.) in the length and weight. However, H-MW-N showed a slightly higher diameter (a 7.7 % increase). Similarly, liquid nitrogen use on freezing has almost no effects on 60-min-crosslinked implants due to

no statistically significant differences (α n.s.) in the diameter and weight between them were found.

Figure 6.2 shows pictures of the lyophilised implants. At first sight, it can be observed that the 60 min-crosslinked implant presented a smoother surface in comparison to the standard high MW implant. Moreover, it is clearly visible the increased diameter of the medium MW implants.

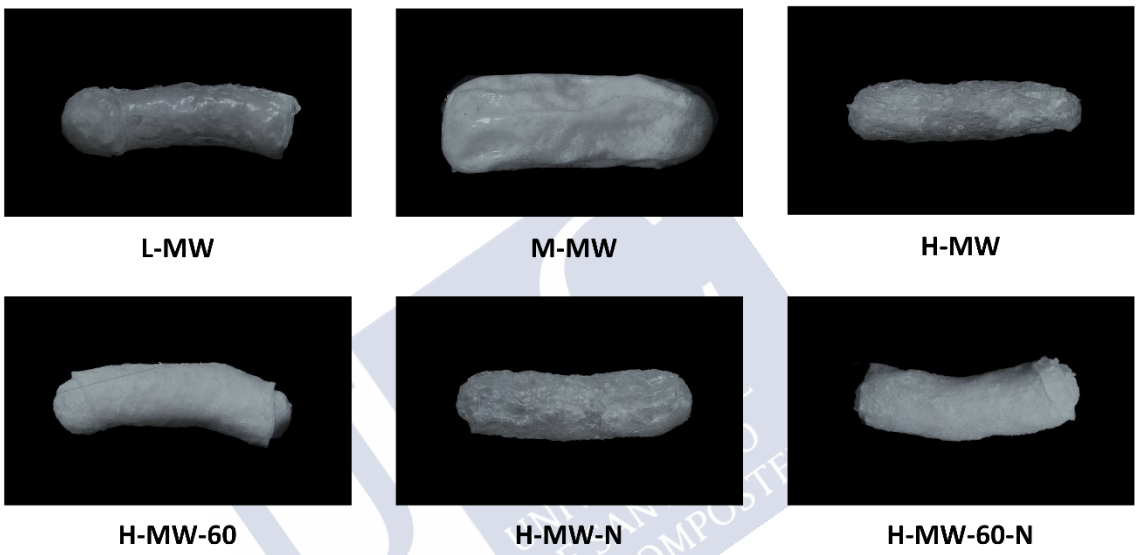

Figure 6.2. Pictures of the lyophilised implants. Top line: implants prepared with three different molecular weight chitosans: low (L-MW), medium (M-MW) and high (H-MW) molecular weight chitosan. Bottom line: modifications in the method of the implant preparation for the high MW chitosan implants: 60-min-crosslinked implants (H-MW-60), liquid nitrogen frozen implants (H-MW-N) and the combination of both modifications (H-MW-60-N).

6.3.3. Swelling analysis

The mean swelling index evolution over 21 days of study can be observed in Figure 6.3. Implant swelling started immediately after placing the implant in the PBS medium. The weight gain was very fast at initial times, followed by an interval of slow swelling until the weight acquired a steady state.

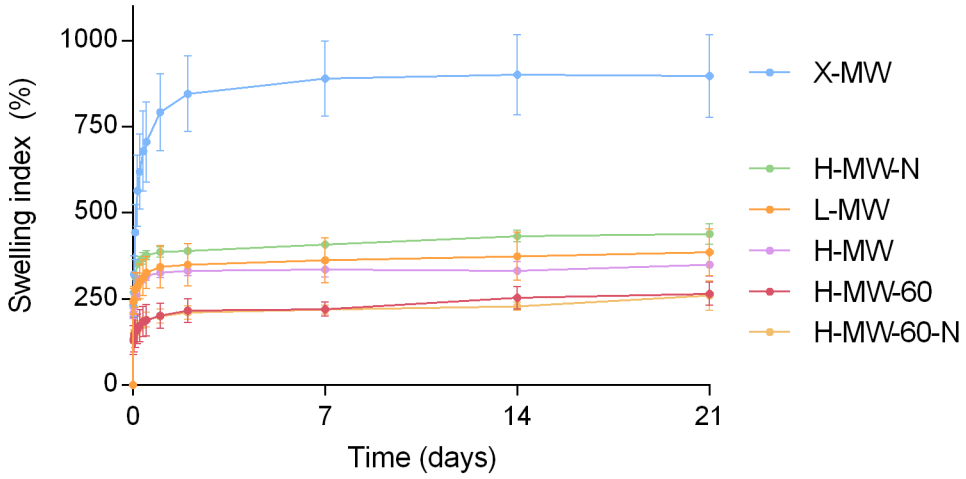

Figure 6.3. Swelling indexes (%) (mean ± SD) of the lyophilised implants in PBS, including implants prepared with three different molecular weight chitosans: low (L-MW), medium (M-MW) and high (H-MW) molecular weight chitosan implants; and the high MW chitosan implants with the modifications in the method of the implant preparation: 60-min-crosslinked implants (H-MW-60), liquid nitrogen frozen implants (H-MW-N) and the combination of both modifications (H-MW-60-N).

Medium MW implants presented the highest value of swelling index in PBS, reaching a swelling index of 897 % at day 21. H-MW and L-MW implants presented a similar swelling behaviour (no statistically significant differences, α n.s.), reaching final swelling index values of 350 % and 386 %, respectively.

Regarding the implants prepared with high MW chitosan, H-MW-60 presented lower values of swelling index in comparison to H-MW (statistically significant differences, $\alpha < 0.05$). H-MW-N showed a similar profile during the first time points (until 7 days) but slightly higher in the following points than H-MW (statistically significant differences, $\alpha < 0.05$). The final swelling index was 439 %. On the contrary, both 60-min-crosslinked implants, H-MW-60 and H-MW-60-N showed the same swelling profile (no statistically significant differences, α n.s.) with swelling indexes after 21 days of 265 % and 260 %, respectively.

6.3.4. *In vitro* aflibercept release from implants

The comparison of the *in vitro* release of the lyophilised implants prepared with the different three molecular weight chitosans can be observed in Figure 6.4. Low and high MW chitosan-based implants presented a very similar release profile, achieving a cumulative release around

75 % of the loaded aflibercept at day 21. Initial burst release was also similar, 52.00 % for H-MW and 50.12 % for L-MW at 24 hours. Conversely, freeze-dried medium MW chitosan implant showed almost no burst release but a very low final cumulative release at 21 days (approximately 12 %).

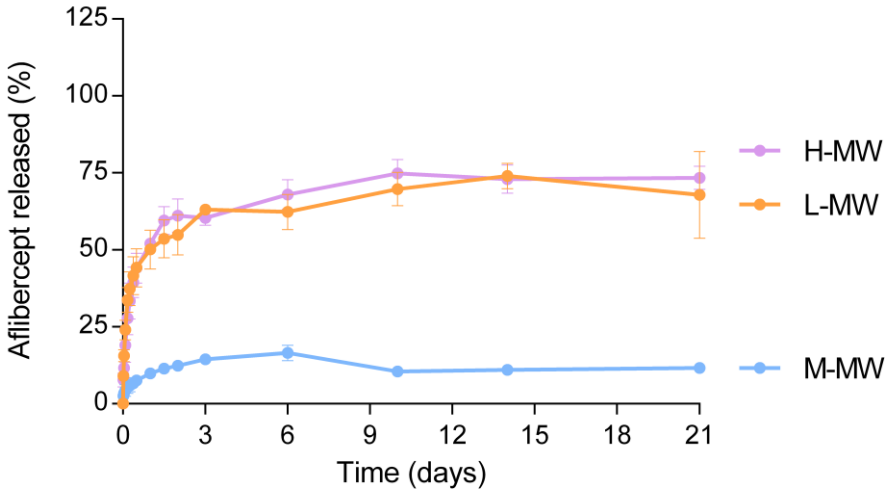

Figure 6.4. Comparison of the aflibercept release data (%) (mean ± SD) from the lyophilised implants prepared with different molecular weight chitosans: high (H-MW), medium (M-MW) and low (L-MW).

The modifications performed on the preparation of high MW implants (Figure 6.5) showed that increasing the crosslinking time to 60 min produced a similar release profile at initial times, with a burst release of 55.42 % until 36 hours. However, final cumulative release was higher for 60-min-crosslinked implants, 96.94 % vs 73.39 % at 21 days. Regarding freezing technique with nitrogen liquid, it can be observed that a considerably reduction of the burst release was obtained (22.83 % at 24 h) compared to the same implants frozen at − 80 °C (52.00 %). Final cumulative release was the very similar for both freezing techniques (73.19 % vs 73.39 %). Finally, combination of both modifications (60 min crosslinking, freezing by nitrogen liquid), showed the more controlled release at initial times (burst release of 19.95 % at 24 h) of the freezing technique with a higher final cumulative release (89.52 %).

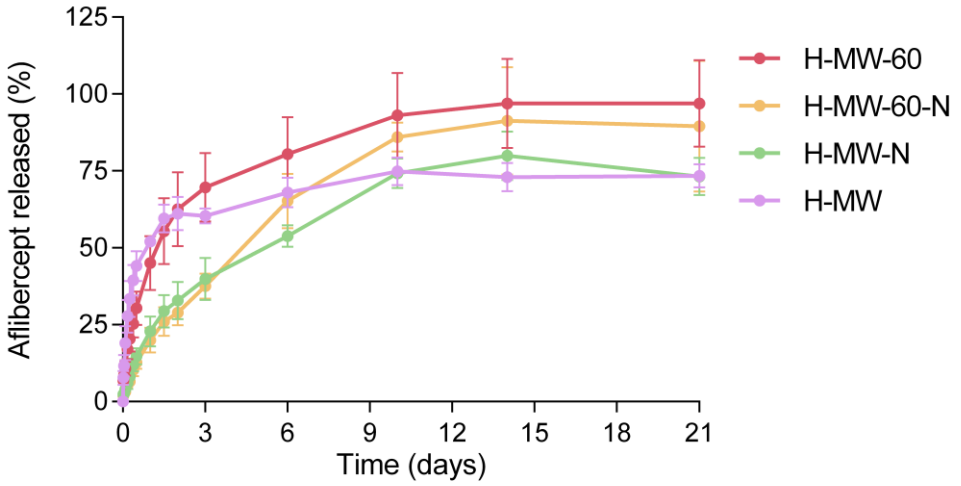

Figure 6.5. Comparison of the aflibercept release data (%) (mean ± SD) from the lyophilised implants prepared with high molecular weight chitosan (H-MW) with three different modifications in the method of preparation: increased crosslinking time to 60 min (H-MW-60), freezing in liquid nitrogen (H-MW-N) and the combination of both (H-MW-60-N).

Drug release data during the first 12 hours from these four types of freeze-dried implants containing high MW chitosan were fitted to the zero-order kinetics, the first-order kinetics, the Korsmeyer-Peppas model, the Korsmeyer-Peppas model adapted to burst release effect and the Higuchi model. The fitting to each model was evaluated based on correlation coefficient (R^2) values. The R^2 values of each model fitting are reported in Table 6.5.

Table 6.5. Correlation coefficient (R2) values of the fitting of the aflibercept released data (%) from the four types of freeze-dried implants containing high MW chitosan (H-MW, H-MW-60, H-MW-N and H-MW-60-N) during the first 12 hours to different mathematical models: zero-order kinetics, first-order kinetics, Korsmeyer-Peppas model both considering and not burst effect, and Higuchi model.

	Zero-order kinetics	**First-order kinetics**	**Korsmeyer-Peppas model**	**Korsmeyer-Peppas model (burst effect)**	**Higuchi model**
Equation	$Q = Q_0 + k_0 \cdot t$	$\ln Q = \ln Q_0 + k_1 \cdot t$	$Q = k_{KP} \cdot t^n$	$Q = A + k_{KP} \cdot t^n$	$Q = k_H \cdot \sqrt{t}$
	R^2	**R^2**	**R^2**	**R^2**	**R^2**
H-MW	0.9209	0.8165	0.9963	0.9965	0.8028
H-MW-60	0.9392	0.9050	0.9957	0.9959	0.8007
H-MW-N	0.9875	0.9477	0.9905	0.9927	0.9567
H-MW-60-N	0.9890	0.9246	0.9920	0.9933	0.9684

Korsmeyer-Peppas model showed the best fit as the four types of high MW implants presented R^2 values above 0.99 (Table 6.5). Moreover, the model which takes into account the burst effect showed slightly higher R^2 values than the standard model. The fitting of the amount of aflibercept released (µg) to Korsmeyer-Peppas model adapted to burst effect can be observed in Figure 6.6 and the parameters obtained from this fitting can be found in Table 6.6. Release rates were statistically significant different for each high MW chitosan implants ($\alpha < 0.05$). H-MW implants showed a considerably higher release rate (60.47 $\mu g \cdot h^{-1}$) in comparison with the others. The 60 min-crosslinked implant (H-MW-60) presented a 39.27 $\mu g \cdot h^{-1}$ release rate, whereas the implants frozen in liquid nitrogen showed considerably lower release rates (9.20 $\mu g \cdot h^{-1}$ for H-MW-N and 7.66 $\mu g \cdot h^{-1}$ for H-MW-60-N).

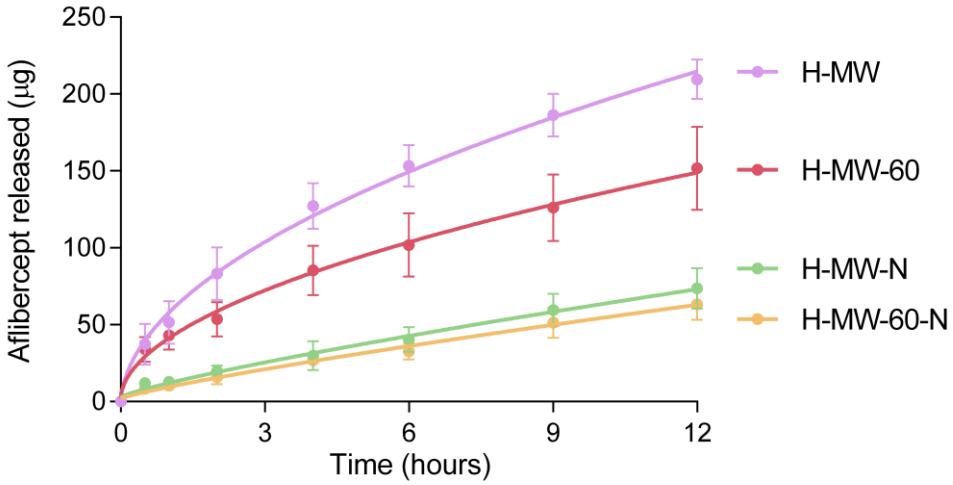

Figure 6.6. Comparison of the aflibercept release data (%) (mean ± SD) from the lyophilised implants prepared with high molecular weight chitosan (H-MW) with three different modifications in the method of preparation: increased crosslinking time to 60 min (H-MW-60), freezing in liquid nitrogen (H-MW-N) and the combination of both (H-MW-60-N).

Table 6.6. Parameters obtained (k_{KP} and n) through the fitting of the aflibercept release data (µg) from the four types of freeze-dried implants containing high MW chitosan (H-MW, H-MW-60, H-MW-N and H-MW-60-N) during the first 12 hours to Korsmeyer-Peppas model adapted to burst release. Data is provided as mean ± standard error.

Implant	k_{KP} ($\mu g \cdot h^{-1}$)	n	R^2
H-MW	60.47 ± 5.40	0.515 ± 0.031	0.9965
H-MW-60	39.27 ± 3.93	0.531 ± 0.035	0.9959
H-MW-N	9.20 ± 1.92	0.818 ± 0.080	0.9927
H-MW-60-N	7.66 ± 1.56	0.836 ± 0.079	0.9933

6.4. DISCUSSION

Delivery of biologicals to the back of the eye has been a challenge largely because of the labile nature of these biomolecules. Most efforts have focused on using the polymer PLGA for the formation of different drug delivery systems, although no promising results have been reported due to the potential instability of the proteins in organic environments. Therefore, in this study, the alternative of using the natural polymer chitosan as gel-matrix forming for intravitreal implants containing aflibercept has been presented. Moreover, ionic crosslinking of chitosan with the polyanion tripolyphosphate (TPP) was performed in order to delay the delivery of aflibercept. An in-house layout adapted to a universal testing machine for the semisolid extrusion printing of chitosan-based intravitreal implants was presented in this work as a valid approach. One advantage of using this layout is that it permits calculating different parameters related to the force required for the implant semisolid extrusion printing. In this sense, an increase in energy, maximum force and elastic modulus is observed when increasing the molecular weight of the chitosan (Table 6.1). The raise in these parameters indicates that an increase in the molecular weight produces implants with less deformation capacity (higher elastic modulus) and therefore they need higher maximum force and energy in order to be able to be extruded through the outlet hole of the syringe. Nevertheless, the differences found are not very high, and therefore the lower deformation capacity does not hinder de formation of the implants using relatively low forces.

From the analysis of the morphology of the different implants prepared it can be concluded that the procedure described is an acceptable approach since reproducibility was achieved in all the different types of implants. Low and high MW chitosan-based implants presented dimensions after printing of 10 mm of length and 2.5 mm of width on average (raw implants). However, medium MW chitosan formed very irregular implants (Figure 6.2), which suffered a considerably dilation in the diameter during the time of TPP crosslinking (Table 6.2). Therefore, it was considered as not a suitable product for the preparation of the intravitreal implants by this method. Regarding the remaining two chitosans, L-MW and H-MW showed a comparable morphology after the lyophilisation process with small differences in the volume reduction. However, the more easiness of processing the gel matrix prepared with high MW

chitosan made that it was chosen as the prototype for the following studies regarding modifications in the method of preparation. Increasing the crosslinking time in the TPP solution from 10 min to 60 min produced smaller implants, more compacted and with a smoother surface (Figure 6.2) due to the increased degree of crosslinking. That could be the reason why the water loss during the lyophilisation was slightly lower in comparison to the 10 min-crosslinked implants, since prior to freeze-drying the implants presented lower water percentage and therefore the water loss was lower. Regarding the modification in the method of freezing to using liquid nitrogen, the implants prepared by the latter procedure showed a slightly increased size. This could be due to the more rapid freezing that produces amorphous and smaller ice solid particles which allowed maintaining the structure through the lyophilisation process. The formation of higher ice crystals at the freezing temperature of − 80 °C can induce the distortion of the polysaccharide matrix, increasing the volume and the porosity of the implant (19).

Regarding the size of the intravitreal implants developed in this work, it must be pointed out that they present a slightly increased dimensions (Table 6.2 and 6.3; e.g., 7.64 x 1.82 mm for H-MW) in comparison to the intravitreal implants available at the market (e.g., Ozurdex®: 6 x 0.46 mm, Iluvien®: 3.5 x 0.37 mm). However, their size goes in line with other implantable devices containing anti-VEGF agents developed in other studies (i.e., 15 x 1.7 mm (20), 7.5 x 1.67 mm (21)), and even some of them even were intravitreally injected into rabbit eyes (i.e., 10 x 10 mm (22), 11.5 x 2.9 mm (23)). Moreover, the implant semisolid extrusion printing with the adapted universal testing machine presented in this work has already been translated into a robotic deposition equipment which permits to print implants with a considerably reduced size. The first experiments were already carried out with implants with initial raw lower diameter (10 x 0.84 mm) (24) and even smaller dimensions of the implants were achieved through this same methodology (5 x 0.41 mm). Therefore, although the size of the implants presented in this study might be a little high for clinical studies, we believed that they are suitable for continuing with preclinical studies.

The swelling behaviour of the implants was characterised by an initial, rapid, and very high increase of the swelling index after immersion in the medium followed by a very slow swelling

index rising. Final swelling indexes were relatively high, at least 350 %, except for the 60 min-crosslinked implants which showed the least swelling indexes (260-265 %), therefore concluding that the increased crosslinking time had a high impact on the swelling behaviour. This effect has also been observed in other studies in which the percentage of swelling ratio decreased with increasing reaction time (25–27). The increased crosslinking time produced a higher degree of crosslinking which resulted in a stronger and denser polymer structure with lower water absorption capacity. This is what caused the decreasing of swelling capability of the 60 min-crosslinked implants. Swelling behaviour after *in vivo* implantation of the chitosan-based implants is not comparable to the one observed in the *in vitro* swelling analysis in PBS. However, the evaluation of the swelling behaviour is PBS is a relative useful measure for evaluating the behaviour among the different types of implants as well as an indication of the future swelling behaviour in the vitreous humour.

Korsmeyer-Peppas model is considered to be a rigorous description of the mixed mechanism of diffusion- and swelling-controlled release, as drug diffusion, polymer relaxation and the conditions where the gel expands heterogeneously as water penetrates and swells the gel are taken into consideration (19). In our case, an adaptation which takes into consideration the burst effect was found to be the most appropriate for the fitting of the high MW chitosan implants (Table 6.5). Freeze-dried implant composed of high MW chitosan crosslinked during 10 and 60 min showed a release exponent close to 0.5. On the contrary, high MW implants frozen by liquid nitrogen showed a release exponent close to 0.82-0.84 (Table 6.6). Siepmann and Siepmann et al. (28) indicates that in specimens with cylindrical shape, as implants, n exponent of 0.45 indicates Fickian diffusion, 0.45 to 0.89 anomalous transport, and values higher than 0.89 polymer swelling. According to these data, all the implants showed anomalous transport, i.e., an overlapping of drug diffusion and polymer swelling. However, the H-MW and H-MW-60 implants probably presented a behavior closer to diffusion-controlled release mechanism, whereas the implants frozen in liquid nitrogen a mixed mechanism with higher effect of the polymer swelling-controlled release (29). The latter release mechanism could be the cause that a lower burst release effect was found for the high MW implants frozen by liquid nitrogen in comparison to the − 80 °C frozen ones. Moreover,

these implants (H-MW-N and H-MW-60-N) are the ones that presented the lowest release rates, at least 6 times lower than the other two.

The bioactivity of aflibercept after gel matrix preparation, semisolid extrusion printing procedure and the different characterisation studies is not addressed in this work. The chitosan dissolution requires using a mild acidic solution of 1 % acetic acid in order to prepare the gel matrix, which could influence the aflibercept stability. However, aflibercept has proven to keep intact its structure and VEGF binding capacity at different pH conditions (30), so it should not be a limitation. In this sense, physical stability and bioactivity of aflibercept is also maintained when incubated at 37 °C (30), so the release study should not either affect aflibercept stability. Moreover, although there are no studies on the effect of lyophilisation on aflibercept stability due to its inclusion in drug delivery systems, lyophilisation has proven to be a suitable technique to obtain a solid dosage form of bevacizumab (23,31–34), another anti-VEGF antibody. However, the addition of a cryoprotectant should also be considered for future studies.

The advantage of the methodology for the chitosan-based implants described in this work stems from using biocompatible and biodegradable materials, no organic solvents, the simplicity of the method and the possibility of translating its preparation to a more automatic manufacturing process. Preliminary studies have shown that the implants prepared with high molecular weight chitosan with 60 min TPP crosslinking time and freezing by immersion in liquid nitrogen (H-MW-60-N) presented the better characteristics of the proposed implants. The advantages of both modifications to the initial method of preparation are reflected in combination in this implant. On the one hand, the increased crosslinked time has a positive influence on the morphology of the implants, producing implants with smaller size (7.00 x 1.87 mm), more compacted and with a smoother surface. Moreover, the implants suffered a very low swelling due to this structure, which is a beneficial characteristic for the future ocular implantation in *in vivo* studies due to the small size of the vitreous cavity. In addition, the aflibercept release test permitted to conclude that the implants with increased crosslinking time presented a higher final cumulative release, which represented almost 90 % of the payload dose for the H-MW-60-N implant. On the other hand, liquid nitrogen freezing

modification produced implants with a considerably reduction of the initial burst effect, which represented approximately 20 % of the aflibercept release at 24 hours in this case. Moreover, this more controlled release during initial times is also reflected in the considerably reduction of the release rate in comparison with the other types of implants, which in the case of the H-MW-60-N implant represented 7.66 µg of aflibercept per hour during the first 12 hours. Finally, H-MW-60-N was able to deliver aflibercept in a controlled manner at least for 21 days. Therefore, this implant seems to be a good candidate for further characterisation and optimisation studies.

6.5. CONCLUSION

In this study, a potential intravitreal implant based on chitosan crosslinked with TPP containing aflibercept has been prepared to improve the treatment of AMD. The high molecular weight chitosan is presented as the better alternative for the preparation of the intravitreal implants. The implants prepared in this way were able to deliver aflibercept in a controlled manner at least for 21 days. Moreover, the incorporation of the modifications in the method of preparation of increased crosslinking time and liquid nitrogen freezing resulted in an implant with improved characteristics regarding morphology, swelling and release rates.

6.6. REFERENCES

1. Falavarjani KG, Nguyen QD. Adverse events and complications associated with intravitreal injection of anti-VEGF agents: a review of literature. Eye Lond Engl. 2013 Jul;27(7):787–94.
2. Williams D, Argáez C. Acute, Sustained, Intraocular Pressure increases following Anti-Vascular Endothelial Growth Factor Treatment for Retinal Conditions: A Review of Clinical Evidence and Guidelines [Internet]. Ottawa (ON): Canadian Agency for Drugs and Technologies in Health; 2019 [cited 2020 Jan 15]. (CADTH Rapid Response Reports). Available from: http://www.ncbi.nlm.nih.gov/books/NBK545133/
3. Bracha P, Moore NA, Ciulla TA, WuDunn D, Cantor LB. The acute and chronic effects of intravitreal anti-vascular endothelial growth factor injections on intraocular pressure: A review. Surv Ophthalmol. 2018 Jun;63(3):281–95.
4. WHO | Priority eye diseases [Internet]. World Health Organization. [cited 2019 Aug 26]. Available from: http://www.who.int/blindness/causes/priority/en/

5. Fogli S, Del Re M, Rofi E, Posarelli C, Figus M, Danesi R. Clinical pharmacology of intravitreal anti-VEGF drugs. Eye Lond Engl. 2018;32(6):1010–20.

6. Gote V, Sikder S, Sicotte J, Pal D. Ocular Drug Delivery: Present Innovations and Future Challenges. J Pharmacol Exp Ther. 2019 May 9;jpet.119.256933.

7. Yasukawa T, Ogura Y, Kimura H, Sakurai E, Tabata Y. Drug delivery from ocular implants. Expert Opin Drug Deliv. 2006 Mar;3(2):261–73.

8. Lee SS, Hughes P, Ross AD, Robinson MR. Biodegradable implants for sustained drug release in the eye. Pharm Res. 2010 Oct;27(10):2043–53.

9. Luaces-Rodríguez A, Mondelo-García C, Zarra-Ferro I, González-Barcia M, Aguiar P, Fernández-Ferreiro A, et al. Intravitreal anti-VEGF drug delivery systems for age-related macular degeneration. Int J Pharm. 2020 Jan 5;573:118767.

10. Agrahari V, Agrahari V, Mandal A, Pal D, Mitra AK. How are we improving the delivery to back of the eye? Advances and challenges of novel therapeutic approaches. Expert Opin Drug Deliv. 2017;14(10):1145–62.

11. van de Weert M, Hennink WE, Jiskoot W. Protein instability in poly(lactic-co-glycolic acid) microparticles. Pharm Res. 2000 Oct;17(10):1159–67.

12. Anwary M, Kumar P, du Toit LC, Choonara YE, Pillay V. Polymeric, injectable, intravitreal hydrogel devices for posterior segment applications and interventions. Artif Cells Nanomedicine Biotechnol. 2018;46(sup2):1074–81.

13. de la Fuente M, Raviña M, Paolicelli P, Sanchez A, Seijo B, Alonso MJ. Chitosan-based nanostructures: a delivery platform for ocular therapeutics. Adv Drug Deliv Rev. 2010 Jan 31;62(1):100–17.

14. Ahsan SM, Thomas M, Reddy KK, Sooraparaju SG, Asthana A, Bhatnagar I. Chitosan as biomaterial in drug delivery and tissue engineering. Int J Biol Macromol. 2018 Apr 15;110:97–109.

15. Hong S-C, Yoo S-Y, Kim H, Lee J. Chitosan-Based Multifunctional Platforms for Local Delivery of Therapeutics. Mar Drugs. 2017 Mar 1;15(3).

16. Kravanja G, Primožič M, Knez Ž, Leitgeb M. Chitosan-based (Nano)materials for Novel Biomedical Applications. Mol Basel Switz. 2019 May 21;24(10).

17. Nayak K, Misra M. A review on recent drug delivery systems for posterior segment of eye. Biomed Pharmacother Biomedecine Pharmacother. 2018 Nov;107:1564–82.

18. Shatz W, Aaronson J, Yohe S, Kelley RF, Kalia YN. Strategies for modifying drug residence time and ocular bioavailability to decrease treatment frequency for back of the eye diseases. Expert Opin Drug Deliv. 2018 Nov 29;

19. Zhao J. Chitosan-Based Gels for the Drug Delivery System. In: Chitosan-Based Hydrogels: Functions and Applications. CRC Press; 2016.

20. Vollrath M, Engert J, Winter G. Long-term release and stability of pharmaceutical proteins delivered from solid lipid implants. Eur J Pharm Biopharm Off J Arbeitsgemeinschaft Pharm Verfahrenstechnik EV. 2017 Aug;117:244–55.

21. Badiee P, Varshochian R, Rafiee-Tehrani M, Abedin Dorkoosh F, Khoshayand MR, Dinarvand R. Ocular implant containing bevacizumab-loaded chitosan nanoparticles intended for choroidal neovascularization treatment. J Biomed Mater Res A. 2018 Aug;106(8):2261–71.

22. Lance KD, Bernards DA, Ciaccio NA, Good SD, Mendes TS, Kudisch M, et al. In vivo and in vitro sustained release of ranibizumab from a nanoporous thin-film device. Drug Deliv Transl Res. 2016;6(6):771–80.

23. Burgalassi S, Monti D, Nicosia N, Tampucci S, Terreni E, Vento A, et al. Freeze-dried matrices for ocular administration of bevacizumab: a comparison between subconjunctival and intravitreal administration in rabbits. Drug Deliv Transl Res. 2018 Jun;8(3):461–72.

24. Luaces-Rodríguez A, Quiroga-Álvarez X, Gil-González Á, Fernández-Ferreiro A, Otero-Espinar FJ. Estudio preliminar de implantes intravítreos para la liberación de anticuerpos anti-VEGF. In: Concheiro-Nine Á, editor. Libro de comunicaciones del XIV Congreso de la Sociedad Española de Farmacia Industrial y Galénica [Internet]. Santiago de Compostela (Spain); 2019 [cited 2020 Apr 25]. p. 113–4. Available from: https://www.sefig.org/sites/default/files/congresos/abstracts_ivx_congreso_sefig_santiago_2019_0.pdf

25. Budianto E, Muthoharoh SP, Nizardo NM. Effect of Crosslinking Agents, pH and Temperature on Swelling Behavior of Cross-linked Chitosan Hydrogel. Asian J Appl Sci [Internet]. 2015 Oct 26 [cited 2020 Mar 17];3(5). Available from: https://ajouronline.com/index.php/AJAS/article/view/3099

26. Khan S, Ranjha NM. Effect of degree of cross-linking on swelling and on drug release of low viscous chitosan/poly(vinyl alcohol) hydrogels. Polym Bull. 2014 Aug 1;71(8):2133–58.

27. Rohindra DR, Nand AV, Khurma JR. Swelling properties of chitosan hydrogels. S Pac J Nat Appl Sci. 2004;22(1):32–5.

28. Siepmann J, Siepmann F. Mathematical modeling of drug delivery. Int J Pharm. 2008 Dec 8;364(2):328–43.

29. Costa P, Sousa Lobo JM. Modeling and comparison of dissolution profiles. Eur J Pharm Sci Off J Eur Fed Pharm Sci. 2001 May;13(2):123–33.

30. Moreno MR, Tabitha TS, Nirmal J, Radhakrishnan K, Yee CH, Lim S, et al. Study of stability and biophysical characterization of ranibizumab and aflibercept. Eur J Pharm Biopharm Off J Arbeitsgemeinschaft Pharm Verfahrenstechnik EV. 2016 Nov;108:156–67.

31. Sousa F, Cruz A, Fonte P, Pinto IM, Neves-Petersen MT, Sarmento B. A new paradigm for antiangiogenic therapy through controlled release of bevacizumab from PLGA nanoparticles. Sci Rep. 2017 16;7(1):3736.

32. Yandrapu SK, Upadhyay AK, Petrash JM, Kompella UB. Nanoparticles in porous microparticles prepared by supercritical infusion and pressure quench technology for sustained delivery of bevacizumab. Mol Pharm. 2013 Dec 2;10(12):4676–86.

33. Sharma G, Khalili A, Awwad S, Malik K, Matejtschuk P, Gaisford S, et al. Freeze Drying to Develop a Bevacizumab-based Tablet for Ocular Implantation. Invest Ophthalmol Vis Sci. 2013 Jun 16;54(15):1082–1082.

34. Taniwaki L, Mendonça R, Cunha-Júnior AS, Faraco A a. G, Ribeiro J a. S, Scott IU, et al. Effect of lyophilization on the in vitro biological activity of bevacizumab. Eye Lond Engl. 2010 Oct;24(10):1628–9.

USC
UNIVERSIDADE
DE SANTIAGO
DE COMPOSTELA

Conclusions

USC
UNIVERSIDADE
DE SANTIAGO
DE COMPOSTELA

CONCLUSIONS

In the **first part** of this doctoral thesis two different types of ocular hydrogels containing cysteamine, one made of hyaluronic acid polymer and the other an ion sensitive hydrogel composed of gellan gum and kappa carrageenan, have been successfully developed.

The *in vitro* release study showed that the cysteamine was able to be released from the hydrogels and that both hydrogels could control its release over time by a zero-order kinetics. Moreover, both hydrogels showed a higher transcorneal permeation of cysteamine than the control solution, concluding that the hydrogels enhanced cysteamine diffusion by acting as corneal absorption promoters.

The ocular surface permanence study by PET/CT showed that these formulations presented high retention time on the ocular surface of rats. This might lead to an increase in the duration of action, decreasing the frequency of administration. In addition, HET-CAM test showed that both hydrogels did not produce any irritation concluding that the formulations can be regarded as safe for ocular application.

The stability study of the hyaluronan hydrogel containing cysteamine showed that transparency, sterility, osmolality, pH and cysteamine concentration remained practically constant during the 30-day study period. Therefore, the recommendation for the preservation of the cysteamine hyaluronan hydrogels is refrigerated storage to prevent microbiological growth and avoiding the addition of the preservative EDTA.

As overall conclusion, the hydrogels containing cysteamine have demonstrated a prolonged retention time on the ocular surface, an adequate cysteamine controlled release, to be safe, and good stability, so the developed formulations present a high potential as vehicles for the topical ocular administration of cysteamine.

In the **second part** of this doctoral thesis, preliminary studies related to intravitreal administration of monoclonal antibodies in age-related macular degeneration (AMD) have been performed. The study of intravitreally injected fluorinated radionuclides permitted to determine the feasibility of using Positron Emission Tomography as a non-invasive methodology for the study of the ocular pharmacokinetics of intravitreal compounds in rats.

The evaluation of the pharmacokinetic profile of three different molecules labelled to 18-Fluorine (^{18}F-FDG, ^{18}F-NaF and ^{18}F-choline) following intravitreal injection in rats demonstrated that the molecular weight and physiochemical properties played a key role in the vitreous elimination.

The intravitreal injection of different volumes of radiotracers (2, 4 and 7 µL) showed that the injected volume had no significant influence on vitreous drug clearance in rat eyes. Four microlitres injection volume was selected as an adequate injected volume based on the results that the 7 µL-volume produced a transitory collapse on the ocular vessels and that allowed optimal visualisation through PET imaging.

The evaluation of the presence of ocular inflammation, such as the lipopolysaccharide-induced uveitis in rats, showed that uveitis was an important factor in vitreous clearance since the elimination of ^{18}F-FDG was clearly increased when this condition was present.

This PET methodology was successfully translated to the study of the pharmacokinetics of intravitreal ^{89}Zr-aflibercept and ^{89}Zr-bevacizumab. This provided for the first time the ocular and blood simultaneous quantification of these antibodies following intravitreal injection in rats.

The ocular and blood half-lives of both antibodies were stablished for the first time in rats. An ocular half-life of 16.4 hours and a blood half-life of 7.1 days were found for bevacizumab. Both half-lives were longer than for aflibercept, which showed a 4.5-hour ocular half-life and a 3.2- day blood half-life.

Therefore, a methodology for the study of intravitreal pharmacokinetics of zirconium-89 labelled antibodies which provides longitudinal data over the same animal was set for future pharmacokinetic studies of under-developed anti-VEGF drug delivery systems.

Finally, the study of chitosan-based intravitreal implants containing aflibercept has shown the potential of this approach as a drug delivery system to improve the treatment of AMD.

High molecular weight chitosan presented the best characteristics for the preparation of aflibercept-loaded implants. The implants prepared in this way were able to deliver aflibercept in a controlled manner at least for 21 days.

Increasing the crosslinking time with tripolyphosphate produced smaller implants, more compacted and with a smoother surface, which subsequently led to a lower swelling capacity. On the other hand, freezing of implants by immersion in liquid nitrogen produced implants with a considerably reduction of the initial burst effect. Therefore, the incorporation of both modifications in the method of preparation resulted in an implant with improved characteristics regarding morphology, swelling and release rates, and consequently, it seems to be a good candidate for further characterisation and optimisation studies.

USC
UNIVERSIDADE
DE SANTIAGO
DE COMPOSTELA

Appendix

USC
UNIVERSIDADE
DE SANTIAGO
DE COMPOSTELA

APPENDIX

The doctoral student declares that there is no conflict of interest regarding the doctoral thesis.

ANIMAL EXPERIMENTS

This thesis used male adult Sprague-Dawley rats with an average weight of 200-300 g supplied by the animal facility of the University of Santiago de Compostela (Santiago de Compostela, Spain). During the experiments, the animals were kept in individual cages with free access to food and water in a room under controlled temperature (22 ± 1 °C) and humidity (60 ± 5 %) and with day–night cycles regulated by artificial light (12/12 hours).

The animals were treated according to the guidelines for the care and use of laboratory animals and animal experiments complied with the ARRIVE guidelines (Kilkenny C, Browne WJ, Cuthill IC, Emerson M, Altman DG. Improving bioscience research reporting: the ARRIVE guidelines for reporting animal research. PLoS Biol. 2010 Jun 29;8(6):e1000412.). Experiments were performed at the Research Imaging Unit (UNIME) of the Health Research Institute of Santiago de Compostela (IDIS) (REGA number: ES1507802928 01).

Experiments were approved by the Consellería de Medio Rural da Xunta de Galicia (15010/2019/005) and were authorised by the Animal Research Committee of the Health Research Institute of Santiago de Compostela (IDIS). They followed the Spanish and European Union (EU) regulations for animal experimentation (86/609/CEE, 2003/ 65/CE, 2010/63/EU, and RD53/2013).

FUNDING

The work presented in this thesis was partially supported by the Spanish Ministry of Science, Innovation and Universities (RTI2018-099597-B-100), the Instituto de Salud Carlos III (PI17/00940, RETICS Oftared: RD16/0008/0003 and RD12/0034/0017), the Xunta de Galicia (GPC2017/015), the Fundación Española de Farmacia Hospitalaria (2019), the Fundación Mutua Madrileña (2019) and the Fundación La lucha de Iker. Moreover, the Hospital Pharmacy Department of the University Clinical Hospital of Santiago de Compostela kindly provided the anti-VEGF antibodies which were used in the experiments.

The doctoral student acknowledges specially the financial support of the Xunta de Galicia and the European Union (predoctoral research fellowship).

ARTICLES DERIVED FROM THIS THESIS

- Luaces-Rodríguez A, Díaz-Tomé V, González-Barcia M, et al. Cysteamine polysaccharide hydrogels: Study of extended ocular delivery and biopermanence time by PET imaging. *Int J Pharm.* 2017;528(1-2):714-722. doi:10.1016/j.ijpharm.2017.06.060.

  - Corresponds to **Chapter 1**.

- Luaces-Rodríguez A, Fernández-Ferreiro A, Díaz-Tomé V, et al. Cysteamine ophthalmic hydrogel for the treatment of ocular cystinosis. *Farm Hosp*. 2017;41(6):678-687. doi:10.7399/fh.10834.

  - Corresponds to **Chapter 2**.

- Luaces-Rodríguez A**,** Mondelo-García C, Zarra-Ferro I, et al. Intravitreal anti-VEGF drug delivery systems for age-related macular degeneration. *Int J Pharm*. 2020;573:118767. doi:10.1016/j.ijpharm.2019.118767.

  - Corresponds to **Chapter 3**.

- Luaces-Rodríguez A**,** Fernández-Ferreiro A, Aguiar P, et al. Preclinical PET Study of Intravitreal Injections. *Invest Ophthalmol Vis Sci*. 2017;58(7):2843-2851. doi:10.1167/iovs.17-21812.

  ➢ Corresponds to **Chapter 4**.

- Luaces-Rodríguez A, del Amo E, Mondelo-García A, et al. PET study of ocular and blood pharmacokinetics of intravitreal bevacizumab and aflibercept in rats. *Eur J Pharm Biopharm*. 2020; S0939-6411(20)30189-2. doi: 10.1016/j.ejpb.2020.06.024

  ➢ Corresponds to **Chapter 5**.

USC
UNIVERSIDADE
DE SANTIAGO
DE COMPOSTELA

USC
UNIVERSIDADE
DE SANTIAGO
DE COMPOSTELA